ACS SYMPOSIUM SERIES 1088

Production and Purification of Ultraclean Transportation Fuels

BIOMASS PRODUCTION
HYDROTREATING
CARBON DIOXIDE SEPARATION AND CONVERSION
DESULFURIZATION
HYDROGEN PRODUCTION

EDITED BY

Yun Hang Hu, Xiaoliang Ma,
Elise B. Fox, and Xinwen Guo

Downloaded by 89.163.34.136 on June 4, 2012 | http://pubs.acs.org
Publication Date (Web): December 14, 2011 | doi: 10.1021/bk-2011-1088.fw001

Production and Purification of Ultraclean Transportation Fuels

Downloaded by 89.163.34.136 on June 4, 2012 | http://pubs.acs.org
Publication Date (Web): December 14, 2011 | doi: 10.1021/bk-2011-1088.fw001

In Production and Purification of Ultraclean Transportation Fuels; Hu, Y., et al.;
ACS Symposium Series; American Chemical Society: Washington, DC, 2011.

ACS SYMPOSIUM SERIES **1088**

Production and Purification of Ultraclean Transportation Fuels

Yun Hang Hu, Editor
Michigan Technological University
Houghton, Michigan

Xiaoliang Ma, Editor
Kuwait Institute for Scientific Research
Safat, Kuwait

Elise B. Fox, Editor
Savannah River National Laboratory
Aiken, South Carolina

Xinwen Guo, Editor
Dalian University of Technology
Dalian, Liaoning, China

Sponsored by the
ACS Division of Fuel Chemistry

American Chemical Society, Washington, DC

Distributed in print by Oxford University Press, Inc.

Downloaded by 89.163.34.136 on June 4, 2012 | http://pubs.acs.org
Publication Date (Web): December 14, 2011 | doi: 10.1021/bk-2011-1088.fw001

Downloaded by 89.163.34.136 on June 4, 2012 | http://pubs.acs.org
Publication Date (Web): December 14, 2011 | doi: 10.1021/bk-2011-1088.fw001

Library of Congress Cataloging-in-Publication Data

Production and purification of ultraclean transportation fuels / Yun Hang Hu ... [et al.], editor ; sponsored by the ACS Division of Fuel Chemistry.
p. cm. -- (ACS symposium series ; 1088)
Includes bibliographical references and index.
ISBN 978-0-8412-2693-7
1. Synthetic fuels. 2. Gases--Purification. I. Hu, Yun Hang. II. American Chemical Society. Division of Fuel Chemistry.
TP360.P766 2011
665.7--dc23
2011046398

The paper used in this publication meets the minimum requirements of American National Standard for Information Sciences—Permanence of Paper for Printed Library Materials, ANSI Z39.48n1984.

Copyright © 2011 American Chemical Society

Distributed in print by Oxford University Press, Inc.

All Rights Reserved. Reprographic copying beyond that permitted by Sections 107 or 108 of the U.S. Copyright Act is allowed for internal use only, provided that a per-chapter fee of $40.25 plus $0.75 per page is paid to the Copyright Clearance Center, Inc., 222 Rosewood Drive, Danvers, MA 01923, USA. Republication or reproduction for sale of pages in this book is permitted only under license from ACS. Direct these and other permission requests to ACS Copyright Office, Publications Division, 1155 16th Street, N.W., Washington, DC 20036.

The citation of trade names and/or names of manufacturers in this publication is not to be construed as an endorsement or as approval by ACS of the commercial products or services referenced herein; nor should the mere reference herein to any drawing, specification, chemical process, or other data be regarded as a license or as a conveyance of any right or permission to the holder, reader, or any other person or corporation, to manufacture, reproduce, use, or sell any patented invention or copyrighted work that may in any way be related thereto. Registered names, trademarks, etc., used in this publication, even without specific indication thereof, are not to be considered unprotected by law.

PRINTED IN THE UNITED STATES OF AMERICA

Downloaded by 89.163.34.136 on June 4, 2012 | http://pubs.acs.org
Publication Date (Web): December 14, 2011 | doi: 10.1021/bk-2011-1088.fw001

Foreword

The ACS Symposium Series was first published in 1974 to provide a mechanism for publishing symposia quickly in book form. The purpose of the series is to publish timely, comprehensive books developed from the ACS sponsored symposia based on current scientific research. Occasionally, books are developed from symposia sponsored by other organizations when the topic is of keen interest to the chemistry audience.

Before agreeing to publish a book, the proposed table of contents is reviewed for appropriate and comprehensive coverage and for interest to the audience. Some papers may be excluded to better focus the book; others may be added to provide comprehensiveness. When appropriate, overview or introductory chapters are added. Drafts of chapters are peer-reviewed prior to final acceptance or rejection, and manuscripts are prepared in camera-ready format.

As a rule, only original research papers and original review papers are included in the volumes. Verbatim reproductions of previous published papers are not accepted.

ACS Books Department

Downloaded by 89.163.34.136 on June 4, 2012 | http://pubs.acs.org
Publication Date (Web): December 14, 2011 | doi: 10.1021/bk-2011-1088.pr001

Preface

As a result of the burning of fossil fuels, toxic air pollution levels are above health-based standards in many areas. The production and utilization of ultraclean fuels for transportation has been considered as the most effective approach to solve the issues of air pollution. To promote the improvement of research and to foster professional collaboration among researchers in clean fuel areas, we organized a symposium on "Ultraclean Fuels Production and Utilization for Sustainable Transportation" as a part of the 241st American Chemical Society National Meeting, March 27-31, 2011. Anaheim, California, U.S.A. This ACS symposium consisted of 33 oral presentations from industrial, university, and national laboratories in clean fuel areas. This ACS Symposium Series book was developed on this Symposium.

The aim of this ACS series book, which contains nine chapters, is to give the reader an appreciation of the state-of-the-art with respect to the production and utilization of clean fuels. The book focuses on the following topics: hydrotreating (Chapters 1 and 2), desulfurization (Chapters 3 and 4), biomass production (Chapters 5 and 6), carbon dioxide separation and conversion (Chapters 7 and 8), and hydrogen production (Chapter 9). All of those nine chapters were recruited from oral presentations at the symposium. All contributed manuscripts were sent to referees, and only those that passed through the peer review process became the chapters in this book.

We would like to express our genuine appreciation to all the authors of the chapters for their contributions to the ACS book and the ACS symposium. We thank all the peer reviewers for their efforts in evaluating the manuscripts to improve the quality of most chapters in the book. We gratefully acknowledge the ACS Division of Fuel Chemistry and the ACS Books Department for the opportunities to organize the symposium and to publish this book, respectively. We also wish to thank Arlene Furman, Tim Marney, and Bob Hauserman at the ACS Books Department for their great efforts and supports in the peer-review process and production of this book.

Yun Hang Hu
Department of Materials Science and Engineering
Michigan Technological University
Houghton, Michigan 49931-1295, U.S.A.

In Production and Purification of Ultraclean Transportation Fuels; Hu, Y., et al.;
ACS Symposium Series; American Chemical Society: Washington, DC, 2011.

Xiaoliang Ma
Kuwait Institute for Scientific Research (KISR)
Safat 13109, Kuwait

Elise B. Fox
Materials Science & Technology
Savannah River National Lab
Aiken, SC 29808, U.S.A.

Xinwen Guo
State Key Laboratory of Fine Chemicals
Dalian University of Technology
Dalian, Liaoning 116024, China

Downloaded by 89.163.34.136 on June 4, 2012 | http://pubs.acs.org
Publication Date (Web): December 14, 2011 | doi: 10.1021/bk-2011-1088.pr001

In Production and Purification of Ultraclean Transportation Fuels; Hu, Y., et al.;
ACS Symposium Series; American Chemical Society: Washington, DC, 2011.

Downloaded by 89.163.34.136 on June 4, 2012 | http://pubs.acs.org
Publication Date (Web): December 14, 2011 | doi: 10.1021/bk-2011-1088.ch001

Chapter 1

Effects of Citric Acid as a Chelating Agent on the Performance of a Heavy Oil Hydrotreatment Catalyst

Qiang Wei,[1] Yasong Zhou,[*,1] Chunming Xu,[1] and Yindong Liu[2]

[1]State Key Laboratory of Heavy Oil Processing,
China University of Petroleum, Beijing 102249, P.R. China
[2]Petrochemical Research Institute of Petrochina Company Limited,
Beijing 100029, P.R. China
[*]Tel: +86 10 89733501. E-mail: zhys01@cup.edu.cn.

Hydrotreatment catalyst was prepared by adding citric acid to improve the metal dispersion and reduce the metal-support interaction (MSI) of the catalyst. The catalyst was characterized by the method of Brunauer–Emmett–Teller (BET), X-ray diffraction (XRD), Fourier-transform infrared (FT-IR), NH_3-temperature-programmed desorption (NH_3-TPD) and thermogravimetry-differential scanning calorimetry (TG-DSC). Experimental and characterization results showed that citric acid intensively interacted with the active metal components of a catalyst. This interaction improved metal dispersion, and lessened the amount by which the specific surface area and pore volume decreased after corresponding decreased amounts of support-loaded metal components. The addition of citric acid favored the interaction of Ni and W with the support. The hydrotreatment performance of the citric acid-modified catalyst CMcat was higher than that of Ni-W/CYCTS. The hydrotreatment performances of the catalysts modified with citric acid were higher than that of the unmodified catalyst. The catalyst with 5% citric acid showed the highest HDS and HDN conversions, reaching 96% and 63%.

In Production and Purification of Ultraclean Transportation Fuels; Hu, Y., et al.;
ACS Symposium Series; American Chemical Society: Washington, DC, 2011.

Downloaded by 89.163.34.136 on June 4, 2012 | http://pubs.acs.org
Publication Date (Web): December 14, 2011 | doi: 10.1021/bk-2011-1088.ch001

Introduction

The hydrotreatment of heavy oil is very significant in petroleum processing. Very large amounts of heavy oils, such as coker gas oil (CGO) and deasphaltene oil (DAO), are produced everyday in refineries. CGO and DAO have very poor properties for processes such as fluid catalytic cracking (FCC) or hydrocracking. Hydrotreatment is the most efficient method for decreasing sulfur and nitrogen concentrations in petroleum fractions. Hence, CGO and DAO should first be hydrotreated before being used as feedstocks in FCC or hydrocracking.

Although most studies on hydrotreatment catalysts focus on hydrodesulfurization (HDS), hydrodenitrogenation (HDN) is becoming increasingly important in hydrotreating petroleum fractions (*1*). The properties of nitrogen-containing compounds greatly differ from those sulfur-containing compounds. Catalysts that may be suitable for HDS may not suit HDN (*2*). Hence, research on HDN catalysts is highly important for the hydrotreatment of heavy oil.

The catalytic activities of hydrotreatment catalysts are efficiently improved by evenly dispersing metal components (*3*). Examples are catalysts with nickel (Ni) and tungsten (W). With improved metal dispersion, the W crystalline slice becomes smaller, exposing more active sites to the catalyst surface (*4*). The Ni species then inhibits the growth of WO_3 crystalline particles as well as decreases the metal-support-interaction (MSI) of W and the support. Consequently, the reduction temperature of the metal component decreases.

Experimental

Chemically modified Y zeolite mixed with composite titania silica (CYCTS) was used as the support for the hydrotreatment catalyst (*5*). Nickel nitrate and ammonium metatungstate were used as the precursors of the metal component. The impregnation solution was first prepared by dissolving 1.35 g of $Ni(NO_3)_2$ and 3.71 g of $(NH_4)_6H_2W_{12}O_{40}$ in deionized water. A certain amount of citric acid was then added, and the solution was heated to 40 °C. After the impregnation solution became clear, it was added dropwise to 10 g support. The support was subjected to the method of equal volume impregnation for 4 h, dried at 120 °C for 5 h, and calcined at 500 °C for 3 h to obtain the citric acid-modified catalyst (CMcat) for heavy oil hydrotreatment. The unmodified catalyst was named as NiW/CYCTS.

The hydrotreating performance of the catalyst was evaluated on a JQ-III hydroprocessing unit, and a commercial CGO sample was chosen as feedstock. The concentrations of S and N in the CGO are 2402 $\mu g \cdot g^{-1}$ and 4800 $\mu g \cdot g^{-1}$, respectively. The catalyst loading was 10 ml. The reaction conditions were 380 °C, 6.0 MPa, 1.0 h^{-1} liquid hour space velocity (LHSV), and volumetric ration of hydrogen to oil 1000. The catalyst presulfidation conditions are as follows: the presulfidation solution 2% CS_2/cyclohexane, 300 °C, 4.0 MPa, 6 h^{-1}, and 4 h.

Downloaded by 89.163.34.136 on June 4, 2012 | http://pubs.acs.org
Publication Date (Web): December 14, 2011 | doi: 10.1021/bk-2011-1088.ch001

Results and Discussion

Effects of Citric Acid Modification on the Pore Structure of the Catalyst

Table I presents the specific surface area, pore volume, and pore diameter of the CYCTS support, the unmodified catalyst NiW/CYCTS prepared via the traditional method, and CMcat. The surface area and pore volume of CMcat were higher than those of NiW/CYCTS, and the pore diameter slightly decreased. When the metal component was loaded to the support, some micropores were blocked, causing the decreased specific surface area. When the catalyst was prepared via citric acid modification, the decrease in the surface area was not as much as in traditionally prepared catalyst. This discrepancy was attributed to the smaller size of the metal component particles on the CMcat surface, and to the fewer micropores blocked by the metal component.

Table I. Brunauer–Emmett–Teller Characterizations of CYCTS, NiW/CYCTS, and CMcat

Samples	*Specific Surface Area* $m^2 \cdot g^{-1}$	*Pore Volume* $ml \cdot g^{-1}$	*Pore Diameter* *nm*
CYCTS	280	0.80	11.4
NiW/CYCTS	177	0.52	11.8
CMcat	188	0.56	11.7

Figure 1 shows the pore distribution of CYCTS, NiW/CYCTS, and CMcat. The volumes of CMcat pores 5–12 and 14–17 nm in size were higher than those of NiW/CYCTS pores. Upon the addition of citric acid, its molecules intensively interacted with the metal components, resulting in improved metal dispersion. Consequently, the decrease in the specific surface area and pore volume after the support loading was not as much as that in traditionally prepared catalysts.

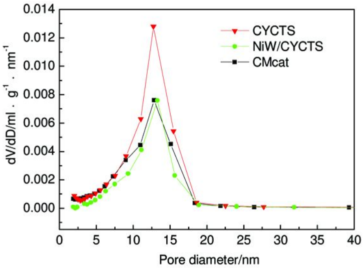

Figure 1. Pore distribution of CYCTS, NiW/CYCTS, and CMcat.

Downloaded by 89.163.34.136 on June 4, 2012 | http://pubs.acs.org
Publication Date (Web): December 14, 2011 | doi: 10.1021/bk-2011-1088.ch001

Effects of Citric Acid on the Metal Species Exposed to the Catalyst Surface

Figure 2 presents the Fourier-transform infrared (FT-IR) spectrum of CYCTS, Ni-loaded CYCTS (Ni/CYCTS), W-loaded CYSTS (W/CYCTS), and the catalyst NiW/CYCTS. From the spectrum of CYCTS, the characteristic peak of Ti-O-Si appeared at 930 cm^{-1}, and that of Si-O-Si appeared at 1040 cm^{-1}. After Ni loading, the characteristic peak of the spectrum did not obviously differ from that of CYCTS, illustrating that the Ni species on the support surface did not affect the CYCTS structure. The spectrum of W/CYCTS showed a characteristic peak at 950 cm^{-1}, which was the stretching vibration peak of W=O. The other peaks were the same with those of CYCTS. These findings revealed that the W species on the surface also did not affect the structure of CYCTS. The peaks at 880 and 730 cm^{-1} in the spectra of W/CYCTS and NiW/CYCTS were more intense than those of CYCTS. This result was due to the fact that the two peaks were not only the characteristic peaks of the support, but were also the peaks of the bridge vibration of W-O-W. Previous studies have reported that with decreased W=O/W-O-W ratio, poly(tungsten acid) species increase (*2*). Therefore, the addition of Ni induced an increase in the amount of poly(tungsten acid) species on the catalyst surface.

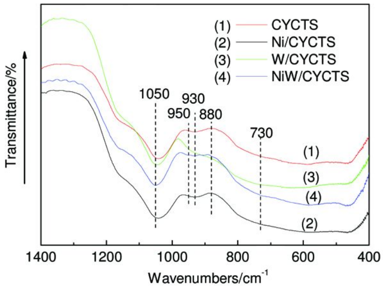

Figure 2. FT-IR spectrum of CYCTS, Ni/CYCTS, W/CYCTS, and NiW/CYCTS.

Figure 3 shows the FT-IR spectrum of CYCTS, NiW/CYCTS, and CMcat. For the spectrum of CMcat, the characteristic peak of the Si-O-Si bond at 1050 cm^{-1} moved 50 cm^{-1} toward a higher wavenumber, and the peak of Ti-O-Si at 930 cm^{-1} became more intense. This result indicated that some Ti-O-Si and Ti-O-Ti bonds were cleaved, and some Ti atoms were removed from the CYCTS structure. This phenomenon induced the movement of the characteristic peaks of Si-O-Si and Ti-O-Si toward a higher wavenumber, and then induced an increase in the Ti/Si atomic ratio on the support surface. Previous studies have demonstrated that TiO_2 favors the reduction and sulfidation of metal components. Hence, an increased Ti/Si atomic ratio on the support surface favors the activity of the catalyst.

Moreover, the intensity of the W=O bond stretching vibration at 950 cm^{-1} of CMcat was weaker than that of NiW/CYCTS. In contrast, the bridge vibration of the W-O-W bond at 880 and 730 cm^{-1} of CMcat was more intense than that of NiW/CYCTS. Hence, the W=O/W-O-W ratio of CMcat was less than that of NiW/CYCTS, illustrating that the addition of citric acid induced an increase in the amount of poly(tungsten acid) species on the catalyst surface.

Downloaded by 89.163.34.136 on June 4, 2012 | http://pubs.acs.org
Publication Date (Web): December 14, 2011 | doi: 10.1021/bk-2011-1088.ch001

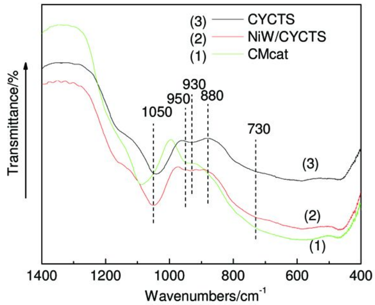

Figure 3. FT-IR spectrum of CYCTS, NiW/CYCTS, and CMcat.

Effects of Citric Acid on the Catalyst Acidity

Figure 4 presents the NH_3-temperature-programmed desorption (NH_3-TPD) profiles of NiW/CYCTS and CMcat. The desorption temperature of NiW/CYCTS and CMcat was between 100 to 300 °C. When the temperature was higher than 375 °C, the desorption curves overlapped with the baseline. Compared with NiW/CYCTS, the weak acidity sites of CMcat moved from 128 and 165 °C to 133 and 173 °C, respectively. This finding indicated that the acidity of the catalysts was mainly weak or within medium levels. The reason for the stronger acidity of CMcat was the increased atomic ratio of Ti/Si, inducing the intense interaction of Ni^{2+} or W^{6+} with TiO_2 (*6*). The interaction of the metal component with the support was also weaker, thereby inducing a strengthened acidity (*7*). Hence, given the weak Lewis acidities of Ni^{2+} and W^{6+} and the increased dispersion of the metal components (*8*), the aggregation of the metal particles was prevented (*9*), and weaker acidity sites were exposed to the CMcat surface.

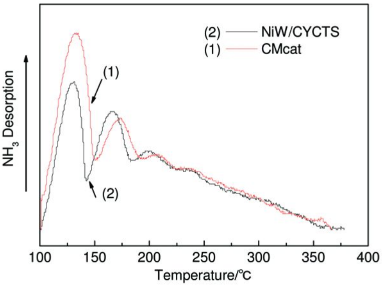

Figure 4. NH_3-TPD profiles of NiW/CYCTS and CMcat.

Downloaded by 89.163.34.136 on June 4, 2012 | http://pubs.acs.org
Publication Date (Web): December 14, 2011 | doi: 10.1021/bk-2011-1088.ch001

Effects of Citric Acid on the MSI of the Catalyst

Figures 5 and 6 show the thermogravimetry-differential scanning calorimetry (TG-DSC) spectra of NiW/CYCTS and CMcat.

For NiW/CYCTS, the endothermic peak from 30 to 200 °C was the support-losing surface-adsorbed water and $Ni(NO_3)_2$-losing crystal water. The intense endothermic peak from 200 to 400 °C was the decomposition peak of the nitrate radical. The wide endothermic peak from 400 to 600 °C was the decomposition peak of $(NH_4)_6H_2W_{12}O_{40}$. The exothermic peak of 600 °C was the generation of WO_3. For CMcat, the decomposition temperature of the nitrate radical decreased from 200 to 155 °C because the interaction of citric acid with Ni^{2+} favored the decomposition of $Ni(NO_3)_2$. However, the decomposition temperature was higher by about 50 °C than that of NiW/CYCTS. The exothermic peak of WO_3 at 600 °C became narrower, indicating the homogeneity of the poly(tungsten acid) (*10*, *11*). Hence, the addition of citric acid favored the interactions of Ni with W, and of both metals with the support.

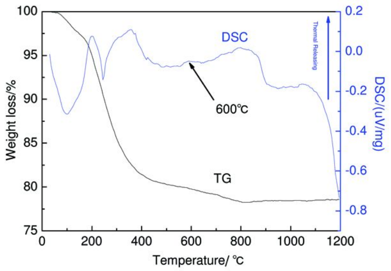

Figure 5. TG-DSC spectrum of NiW/CYCTS.

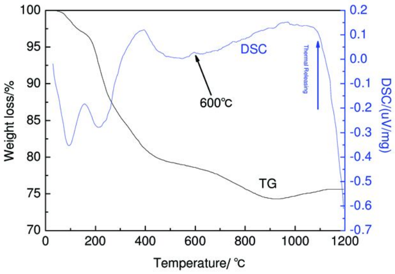

Figure 6. TG-DSC spectrum of CMcat.

Effects of the Catalyst Preparation Method on the Dispersion of the Metal Component

Figure 7 exhibits the X-ray diffraction (XRD) patterns of catalysts A, B, and C. Catalyst A was prepared by a sub-step impregnation method, and by mixing citric acid with a $Ni(NO_3)_2$ solution. In the sub-step impregnation method, Ni

Downloaded by 89.163.34.136 on June 4, 2012 | http://pubs.acs.org
Publication Date (Web): December 14, 2011 | doi: 10.1021/bk-2011-1088.ch001

was first loaded and calcined before W. Catalyst B was also prepared using the sub-step impregnation method. Ni was first loaded, and citric acid was mixed with the W-containing impregnating solution. The solution was then loaded to the support. Catalyst C was prepared via co-impregnation. Citric acid was added to the impregnating solution before the metal component was loaded, yielding CMcat.

The spectrum of the catalyst prepared by sub-step impregnation showed obvious characteristic peaks of WO_3 at 23.7°, 29°, and 33.6°. The intensity of the WO_3 characteristic peak of catalyst A was weaker than that of the sub-stepped catalyst. The spectrum of catalyst B showed a barely visible WO_3 characteristic peak, but the characteristic peak of $NiWO_4$ was more intense than that of catalyst A. The spectrum of catalyst C also demonstrated a very weak WO_3 characteristic peak. Similar with catalyst B, the characteristic peak of $NiWO_4$ was more intense than that of catalyst A. The characteristic peaks of the four catalysts revealed that the citric acid evenly dispersed the active metal Ni, and prevented the aggregation of WO_3 particles (*12*, *13*). For catalyst B, the interaction of citric acid with W efficiently prevented the aggregation and growth of WO_3. For catalyst C, citric acid simultaneously interacted with Ni and W, and improved metal dispersion by changing the interaction of the metal with the support (*14*, *15*). Consequently, the formation of $NiWO_4$ was favored.

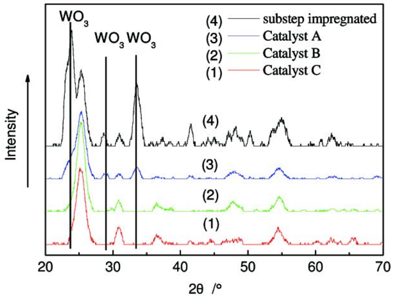

Figure 7. XRD patterns of catalysts prepared via different methods.

Effects of the Catalyst Preparation Method on HDS and HDN Conversions

Figure 8 shows the hydrotreatment performances of the catalysts prepared via different methods. The hydrotreatment performances of the catalysts were closely related with the metal oxide species on the catalyst surface (*13–15*). WO_3 species are difficult to reduce, and the active metal sites contained sulfides (*16*). Hence, the activities of the catalysts with more WO_3 exposed to the surface were not as high as those with less WO_3 characteristic peaks in their XRD spectra. $NiWO_4$ species, the precursor of the active sites, favored the improvement of the hydrotreatment performances of the catalysts (*4*, *17*). The amounts of HDS and HDN conversions of catalysts A and B were higher than those of the unmodified catalyst NiW/CYCTS. The hydrotreatment performance of catalyst C was the highest among the 4 catalysts. The HDS and HDN conversions were improved by 3% and 16% compared with the unmodified catalyst, respectively.

Downloaded by 89.163.34.136 on June 4, 2012 | http://pubs.acs.org
Publication Date (Web): December 14, 2011 | doi: 10.1021/bk-2011-1088.ch001

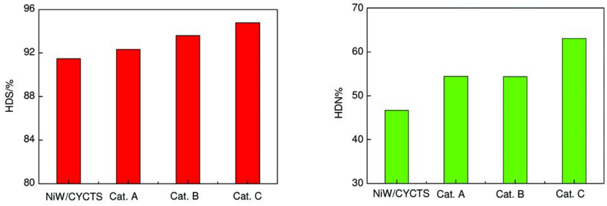

Figure 8. Hydrotreatment performances of catalysts prepared via different methods.

Effects of Additional Amount of Citric Acid on HDS and HDN Conversions

Figure 9 presents the XRD patterns of citric acid-modified catalysts with different amounts of citric acid added to the impregnating solution. A characteristic shoulder peak appeared at 23.7° in the pattern of the unmodified catalyst NiW/CYCTS. The patterns of the citric acid-modified catalysts showed no peak at this position. The intensity of the $NiWO_4$ characteristic peak increased with increasing amount of citric acid, indicating that the addition of citric acid prevented the growth of WO_3 particles (*18–21*).

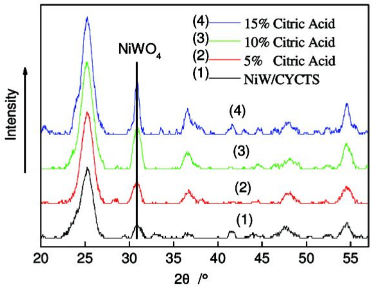

Figure 9. XDR patterns of catalysts with different citric acid amounts.

Figure 10 shows the HDS and HDN conversions of the modified catalysts with different citric acid amounts. The catalyst with 0% citric acid was the catalyst prepared via co-impregnation without citric acid modification.

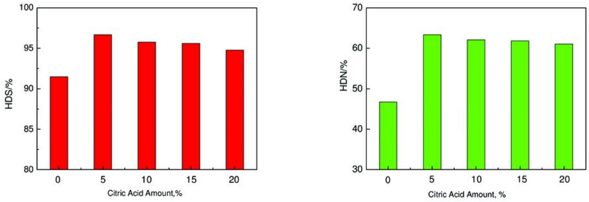

Figure 10. Hydrotreatment performances of CMcat with different citric acid amounts.

The hydrotreatment performances of the catalysts modified with citric acid were higher than that of the unmodified catalyst. The catalyst with 5% citric acid showed the highest HDS and HDN conversions, reaching 96% and 63%, respectively. With increasing citric acid content, the HDS and HDN conversions decreased. This result was due to very easy transformation of citric acid into coke during catalyst calcination. Consequently, some of the active metal sites were covered by coke, the amount of active sites decreased, and the hydrotreatment performances decreased.

Conclusions

Citric acid intensively interacted with the active metal components of a catalyst. This interaction improved metal dispersion, and lessened the amount by which the specific surface area and pore volume decreased after corresponding decreased amounts of support-loaded metal components. The addition of citric acid favored the interaction of Ni and W with the support. The aggregation of metal component particles during calcination was also prevented. The formation of $NiWO_4$, which was the active species of the hydrotreatment sites, was improved by citric acid as well.

The hydrotreatment performance of the citric acid-modified catalyst CMcat was higher than that of Ni-W/CYCTS. The preparation method affected the HDS and HDN conversions of CMcat.

Downloaded by 89.163.34.136 on June 4, 2012 | http://pubs.acs.org
Publication Date (Web): December 14, 2011 | doi: 10.1021/bk-2011-1088.ch001

Acknowledgments

The authors acknowledge the financial support of the Ministry of Science and Technology of China through the National Basic Research Program (Grant No. 2010CB226905), and of the National Natural Science Foundation of China through the General Program (Grant No. 20876172).

References

1. Viviane, S.; Oyama, S. T. Reaction network of pyridine hydrodenitrogenation over carbide and sulfide catalysts. *J. Mol. Catal. A: Chem.* **2000**, *163*, 269–282.
2. Dujardin, C.; Le´lias, M. A.; van Gestel, J.; Travert, A.; Duchet, J. C.; Mauge, F. Towards the characterization of active phase of (Co)Mo sulfide catalysts under reaction conditions—Parallel between IR spectroscopy, HDS and HDN tests. *Appl. Catal., A* **2007**, *322*, 46–57.
3. Atanasova, P.; Tabakova, T.; Vladov, Ch.; Halachev, T.; Lopez Agudo, A. Effect of phosphorus concentration and method of preparation on the structure of the oxide form of phosphorus-nickel-tungsten/alumina hydrotreating catalysts. *Appl. Catal. A* **1997**, *161*, 105–119.
4. Scheffer, B.; Heijeinga, J. J.; Moulijn, J. An electron spectroscopy and X-ray diffraction study of NiO/Al_2O_3 and $NiO-WO_3/Al_2O_3$ catalysts. *J. Phys. Chem.* **1987**, *18*, 4752–4759.

5. Wei, Q.; Zhou, Y.; Wen, S.; Xu, C. Preparation and properties of nickel preimpregnated CYCTS supports for hydrotreating coker gas oil. *Catal. Today* **2010**, *149*, 76–81.
6. Escobar, J.; Barrera, M. C.; de los Reyes, J. A.; Toledo, J. A.; Santes, V.; Colin, J. A. Effect of chelating ligands on Ni–Mo impregnation over wide-pore ZrO_2–TiO_2. *J. Mol. Catal. A: Chem.* **2008**, *287*, 33–40.
7. Martin, C.; Lamonier, C.; Fournier, M.; Mentré, O.; Harlé, V.; Guillaume, D.; Payen, E. Preparation and characterization of 6-molybdocobaltate and 6-molybdoaluminate cobalt salts. Evidence of a new heteropolymolybdate structure. *Inorg. Chem.* **2004**, *43*, 4636.
8. Rana, M. S.; Ramirez, J.; Gutierrez-Alejandre, A.; Ancheyta, J.; Cedeño, L.; Maity, S. K. Support effects in CoMo hydrodesulfurization catalysts prepared with EDTA as a chelating agent. *J. Catal.* **2007**, *246*, 100–108.
9. Mazoyer, P.; Geantet, C.; Diehl, F.; Loridant, S.; Lacroix, M. Role of chelating agent on the oxidic state of hydrotreating catalysts. *Catal. Today* **2008**, *130*, 75–79.
10. Kubota, T.; Rinaldi, N.; Okumura, K.; Honma, T.; Hirayama, S.; Okamoto, Y. In situ XAFS study of the sulfidation of Co-Mo/B_2O_3/Al_2O_3 hydrodesulfurization catalysts prepared by using citric acid as a chelating agent. *Appl. Catal. A* **2010**, *373*, 214–221.
11. Fan, Y.; Xiao, H.; Shi, G.; Liu, H.; Qian, Y.; Wang, T.; Gong, G.; Bao, X. Citric acid-assisted hydrothermal method for preparing NiW/USY–Al_2O_3 ultradeep hydrodesulfurization catalysts. *J. Catal.* **2011**, *279*, 27–35.
12. Okamoto, Y.; Kawano, M.; Kawabata, T.; Kubota, T.; Hiromitsu, I. Structure of the active sites of Co-Mo hydrodesulfurization catalysts as studied by magnetic susceptibility measurement and NO adsorption. *J. Phys. Chem. B* **2005**, *109*, 288–296.
13. Lelias, M. A.; Kooyman, P. J.; Mariey, L.; Oliviero, L.; Travert, A.; van Gestel, J.; van Veen, J. A. R.; Mauge, F. Effect of NTA addition on the structure and activity of the active phase of cobalt-molybdenum sulfide hydrotreating catalysts. *J. Catal.* **2009**, *267*, 14–23.
14. Chu, W.; Chernavskii, P. A.; Gengembre, L.; Pankina, G. A.; Fongarland, P.; Khodakov, A. Y. Cobalt species in promoted cobalt alumina-supported Fischer–Tropsch catalysts. *J. Catal.* **2007**, *252*, 215–230.
15. Rinaldi, N.; Kubota, T.; Okamoto, Y. Effect of citric acid addition on Co-Mo/B_2O_3/Al_2O_3 catalysts prepared by a post-treatment method. *Ind. Eng. Chem. Res.* **2009**, *48*, 10414–10424.
16. Fujikawa, T.; Kimura, H.; Kiriyama, K.; Hagiwara, K. Development of ultra-deep HDS catalyst for production of clean diesel fuels. *Catal. Today* **2006**, *111*, 188–193.
17. Quintana-Melgoza, J. M.; Cruz-Reyes, J.; Avalos, M. Synthesis and characterization of $NiWO_4$ crystals. *Mater. Lett.* **2001**, *47*, 314–318.
18. Lélias, M. A.; van Gestel, J.; Maugé, F.; van Veen, J. A. R. Effect of NTA addition on the formation, structure and activity of the active phase of cobalt–molybdenum sulfide hydrotreating catalysts. *Catal. Today* **2008**, *130*, 109–116.

Downloaded by 89.163.34.136 on June 4, 2012 | http://pubs.acs.org
Publication Date (Web): December 14, 2011 | doi: 10.1021/bk-2011-1088.ch001

In Production and Purification of Ultraclean Transportation Fuels; Hu, Y., et al.;
ACS Symposium Series; American Chemical Society: Washington, DC, 2011.

19. Valencia, D.; García-Cruz, I.; Klimova, T. Effect of citrate addition in NiMo/SBA-15 catalysts on selectivity of DBT hydrodesulfurization. *Stud. Surf. Sci. Catal.* **2010**, 529–532.
20. Rinaldi, N.; Kubota, T.; Okamoto, Y. Effect of citric acid addition on the hydrodesulfurization activity of MoO3/Al2O3 catalysts. *Appl. Catal. A* **2010**, *374*, 228–236.
21. Rinaldi, N.; Usman; Al-Dalama, K.; Kubota, T.; Okamoto, Y. Preparation of Co–Mo/B_2O_3/Al_2O_3 catalysts for hydrodesulfurization: Effect of citric acid addition. *Appl. Catal. A* **2009**, *360*, 130–136.

Downloaded by 89.163.34.136 on June 4, 2012 | http://pubs.acs.org
Publication Date (Web): December 14, 2011 | doi: 10.1021/bk-2011-1088.ch001

Downloaded by UNIV OF DELAWARE MORRIS LIB on June 5, 2012 | http://pubs.acs.org
Publication Date (Web): December 14, 2011 | doi: 10.1021/bk-2011-1088.ch002

Chapter 2

Hydrotreating of Coker Light Gas Oil on MCM-41 Supported Nickel Phosphide Catalysts

Kapil Soni, P. E. Boahene, and A. K. Dalai[*]

Catalysis and Chemical Reaction Engineering Laboratories,
Department of Chemical Engineering, University of Saskatchewan,
Saskatoon, Saskatchewan, Canada S7N 5A9
[*]**E-mail: ajay.dalai@usask.ca. Tel.: +1-306-966-4771. Fax: +1-306-966-4777.**

Siliceous MCM-41-supported nickel phosphides with a Ni/P atomic ratio of 2 and 0.5 were prepared by Temperature programmed reduction method. The phase purity and structural/surface properties were studied by X-ray diffraction and N_2 sorption measurements respectively. X-ray diffraction (XRD) analysis of the passivated catalysts confirmed the presence of Ni_2P and $Ni_{12}P_5$ in all catalysts prepared from oxidic precursors. Supports and catalysts were thoroughly characterized by using other techniques also; such as EDAX, SEM, and TEM. Results from low angle XRD measurements confirm the presence of hexagonally ordered mesoporous structure in MCM-41 material. Hydrotreating experiments were conducted under industrial conditions using Coker light gas oil (CLGO) as feed which contains 2,439 ppm nitrogen 23,420 ppm sulfur respectively. The activities with high Ni/P ratio (Ni/P=2 or $Ni_{12}P_5$/MCM-41 catalyst) exhibited higher hydrotreating activities than the catalysts with lower Ni/P ratio (Ni/P=0.5 or Ni_2P/MCM-41 catalyst) due to higher activity of $Ni_{12}P_5$ phosphides. The ratios of HDN over HDS activities are much higher over both phosphide catalysts than over the NiMo reference sample, due to the higher dispersion of metals in the former one. It was confirmed from this research work that $Ni_{12}P_5$/MCM-41 has shown very promising catalytic activity for hydrotreating of Coker light gas oil than the NiMo catalysts prepared by conventional method.

In Production and Purification of Ultraclean Transportation Fuels; Hu, Y., et al.;
ACS Symposium Series; American Chemical Society: Washington, DC, 2011.

Keywords: HDN; HDS; CLGO; $Ni_{12}P_5$; Ni_2P; MCM-41; BET; XRD

Downloaded by UNIV OF DELAWARE MORRIS LIB on June 5, 2012 | http://pubs.acs.org
Publication Date (Web): December 14, 2011 | doi: 10.1021/bk-2011-1088.ch002

Introduction

Stringent environmental regulations of the sulfur and nitrogen content of transportation fuels and non-road fuels have put considerable pressure on the refining industry worldwide to produce cleaner fuels and have motivated much research for the development of new hydrotreating catalysts. For example, in the case of sulfur, the U.S. Environmental Protection Agency (EPA) has issued regulations that had lowered its allowed content in diesel fuel from the 500 to 15 ppmw in 2006, and in gasoline from 300 to 30 ppmw in 2004 (*1*, *2*). For these reasons there are considerable efforts being expended to develop new technologies for the production of clean fuels, like adsorption, extraction, oxidation, alkylation, and hydroprocessing (*3*). However, out of these technologies hydroprocessing appears to be the technologically preferred solution. Hydroprocessing refers to a variety of catalytic hydrogenation processes that saturate heteroatomatic rings and remove S, N, O, and metals from different petroleum streams in a refinery (*4*). The existing challenge for hydroprocessing is deep desulfurization of diesel fuels which has refractory sulfur and nitrogen compounds.

Traditional hydrotreating catalysts consist of MoS_2-type phases supported on γ-Al_2O_3 and promoted by Co or Ni, which often contain phosphorous as a secondary promoter. These conventional catalysts are active in HDT of smaller S and N compounds, but not active enough in HDT of most refractory sulfur and nitrogen containing polyaromatic compounds (*5*, *6*). This has led to a worldwide search for better catalysts for hydrotreating of these compounds. Current approaches include the improvement of existing sulfide catalysts and the investigation of new compositions such as carbides, nitrides, zeolites and materials containing noble metals (*7–10*). One of the approaches to improve HDS catalysts is to find new active phases by including other cations (e.g., Ru, Pt, Pd) and anions (e.g., carbides, nitrides) (*11*). Transition metal phosphides have recently been reported to be promising as a new class of high-performance hydroprocessing catalysts. Among the phosphides studied, MoP and WP were reported to be more active than the corresponding group VI metal sulfides (*12–14*). Ni_2P was found to be the most active phase in the iron group compounds, although Fe_2P, CoP, and Co_2P also showed substantial HDS activities (*15–19*). Moreover, Ni_2P showed higher HDS and HDN activities than MoP or WP (*20*) and have recently been reported as a new class of high activity hydroprocessing catalysts that have substantial promise as next-generation catalysts. These phosphides are regarded as a group of stable, sulfur-resistant, metallic compounds that have exceptional hydroprocessing properties (*17*, *20*). Several articles have appeared in the literature describing the HDS and HDN properties of these metal phosphide catalysts (*21–26*). The hydrotreating activities of monophosphides (MoP and WP), metal rich phosphides (Co_2P and Ni_2P) as well as ternary phosphides (CoMoP and NiMoP) have been reported in a number of studies, most often using model compounds to determine catalyst activity (*17*, *20*). Oyama (*27*) reported the HDS of dibenzothiophene using different metal phosphides in this order Fe_2P < CoP < MoP < WP < Ni_2P. These catalysts were also shown to be more effective in removing S from refractory compounds such as 4-methyldibenzothiophene and 4,6-dimethyldibenzothiophene (4,6-DMDBT), than a conventional Co-Mo-S/Al_2O_3 catalyst (*28*).

These metal phosphides (e.g., Ni_2P) catalysts can be prepared by using a variety of methods. These methods include the temperature-programmed reduction (TPR) of nickel phosphates (*20*) and nickel dihydrogenphosphite (*29*), the decomposition of nickel thiophosphate ($NiPS_3$) (*30*) and nickel dihypophosphite (*31*), and the reduction of oxide precursors in nonthermal H_2 plasma (*32*). Among these methods, Ni_2P catalysts which are prepared by the temperature programmed reduction of phosphate exhibits excellent hydrotreating activity for the removal of organic sulfur and nitrogen in the liquid fuels (*20*, *33–36*). Such metal phosphide catalysts were even believed to be the next generation catalysts in replace of the transitional sulfide catalysts for the hydrotreating reactions. In the preparation of metal phosphides, it is essential to passivate the obtained metal phosphides prior to exposure to air or moisture because they react vigorously with oxygen and water, leading to the formation of metal oxides. In a typical passivation, a low concentration of O_2 (0.5–1.0%) in inert gas is used to mildly oxidize the surface of the metal phosphides in order to form a protective layer, which prevents the bulk oxidation of the phosphides. Since the oxides are not catalytically active, the catalyst has to be reduced at elevated temperatures prior to the hydrotreating reaction. However, temperature programmed reduction method has the disadvantage of requiring high reaction temperatures (usually above 873 K. This reduction process led to the low surface areas of the metal phosphides or the low dispersion of the metal phosphides on supports. In order to increase the dispersion of Ni_2P, the high surface area materials are being used as the supports, such as MCM-41 (*34*), SBA-15 (*37–40*), KIT-6 (*37*), MFI (*37*) and CMK-5 (*39*). Although alumina is a very good carrier for supported sulfides, but in the case of Ni_2P catalyst, it reacts with phosphate to form aluminum phosphates on the surface (*41*). Silica was reported to be a superior support because of its weak interaction with phosphates (*18*). In this current study, siliceous MCM-41 was used as support for preparing NixPy catalysts. The MCM-41 silica has much higher surface area, which helps in high dispersion of the active phases. To obtain the desired stoichiometry, phosphorus was added in different quantities to the MCM-41 support.

Although metal phosphides acts as promising alternative hydrotreating catalysts, but the assessment of these catalysts using typical refinery feedstocks are rare. In the present study, we are reporting the effect of Ni/P ratio on the HDN and HDS of Coker light gas oil (CLGO) derived from Athabasca bitumen using NixPy/MCM-41 catalysts. To our knowledge, no published work has been found NixPy catalysts were screened using CLGO as feed. For comparison, NiMo/MCM-41 catalyst was also prepared through conventional methods using ammonium hepta molybdate and nickel nitrate hexa hydrate as Mo and Ni source respectively.

Downloaded by UNIV OF DELAWARE MORRIS LIB on June 5, 2012 | http://pubs.acs.org
Publication Date (Web): December 14, 2011 | doi: 10.1021/bk-2011-1088.ch002

Downloaded by UNIV OF DELAWARE MORRIS LIB on June 5, 2012 | http://pubs.acs.org
Publication Date (Web): December 14, 2011 | doi: 10.1021/bk-2011-1088.ch002

Experimental

The MCM-41 material was synthesized using Cetyl trimethyl ammonium bromide (CTAB) as template, followed by a procedure reported elsewhere (*42*). In a typical synthesis procedure 35 g of Ludox HS-40 was added to 14.55 mL of water under stirring, and 18.2 mL of 40% tetramethylammonium hydroxide was added. Independently, 18.25 g of the template was dissolved in 33 mL of water, and subsequently, 7 mL of 28% NH_4OH was introduced. Finally, the above two solutions containing Ludox and template were mixed together. The final mixtures were stirred together for 30 min and then transferred into a polypropylene bottle for hydrothermal treatment at 100°C for 2 days. The resulting solids were filtered, washed, dried, and calcined at 550°C for 10 h under airflow at 2°C/min ramping rate. The synthesized siliceous MCM-41 has a specific surface area of 899 m^2 g^{-1}, a pore volume of 0.90 cm^3 g^{-1}, and a BJH average pore size of 3.6 nm.

MCM-41-supported nickel phosphides (Ni_2P) were prepared according to a procedure adapted from the literature (*39*). The procedure mainly includes two steps: (1) the oxidic precursor was obtained by incipient wetness impregnation method using a solution of nickel nitrate hexa hydrate (NNA) and ammonium hydrophosphate (AHP) precursors with Ni/P atomic ratio of 2.0 and 0.5 followed by drying and calcination; (2) the precursor was converted to nickel phosphide in flowing H_2 by temperature-programmed reduction. In a typical preparation of NixPy/MCM-41, a required amount of AHP was dissolved in 20 mL of deionized water to form a transparent colorless solution, then 1.96 g $Ni(NO_3)_2.6H_2O$ was added. The clear solution immediately became cloudy but, when the pH of the mixture was adjusted to 2–3 using 0.5 M HNO_3, it became clear again. A quantity of 4.00 g of MCM-41 was evacuated for 0.5 h and then wet-impregnated with the prepared solution for 0.5 h at room temperature. The mixture was heated to evaporate the water, and then the obtained solid was dried at 120°C overnight, followed by calcination in air at 500°C for 3 h. The oxidic precursor was pelletized, crushed, and sieved to ~20 mesh. The supported oxidic precursor was subjected to a temperature-programmed hydrogen reduction in a tubular reactor. The temperature program included two stages: (1) heating at 5 °C min^{-1} from room temperature to 120°C and maintaining at 120°C for 1 h to remove adsorbed moisture in a H_2 flow of 150 mL min^{-1} (2) further heating from 120 to 400 °C at 5°C min^{-1} and from 400 to 550°C at 1°C min^{-1}, then holding the temperature at 550°C for 3 h. To protect the metal phosphide structures, the prepared Ni_2P is passivated in a 1.0 mol% O_2/He flow (30 mL min^{-1}) at ambient temperature and pressure for 2 h. The synthesized catalysts are denoted as NixPy(z), where z represents the Ni/P atomic ratio in the precursor. Both of the oxidic precursors were prepared with the same procedure, using constant amount of $Ni(NO_3)_2.6H_2O$ with varying AHP amount to keep desired Ni/P ratio.

Downloaded by UNIV OF DELAWARE MORRIS LIB on June 5, 2012 | http://pubs.acs.org
Publication Date (Web): December 14, 2011 | doi: 10.1021/bk-2011-1088.ch002

Characterization

Measurement of N_2 Adsorption–Desorption Isotherms

The BET surface area, pore volume, and pore size distribution of the samples were measured with a Micromeritics ASAP 2000 instrument using low temperature N_2 adsorption–desorption isotherms. Before measuring, the sample was degassed in vacuum at 200°C. The surface area was computed from these isotherms using the multi-point Brunauer–Emmett–Teller (BET) method based on the adsorption data in the partial pressure P/P_0 range from 0.01 to 0.2. The value of 0.1620 nm^2 was taken for the cross-section of the physically adsorbed N_2 molecule. The mesopore volume was determined from the N_2 adsorbed at a $P/P_0 = 0.4$. The total pore volume was calculated from the amount of nitrogen adsorbed at $P/P_0 = 0.95$, assuming that adsorption on the external surface was negligible compared to adsorption in pores.The pore diameter and pore volume were determined using the (BJH) method. In all cases, correlation coefficients above 0.999 were obtained.

X-ray Diffraction (XRD) Analysis

The low-angle X-ray diffraction patterns of the samples were measured using a Bruker D8 Advance Powder diffractometer with a Ge monochromator producing a monochromatic Cu Kα radiation. The scanning was made from 1.5° to 10° with a 2θ step size of 0.02 and a step time of 2 s. In all cases, the generator was operated at 40 kV and 30 mA. To avoid the problem of illuminated areas at low 2θ angles, all samples were measured using the same sample holder. Broad angle powder X-ray diffraction patterns of all catalysts were recorded on a Rigaku diffractometer using Cu Kα radiation in the range 10–80° with a scan rate of 2°/min.

Transmission Electron Microscopy (TEM) and Scanning Electron Microscopy (SEM)

The morphological features of the support and catalysts were studied from electron micrographs obtained with a JEOL 2011 scanning transmission electron microscope. The powder samples were grounded softly in an agate mortar and dispersed in heptane in an ultrasonic bath for several minutes. A few drops were then deposited on 200 mesh copper grids covered with a holey carbon film. The electron micrographs were recorded in electron negative films and in a digital PC system attached to the electron microscope. Scanning electron microscopy (SEM) micrographs were observed on a Hitachi-S4700 microscope.

Energy Dispersive X-ray Analysis

Quantitative compositional analysis was carried out with an energy-dispersive X-ray analysis (EDAX) system attached to the electron microscope, which was operated at 25 kV. Determination of the chemical composition was based on the average analytical data of individual particles.

Catalytic Activity

Hydrotreating experiments were performed in a trickle bed reactor under typical industrial conditions. The coker light gas oil (CLGO) derived from Athabasca bitumen was used as a feed for the hydrotreating studies. CLGO is a complex combination of hydrocarbons from the distillation of the products from a thermal cracking process (fluid coker). It consists of hydrocarbons having carbon numbers predominantly in the range of C11 through C28 and boiling in the range of 200–450°C (Table 1) with specific gravity of 0.95 at 20°C and contains 0.24 and 2.3 wt % of nitrogen and sulfur, respectively. The high pressure reaction set up used in this study simulates the process that takes place in industrial hydrotreaters. The system consists of liquid and gas feeding sections, a high pressure reactor, a heater with temperature controller for precisely controlling the temperature of the catalyst bed, a scrubber for removing the ammonium sulfide from the reaction products, and a high pressure gas–liquid separator. The length and internal diameter of the reactor were 240 and 14 mm, respectively. The details of catalyst loading into the reactor are described elsewhere (*43*). Typically, the catalyst bed, approximately 10.5 cm long, was packed with 5 cm^3 of catalyst (2.0 g) and 12 cm^3 of 90 mesh silicon carbide.

Downloaded by UNIV OF DELAWARE MORRIS LIB on June 5, 2012 | http://pubs.acs.org
Publication Date (Web): December 14, 2011 | doi: 10.1021/bk-2011-1088.ch002

Table 1. Characteristics of Coker Light Gas Oil derived from Athabasca bitumen

Characteristic	*Coker Light Gas Oil*
Nitrogen (ppm)	2439
Sulfur (ppm)	23,420
Density (g/ml)	0.95
Boiling point distribution	
IBP (°C)	169
FBP (°C)	548
Boiling range (°C)	
IBP–250	6
250–300	22
300–350	31
350–400	23
401–450	9
450–500	6
500–FBP	3

Before reaction, the phosphide catalysts were activated by *in situ* reduction in an H_2 stream at atmospheric pressure (25 cm^3/min) while being heated at a rate of 3°C/min to 400°C and held at this temperature for 2 h. Following activation, the catalyst was precoked (stabilized) with CLGO for 5 days at a temperature of 370°C, pressure of 8.8 MPa, and LHSV of 2.0 h^{-1}. After precoking, HDN and HDS activities of the catalysts were studied at three different temperatures of 370°C, 350°C, and 330°C using CLGO for 3 days at each temperature. The pressure, H_2/feed ratio and LHSV were maintained constant at 8.8 MPa, 600 ml/ml and 2.0 h^{-1}, respectively. The products were collected at 12 h intervals and the products stripped with nitrogen for removing the dissolved ammonia and hydrogen sulfide. The total nitrogen content of the liquid product was measured by combustion/chemiluminence technique following ASTM D4629 method, and the sulfur content was measured using combustion/fluorescence technique following ASTM 5463 method. Both sulfur and nitrogen were analyzed in an Antek 9000 NS analyzer. The instrumental error in N and S analysis was 3%.

Downloaded by UNIV OF DELAWARE MORRIS LIB on June 5, 2012 | http://pubs.acs.org
Publication Date (Web): December 14, 2011 | doi: 10.1021/bk-2011-1088.ch002

Results and Discussion

Low Angle XRD

Powder XRD and N_2 sorption studies are regularly used to assess the quality and structural ordering of MCM-41 materials. These techniques provide important information regarding mesopores ordering in these materials. Powder XRD patterns obtained for the purely siliceous MCM-41 and NixPy/MCM-41 materials are shown in Figure 1. The pure silica, Si-MCM- 41, sample exhibits an XRD pattern which is typical of a well ordered material and shows an intense (100) diffraction peak and at least two higher order peaks (*42*). The incorporation of metals in MCM-41 support (NixPy/MCM-41: 2.0) results in a reduction in the intensity of the (100) peak due to slight modification in MCM-41 structure. In the case of NixPy/MCM-41 catalyst with Ni/P =0.5, all peaks are disappeared due to loss in the periodicity of the MCM-41 structure. The (100) peak for NixPy/MCM-41(2.0) samples is shifted to higher 2-theta values compared to pure MCM-41 indicating a decrease in basal (*d*100) spacing (*44*).

Broad Angle XRD

The effects of ratio of Ni/P can be clearly seen in the broad angle XRD pattern of MCM-41 supported Ni_xP_y catalysts (Figure 2). At higher Ni/P ratios (2.0), significant amount of catalytic active phases are present as $Ni_{12}P_5$ species. Henceforth, this catalyst is referred as $Ni_{12}P_5$/MCM-41 catalyst. The characteristic peaks corresponding to $Ni_{12}P_5$ are visible at 2θ value of 39°, 42°, and 49.3°. As the amount of phosphorus in the oxidic precursor is increased to a molar ratio Ni/P =0.5, the XRD pattern for the NixPy/MCM-41 catalysts shows dominant Ni_2P phase. The characteristic peaks corresponding to Ni_2P are visible at 2θ value of 41°, 44°, 47°, and 54° for Ni_2P/SiO_2, which confirms the formation of Ni_2P on the support. These catalysts can be referred as Ni_2P/MCM-41 catalyst (Figure 2). Similar type of results are found by other research groups also

(*45*, *46*). These results clearly explain that ratio of Ni/P changes the active phase in the final catalysts.

N_2 Adsorption-Desorption Isotherms and Pore Size Distribution

The N_2 adsorption-desorption isotherms, pore size distribution and textural properties of the prepared MCM-41 support and supported catalysts are shown in Figure 3 and Table 2. All the isotherms are corresponding to a Brunauer type IV isotherm of adsorption and desorption. Three well-distinguished regions of the adsorption isotherm are present, indicating the presence of monolayer-multilayer adsorption, capillary condensation, and multilayer adsorption on the outer surface. The hysteresis loop with features of H2-type hysteresis and the occurrence of pore filling over a relatively wide P/P_0 range (0.25-0.60) suggest a broad pore size distribution for MCM-41 material. These results indicate that the supports and the catalysts exhibit a uniform textural porosity. It can be seen from Figure 3 and Table 2 that as metal content increases, the surface area, pore volume and pore diameter decreases continouosly due to pore blocking effect. In the case of NixPy/MCM-41(0.5), the pore channels significantly blocked by P species, which might formed from the deposition of excess volatile P species (P and PH_3) during the transformation of oxidic precursors to Ni_2P. It can be seen in Figure 3C that the shape of the isotherm is quite different from Figure 3A and 3B due to very high metal loadings which causes a significant amount of pore blockage and a reason for distorting the pore structure.

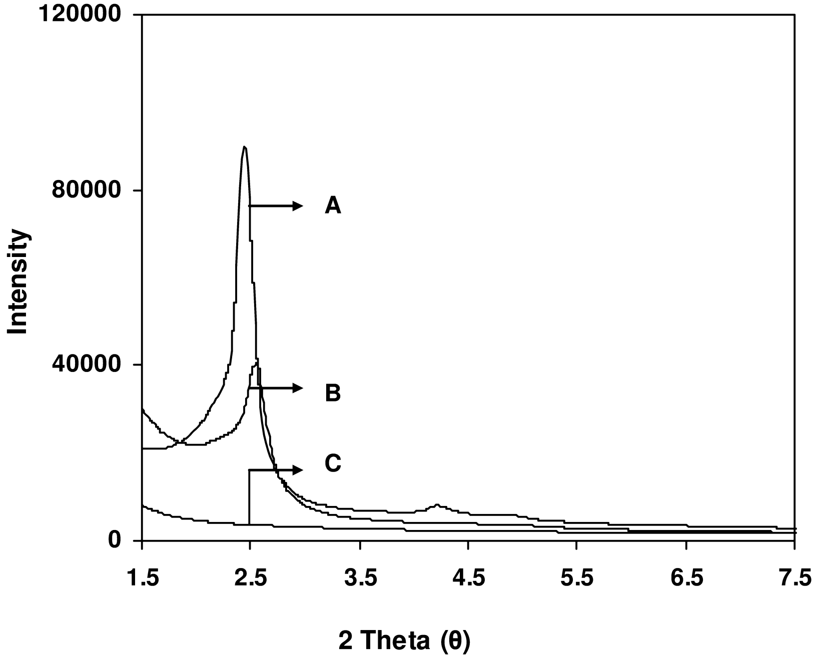

Figure 1. Low angle XRD Pattern of MCM-41 supported catalysts (A) MCM-41, (B) NixPy/MCM-41 (2.0), and (C) NixPy/MCM-41 (0.5).

Downloaded by UNIV OF DELAWARE MORRIS LIB on June 5, 2012 | http://pubs.acs.org
Publication Date (Web): December 14, 2011 | doi: 10.1021/bk-2011-1088.ch002

Downloaded by UNIV OF DELAWARE MORRIS LIB on June 5, 2012 | http://pubs.acs.org
Publication Date (Web): December 14, 2011 | doi: 10.1021/bk-2011-1088.ch002

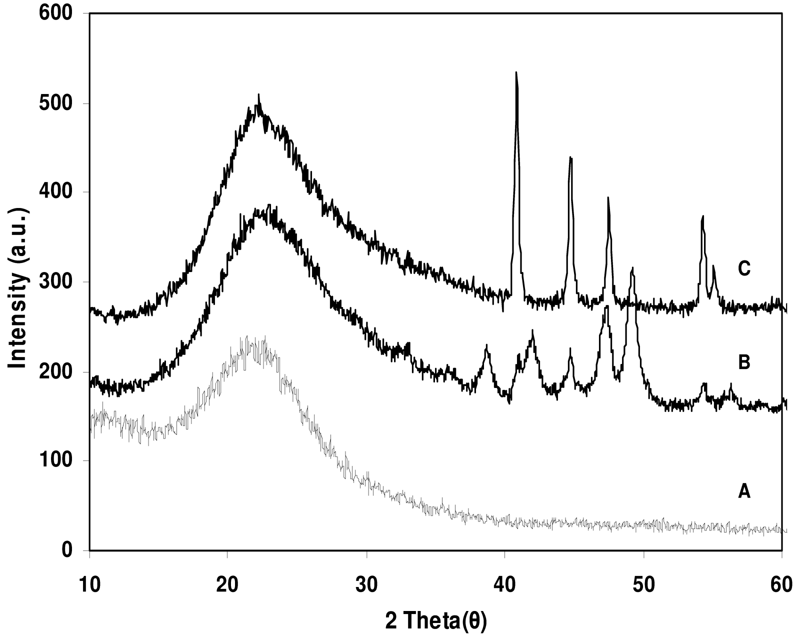

Figure 2. Broad angle XRD pattern of MCM-41 supported catalysts (A) MCM-41, (B) NixPy/MCM-41 (2.0), and (C) NixPy/MCM-41 (0.5).

Table 2. Textural characterization of MCM-41 and supported catalysts NixPy with different Ni/P ratio

Sample	*Metal composition (wt %)*		*S_{BET} (m^2/g)*	*D_p (nm)*	*V_p (cm^3/g)*
	Ni	*P*			
MCM-41	-	-	899	3.6	0.90
NixPy/MCM-41 (2.0)	11.68	2.68	443	3.4	0.75
NixPy/MCM-41 (0.5)	11.68	7.50	376	3.1	0.51

S_{BET}, specific surface area calculated by the BET method. **D_p**, mesopore diameter corresponding to the maximum of the pore size distribution obtained from the adsorption isotherm by the BJH method. **V_p**, pore volume determined by nitrogen adsorption at a relative pressure of 0.98.

Downloaded by UNIV OF DELAWARE MORRIS LIB on June 5, 2012 | http://pubs.acs.org
Publication Date (Web): December 14, 2011 | doi: 10.1021/bk-2011-1088.ch002

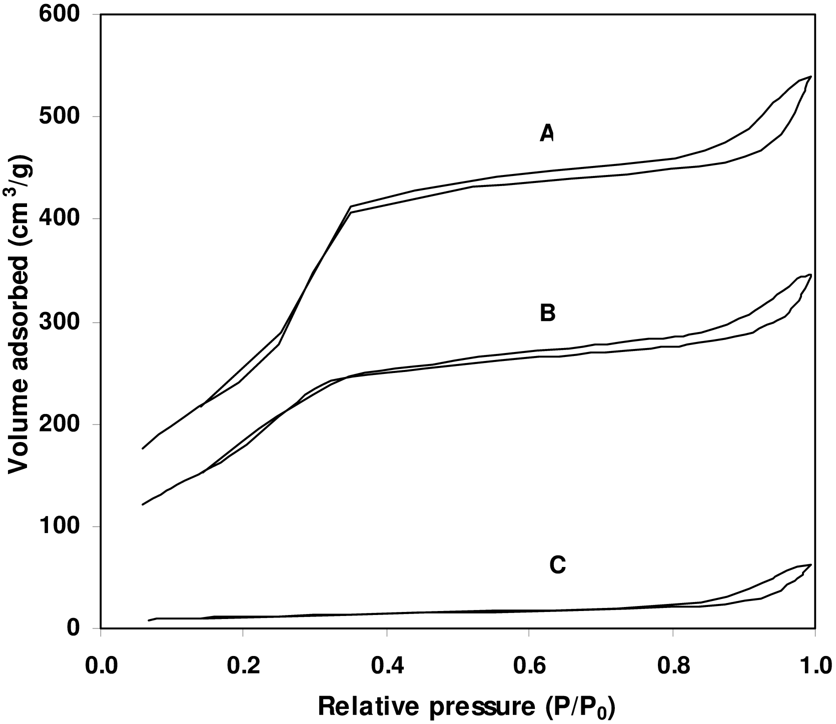

Figure 3. N_2 adsorption-desorption isotherm of MCM-41 supported catalysts (A) MCM-41, (B) NixPy/MCM-41 (2.0), and (C) NixPy/MCM-41 (0.5).

Transmission Electron Microscopy (TEM) and Scanning Electron Microscopy (SEM) Analysis

Distinct differences in the morphology and particle sizes of the samples are observed using transmission electron micrographs (TEM). The TEM image shown in Figure 4 provides insight into the porous framework of MCM-41 and NixPy/MCM-41(2.0) materials. A typical hexagonal pore structure of MCM-41 materials with network channels, uniform pore sizes, and long-range ordering can be seen in Figure 4A, that was also confirmed by low angle XRD patterns. The TEM micrographs of NixPy/MCM-41(2.0) illustrated in Figure 4B show no significant changes in the catalyst morphology, suggesting that the metals are uniformly dispersed on the surface of the MCM-41 support. Some metal agglomerates are present on the external surface of the support and some particles seem to be distributed into the support porosity. From the TEM micrograph, the calculated pore diameter is about 3 nm, which is close to that estimated from the nitrogen sorption isotherms. It is clear from Figure 4C that, at high metal loading (NixPy/MCM-41(0.5), most of the pores has been blocked by metal content which causes less dispersed species"

In Production and Purification of Ultraclean Transportation Fuels; Hu, Y., et al.;
ACS Symposium Series; American Chemical Society: Washington, DC, 2011.

Scanning electron microscopy pictures of pure MCM-41 material are illustrated in Figure 5A. These images reveal that MCM-41 is made up of aggregate with fine particles of smaller than 1 μm. The SEM picture of MCM-41 supported NixPy (2.0) catalysts is also shown in Figure 5B. The supported catalysts have similar morphology as pure support has indicating that MCM-41 support helps to maintain good dispersion of active species without losing morphology.

Downloaded by UNIV OF DELAWARE MORRIS LIB on June 5, 2012 | http://pubs.acs.org
Publication Date (Web): December 14, 2011 | doi: 10.1021/bk-2011-1088.ch002

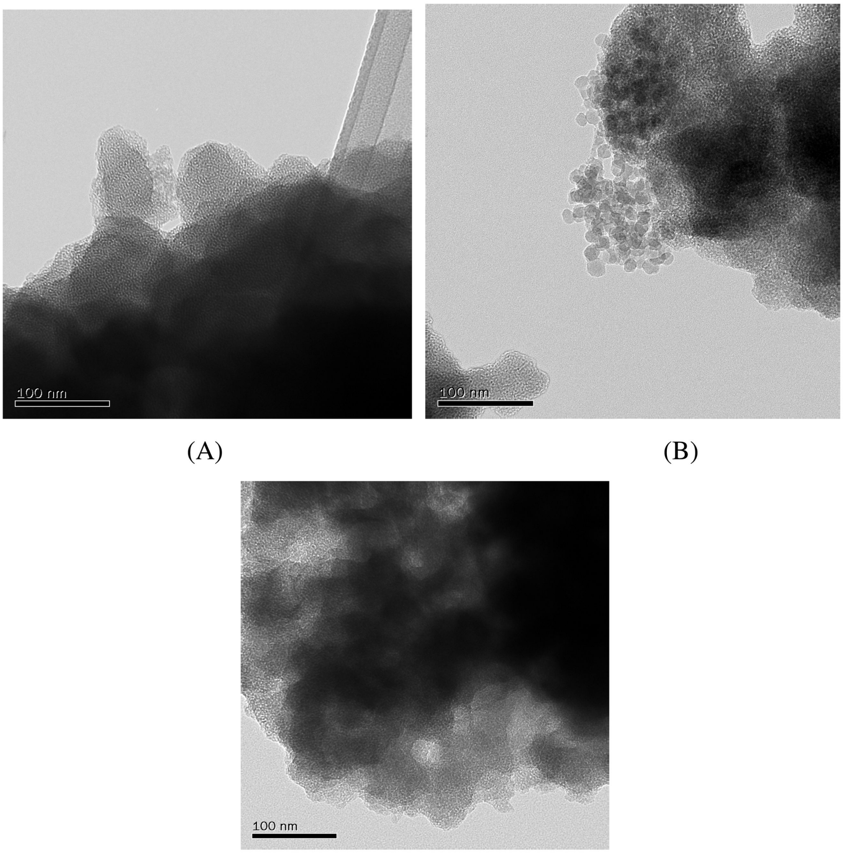

(A) (B)

(C)

Figure 4. TEM images of MCM-41 supported catalysts (A) MCM-41, (B) NixPy/MCM-41 (2.0), and (C) NixPy/MCM-41 (0.5).

Downloaded by UNIV OF DELAWARE MORRIS LIB on June 5, 2012 | http://pubs.acs.org
Publication Date (Web): December 14, 2011 | doi: 10.1021/bk-2011-1088.ch002

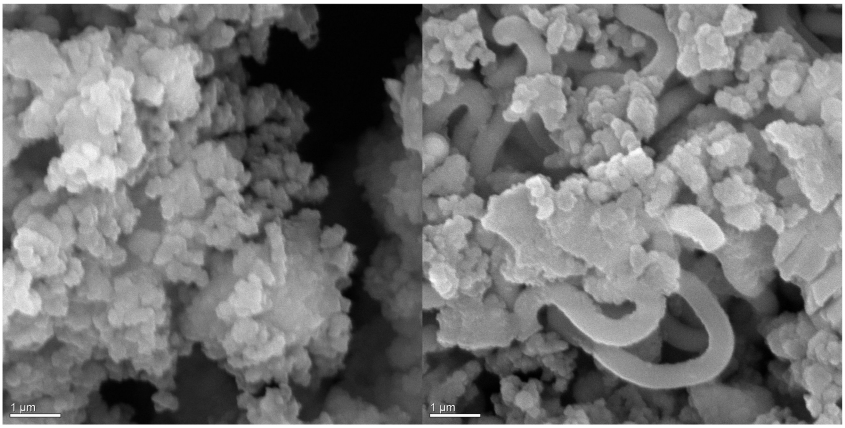

(A) (B)

Figure 5. SEM image of MCM-41 support and supported NixPy(2.0) catalysts.

Energy Dispersive X-ray Analysis

To obtain evidence of the uniform dispersed deposition of the active phase in the MCM-41 supported NixPy (2.0) catalyst utilization of elemental composition determination using EDAX was carried out while performing TEM. Ni and P were detected at two arbitrary points of a newly synthesized catalyst. The quantitative analysis of different elements showed ~11 wt. % Ni and ~2wt. % P content for this sample in the two arbitrary chosen points. The obtained EDAX spectra of the two arbitrary points of the newly synthesized catalyst sample showed no significant change in relative intensities (figure not shown). The EDAX results provide a strong indication that most of the Ni and P in the synthesized catalyst are uniformly distributed in the MCM-41 support.

Catalytic Activity Studies

In this study, the HDN and HDS activities, expressed as percent conversion, were measured using synthesized NixPy/MCM-41 catalysts with different Ni/P ratios. For comparison, the activity studies of NiMo/MCM-41 was also measured (Figure 6). Before reaction, the phosphide catalysts were activated by H_2 stream at atmospheric pressure (25 cm^3/min) while being heated at a rate of 3°C/min to 400°C and held at this temperature for 2 h. After activation, the temperature was lowered to 370°C. The NiMo/MCM-41 catalysts were sulfided before reaction by injecting sulfidation solution containing 2.9 vol % of butanethiol in straight run atmospheric gas oil at a pressure and temperature of 8.8 MPa and 193°C, respectively, for 24 h. The flow rate of the sulfiding solution was 5 mL/min. The H_2 flow rate was kept at a rate corresponding to H_2/sulfiding solution ratio of 600 mL/mL. The temperature of the reactor was increased to 343°C and maintained for another 24 h.

In Production and Purification of Ultraclean Transportation Fuels; Hu, Y., et al.;
ACS Symposium Series; American Chemical Society: Washington, DC, 2011.

To achieve steady-state activity, all the catalysts were stabilized by precoking using CLGO at a temperature, pressure, LHSV, and H_2/feed ratio of 370°C, 8.8 MPa, 2 h^{-1}, and 600 ml/ml, respectively for 5 days. HDN and HDS activities of the MCM-41 supported NixPy catalysts are higher than MCM-41 supported NiMo catalysts. At initial stage of the reaction, the HDN and HDS activities of these catalysts are very high due to high number of active sites. The N and S conversions of the CLGO catalysts decreased with time on stream and reached steady-state after 3 days, probably due to coking of active sites.

After precoking, the steady-state activity of all prepared catalysts were studied using the same feed at reaction temperatures of 330, 350, and 370°C, a pressure of 8.8MPa, an LHSV of 2 h^{-1}, and a hydrogen-to-gas oil ratio of 600 mL/mL. The activity was studied for 72 h at each temperature and samples collected after every 12 h. The average N and S conversions of the last four samples at each reaction temperature are shown in Figure 6, respectively. The activity results show that MCM-41 supported NixPy catalysts show much higher catalytic activities compared to reference NiMo/MCM-41 catalysts under similar reaction conditions. The N-S conversion confirms the following order of activity: NixPy/MCM-41(2.0) > NixPy/MCM-41(0.5) > NiMo/MCM-41. These results are in agreement with the fact that MCM-41 supported NixPy catalysts have optimum metal support interaction, which helps to high and homogeneous dispersion of Ni and phosphate species and causes higher hydrotreating activity.

Downloaded by UNIV OF DELAWARE MORRIS LIB on June 5, 2012 | http://pubs.acs.org
Publication Date (Web): December 14, 2011 | doi: 10.1021/bk-2011-1088.ch002

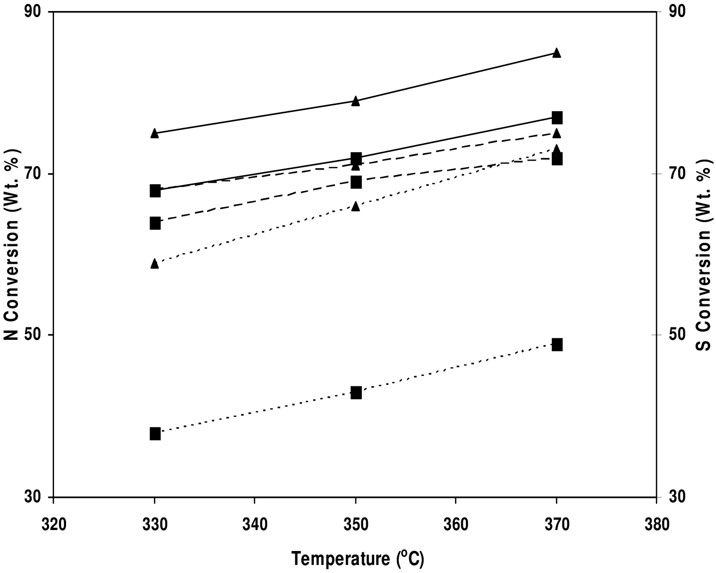

Figure 6. (▲) HDS and (■) HDN activities of MCM-41 supported catalysts (·····NiMo, ----- NixPy (0.5), and —— NixPy (2.0) with CLGO at different temperatures (Catalyst = 5 cm^3, P = 8.8 MPa, LHSV = 2 h^{-1}, and H_2/oil ratio = 600 (v/v)).

Downloaded by UNIV OF DELAWARE MORRIS LIB on June 5, 2012 | http://pubs.acs.org
Publication Date (Web): December 14, 2011 | doi: 10.1021/bk-2011-1088.ch002

Conclusions

In the present work, a series of NixPy catalysts supported on MCM-41 were prepared. The high surface area (~900m^2/g) in the range of mesopores makes them suitable carriers for better and uniform distribution of metal species. It was observed that Ni/P ratio played an important role in improving dispersion and, subsequently, reduction of the Ni and P species, which makes the active for hydrotreating reaction. The N and S conversions of the MCM-41 supported NixPy catalyst are significantly higher than that of the MCM-41 supported NiMo catalysts, indicating that MCM-41 supported NixPy catalysts have optimum metal support interaction and greater dispersion of Ni and P species, which causes greater activity in hydrotreatment reactions. The catalytic activity for NixPy/MCM-41 (2.0) is high compared to NixPy/MCM-41 (0.5) due to more dispersion and less pore blocking.

Acknowledgments

The authors are grateful to Syncrude Canada Ltd. and the Natural Sciences and Engineering Research Council of Canada for financial support of this research.

References

1. U.S. Environmental Protection Agency; Press Release, May 1, 1999; December 21, 2000.
2. *Federal Register*, Vol. 65, No. 28; Washington, DC, 2000.
3. O'Connor, P.; Mayo, S. *Prepr. Pap. - Am. Chem. Soc., Div. Fuel Chem.* **2001**, *46*, 381.
4. Topsøe, H.; Clausen, B. S.; Massoth, F. E. In *Hydrotreating Catalysis, Science and Technology*; Anderson, J. R., Boudart, M., Eds.; Springer-Verlag: Berlin/Heidelberg/New York, 1991; Vol. 11.
5. Whitehurst, D. D.; Isoda, T.; Mochida, I. *Adv. Catal.* **1998**, *42*, 345.
6. Wang, A. J.; Wang, Y.; Kabe, T.; Chen, Y. Y.; Ishihara, A.; Qian, W. H. *J. Catal.* **2001**, *199*, 19.
7. Oyama, S. T.; Yu, C. C.; Ramanathan, S. *J. Catal.* **1999**, *184*, 535.
8. Aegerter, P. A.; Quigley, W. W. C.; Simpson, G. J.; Ziegler, D. D.; Logan, J. W.; McCrea, K. R.; Glazier, S.; Bussell, M. E. *J. Catal.* **1996**, *164*, 109.
9. Qian, W.; Yoda, Y.; Hirai, Y.; Ishihara, A.; Kabe, T. *Appl. Catal., A* **1999**, *184*, 81.
10. Song, C.; Reddy, K. M. *Appl. Catal., A* **1999**, *176*, 1.
11. Kabe, T.; Ishihara, A.; Qian, W. *Hydrodesulfurization and Hydrodenitrogenation: Chemistry and Engineering*; Wiley–VCH: Weinheim, 1999.
12. Stinner, C.; Prins, R.; Weber, T. *J. Catal.* **2000**, *191*, 438.
13. Clark, P.; Wang, X.; Oyama, S. T. *J. Catal.* **2002**, *207*, 256.
14. Phillips, D. C.; Sawhill, S. J.; Self, R.; Bussell, M. E. *J. Catal.* **2002**, *207*, 266.
15. Wang, X.; Clark, P.; Oyama, S. T. *J. Catal.* **2002**, *208*, 321.

16. Oyama, S. T.; Wang, X.; Lee, Y.-K.; Bando, K.; Requejo, F. G. *J. Catal.* **2002**, *210*, 207.
17. Stinner, C.; Prins, R.; Weber, T. *J. Catal.* **2001**, *202*, 187.
18. Robinson, W. R. A. M.; Van Gestel, J. N. M.; Korányi, T. I.; Eijsbouts, S.; van der Kraan, A. M.; Van veen, J. A. R.; De beer, V. H. J. *J. Catal.* **1996**, *161*, 539.
19. Korányi, T. I. *Appl. Catal., A* **2003**, *239*, 253.
20. Oyama, S. T. *J. Catal.* **2003**, *216*, 343.
21. Duan, X.; Tenga, Y.; Wang, A.; Koganb, V. M.; Li, X.; Wanga, Y. *J. Catal.* **2009**, *261*, 232–240.
22. Ibeh, B.; Zhang, S.; Hill, J. M. *Appl. Catal., A* **2009**, *368*, 127–131.
23. Burns, A. W.; Gaudette, A. F.; Bussell, M. E. *J. Catal.* **2008**, *260*, 262–269.
24. Guan, Q.; Li, W. *J. Catal.* **2010**, *271*, 413–415.
25. Duan, X.; Li, X.; Wanga, A.; Teng, Y.; Wangb, Y.; Hua, Y. *Catal. Today* **2010**, *149*, 11–18.
26. Zhao, H. Y.; Lia, D.; Bui, P.; Oyama, S. T. *Appl. Catal., A* **2011**, *391*, 305–310.
27. Oyama, S. T.; Gott, T.; Zhao, H.; Lee, Y. K. *Catal. Today* **2009**, *143*, 94–107.
28. Oyama, S. T.; Wang, X. T.; Requejo, F. G.; Sato, T.; Yoshimura, Y. *J. Catal.* **2002**, *209*, 1.
29. Cecilia, J. A.; Infantes-Molina, A.; Rodríguez-Castellón, E.; Jiménez-López, A. *J. Catal.* **2009**, *263*, 4.
30. Loboué, H.; Guillot-Deudon, C.; Popa, A. F.; Lafond, A.; Rebours, B.; Pichon, C.; Cseri, T.; Berhault, G.; Geantet, C. *Catal. Today* **2008**, *130*, 63.
31. Guan, Q. X.; Li, W.; Zhang, M. H.; Tao, K. Y. *J. Catal.* **2009**, *263*, 1.
32. Wang, A. J.; Li, M.; Qin, Guan J.; Wang, L.; Guo, H. C.; Li, X.; Wang, Y.; Prins, R.; Hu, Y. K. *Angew. Chem., Int. Ed.* **2008**, *47*, 6052.
33. Sawhill, S. J.; Phillips, D. C.; Bussell, M. E. *J. Catal.* **2003**, *215*, 208.
34. Oyama, S. T.; Lee, Y. *J. Catal.* **2008**, *258*, 393.
35. Yang, S.; Prins, R. *Chem. Commun.* **2005**, 4178.
36. Yang, S.; Lang, C.; Prins, R. *J. Catal.* **2006**, *237*, 118.
37. Korányi, T. I.; Coumans, A. E.; Hensen, E. J. M.; Ryoo, R.; Kim, H. S.; Pfeifer, É.; Kasztovszky, Z. *Appl. Catal., A* **2009**, *365*, 48.
38. Korányi, T. I.; Vít, Z.; Poduval, D. G.; Ryoo, R.; Kim, H. S.; Hensen, E. J. M. *J. Catal.* **2008**, *253*, 119–131.
39. Korányi, T. I.; Vít, Z.; Nagy, J. B. *Catal. Today* **2008**, *130*, 80.
40. Wei, N.; Ji, S.; Wu, P.; Guo, Y.; Liu, H.; Zhu, J.; Li, C. *Catal. Today* **2009**, *147S*, S66–S70.
41. Stinner, C.; Tang, Z.; Haouas, M.; Weber, Th.; Prins, R. *J. Catal.* **2002**, *208*, 456.
42. Reddy, E. P.; Davydov, L.; Smirniotis, P. G. *J. Phys. Chem. B* **2002**, *106*, 3394–3401.
43. Sundaramurthy, V.; Dalai, A. K.; Adjaye, J. *Catal. Lett.* **2005**, *102*, 299.
44. Wang, A.; Wang, Y.; Kabe, T.; Chen, Y.; Ishihara, A.; Qian, W. *J. Catal.* **2001**, *199*, 19.
45. Song, L.; Zhang, S. *Powder Technol.* **2011**, *208*, 713–716.
46. Song, L.; Zhang, S.; Wei, Q. *Catal. Commun.* **2011**, *12*, 1157–1160.

Downloaded by UNIV OF DELAWARE MORRIS LIB on June 5, 2012 | http://pubs.acs.org
Publication Date (Web): December 14, 2011 | doi: 10.1021/bk-2011-1088.ch002

Downloaded by UNIV OF DELAWARE MORRIS LIB on June 5, 2012 | http://pubs.acs.org
Publication Date (Web): December 14, 2011 | doi: 10.1021/bk-2011-1088.ch003

Chapter 3

Adsorptive Pretreatment of Light Cycle Oil and Its Effect on Subsequent Hydrodesulfurization

Masoud Almarri,*,[1] Xiaoliang Ma,[2] Na Li,[2] and Chunshan Song[2]

[1]Petroleum Refining Department, Kuwait Institute for Scientific Research,
P.O. Box 24885, Safat 13109, Kuwait
[2]Clean Fuels and Catalysis Program, EMS Energy Institute,
and Department of Energy & Mineral Engineering,
Pennsylvania State University, 209 Academic Projects Building,
University Park, Pennsylvania 16802, U.S.A.
***E-mail: mmerri@kisr.edu.kw**

Adsorptive denitrogenation of light cycle oil (LCO) over the carbon-based adsorbents was conducted in both batch and flow adsorption systems. The effects of the physical and chemical properties of the carbon materials as well as the adsorption conditions on the adsorption performance were examined. It was found that some activated carbons could efficiently remove the nitrogen compounds from LCO. Oxidative modification of the activated carbons greatly enhanced the adsorption capacity and selectivity for nitrogen compounds, but not for the coexisting sulfur compounds. The regeneration of the spent activated carbon by solvent washing was also studied. The results indicate that the majority of the capacity of the adsorbents can be recovered by washing the spent adsorbents with toluene. In addition, the effect of the pre-denitrogenation on the performance of the subsequent HDS was examined. It was confirmed that the pretreatment of LCO by adsorption over the activated carbon improved the HDS performance significantly, especially for removing the refractory sulfur compounds that have one or two alkyl groups at the 4- and/or 6- positions of dibenzothiophenes, due to the substantial pre-removal of the coexisting carbazole compounds from LCO.

In Production and Purification of Ultraclean Transportation Fuels; Hu, Y., et al.;
ACS Symposium Series; American Chemical Society: Washington, DC, 2011.

Downloaded by UNIV OF DELAWARE MORRIS LIB on June 5, 2012 | http://pubs.acs.org
Publication Date (Web): December 14, 2011 | doi: 10.1021/bk-2011-1088.ch003

Introduction

Deep denitrogenation (*1–3*) and desulfurization (*4–6*) of fuels have gained great attention worldwide in recent years. Heightened concerns regarding global climate change and air pollution are driving the movement towards production of ultraclean transportation fuels (gasoline and diesel fuel). Over the last two decades, a continuous move towards the ultraclean fuels has taken place. While legislation moves at different paces in various parts of the world, most likely, the ultraclean fuels will be the standard in a few years.

Conventional hydrotreating technologies with the current advanced catalysts have been effective for the removal of sulfur compounds in gasoline. However, current catalysts are less effective for the removal of heterocyclic sulfur and nitrogen compounds. It is well-known that 4-methyldibenzothiophene (4-MDBT) and 4,6-dimethyldibenzothiophene (4,6-DMDBT) are among the most refractory sulfur compounds in gas oil (*4–9*) and are difficult to remove by hydrodesulfurization (HDS). The coexisting presence of nitrogen compounds, such as quinoline, indole, carbazole, and their derivatives, in the gas oil significantly inhibits the hydrodesulfurization (HDS) (*10–16*), although the concentration of nitrogen is much lower than the sulfur concentration. Due to the stronger N-C bond in comparison to the S-C bond in the heterocyclic N- S-compounds, the nitrogen compounds in gas oil are much less reactive than sulfur compounds, and they are converted under severer conditions (*17*). As a result, for the effective catalytic removal of refractory sulfur compounds, it is important to remove coexisting nitrogen compounds.

On the other hand, it has been reported that the United States and Europe will face increasing demand for diesel fuel in the future (*5*). Therefore, it is extremely important to blend more of other refinery hydrocarbon streams, such as light cycle oil (LCO) and coker gas oil (CGO), into the diesel pool. LCO and CGO typically contain much more nitrogen, sulfur, and aromatic compounds in comparison with the straight run gas oil (SRGO). Shin et al. (*18*) determined the nitrogen compounds in LCO derived from Venezuelan heavy crude oil using gas chromatography with an atomic emission detector (AED) and mass spectrometer (GC-MS). They found that most abundant nitrogen compounds in the LCO sample were aniline derivatives, indole, quinoline, and their alkyl substituent derivatives. In addition, carbazole and its derivatives were found in low concentrations in the LCO sample. The reactivity order of nitrogen compounds in LCO during the hydrotreating was found as: indole > methylated aniline > methylated indole > quinoline > benzoquinoline > methylated benzoquinoline > carbazole > methylated carbazoles (*18*). On the other hand, Depauw and Froment (*19*) reported the detailed characterization of sulfur compounds present in a LCO sample. They showed that over 40% of the sulfur, represented by the highly refractory sulfur compounds, alkylated DBT. The coexisting presence of nitrogen seems to make the catalytic removal of refractory sulfur compounds from LCO more difficult.

In order to achieve deep denitrogenation, the use of adsorbents to selectively remove the nitrogen compounds has attracted great attention (*3*, *20–22*). Recently, several types of adsorbents have been reported for the adsorptive denitrogenation of liquid hydrocarbon fuels, including zeolite (*20*, *23*, *24*), activated carbon (*3*, *25–27*), activated alumina (*3*, *26*, *28*), and silica gel (*21*, *29*, *30*). For example, SK Company has developed a new process based on the adsorptive removal of nitrogen compounds from diesel fuel using silica gel as an adsorbent. The process was capable of removing over 90 % of nitrogen compounds from the diesel fuel (*30*). They claim that the SK pretreatment process is a cost-effective method for refineries to achieve 10 ppmw ultra low sulfur diesel fuels. However, regeneration of silica gel has been known to be difficult (*25*). On the other hand, we have shown in a previous study (*26*) that the spent activated carbon used for adsorptive denitrogenation and desulfurization of model diesel fuel can easily be regenerated at 80 °C by toluene, which is readily available in the refinery.

The objective of this study was to evaluate the modified activated carbon for selective adsorptive denitrogenation of LCO and to determine the influence of the adsorptive removal of nitrogen compounds on subsequent HDS of LCO.

Downloaded by UNIV OF DELAWARE MORRIS LIB on June 5, 2012 | http://pubs.acs.org
Publication Date (Web): December 14, 2011 | doi: 10.1021/bk-2011-1088.ch003

Experimental Section

Materials

Various commercial activated carbons with different physical and chemical properties were used in the current study. Table 1 shows some manufacturing parameters for all commercial activated carbons used in this study. In order to broaden the spectrum of surface features, the surfaces of some commercial samples were modified by concentrated H_2SO_4 (98%) and HNO_3 (70%). For each modification, 4 g of AC were transferred into a flask fitted with a water reflux condenser. 50 ml of desired oxidant was then slowly added into the corresponding flask. Based on previous modification treatment experiments (*31*), the modification with H_2SO_4 and HNO_3 was carried out at 140 ºC and 80 ºC respectively. After oxidation treatments, each mixture was mixed with 2,000 ml of distilled water and stirrer for 1 h at room temperature. The mixture was then filtered and washed thoroughly until the pH of the filtrate was approximately equal to the pH of distilled water. The modified samples were placed in a vacuum oven at 110 ºC overnight. The samples obtained were named: AC-S*t*, AC-N*t* (S and N refer to H_2SO_4, and HNO_3 respectively; and *t* denoted the modification temperature).

Before use in experiments, all activated carbon samples were washed by deionized water and then heated at 110ºC in a vacuum oven overnight for drying.

A commercial catalyst $CoMo/Al_2O_3$ (Cr447), obtained from the Criterion Catalyst Company, was used for the HDS of LCO and pretreated-LCO. The catalyst was crushed to a particle size of <1 mm and presulfided at 350 °C for 4 h in a flow of 5 vol. % H_2S-H_2 at a flow rate of 200 ml/min. It was subsequently stored in hexane to minimize oxidation.

The light cycle oil (LCO) sample was obtained from United Refining Company through Intertek-PARC Technical Services. The key properties of the LCO sample are listed in Table 2. The simulated distillation results were obtained at the Kuwait Institute for Scientific Research.

Downloaded by UNIV OF DELAWARE MORRIS LIB on June 5, 2012 | http://pubs.acs.org
Publication Date (Web): December 14, 2011 | doi: 10.1021/bk-2011-1088.ch003

Table 1. Some Parameters of the Studied Activated Carbons

Carbon ID	*Source*	*Activation*	*Commercial ID*	*Maker*
AC1	Coconut	Steam	PCB-G	Calgon
AC2	Wood	Chemical	Nuchar AC20	WESTVACO
AC3	Wood	Chemical	Nuchar AC1500	WESTVACO
AC5	Lignite coal	Steam	Darco-G60	Norit
AC6	Coal	Steam	Norit SA 4 PAH	Norit

Table 2. Key Properties of LCO Sample

Analysis	*Value*
Sulfur, wt%	1.81
N, ppmw	598
Aromatics, wt%	89
Distillation characteristics, °C	
Initial boiling point175	1751
5 wt%	203
50 wt%	275
90 wt%	329
Final boiling point	376

Characterization of Samples

Textural characterization of selected activated carbons was performed by the adsorption of N_2 at 77 K using the Autosorb-1 MP system (Quantachrome Corp.). The surface areas were obtained from the N_2 adsorption data at relative pressures $0.05 < P/Po < 0.2$ using the BET equation. The total pore volumes (V_{Total}) were estimated from the volume of N_2 (as liquid) held at a relative pressure (P/P^o) of 0.98. The average pore diameter was estimated from the pore volume assuming cylindrical pore geometry.

The surface chemistry was analyzed by temperature-programmed desorption (TPD). A TPD procedure up to 950 °C was used to evaluate the amount and nature of the surface functionalities. About 100 mg of the samples were placed in a quartz tube reactor. After drying the samples for 2 h at 110 °C under a He flow, the temperature was then increased to 950 °C at a rate of 10 °C/min under a He flow of 50 ml/min. The evolved amounts of CO_2, CO, and H_2O were monitored by a mass spectrometer as a function of the temperature. The details were discussed previously (*27*).

Downloaded by UNIV OF DELAWARE MORRIS LIB on June 5, 2012 | http://pubs.acs.org
Publication Date (Web): December 14, 2011 | doi: 10.1021/bk-2011-1088.ch003

Extraction of Nitrogen Compounds

A diagram of the extraction procedure is shown in Figure 1. The non-polar compounds in the LCO were first removed by adsorption chromatography using a column packed with 100 g activated neutral alumina to eliminate their interference in the following separation and identification procedures. Approximately 5 g of the LCO sample were dissolved in a few milliliters of *n*-hexane and mixed with 20 g of activated neutral alumina. The mixture was placed in the top of the column. The sample was eluted first with 600 ml of benzene for the non-polar fraction and then with 300 ml of benzene-methanol (1:1) for the polar fraction. The two fractions were then concentrated by evaporation to remove the solvent.

The solvents used in this work were HPLC grade. Neutral aluminum oxide powder was obtained from Aldrich Chemical Co. The activated neutral alumina was dried at 110 °C overnight before use.

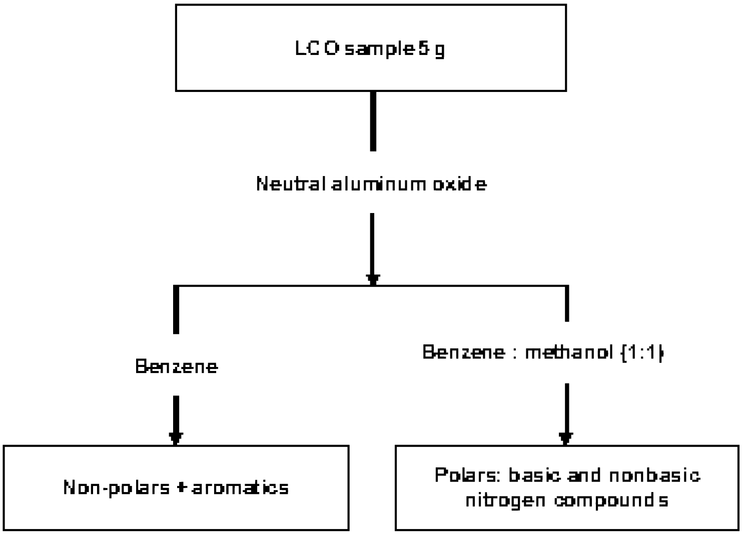

Figure 1. Separation scheme of the extraction of nitrogen compounds from LCO.

Adsorption and Regeneration Experiments

The screening adsorption experiments were conducted in a batch system. About 6.0 g of LCO and 0.40 g of the tested adsorbent were added into a glass tube with a magnetic stirrer at desired temperatures. After the desired time was reached, the mixture was filtered, using centrifugal system, and the products were analyzed to estimate the adsorption capacity of various carbons for total nitrogen and sulfur.

Based on the screening adsorption experiments, a modified sample with concentrated H_2SO_4, which had the best performance for nitrogen removal, was further examined and compared with the original sample for adsorptive denitrogenation and desulfurization of LCO using a fixed-bed flow system.

In order to explore the regenerability of the activated carbons for LCO, the activated carbon after saturation in the fixed-bed adsorption experiment was subjected to a regeneration test. Toluene was used as a solvent to wash out the adsorbates from the spent activated carbons at 80ºC and 4.8 h^{-1} LHSV. The washing continued until the nitrogen and sulfur concentrations in the eluted toluene were close to zero. Following the toluene washing, a mixture of toluene and methanol (1:1 v/v) was introduced. After washing, the system was purged with N_2 at 200 ºC for 8 h to remove the remaining solvent, and the temperature of the adsorption bed was reduced to room temperature for the adsorption test of the regenerated adsorbent.

Downloaded by UNIV OF DELAWARE MORRIS LIB on June 5, 2012 | http://pubs.acs.org
Publication Date (Web): December 14, 2011 | doi: 10.1021/bk-2011-1088.ch003

Hydrotreating Experiments

The eluted LCO was hydrodesulfurized using a batch reactor with a volume of 25 ml. The reactor was first loaded with 0.1 g of catalyst and 3 g of LCO, and the assembly was then purged five times using nitrogen and hydrogen before being pressurized with hydrogen to 50 bars. The reactor was placed in a fluidized sand bath for 2 h, which was preheated to 350 ˚C, and then was agitated at 200 strokes/min. The temperature inside the reactor was monitored by a thermocouple. Following the reaction, the reactor was removed from the sand bath and immediately quenched in a cold-water bath. The product was then sucked from the reactor using a glass pipette, and the total sulfur was analyzed to estimate the HDS conversion. The HDS conversion (HDS%) was calculated according to the following equation:

$$HDS\% = \frac{(C_i - C_f)}{C_i} \times 100$$

where Ci and C_f are the sulfur concentration in the feed and product, respectively.

Analysis of Treated Samples

In most cases, the treated LCO was diluted with toluene at the desired toluene/LCO ratio. For total nitrogen and sulfur analysis, an Antek 9000 series nitrogen and sulfur analyzer was used. A detailed description of the analytical method was described elsewhere (*32*). Qualitative analysis of the nitrogen compounds in the treated LCO was performed using a Varian CP 3800 gas chromatograph with a capillary column (30 m length, 0.25 mm internal diameter, and 0.25 mm film thickness) and a nitrogen-phosphorus detector (NPD). Column temperature was held at 40 °C for 4 minutes, then programmed from 40 °C to 290 °C at a rate of

Downloaded by UNIV OF DELAWARE MORRIS LIB on June 5, 2012 | http://pubs.acs.org
Publication Date (Web): December 14, 2011 | doi: 10.1021/bk-2011-1088.ch003

6 °C/min, and held for 5 min. The injector and detector temperatures were set to 290 °C. The analytical method was the same as the GC-FID.

Qualitative analysis of sulfur compounds in the LCO was conducted using an HP 5890 gas chromatograph with a capillary column (XTI-5, Restek, 30 m in length and 0.25 mm in internal diameter) and a pulsed-flame photometric detector (PFPD).

Gas chromatography-mass spectrometry (GC-MS) was used for identification of the nitrogen compounds in the concentrated nitrogen-containing fuel. The GC-MS consisted of a Shimadzu GC-17A gas chromatograph coupled to a Shimadzu QP-5000 mass spectrometer. The gas chromatograph was fitted with a fused silica capillary column (Rxi-5ms, 30 m x 0.25 mm I.D. x 0.25 um film thickness) purchased from Restek. The separation conditions were as follows: the flow of carrier gas (ultra high purity helium) was 1 mL/min. Column temperature was held at 40 °C for 4 min, then programmed from 40 °C to 290 °C at a rate of 6 °C/min, and then held for 5 min. The injector and detector temperatures were set at 290 °C. The injection volume was 1 μL, and the split ratio was 15:1. The mass spectrometer was operated in the electron impact mode using ionization energy of 70 eV. Identification was performed by similarity search of the spectra of the compound in the sample and the NIST 107 mass spectral library.

Results and Discussion

Identification of Nitrogen and Sulfur Compounds in LCO

For reference, the chemical structures and nomenclature of carbazole and its sulfur analogue dibenzothiophene are as follows:

Carbazole

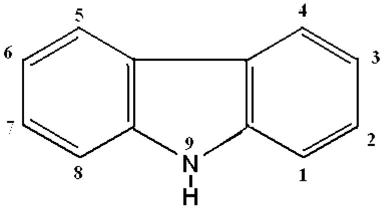

Dibenzothiophene

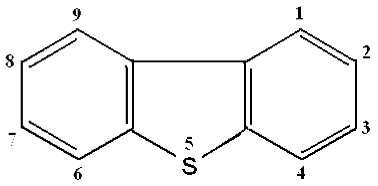

Figure 2 shows the nitrogen chromatogram measured by the nitrogen-selective detector (GC-NPD). The nitrogen concentration in the LCO sample was 598 ppmw. The first compound eluted at a retention time of 32 min. Analysis of the extracted sample by GC-MS showed that the LCO sample contained almost only carbazole and methyl-substituted carbazoles. The identification of carbazole, monomethylcarbazoles dimethylcarbazoles, and trimethylcarbazoles were conducted by a combination of GC-MS, standard samples and comparison with the relative retention time reported in the literature (*18*, *33*).

Downloaded by UNIV OF DELAWARE MORRIS LIB on June 5, 2012 | http://pubs.acs.org
Publication Date (Web): December 14, 2011 | doi: 10.1021/bk-2011-1088.ch003

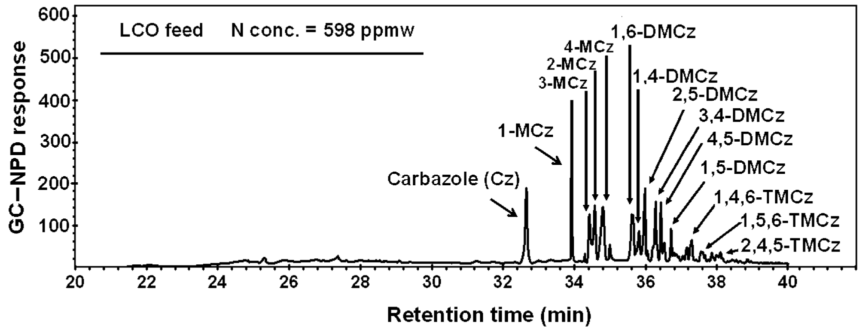

Figure 2. Nitrogen-selective chromatogram for LCO feed.

Figure 3 shows the sulfur chromatogram measured by the sulfur-selective detector (GC-PFPD). The sulfur concentration in the LCO sample was about 1.81 wt%. The sulfur chromatogram profile in the current research was found similar to the chromatograms reported in the literature (*4*, *5*). It was convenient to identify the sulfur compounds in the LCO sample by comparison with the reported chromatograms. In order to confirm the identification, the retention times of several sulfur model compounds, including 1,5-dimethylbenzothiophene, dibenzothiophene, and 4,6-dimethyledibenzothiophene, were identified and compared with the assigned peaks.

The predominant sulfur compounds in LCO are alkylated benzothiophene, dibenzothiophene, and alkylated dibenzothiophene. 4-methylbenzothiophene was the predominant refractory sulfur compound in the LCO sample, which is typically difficult to remove by the conventional HDS process.

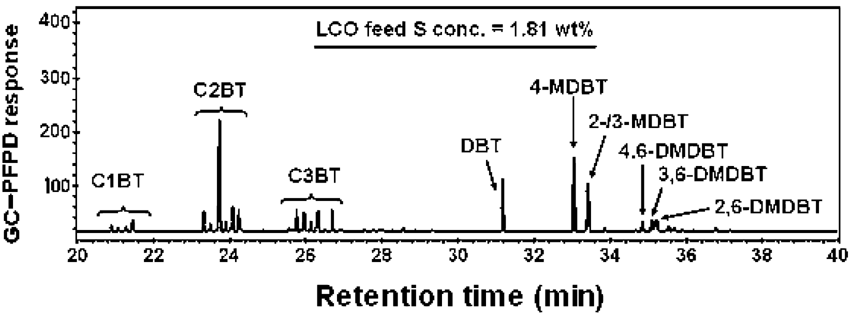

Figure 3. Sulfur-selective chromatogram for LCO feed.

Downloaded by UNIV OF DELAWARE MORRIS LIB on June 5, 2012 | http://pubs.acs.org
Publication Date (Web): December 14, 2011 | doi: 10.1021/bk-2011-1088.ch003

Effect of Adsorption Conditions on the Adsorption Capacity

The effects of the adsorption time and adsorption temperature on adsorption capacities of AC1 and AC3 were examined in the batch mode using an LCO/AC3 ratio of 15. It should be pointed out that these activated carbons were selected because they represent the microporous and micro-mesoporous activated carbons. The results of the adsorption capacities as a function of adsorption time are shown in Figure 4. The adsorption capacities for nitrogen compounds over both the carbons reached adsorption equilibrium at an adsorption time of 2 h.

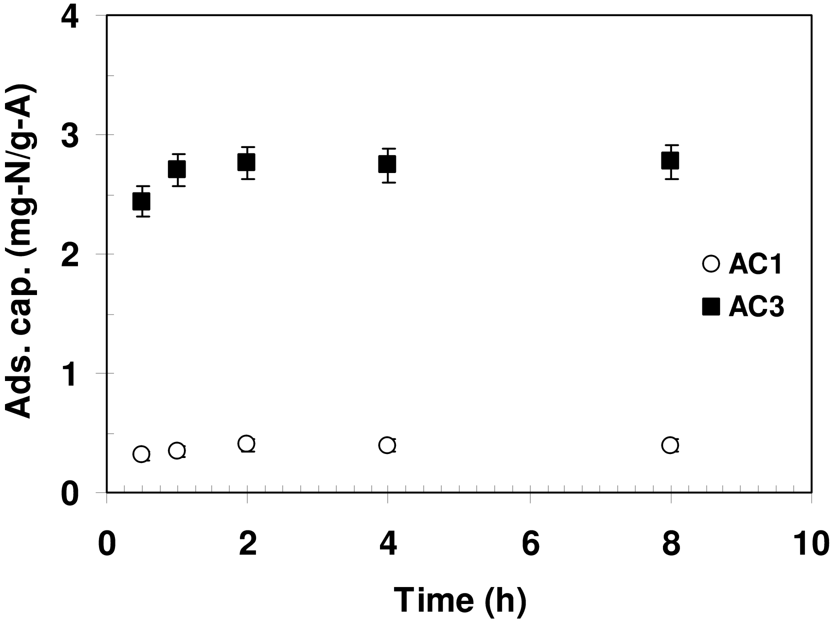

Figure 4. Effect of adsorption time on adsorption capacity on nitrogen compounds; adsorption temperature is 25 °C; AC1: microporous carbon and AC3: micro-meso-porous carbon.

The adsorption pretreatment of LCO over AC1 and AC3 for 4 h and different adsorption temperatures was performed to evaluate the effect of temperature on the adsorption capacity of nitrogen compounds. Figure 5 shows that the temperature negatively affects the adsorption of nitrogen compounds over the mesoporous carbon (AC3). When the temperature increased from 25 to 100 °C, the adsorption capacity decreased from 2.7 to 2.5 mg-N/g-A. On the other hand, the increase in the adsorption temperature significantly increased the adsorption uptake of nitrogen compounds over the microporous carbon (AC1). When the adsorption temperature increased from 25 to 100 °C, over 69% increase in the adsorption of nitrogen compounds was achieved. The increase in the adsorption capacity as a function of adsorption temperature over AC1 may be attributed to

In Production and Purification of Ultraclean Transportation Fuels; Hu, Y., et al.;
ACS Symposium Series; American Chemical Society: Washington, DC, 2011.

the fact that the diffusion of nitrogen compounds into the pore of the activated carbon might be a rate-controlled step in the adsorption process, and that an increase in temperature facilitates the diffusion of nitrogen compounds and helps to drive nitrogen compounds through the narrow pore network of activated carbon. Subsequently, the adsorption capacity is enhanced. However, in the case of the adsorption of nitrogen compounds over the mesoporous carbon (AC3), the adsorption capacity might depend on the thermodynamic equilibrium, so an increase in the adsorption temperature facilitates the desorption rate and thereby reduces the adsorption capacity for nitrogen compounds.

Downloaded by UNIV OF DELAWARE MORRIS LIB on June 5, 2012 | http://pubs.acs.org
Publication Date (Web): December 14, 2011 | doi: 10.1021/bk-2011-1088.ch003

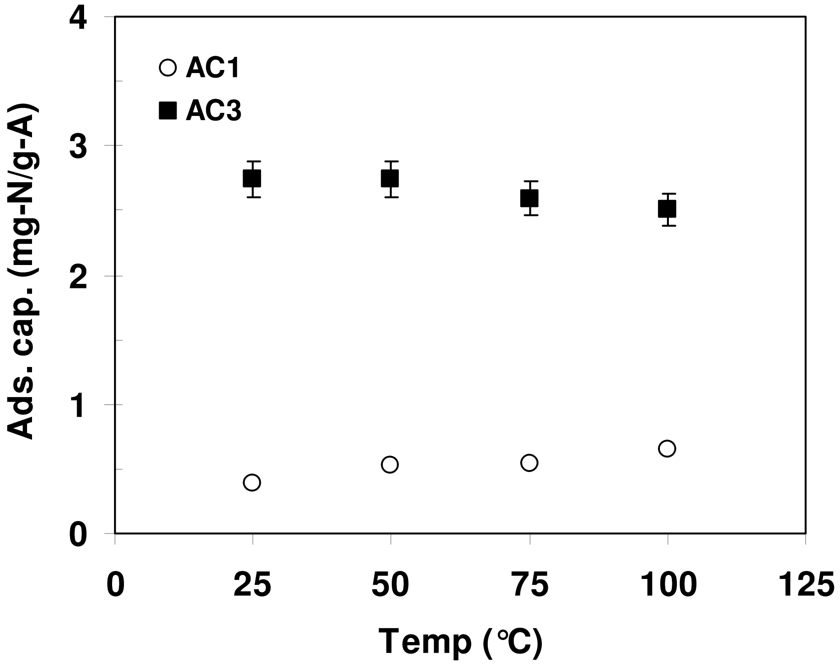

Figure 5. Effect of adsorption temperature on adsorption capacity of nitrogen compounds; adsorption time is 4h; AC1: microporous carbon and AC3: micro-meso-porous carbon.

The results obtained above reveal that diffusion has a negligible effect on the adsorption capacity over mesoporous activated carbon even at room temperature when the adsorption time is longer than 2 h. Based on these results, optimum conditions of 25 °C, a 4-h contact time, and a LCO/AC3 ratio of 15 were selected for evaluating the adsorption pretreatment process of LCO using mesoporous activated carbon.

Downloaded by UNIV OF DELAWARE MORRIS LIB on June 5, 2012 | http://pubs.acs.org
Publication Date (Web): December 14, 2011 | doi: 10.1021/bk-2011-1088.ch003

Evaluation of Adsorbents

Adsorptive denitrogenation and desulfurization of LCO over a series of the activated carbons at 25 ºC for 4 h were conducted in the batch mode for screening adsorbents. The adsorption capacities for nitrogen and sulfur compounds with the textural properties and oxygen concentration of the various adsorbents are listed in Table 3. The oxidized activated carbon with H_2SO_4 at 140 °C, denoted as AC3-S140, showed the highest adsorption capacity for nitrogen compounds at 257 µmol/g-A, while AC6 was the worst among the all activated carbon samples with a capacity around 29 µmol/g-A. For sulfur removal, all activated carbons showed low adsorptive desulfurization capacities.

Oxidative modification of the activated carbon greatly enhanced the adsorptive denitrogenation capacity. The oxidized adsorbents including AC3-S140, AC6-N80, and AC6-S140 showed significant improvement in the adsorptive denitrogenation of LCO compared with their parent adsorbents. This was not the case for sulfur removal, where the performance of the oxidized adsorbents noticeably decreased.

Table 3. Key Characteristics of the Studied Activated Carbons

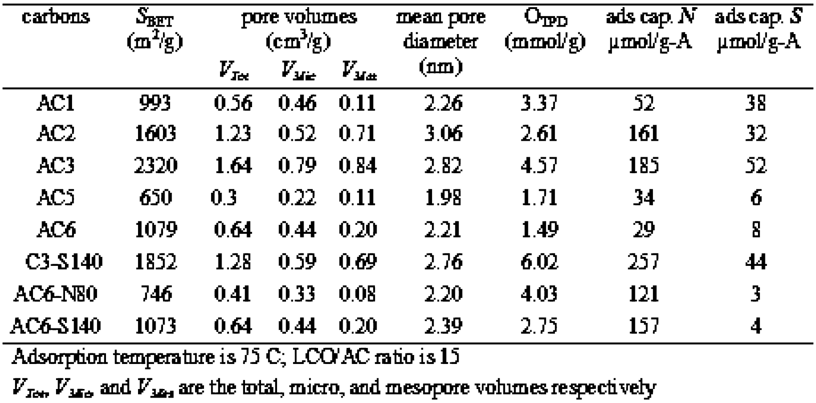

carbons	S_{BET} (m^2/g)	pore volumes (cm^3/g)			mean pore diameter (nm)	O_{TPD} (mmol/g)	ads cap. *N* µmol/g-A	ads cap. *S* µmol/g-A
		V_{Tot}	V_{Mic}	V_{Mes}				
AC1	993	0.56	0.46	0.11	2.26	3.37	52	38
AC2	1603	1.23	0.52	0.71	3.06	2.61	161	32
AC3	2320	1.64	0.79	0.84	2.82	4.57	185	52
AC5	650	0.3	0.22	0.11	1.98	1.71	34	6
AC6	1079	0.64	0.44	0.20	2.21	1.49	29	8
C3-S140	1852	1.28	0.59	0.69	2.76	6.02	257	44
AC6-N80	746	0.41	0.33	0.08	2.20	4.03	121	3
AC6-S140	1073	0.64	0.44	0.20	2.39	2.75	157	4

Adsorption temperature is 75 C; LCO/AC ratio is 15

V_{Tot}, V_{Mic}, and V_{Mes} are the total, micro, and mesopore volumes respectively

Effect of Surface Properties on Adsorptive Denitrogenation of LCO

It is well-known that the activated carbon surface physical and chemical properties play an important role in many selective adsorption processes. According to a study by Sano et al., (*22*) for adsorptive denitrogenation and desulfurization of real gas oil, they found that oxygen functional groups, in particular, phenol groups are crucial for selective adsorption of nitrogen compounds. However, in our previous study (*27*), for the adsorptive denitrogenation of model diesel fuel, it was concluded that carboxylic and anhydride were the primary oxygen functional groups involved in the binding of basic nitrogen compounds such as quinoline, whereas basic oxygen functional

Downloaded by UNIV OF DELAWARE MORRIS LIB on June 5, 2012 | http://pubs.acs.org
Publication Date (Web): December 14, 2011 | doi: 10.1021/bk-2011-1088.ch003

groups, including carbonyl and quinone contributed more for the adsorption of nonbasic nitrogen compounds such as indole.

In our previous study, a model fuel with a density about 0.73 g/ml containing 9 molecules was used. However, in the current study, LCO with a density of about 1.00 g/ml, relatively high viscosity, and contains thousands of molecules is used. This makes establishing a relation between the physio-chemical properties of carbon and the adsorptive denitrogenation performance is a challenging task.

Figure 6 shows the adsorption capacity for nitrogen compounds as a function of the oxygen concentration. Although, the relationship between the capacity and the oxygen concentration is not perfectly linear, certainly the oxygen concentrations on the surface of the activated carbon significantly contribute to the adsorption performance for nitrogen removal. The adsorption capacity for nitrogen compounds increases with increase in the oxygen concentration of the activated carbons.

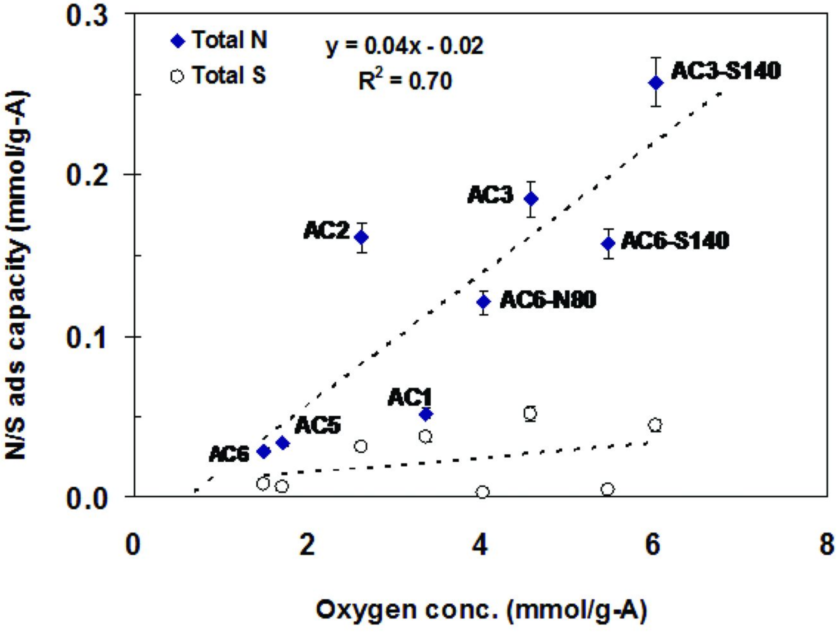

Figure 6. Relationship between oxygen concentrations and adsorption capacity of nitrogen compounds.

Interestingly, close examination of the data in Figure 6 shows that the adsorption capacity for nitrogen compounds of the activated carbons with major microporosity such as AC1, AC5, AC6, AC6-S140, and AC6-N80 deviate negatively from the straight line, whereas the activated carbons with major mesoporosity such as AC2, AC3, and AC3-S140 showed positive deviation for the adsorption of nitrogen compounds. The trend suggests that the contribution of oxygen functional groups in the mesoporous activated carbons for nitrogen removal is greater than those for the activated carbons with major microporosity.

This finding implies that some oxygen functional groups in the microporous activated carbons may not be accessible for nitrogen compounds, especially when viscous fuel such as LCO is used, as the diffusion rate of a molecule is proportional to the fuel viscosity. Consequently, moving from micro pores to meso pores seems to facilitate large nitrogen molecules to penetrate into surface functionalities. Song et al. have investigated the effect of catalyst pore size on the adsorption of large molecules of heavy fractions. It was evident that the adsorption of large molecules is proportional to catalyst pore size distribution (*34*).

Several studies (*35–37*) have suggested that oxygen functional groups, and acidic groups in particular, play a decisive important role in enhancing the adsorption selectivity of sulfur compounds, such as dibenzothiophene (DBT) and 4,6-dimethyldibenzothiophene (4,6-DMDBT), from liquid hydrocarbon fuels. However, these studies did not consider the presence of co-existing nitrogen compounds. Clearly, this is not the case for the adsorptive desulfurization of LCO, and the increase in surface oxygen concentrations showed no positive effect for the removal of sulfur compounds.

Pretreatment of LCO in a Fixed-Bed Flow System

The original and modified AC3 were evaluated in a fixed-bed adsorber using LCO at 25 °C and 2.4 h^{-1} of LHSV. The breakthrough profiles for nitrogen compounds over AC3 occurred at a treated amount of 6 g of LCO/g-A, as shown in Figure 7. The nitrogen outlet concentration approached 200 ppmw at a treated LCO amount of 11.2 g of LCO/g-A. The adsorption performance of the modified carbon was remarkably improved. The treated amount of LCO was 18.1 g-LCO/g-A when the nitrogen outlet concentration was around 200 ppmw. This performance of the modified carbon is superior to the activated alumina and the silica gel for the removal of nitrogen compounds (*22*, *25*).

The results of Figure 7 suggest that carbon materials are promising adsorbents for deep denitrogenation and can easily be tailored for the selective adsorption of nitrogen compounds from light and heavy gas oils.

Figure 8 shows the breakthrough profiles for sulfur compounds during the adsorptive desulfurization of LCO over the original and modified AC3. Unlike the adsorptive denitrogenation, the performance of both activated carbons showed poor adsorption uptake for sulfur compounds. Moreover, upon oxidative modification of carbon, a significant decrease in the adsorptive desulfurization of LCO was observed.

Hydrocarbon, sulfur, and nitrogen chromatograms of the original and adsorptive pretreated LCO are shown in Figure 9. There were no significant differences between the hydrocarbon and sulfur chromatograms of the original and pretreated LCO, indicating that modified activated carbon was not selective for hydrocarbon and sulfur compounds, in agreement with the results of breakthrough curves of sulfur compounds, as shown in Figure 8. On the other hand, a comparison between the nitrogen chromatograms of the original and pretreated LCO shows the excellent adsorption selectivity of modified carbon for nitrogen compounds from LCO.

Downloaded by UNIV OF DELAWARE MORRIS LIB on June 5, 2012 | http://pubs.acs.org
Publication Date (Web): December 14, 2011 | doi: 10.1021/bk-2011-1088.ch003

Downloaded by UNIV OF DELAWARE MORRIS LIB on June 5, 2012 | http://pubs.acs.org
Publication Date (Web): December 14, 2011 | doi: 10.1021/bk-2011-1088.ch003

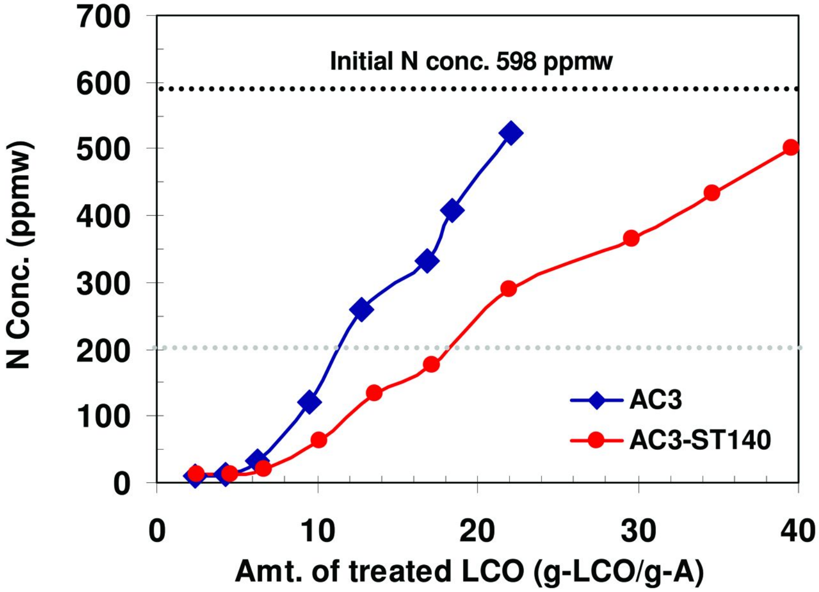

Figure 7. Breakthrough curves of nitrogen compounds in LCO over activated carbon AC3 and modified AC3 at 25 °C and 2.4 h^{-1} LHSV.

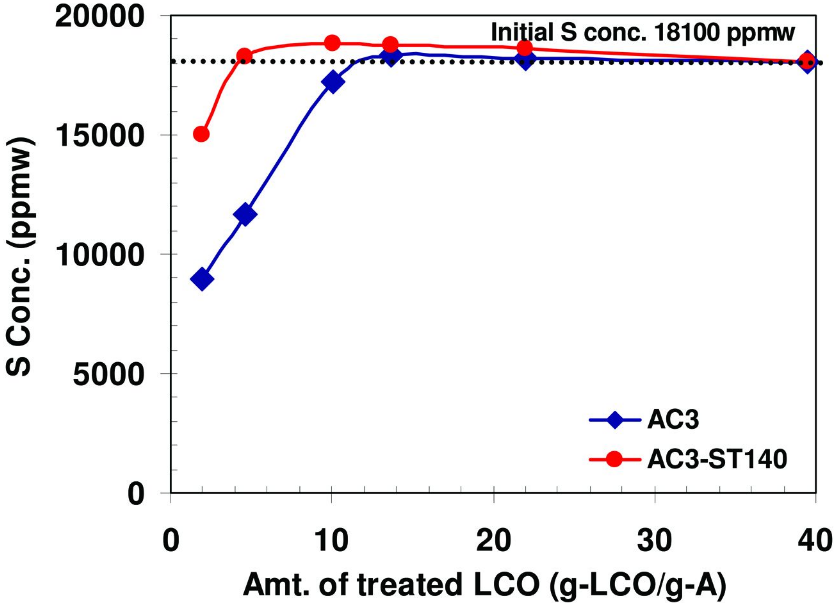

Figure 8. Breakthrough curves of sulfur compounds in LCO over activated carbon AC3 and modified AC3 at 25 °C and 2.4 h^{-1} LHSV.

Downloaded by UNIV OF DELAWARE MORRIS LIB on June 5, 2012 | http://pubs.acs.org
Publication Date (Web): December 14, 2011 | doi: 10.1021/bk-2011-1088.ch003

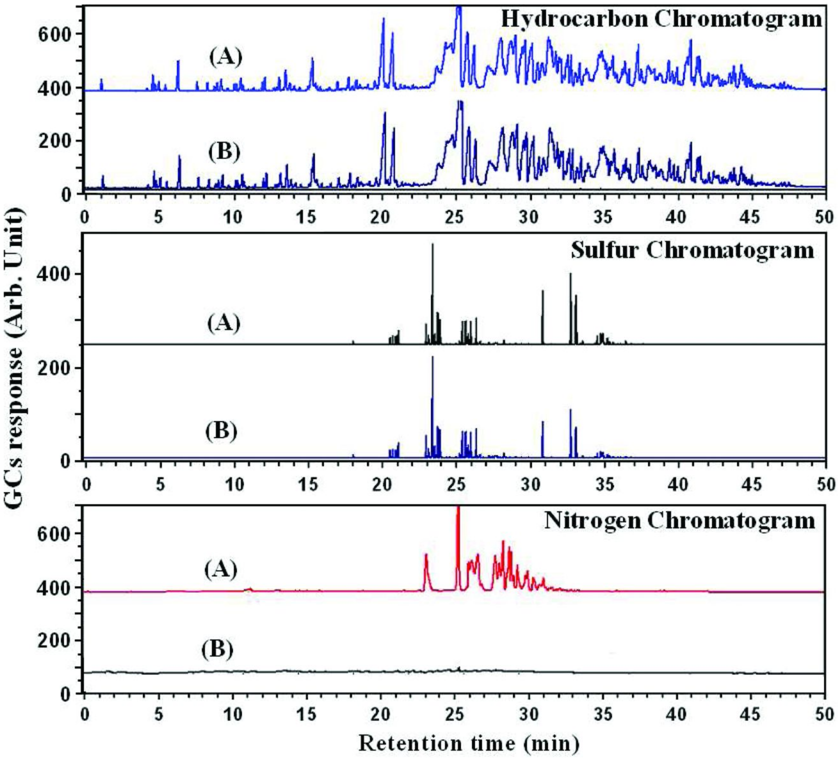

Figure 9. Hydrocarbon, sulfur, and nitrogen chromatograms of (A) LCO and (B) adsorptively treated LCO.

Figure 10 shows the NPD chromatograms for adsorptive pretreated LCO sampled at various elution times. The predominant nitrogen compounds in the LCO feed are carbazole, methylcarbazole (C1-carbazole), dimethylcarbazole (C2-carbazole), and trimethylecarbazole (C3-carbazole). After the pretreatment of 6.7 g ofLCO/g-A, almost no peaks were observed in the eluted LCO. The first peak to appear in the chromatogram at the treated amount of 13.6 g of LCO/g-A was for 1-methylcarbazole (1-MCz). The high peak of 1-MCz in the pretreated fuel was due to the fact that it had the highest concentration in the feed. A comparison between the chromatograms of the original LCO and the eluted LCO at 22.0 g-LCO/g-A shows that they have very similar profiles, although most of the peaks in the treated sample were smaller. This indicates that the modified carbon might have similar adsorption selectivity for all carbazole and alkylated carbazoles.

Downloaded by UNIV OF DELAWARE MORRIS LIB on June 5, 2012 | http://pubs.acs.org
Publication Date (Web): December 14, 2011 | doi: 10.1021/bk-2011-1088.ch003

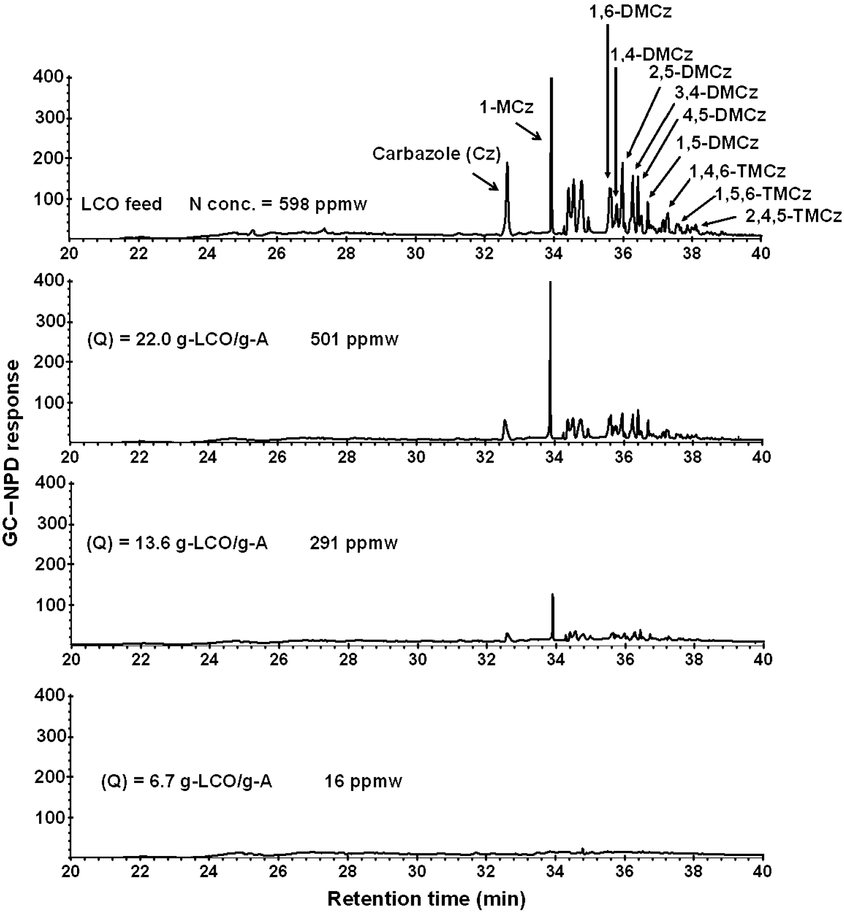

Figure 10. Nitrogen chromatograms of the LCO-feed and the treated LCO at different treated amount.

Regeneration

In our previous study (*26*), using model diesel fuel containing an equimolar concentration of nitrogen, sulfur, and aromatic compounds, it was confirmed that spent activated carbons can be completely regenerated by washing with toluene at 80 °C. In the current study, the spent activated carbon exposed to LCO was also examined for regeneration by washing with toluene followed by washing with a mixture of toluene and methanol at 80 °C and 4.8 h^{-1} LHSV. Figure 11 shows the comparison of the breakthrough profiles of the fresh and regenerated activated carbons. It is seen that the regenerated carbon shows a slightly lower adsorption compared with the fresh one. For the fresh carbon, the outlet-treated LCO reached 200 ppmw when the amount of treated LCO was 18.1 g-LCO/g-A, while for the regenerated carbon, 15.7 g-LCO/g-A was processed when the outlet concentration reached 200 ppmw, corresponding to a decrease by 12 %.

Downloaded by UNIV OF DELAWARE MORRIS LIB on June 5, 2012 | http://pubs.acs.org
Publication Date (Web): December 14, 2011 | doi: 10.1021/bk-2011-1088.ch003

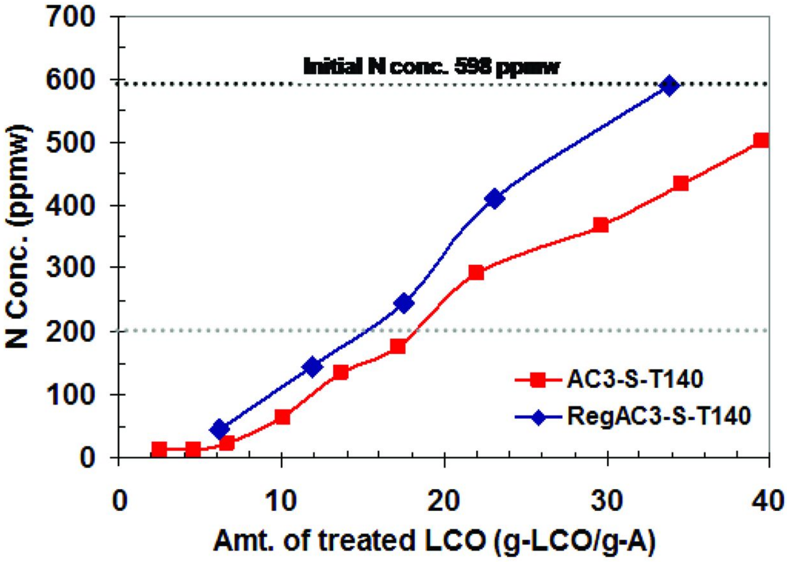

Figure 11. Total nitrogen breakthrough curve for fresh and regenerated AC3-S140 at 25 °C and 2.4 h^{-1} LHSV.

In order to estimate the required amount of the solvent for the regeneration, the total nitrogen and sulfur content in the outlet as a function of the amount of the used solvent was measured, as shown in Figure 12. Washing with toluene continued until the nitrogen and sulfur concentrations in the outlet approached zero. A mixture of toluene and methanol was then introduced to remove the molecules that strongly interacted with the active sites. Upon the introduction of the mixture, both the N and S profiles showed small peaks, indicating that the mixture was more effective than toluene and that some nitrogen and sulfur compounds were still adsorbed. It is important to point out that although the concentration of sulfur in the LCO is 40 times greater than nitrogen, the rate at which nitrogen washed out was much slower than sulfur, as shown in the slope (Figure 12). This suggests that due to the higher adsorption affinity for nitrogen compounds, they are strongly interacting with the active sites as compared with sulfur compounds.

From a practical point of view, it is desired to shorten the regeneration cycle. The regeneration cycle may seem quite long, as almost 250 g-Sol/g-A was used. However, the washout profile clearly showed that at a solvent washout amount of 70 g-Sol/g-A, most of the sulfur and nitrogen were already washed out.

Downloaded by UNIV OF DELAWARE MORRIS LIB on June 5, 2012 | http://pubs.acs.org
Publication Date (Web): December 14, 2011 | doi: 10.1021/bk-2011-1088.ch003

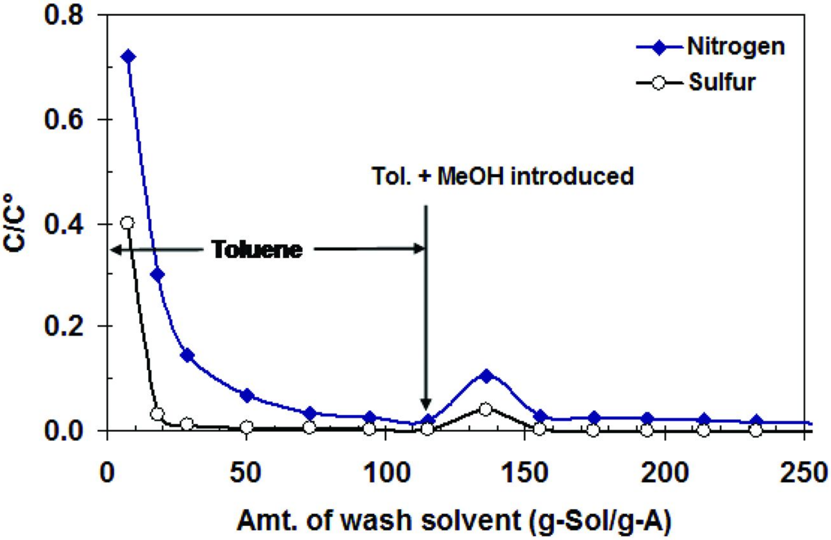

Figure 12. Nitrogen and sulfur concentrations in the effluent as a function of washing-solvent amount for AC3-S140; washing solvent: toluene-followed by a mixture of toluene and methanol; temperature: 80 °C and LHSV: 2.4 h^{-1}.

Effect of Adsorptive Pretreatment on HDS

Both types, basic and nonbasic nitrogen compounds, have been reported to inhibit deep hydrodesulfurization (*10*, *38–42*). Three-ring nitrogen compounds such as carbazole, acridine and their alkylated derivatives have been suggested to have higher inhibition effects on the deep HDS than quinoline and indole (*38*). It is well known that 4-MDBT and 4,6-DMDBT are among the most refractory sulfur compounds in gas oil, even though the alkyl carbazole with a similar structure of 4,6-DMDBT has been shown to react at rates about 1/10 of those of 4,6-DMDBT (*38*, *40*). Therefore, removing carbazole and alkylated carbazoles from the LCO in the adsorption step should enhance the removal of refractory sulfur compounds in the subsequent HDS.

The HDS of the adsorptive pretreated LCO, which contains different nitrogen concentrations, is illustrated in Figure 13. The HDS conversion was found to be proportional to the degree of nitrogen removal in the adsorptive pretreatment process. For example, the HDS conversion of the pretreated LCO containing 7 ppmw nitrogen concentrations was over 84%. On the other hand, HDS of the LCO without adsorptive pretreatment (N=598 ppmw) showed only 52% HDS conversion. Interestingly, when the nitrogen concentration increased from 7 to 88 ppmw, only slight decrease in the HDS conversion was observed. However, significant reduction in the HDS conversion was noticed, by a decrease from 83% down to 67%, when the nitrogen increased from 88 to 209 ppmw. This can be explained as follows: when the nitrogen content in the fuel increased to 88 ppmw, the predominant nitrogen compounds were carbazole and methyl carbazole, which might have a relatively less inhibition effect on the HDS reaction, as compared with di- and trimethylcarbazoles. However, when the fuel contained 209 ppmw nitrogen content, methyl-, dimethyl-, and trimethylcarbazoles were observed in the fuel, which has been reported (*38*) to strongly inhibit the HDS reaction.

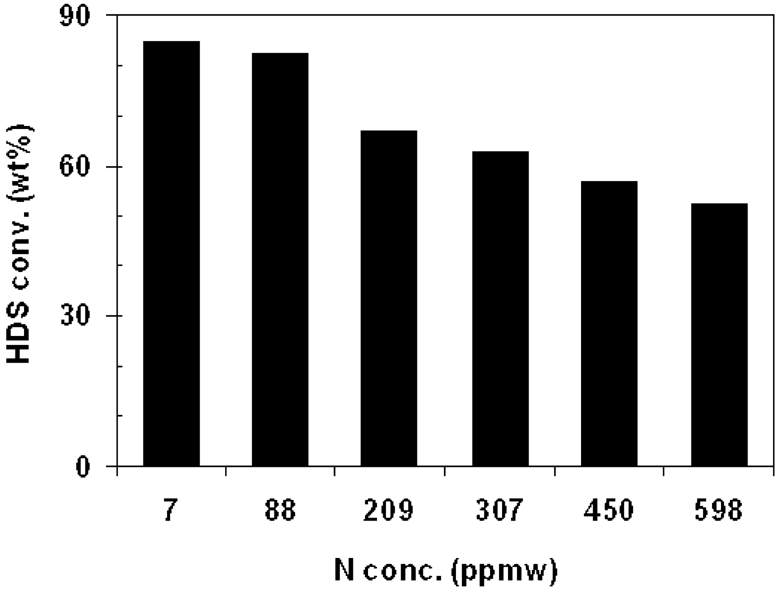

Figure 13. Relationship between nitrogen content in the adsorptive pretreated LCO and the corresponding HDS conversion %.

Figure 14 shows the sulfur-selective GC-PFPD chromatograms of the original LCO, the hydrodesulfurised LCO, and the product from the HDS of the adsorptive pretreated LCO. The HDS of LCO was found effective for the removal of reactive sulfur compounds, such as methylbenzothiophene (MBT), dimethylbenzothiophene (DMBT), and trimethylbenzothiophene (TMBT), but has poor performance for the removal of refractory sulfur compounds, such as 2-MDBT, 4-MDBT, and 4,6-DMDBT. On the other hand, the adsorptive pretreatment of LCO was found very effective to enhance the HDS performance, not only for reactive sulfur, but also for the refractory sulfur compounds. While the HDS of LCO decreased the sulfur content from 1.81 to 0.67 wt%, the HDS of the adsorptively pretreated LCO was able to reduce the sulfur content down to 0.28 wt%. It is worth mentioning that adsorptively pretreated of LCO was very selective for nitrogen removal and did not reduce the sulfur content in the LCO.

Downloaded by UNIV OF DELAWARE MORRIS LIB on June 5, 2012 | http://pubs.acs.org
Publication Date (Web): December 14, 2011 | doi: 10.1021/bk-2011-1088.ch003

Downloaded by UNIV OF DELAWARE MORRIS LIB on June 5, 2012 | http://pubs.acs.org
Publication Date (Web): December 14, 2011 | doi: 10.1021/bk-2011-1088.ch003

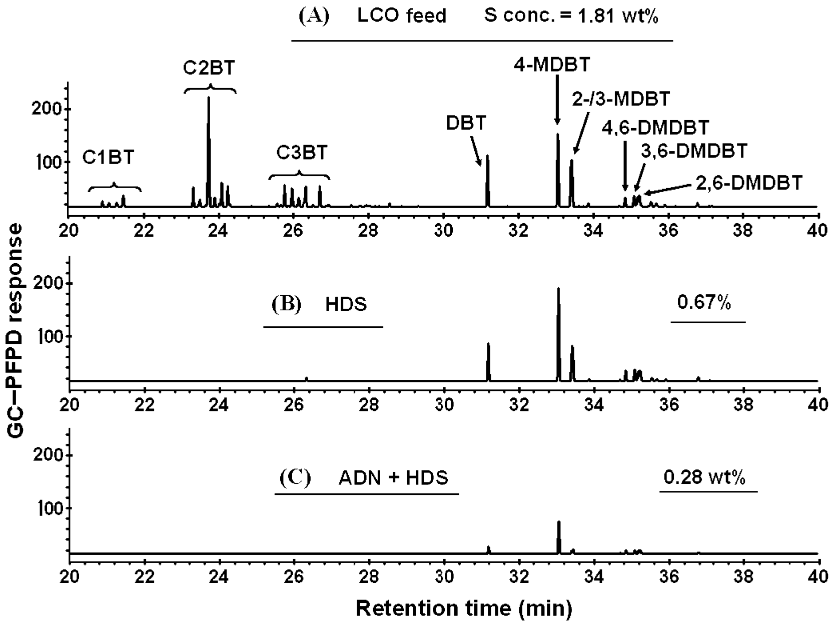

Figure 14. Sulfur chromatograms of (A) original LCO, (B) HDS of LCO, and (C) adsorptive denitrogenation (ADN) LCO + HDS.

Both, the direct HDS of LCO and the adsorptive pretreatment followed by HDS, were able to remove most of the reactive sulfur compounds. However, the latter greatly enhanced the removal of the refractory sulfur compounds. As shown in Figure 10, carbazole and its alkylated derivatives are the predominant nitrogen compounds in LCO. The current results confirm that the removal of such nitrogen compounds from LCO enhances the HDS performance for removing the refractory sulfur compounds.

Conclusions

The carbon-based adsorbent is a promising material for the efficient removal of the nitrogen compounds from LCO. Oxidative modification of the activated carbons greatly improves the adsorption performance for nitrogen removal, but not for sulfur removal, from LCO. The adsorption capacity of the activated carbons for nitrogen compounds highly depends on their concentration of the oxygen functional groups on the surface. Adsorptive pretreatment of LCO on the oxidatively modified activated carbon significantly improves the subsequent HDS performance, especially for the removal of the refractory sulfur compounds. The majority of the capacity of the spent adsorbent can be recovered by washing with toluene.

Downloaded by UNIV OF DELAWARE MORRIS LIB on June 5, 2012 | http://pubs.acs.org
Publication Date (Web): December 14, 2011 | doi: 10.1021/bk-2011-1088.ch003

References

1. Prins, R. *Adv. Catal.* **2002**, *46*, 399.
2. Furimsky, E. *Catal. Rev.: Sci. Eng.* **2005**, *47*, 297.
3. Kim, J. H.; Ma, X. L.; Zhou, A. N.; Song, C. S. *Catal. Today* **2006**, *111*, 74.
4. Song, C. S. *Catal. Today* **2003**, *86*, 211.
5. Song, C. S.; Ma, X. L. *Appl. Catal., B* **2003**, *41*, 207.
6. Babich, I. V.; Moulijn, J. A. *Fuel* **2003**, *82*, 607.
7. Gates, B. C.; Topsoe, H. *Polyhedron* **1997**, *16*, 3213.
8. Ho, T. C. *Catal. Today* **2004**, *98*, 3.
9. Vasudevan, P. T.; Fierro, J. L. G. *Catal. Rev.: Sci. Eng.* **1996**, *38*, 161.
10. Turaga, U. T.; Ma, X. L.; Song, C. S. *Catal. Today* **2003**, *86*, 265.
11. Niquille-Rothlisberger, A.; Prins, R. *Top. Catal.* **2007**, *46*, 65.
12. Murti, S. D. S.; Yang, H.; Choi, K. H.; Korai, Y.; Mochida, I. *Appl. Catal., A* **2003**, *252*, 331.
13. Mizutani, H.; Godo, H.; Ohsaki, T.; Kato, Y.; Fujikawa, T.; Saih, Y.; Funamoto, T.; Segawa, K. *Appl. Catal., A* **2005**, *295*, 193.
14. Laredo, G. C.; De los Reyes, J. A.; Cano, J. L.; Castillo, J. J. *Appl. Catal., A* **2001**, *207*, 103.
15. Gutberlet, L. C.; Bertolacini, R. J. *Ind. Eng. Chem. Prod. Res. Dev.* **1983**, *22*, 246.
16. Yang, H.; Chen, J. W.; Fairbridge, C.; Briker, Y.; Zhu, Y. J.; Ring, Z. *Fuel Process. Technol.* **2004**, *85*, 1415.
17. Eijsbouts, S.; Debeer, V. H. J.; Prins, R. *J. Catal.* **1991**, *127*, 619.
18. Shin, S. H.; Sakanishi, K.; Mochida, I.; Grudoski, D. A.; Shinn, J. H. *Energy Fuels* **2000**, *14*, 539.
19. Depauw, G. A.; Froment, G. F. *J. Chromatogr., A* **1997**, *761*, 231.
20. Hernandez-Maldonado, A. J.; Yang, R. T. *Angew. Chem., Int. Ed.* **2004**, *43*, 1004.
21. Min, W. *Korean J. Chem. Eng.* **2002**, *19*, 601.
22. Sano, Y.; Choi, K. H.; Korai, Y.; Mochida, I. *Energy Fuels* **2004**, *18*, 644.
23. Ellis, J.; Korth, J. *Fuel* **1994**, *73*, 1569.
24. Liu, D.; Gui, J. Z.; Sun, Z. L. *J. Mol. Catal. A: Chem.* **2008**, *291*, 17.
25. Sano, Y.; Choi, K. H.; Korai, Y.; Mochida, I. *Appl. Catal., B* **2004**, *49*, 219.
26. Almarri, M.; Ma, X. L.; Song, C. S. *Ind. Eng. Chem. Res.* **2009**, 951.
27. Almarri, M.; Ma, X. L.; Song, C. S. *Energy Fuels* **2009**, *23*, 3940.
28. Wu, J. C. S.; Sung, H. C.; Lin, Y. F.; Lin, S. L. *Sep. Purif. Technol.* **2000**, *21*, 145.
29. Choi, K. H.; Korai, Y.; Mochida, I.; Ryu, J. W.; Min, W. *Appl. Catal., B* **2004**, *50*, 9.
30. Min, W.; Choi, K. I.; Khang, S. Y.; Min, D. S.; Ryu, J. W.; Yoo, K. S.; Kim, J. H. U.S. Patent 6,248,230, 2001.
31. Almarri, M., Ph.D. Thesis, Pennsylvania State University, University Park, PA, 2009.
32. Ma, X. L.; Velu, S.; Kim, J. H.; Song, C. S. *Appl. Catal., B* **2005**, *56*, 137.
33. Li, N.; Ma, X.; Zha, Q.; Song, C. *Energy Fuels* **2010**, *24*, 5539.

In Production and Purification of Ultraclean Transportation Fuels; Hu, Y., et al.;
ACS Symposium Series; American Chemical Society: Washington, DC, 2011.

34. Song, C. S.; Nihonmatsu, T.; Nomura, M. *Ind. Eng. Chem. Res.* **1991**, *30*, 1726.
35. Ania, C. O.; Bandosz, T. J. *Langmuir* **2005**, *21*, 7752.
36. Yang, Y. X.; Lu, H. Y.; Ying, P. L.; Jiang, Z. X.; Li, C. *Carbon* **2007**, *45*, 3042.
37. Zhou, A. N.; Ma, X. L.; Song, C. S. *J. Phys. Chem. B* **2006**, *110*, 4699.
38. Zeuthen, P.; Knudsen, K. G.; Whitehurst, D. D. *Catal. Today* **2001**, *65*, 307.
39. van Looij, F.; van der Laan, P.; Stork, W. H. J.; DiCamillo, D. J.; Swain, J. *Appl. Catal., A* **1998**, *170*, 1.
40. Kwak, C.; Lee, J. J.; Bae, J. S.; Moon, S. H. *Appl. Catal., B* **2001**, *35*, 59.
41. Nagai, M.; Sato, T.; Aiba, A. *J. Catal.* **1986**, *97*, 52.
42. Lavopa, V.; Satterfield, C. N. *J. Catal.* **1988**, *110*, 375.

Downloaded by UNIV OF DELAWARE MORRIS LIB on June 5, 2012 | http://pubs.acs.org
Publication Date (Web): December 14, 2011 | doi: 10.1021/bk-2011-1088.ch003

Downloaded by PENNSYLVANIA STATE UNIV on June 5, 2012 | http://pubs.acs.org
Publication Date (Web): December 14, 2011 | doi: 10.1021/bk-2011-1088.ch004

Chapter 4

Ultra-Deep Desulfurization of Ultra-Low Sulfur Diesel over Nickel-Based Sorbents in the Presence of Hydrogen for Fuel Cell Applications

C. Sentorun-Shalaby, X. L. Ma,* and C. S. Song*

Clean Fuels and Catalysis Program, EMS Energy Institute, and
Department of Energy & Mineral Engineering,
The Pennsylvania State University,
209 Academic Projects Building, University Park, Pennsylvania 16802
***E-mails: mxx2@psu.edu (Ma); csong@psu.edu (Song)**

This study explored the addition of H_2 to improve the sorption performance of the nickel-based sorbents in ultra-deep desulfurization of ultra-low sulfur diesel (ULSD). The desulfurization of ULSD over Raney Nickel and Ni20/SBA-15 was conducted in a fixed-bed sorption system at 220°C and ambient pressure in the absence and presence of H_2. The ADS performances of the prepared nickel-based sorbent and commercial Raney Nickel in the absence and presence of H_2 were evaluated and compared. Addition of very small amount of H_2 into the sorption system significantly increases the adsorptive capacity of the SBA-15-supported nickel-based sorbent for desulfurization of ULSD. The improvement of the sorption performance is through accelerating the C-S bond cracking of the adsorbed sulfur compounds to release the corresponding hydrocarbon part from the surface, and thus to provide more exposed nickel atoms on the surface to interact with other sulfur compounds. Each kilogram of the prepared Ni20/SBA-15 sorbent is able to treat about 240 L of the commercial ULSD with sulfur content of 14.5 ppmw to get a desulfurized fuel with sulfur content less than 1 ppmw in the presence of H_2.

In Production and Purification of Ultraclean Transportation Fuels; Hu, Y., et al.;
ACS Symposium Series; American Chemical Society: Washington, DC, 2011.

Downloaded by PENNSYLVANIA STATE UNIV on June 5, 2012 | http://pubs.acs.org
Publication Date (Web): December 14, 2011 | doi: 10.1021/bk-2011-1088.ch004

Introduction

The commercial ultra-low sulfur diesel (ULSD) is a preferred liquid hydrocarbon fuel for automotive, portable, resident, and military fuel cells due to its high energy density, availability, safety, and/or ease for delivery and storage. The current sulfur level of the commercial ULSD is less than 15 ppmw. However, even at this sulfur level, the sulfur content in ULSD is still too high for fuel cell applications, as the sulfur compounds in the fuel and H_2S produced from them in the fuel processor poison the catalysts used in reforming and water-gas-shift processes and fuel cell stacks (*1–4*).

In our previous studies (*5*, *6*), we have developed the high-performance nickel-based sorbent by loading nickel on the mesoporous molecular sieves, such as MCM-48 and SBA-15 for adsorptive desulfurization (ADS) of the commercial ULSD for fuel cell applications. The high breakthrough capacity for ADS of the ULSD at a breakthrough sulfur level of 1 ppmw has been achieved. However, we found that each sulfur-containing molecule was adsorbed approximately on the twenty exposed nickel atoms. This value is much lower than the stoichiometry (from 0.48 to 1.09 for different crystal faces of nickel) of the S atoms per exposed Ni atom when the nickel surface is saturated by sulfur (*7*), indicating that the majority of the exposed Ni atoms still remain intact after the breakthrough. Our further investigation found that more than 95 % of the sulfur compounds were adsorbed on the surface without occurrence of the C-S bond cracking to release the corresponding hydrocarbon part from the surface. The results suggest that introducing hydrogen to the nickel surface may accelerate the hydrogenolysis of the adsorbed sulfur compounds and the release of corresponding hydrocarbon part, and thus, provide more accessible nickel atoms to interact with other sulfur compounds.

In the present study, we explored the ultra-deep desulfurization of ULSD on the nickel-based sorbents in the presence of hydrogen to improve the ADS performance of the nickel-based sorbents. The ultra-deep desulfurization of ULSD over Raney Nickel and SBA-15 supported nickel-based sorbents was conducted in a fixed-bed sorption system in the absence and presence of H_2 at atmospheric pressure. The ADS performance of the nickel-based sorbents in the absence and presence of H_2 was evaluated and compared.

Experimental

Nickel-Based Sorbents

The mesoporous-molecular-sieve-supported nickel sorbent, Ni20/SBA-15, was prepared by loading 20 wt % of Ni on SBA-15 using an incipient wetness impregnation (IWI) method with ultrasonic aid. The SBA-15 was synthesized according to the procedure reported by Wang et al. (*8*, *9*) based on the method initially reported by Zhao et al. in 1998 (*10*). Typically, a homogeneous mixture, which was composed of triblock copolymer Pluronic of P123 (MW = 5800,

Downloaded by PENNSYLVANIA STATE UNIV on June 5, 2012 | http://pubs.acs.org
Publication Date (Web): December 14, 2011 | doi: 10.1021/bk-2011-1088.ch004

Aldrich) and tetraethyl orthosilicate (TEOS) in hydrochloric acid, was stirred at 40°C for 20 h, and then further treated at 100°C for 24 h. The solid product was filtered and washed with plenty of water, dried in an oven at 100°C, and subsequently calcined at 550°C for 6 h under an air flow (100 ml/min). The mesoporous-molecular-sieve-supported nickel sorbent was prepared using an incipient wetness impregnation (IWI) method. Tetrahydrofuran (THF) was used as a solvent to prepare the $Ni(NO_3)_2$ solution. The nickel sorbent preparation method is given in Figure 1. The desired amount of $Ni(NO_3)_2{\cdot}6H_2O$ was dissolved in THF, and the solution was slowly added into the support material at room temperature with ultrasonic aid in a VWR-Model 75T ultrasonic bath. After adding the solution, the mixture was kept in the ultrasonic bath for 3 h at room temperature. The mixture was then dried in an oven at 100°C overnight. The dried samples were then reduced in situ in a fixed-bed reactor under a pure hydrogen gas flow at 550°C for 4 h before use.

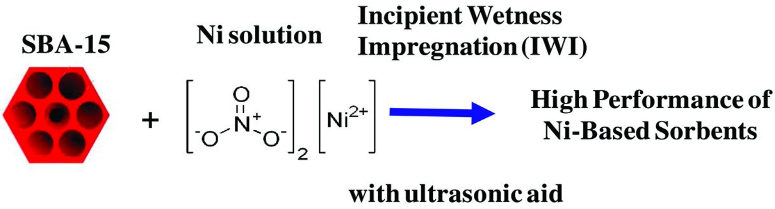
SBA-15
Ni solution
Incipient Wetness Impregnation (IWI)
+
O
N+
-O
O-
2
Ni2+
High Performance of Ni-Based Sorbents
with ultrasonic aid

Figure 1. The nickel sorbent preparation method.

All chemicals that were used in the preparation of the sorbents, including Pluronic (P123) (Mn: 5800), TEOS with a purity of 98%, THF with a purity of 99%, hydrochloric acid solution (HCl) with a purity of 37%, and nickel nitrate hexahydrate ($Ni(NO_3)_2{\cdot}6H_2O$), were purchased from Sigma–Aldrich (Allentown, PA), and were used as received without further purification. A commercial Raney Nickel®2800 was also used in this study, which was purchased from Sigma-Aldrich. Some physical properties of the nickel-based sorbents and SBA-15 used in this study are listed in Table 1. The nitrogen adsorption–desorption at −196°C was conducted using a Micromeritics ASAP2020 instrument. Samples were degassed for 3 h at 400°C under vacuum ($P<10^{-2}$ Pa) and subsequently analysed. The specific BET surface areas were determined from the N_2 adsorption at relative pressures of $0.05 < P/P_0 < 0.3$. The pore size distribution (PSD) was calculated from the adsorption branch of the N_2 physisorption isotherms employing the Barret–Joyner–Halenda (BJH) formula (*11*). The total pore volumes (V_{Total}) were estimated from the volume of N_2 (as liquid) held at a relative pressure (P/P_0) of 0.98. The ULSD with 14.5 ppmw total sulfur used in this study was supplied from British Petroleum (BP).

Table 1. Physical properties of the nickel-based sorbents and SBA-15

Sample	*Surface area*	*Total pore vol.*	*Micro-pore vol.*	*Meso-pore vol.*	*Pore size*
	(m^2/g)	*(cm^3/g)*	*(cm^3/g)*	*(cm^3/g)*	*(nm)*
SBA-15	889	1.24	0.36	0.88	6.4
Ni20/SBA-15	260	0.36	0.10	0.26	5.5
Raney Nickel®2800	33	0.12	0.01	0.11	14.4

Downloaded by PENNSYLVANIA STATE UNIV on June 5, 2012 | http://pubs.acs.org
Publication Date (Web): December 14, 2011 | doi: 10.1021/bk-2011-1088.ch004

ADS Tests

Evaluation of the ADS performance of sorbents was conducted in a fixed-bed flow sorption system with a stainless steel column (4.6 mm I.D. x 150 mm length). A commercial ULSD with sulfur concentration of 14.5 ppmw was fed into the column from the bottom by a HPLC pump. The adsorption conditions were controlled at 220˚C and ambient pressure under a liquid hourly speed velocity (LHSV) of 4.8 h^{-1}. When H_2 was used in the tests, the H_2 flow rate was 1 mL/min at the atmospheric pressure. The effluent fuel from the top of the column was periodically sampled at an interval of 15-20 min for analysis.

Analysis of Untreated and Treated ULSD

The total sulfur concentration of the treated fuel samples was analyzed by using ANTEK 9000 series sulfur analyzer. The sulfur compounds in the un-treated fuel was analysed by using a Hewlett-Packard gas chromatograph equipped with a sulfur-selective pulsed flame photometric detector (GC–PFPD). A Hewlett Packard 5890 series II gas chromatograph with a capillary column (XTI-5, Restek, bonded 5%, 30 m × 0.25 mm I.D. × 0.25 m film thickness) and a split mode injector (ratio: 100:1) was used with ultra high-purity helium as a carrier gas. The oven temperature was initially set at 120˚C and ramped immediately at 6 ˚C/min to 170˚C, followed by a ramp at 20 ˚C/min from 170 to 290˚C, and held at 290˚C for 5 min. The injection sample volume was 1 µL.

Results and Discussion

Sulfur Compounds in ULSD

The GC-PFPD chromatogram of the initial ULSD is shown in Figure 2. The major sulfur compounds in the ULSD with 14.5 ppmw sulfur are the alkyl DBTs with two alkyl substituents at the 4- and 6-positions respectively. This type of the sulfur compounds have been reported to be the most refractory sulfur compounds in gas oil (*12*), thus remain in the commercial ULSD.

Downloaded by PENNSYLVANIA STATE UNIV on June 5, 2012 | http://pubs.acs.org
Publication Date (Web): December 14, 2011 | doi: 10.1021/bk-2011-1088.ch004

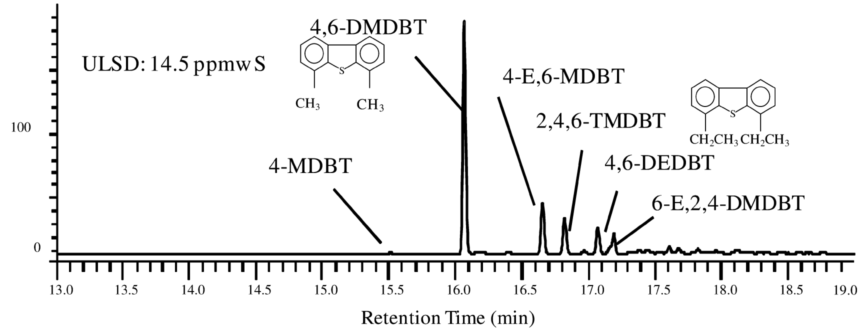

Figure 2. The GC-PFPD chromatogram of the initial ULSD.

Effect of the Presence of H_2 on ADS Performance of the Nickel-Based Sorbents

ADS performances of the prepared sorbent Ni20/SBA-15 and the commercial Raney Nickel were evaluated in the fixed-bed flow sorption system in the absence and presence of H_2 at 220°C and 4.8 h^{-1} of LHSV. The breakthrough curves for Ni20/SBA-15 and Raney Nickel are shown in Figure 3 and the corresponding breakthrough capacities at the breakthrough sulfur level of 1 ppmw are listed in Table 2. In the absence of H_2, the breakthrough capacity over Raney Nickel and Ni20/SBA-15 was 0.19 and 0.98 mg-S/g-sorb, respectively. Ni20/SBA-15 showed the higher breakthrough capacity than that of Raney Nickel by a factor of 5.2. As expected, when introducing only very small amount of H_2 (1.0 ml/min) into the system at ambient pressure, the breakthrough capacity increased dramatically for both nickel-base sorbents. For Raney Nickel, the breakthrough capacities increased from 0.19 mg-S/g-sorb in the absence of H_2 to 2.2 mg-S/g-sorb in the presence of H_2, by a factor of 11.6. For Ni20/SBA-15, the breakthrough capacities increased from 0.98 mg-S/g-sorb in the absence of H_2 to 3.2 mg-S/g-sorb in the presence of H_2, by a factor of 3.3. The results clearly show that introduction of H_2 into the surface of the nickel-based sorbents significantly improves the sorption performance of the sorbents.

In comparison of Raney Nickel and Ni20/SBA-15 in the presence of H_2, the breakthrough capacity of Ni20/SBA-15 is higher than that of Raney Nickel by 45 %. The results indicate that each kilogram of Ni20/SBA-15 is able to treat 240 L of the commercial ULSD with sulfur content of 14.5 ppmw to get the treated ULSD with sulfur content less than 1 ppmw, and to treat about 160 L of the commercial ULSD to get the treated ULSD with sulfur content less than 0.1 ppmw.

The schematic diagram for adsorption mechanism of the nickel-based sorbents in the absence and presence of H_2 is shown in Figure 4. In the absence of H_2, adsorbed sulfur compounds cover the nickel surface, which limits the further adsorption of the sulfur compounds on the surface. The presence of H_2 accelerates the C-S bond cracking of the adsorbed sulfur compounds to release the corresponding hydrocarbon part from the surface. It results in providing more exposed nickel atoms, which are covered by the adsorbed sulfur compounds in the absence of H_2, to interact with other sulfur compounds.

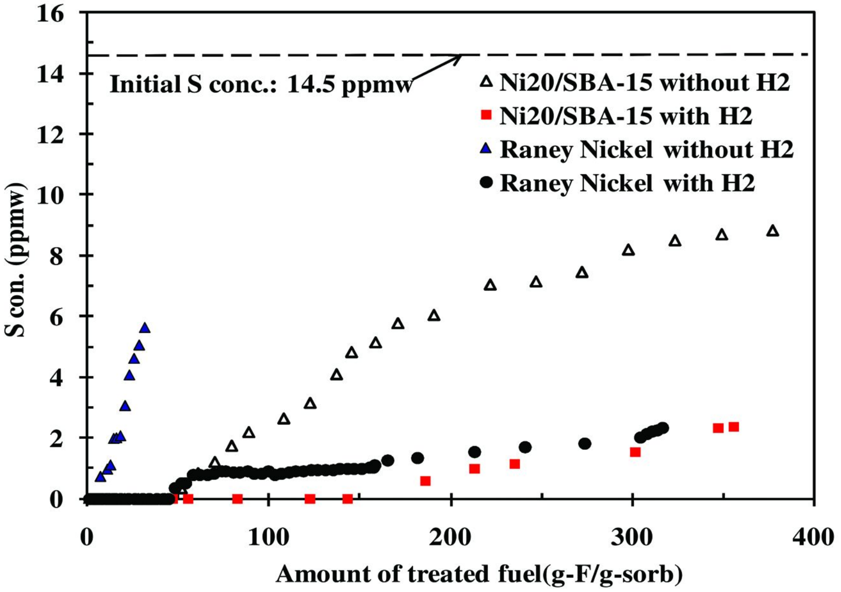

Figure 3. Breakthrough curves for ADS of ULSD over Ni20/SBA-15 and Raney Nickel in the absence/presence of H_2. Sorption conditions: 220̊C, ambient pressure and 4.8 h^{-1} of LHSV.

Table 2. Breakthrough capacities of Ni20/SBA-15 and Raney Nickel at a sulfur level of 1 ppmw at 220°C, ambient pressure and 4.8 h^{-1} of LHSV in the absence/presence of H_2

	Raney Nickel®2800	*Ni20/SBA-15*
	(mg-S/g-sorb)	*(mg-S/g-sorb)*
Without H_2	0.19	0.98
With H_2	2.2	3.2
Increase factor	11.6	3.3

In Production and Purification of Ultraclean Transportation Fuels; Hu, Y., et al.;
ACS Symposium Series; American Chemical Society: Washington, DC, 2011.

Downloaded by PENNSYLVANIA STATE UNIV on June 5, 2012 | http://pubs.acs.org
Publication Date (Web): December 14, 2011 | doi: 10.1021/bk-2011-1088.ch004

Downloaded by PENNSYLVANIA STATE UNIV on June 5, 2012 | http://pubs.acs.org
Publication Date (Web): December 14, 2011 | doi: 10.1021/bk-2011-1088.ch004

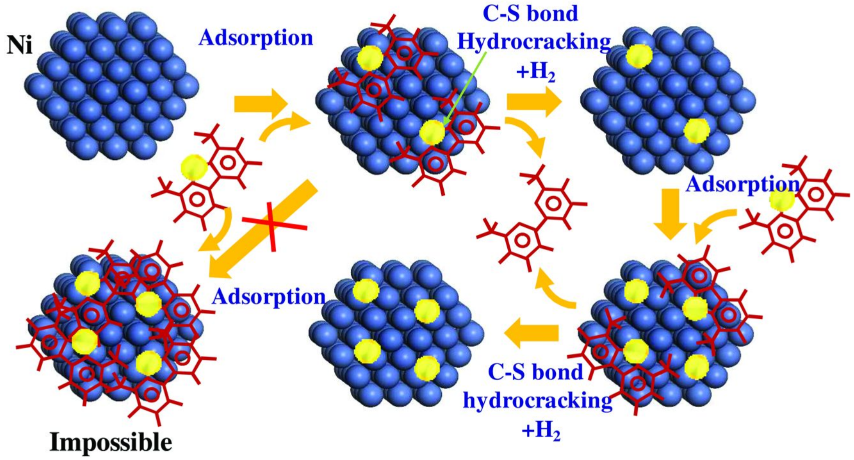

Figure 4. The schematic diagram for sorption mechanism of the sulfur compounds on the nickel-based sorbents in the absence and presence of H_2*: In the absence of* H_2*, adsorbed sulfur compounds cover the nickel surface which limits the further adsorption. The presence of* H_2 *accelerates the C-S bond cracking of the adsorbed sulfur compounds to release the corresponding hydrocarbon part.*

Conclusions

Addition of very small amount of H_2 into the sorption system significantly increases the adsorptive capacity of the nickel-based sorbents for ADS of ULSD. The improvement of the sorption performance by the addition of H_2 is through accelerating the C-S bond cracking of the adsorbed sulfur compounds to release the corresponding hydrocarbon part from the surface, and thus to provide more exposed nickel atoms on the surface to interact with other sulfur compounds. Each kilogram of the prepared Ni20/SBA-15 with 20 % nickel loading on SBA-15 in the presence of H_2 is able to treat about 240 L of the commercial ULSD with initial sulfur content of 14.5 ppmw to get a desulfurized fuel with sulfur content less than 1 ppmw.

Acknowledgments

This work was supported in part by the U.S. Department of Energy, National Energy Technology Laboratory under Contract No. DE-FC26-08NT0004396.

References

1. Song, C. S. *Catal. Today* **2002**, *77*, 17–49.
2. Farrauto, R.; Hwang, S.; Shore, L.; Ruettinger, W.; Lampert, J.; Giroux, T.; Liu, Y.; Ilinich, O. *Annu. Rev. Mater. Res.* **2003**, *33*, 1–27.
3. Dayton, D. C.; Ratcfliff, M.; Bain, R. *Fuel Cell Integration: A Study of the Impacts of Gas Quality and Impurities*; Milestone Completion Report,

NREL/MP-510-30298; National Renewable Energy Laboratory: Golden, CO, June 2001.

4. Haberbauer, M. In *Biofuels for Fuel Cells*; Lens, P., Westermann, P., Haberbauer, M., Moreno, A., Eds.; IWA Publishing: London, 2005; pp 403−412.
5. Sentorun-Shalaby, C.; Ma, X. L.; Song, C. S. *Prepr. Pap.- Am. Chem. Soc., Div. Pet. Chem.* **2010**, *55* (2), 31.
6. Sentorun-Shalaby, C.; Saha, S. K.; Ma, X. L.; Song, C. S. *Appl. Catal., B* **2011**, *101*, 718–726.
7. Bartholomew, C. H.; Agrawal, P. K. In *Advances in Catalysis*; Eley, D. D., Pines, H.; Weiez, P. B. Eds.; Academic Press: New York, 1982.
8. Wang, X. X.; Ma, X. L.; Sun, L.; Song, C. S. *Green Chem.* **2007**, *9*, 695–702.
9. Wang, X. X.; Zhang, Q. H.; Yang, S. F.; Wang, Y. *J. Phys. Chem. B* **2005**, *109*, 23500–23508.
10. Zhao, D.; Feng, J.; Huo, Q.; Melosh, N.; Fredrickson, G. H.; Chmelka, B. F.; Stucky, G. D. *Science* **1998**, *279*, 548–552.
11. Barrett, E. P.; Joyner, L. J.; Halenda, P. P. *J. Am. Chem. Soc.* **1951**, *73*, 373–380.
12. Ma, X. L.; Sakanishi, K.; Mochida, I. *Ind. Eng. Chem.* **1994**, *33*, 218–222.

Downloaded by PENNSYLVANIA STATE UNIV on June 5, 2012 | http://pubs.acs.org
Publication Date (Web): December 14, 2011 | doi: 10.1021/bk-2011-1088.ch004

Downloaded by DUKE UNIV on June 5, 2012 | http://pubs.acs.org
Publication Date (Web): December 14, 2011 | doi: 10.1021/bk-2011-1088.ch005

Chapter 5

The Potential of Biomass in the Production of Clean Transportation Fuels and Base Chemicals

Jacob A. Moulijn* **and Igor V. Babich**

BiCHEM Technology BV, High Tech Campus 48-2,
5656 AE Eindhoven, The Netherlands
***E-mail: J.A.Moulijn@tudelft.nl**

Biomass is shown to have a large potential as energy carrier and feedstock for the chemical industry. Besides direct utilization by combustion many options exist for upgrading by conversion into valuable products in the sector of transport fuels and base chemicals. Because biomass is highly functionalized, dependent on the specific feedstock subtle technology in the liquid phase is most appealing. Processing in the liquid phase calls for a suitable solvent. An innovative example of a concept based on dissolution, hydrolysis and further conversion of biomass in a metal hydrate solvent is discussed. The process potential for producing relevant platform molecules at high yields has been demonstrated.

Biomass is well spread over the globe and compared with other energy carriers, in particular nuclear energy, its use has a long tradition for mankind. In this chapter the potential of biomass for energy and as a feedstock for the chemical industry will be evaluated. A general concern exists with regard to the resources of biomass whether the amounts present are sufficiently large to play a major role in the supply of energy and chemicals. In Table I key numbers are compared for main energy carriers. Among renewable energy resources solar energy has by far the largest theoretical potential.

Biomass produced via photosynthesis is directly coupled with solar energy. Although in natural photosynthesis only a fraction of a percent of the solar radiation is used, the absolute amount is considerable, being one order of magnitude higher than the present energy consumption. Thus, at first sight the

In Production and Purification of Ultraclean Transportation Fuels; Hu, Y., et al.;
ACS Symposium Series; American Chemical Society: Washington, DC, 2011.

volume of the energy resources might not seem alarming. However, we should realize that for a modest growth rate of 2-3 % annually the consumption of energy increases considerably. For instance, in 2050 this growth rate implies an energy consumption of 1550 instead of the 490 EJ/a in 2006. The question arises if biomass resources really are sufficiently large and easily accessible to have a significant impact in the future.

Several research groups have evaluated the potential for an increase in biomass production. A recent study of Ladanai and Vinterbäck (*2*) is a good example. Based on an evaluation by Hoogwijk *et al.* (*3*) a positive conclusion can be drawn.

Downloaded by DUKE UNIV on June 5, 2012 | http://pubs.acs.org
Publication Date (Web): December 14, 2011 | doi: 10.1021/bk-2011-1088.ch005

Table I. Comparison of main energy sources and their potential in energy supply (numbers adapted from (*1*))

	Energy flow		*Reserves (years)*	*Option for chemicals*	*Remarks*
	TW	EJ/a			
Theoretical potential of renewable energy resources					
Solar energy	125,000	4,000,000		R&D has started	1 kW/m^2
Hydropower	4.6	147			
Wind energy	187	6,000			
Ocean energy	230	7,400			
Energy consumption					
Present	15.8	490			2006
Coal	4.4	127.4	190	Yes, mainly syngas route	
Oil	5.2	166.5	42	Yes, relatively easy	
Natural gas	3.6	102.9	63	Yes, mainly syngas route	
Biomass	1.5	49	Sustainable	Promising	Heating, cooking
For 2050	49	1.550			3.5*2005
Energy potential via photosynthesis					
	130	4,000			

Figure 1 gives a clear message regarding the origin of the biomass potentially to be used for energy and chemicals production in 2050. Waste streams are sizeable but not sufficient and agriculture methodology for production of biomass has to be critically evaluated. The present agriculture cannot provide the amounts of biomass needed without affecting food industry. Surplus land, which is not used for forestry production, nature reserves and animal grazing, has to be involved in biomass production, and the good news is that this land is available in the world (*4*). In the study algae were not taken into account. Undoubtedly, they can provide significant additional amounts of energy.

Biomass is not only a sustainable basis for energy. Similar to fossil fuels it is a feedstock for the chemical industry. Assuming that the worldwide energy consumption in chemical sector is about 10 % of the total energy consumption (*5*), it is clear from the data presented that there is plenty of biomass available to serve as a feedstock for the chemical industry.

From this evaluation we conclude that biomass can play a major role in making the world sustainable but energy conservation should keep high priority.

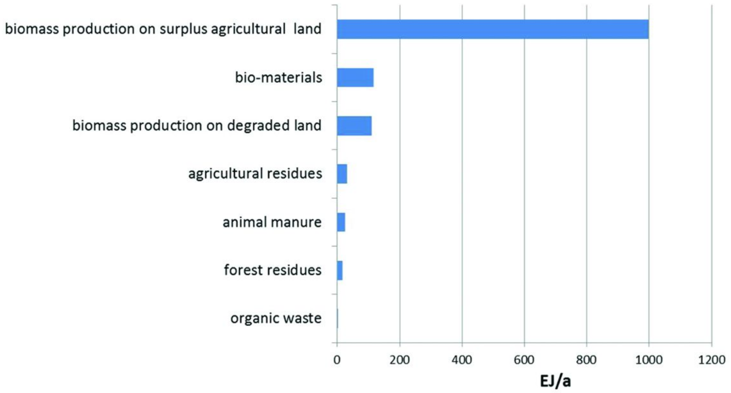

Figure 1. Biomass resources assessed to be theoretically available. (Adapted from ref. (3)).

Lignocellulosic Biomass

In a simplified analysis biomass can be divided in three groups, namely, oils, sugars and lignocellulosic biomass. A simple economic analysis shows that lignocellulosics are most attractive both from the point of resouces and price.

Lignocellulosic biomass consists mainly of three components, cellulose (~40%), hemicellulose (~35%) and lignin (~25%). Plant oils, proteins, different extractives and ashes make up the rest of lignocellulosic biomass structure (Figure 2).

The structure of lignocellulosics is given Figure 3. Cellulose is the most abundant organic polymer on the earth and it's chemical structure is remarkably simple and it is largely crystalline. Cellulose is a linear polymer of cellobiose, a dimer of glucose. The multiple hydroxyl groups of the glucose molecule form hydrogen bonds within the same chain or with a neighbor cellulose chain making cellulose fibrils of high strength and crystallinity. Hemicellulose is chemically related but amorphous and has a more complex composition, see figure for xylan, a representative of hemicellulose. Whereas cellulose is completely built

Downloaded by DUKE UNIV on June 5, 2012 | http://pubs.acs.org
Publication Date (Web): December 14, 2011 | doi: 10.1021/bk-2011-1088.ch005

Downloaded by DUKE UNIV on June 5, 2012 | http://pubs.acs.org
Publication Date (Web): December 14, 2011 | doi: 10.1021/bk-2011-1088.ch005

up from six-membered rings, hemicellulose consists of a mixture of pentoses (xylose, arabinose), hexoses (glucose, mannose, galactose) and uronic acids. Xylose is the monomer present in the largest amount. Chemically, cellulose and hemicellulose are strongly related, they are referred to as carbohydrates. In practice hemicellulose and sugar are often referred to as simple carbohydrates and cellulose as a complex carbohydrate. These terms are related to the easiness of fermentation. Cellulose is difficult to digest, as might have been expected because of the poor accessibility of cellulose chains and because the chemical bond (β-glucosidic bond) is relatively stable. Lignin, the third main component, is an amorphous three-dimensional polymer. It is aromatic and compared with cellulose and hemicellulose hydrophobic. The complexity and variability of lignin composition, and its chemical resistance make its utilization quite difficult. A comprehensive review on the catalytic lignin valorization was published recently (*6*).

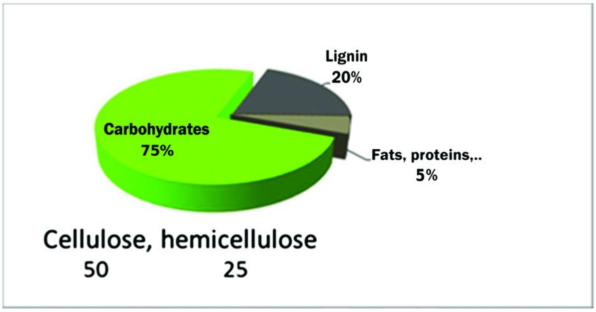

Figure 2. Average composition of lignocellusic biomass.

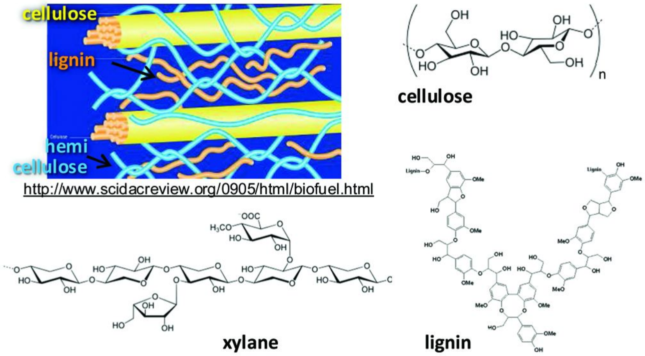

http://www.scidacreview.org/0905/html/biofuel.html

Figure 3. Structure and chemical composition of lignocellulosic biomass.

Not surprisingly, the composition of different crops is very different, see Figure 4, where some typical representatives are compared. Obviously, energy based on biomass can compete with the food chain. Ethically, it is preferable

Downloaded by DUKE UNIV on June 5, 2012 | http://pubs.acs.org
Publication Date (Web): December 14, 2011 | doi: 10.1021/bk-2011-1088.ch005

to give priority to food applications. As an example, in sugar cane processing first sugars are taken out at sugar mills and the remaining bagasse is used as a primary fuel source to provide heat energy used in the mills and in co-generation of electricity.

Besides the composition of the crops, the productivity in harvesting solar energy, characterized as dry weight/ha/a, is the most important characteristic (Table II). Sugar cane shows the highest productivity followed by sugar beet. Soya beans are of a low productivity (*7*).

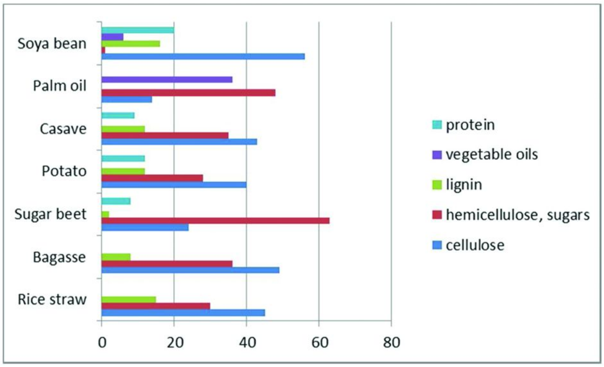

Figure 4. Composition of some major lignocellusic crops. (Reproduced from ref. (7). Copyright 2009, Elsevier).

Table II. Productivity of selected crops. (Reproduced from ref. (*7*)). Copyright 2009, Elsevier)

Crop	*Country*	*Production* (t/ha/a)*
Cassava	Nigeria	50
Grass	Holland	14
Maize	Ioawa	14
Palm oil	Malaysia	25
Potato	Holland	65
Soya bean	Illinois	4
Sugar beet	Germany	100
Sugar cane	Brasil	125
Sun flower	Franca	5
Jatropha seeds	Zimbabwe	8
Rice straw	Egypt	11

* Best practice technology.

Downloaded by DUKE UNIV on June 5, 2012 | http://pubs.acs.org
Publication Date (Web): December 14, 2011 | doi: 10.1021/bk-2011-1088.ch005

Processes

Similar to fossil oil, biomass is utilized in heating, cooking and power generation, providing about 10 % of the total energy consumption. Biomass can be gasified and via the syngas route the 'normal' product spectrum is within reach, for example, methanol and Fischer-Tropsch liquids (*8*). In pyrolysis, a simple process similar to coking in the refinery, biomass is converted to a liquid phase, bio-oil (*9*). The easy separation of the oil is an asset of this process. Moreover, it is robust with respect to the specific feedstock used.

Not all processes are analogous to oil related processes. Also completely different approaches suggest themselves. The underlying reason is the completely different structure of biomass compared to fossil oil. Figure 3 shows that biomass is a highly functionalized structure and contains a large amount of oxygen in sharp contrast with fossil oil. Figure 5 gives an overview showing different approaches and processes for biomass conversion. The highly functionalized structure has resulted in an extensive biotechnological industry, the most important being the production of ethanol by fermentation. It should be noted that in fact this process goes well for sugar and hemicellulose but for cellulose it requires a severe pretreatment of the feedstock and it is not appropriate for lignin. In another category of potential processes the biomass is dissolved and depolymerized into the corresponding monomers. Obvious monomers are sugars, glucose and xylose from cellulose and hemicellulose respectively. These processes are in the R&D stage.

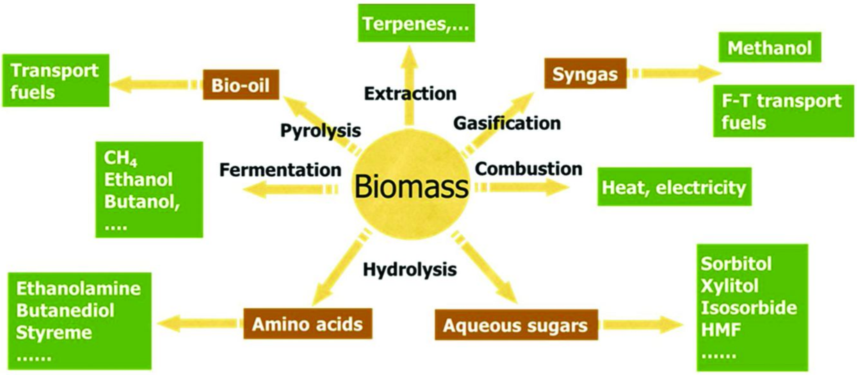
Terpenes,...
Extraction
Transport fuels
Bio-oil
Pyrolysis
Syngas
Gasification
Methanol
F-T transport fuels
CH4
Ethanol
Butanol,
....
Fermentation
Biomass
Combustion
Heat, electricity
Hydrolysis
Ethanolamine
Butanediol
Styreme
......
Amino acids
Aqueous sugars
Sorbitol
Xylitol
Isosorbide
HMF
......

Figure 5. Routes and products in biomass conversion processes.

Thus, the processes range from high-temperature processes, *viz.*, combustion, pyrolysis and gasification, to more subtle processes in the liquid phase, *viz.*, fermentation and hydrolysis. The first category is very robust because the detailed structure of the biomass does play only a minor role and the complete organic part of biomass is converted to a large pool of chemical compounds of different nature. The last category is different due to possibilities for selective conversion under milder conditions. Here, the structure does give the potential of efficient processes with high yields of target products.

Downloaded by DUKE UNIV on June 5, 2012 | http://pubs.acs.org
Publication Date (Web): December 14, 2011 | doi: 10.1021/bk-2011-1088.ch005

Biorefinery

One might wonder if it would not be advisable to process biomass in the existing industrial infrastructure such as oil refineries. The simplest way would be to defunctionalize the biomass so that the stoichiometry of products approaches that of crude oil and subsequently to apply them as feedstock for the refinery. It has been proposed to do this by hydrodeoxygenation (HDO), similar to hydrotreating processing (*10*). However, it is easily shown that the economics of such a process is unsatisfactory. In Table III prices are listed for reactants and products of hydrogenation of glucose, being a model for lignocellulosic biomass, into hexane:

$$C_6H_{12}O_6 + 6\ H_2 \rightarrow C_6H_{12} + 6\ H_2O$$

Table III. The hydrogenation of glucose into hexane, prices of the components involved

	Amount (t)	*Price (Euro/t)*	*Costs (kEuro/t C_6H_{12})*
Reactant			
Glucose	180	500 200*	1.07 0.43*
Hydrogen	12	2200	0.31
Product			
Hexane	84	700	0.7

* Price in Brazil.

It is clear that such a process cannot be cost-effective. Even when sugar is replaced by lignocellulosic biomass (30-40 Euro/t) the costs of hydrogen probably will be prohibitive.

Besides the cost factor one might wonder what the optimal products of biomass conversion are. A priori there is no need to copy the hydrocarbon industry. In principle it is more attractive to produce O-containing products for several reasons. First, less O has to be removed, saving process steps and hydrogen (when hydrogen is used as a reactant). Second, the product quality might be better when O is present. For instance, in the case of diesel, O-containing molecules often are smokeless and give less pollution. Third, when less O is removed less mass is lost.

A fundamental point is the following. Intuitively, it will be clear that it is attractive that the products have a structure similar to that of the feedstock monomers. The consequence will be that the number of bond breaking and forming steps can be minimal. Usually this leads to an efficient process as far as the chemistry is concerned. Therefore, in deciding upon the desired products

Downloaded by DUKE UNIV on June 5, 2012 | http://pubs.acs.org
Publication Date (Web): December 14, 2011 | doi: 10.1021/bk-2011-1088.ch005

the structure of the feedstock should be taken into account. One of the great challenges in biomass applications is to identify such molecules.

Returning to the question of a possible integration of biomass processing with the oil refinery it is instructive to evaluate the processes in Figure 5 with respect to the potential of merging them with the oil refinery. For combustion purposes biomass can be used directly in the oil refinery. Also the pyrolysis process nicely fits with an oil refinery: a bio-oil is formed that easily is separated from the hydrophilic biomass (product mixture) and can be used as a feedstock for further upgrading (*9*). These feedstocks are referred to as “drop-in fuels”. They allow maximum integration with the refinery infrastructure. For gasification this is also the case in the sense that the product can be used in the blending section. For the fermentation and depolymerization (via hydrolysis) processes a fit with the refinery is hardly realistic, except for some final products, for example ethanol and isosorbide derivatives, that can be blended with existing products of the refinery. Thus, we conclude that for most processes a dedicated plant system is needed for efficient biomass conversion. Usually, a complex product spectrum will be produced. Analogous to the oil refinery this system is referred to as a biorefinery.

For economical reasons in general biomass processing will be done on a large scale. Figure 6 gives a schematic listing of the main criteria for the design of a biorefinery and the product spectrum to be expected. It was not attempted to give a full list of potential products. This is done extensively in literature (*11*).

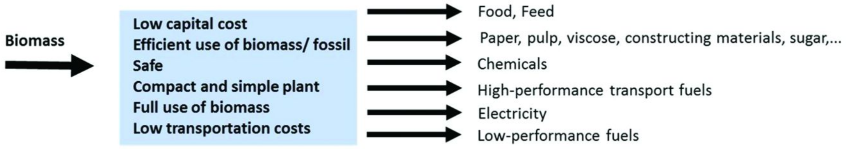

Figure 6. Criteria for design of a biorefinery with its products

In view of the list of criteria and the product spectrum it is not surprising that a large variety of designs of a biorefinery are conceivable (*12*). In addition, the type of biomass to be processed has to be decided upon. In the following an innovative example of a concept based on a hydrolysis step is presented.

Lignocellosic Biomass Biorefinery Based on Separation, Hydrolysi, and *in Situ* Conversions: An Example of a New Promising Technology

The key of the technology presented is the depolymerization of cellulose in an adequate solvent. For the dissolution of cellulose several systems have been reported including ionic liquids (*13*), aqueous alkali solutions (*14*) and salt hydrates (*15*). Figure 7 shows the superb performance of zinc chloride hydrate: at 60 °C all cellulose is dissolved in 7 (!) min.

In one respect the photogaphs might be misleading. Under the conditions of the experiment in Figure 7 cellulose is dissolved but the polymeric chains are not

Downloaded by DUKE UNIV on June 5, 2012 | http://pubs.acs.org
Publication Date (Web): December 14, 2011 | doi: 10.1021/bk-2011-1088.ch005

hydrolyzed. Hydrolysis is catalyzed by $ZnCl_2$ hydrate but compared to dissolution more severe conditions are needed. Dissolution and depolymerization take place sequentially, see Figure 8.

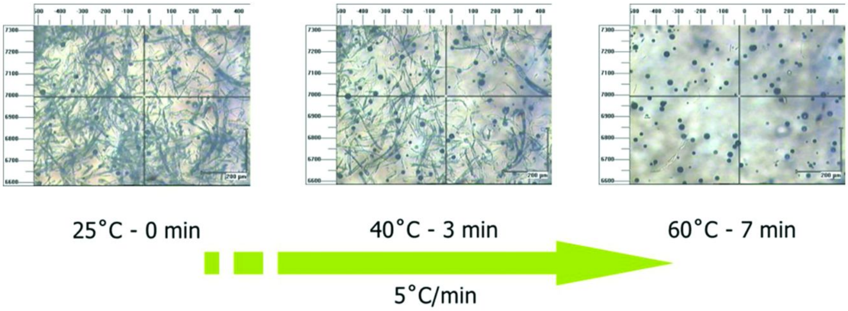

Figure 7. Dissolution of cellulose in $ZnCl_2$ *hydrate. 2 wt.% cellulose in* $ZnCl_2$*(70 wt.%)/*H_2O *solution; Leika DMLM microscope equipped with Leica DFC290 camera, Lynkam TS600 heating stage at heating rate 5°C/min.*

Hydrolysis is a critical step in the total process because glucose is formed, a well-known rather unstable molecule that can undergo all types of degradation reactions. Sorbitol, the monohydrogenated product of glucose, is rather stable. Therefore, we decided to hydrogenate glucose into sorbitol in a first step in the process. Using proper conditions and a catalyst, it is possible to fully hydrogenate glucose to sorbitol in $ZnCl_2$ hydrate medium with acceptable rates and selectivities (*16*).

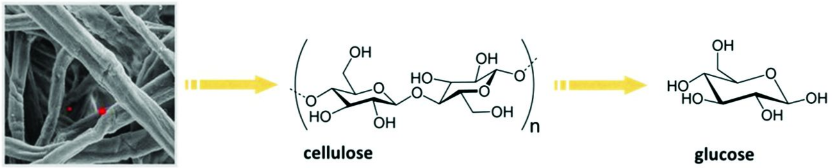

Figure 8. Dissolution of cellulose followed by depolymerization in $ZnCl_2$ *hydrate.*

In biomass conversion separation is often a key issue. The underlying reason is that biomass hydrolysis products are highly polar and sorbitol is no exception. If sorbitol would be transformed to a less polar product, the separation would be easier. We have anticipated that a dehydration step giving isosorbide is an efficient route to a lower-polarity product, see Figure 9.

Fortunately all reactions – hydrolysis, hydrogenation, and dehydration - can be carried out in the solvent used. In fact, the solvent is the basis of an excellent catalyst for the two dehydration reactions. From HPLC analysis it is clear that the reacting system is clean in the sense that the selectivity is very high. Under not yet fully optimized conditions degradation reactions are < 5% and isosorbide is the largest product with a yield of 80-90%, the remainder being for a large part sorbitan (also a useful product).

Downloaded by DUKE UNIV on June 5, 2012 | http://pubs.acs.org
Publication Date (Web): December 14, 2011 | doi: 10.1021/bk-2011-1088.ch005

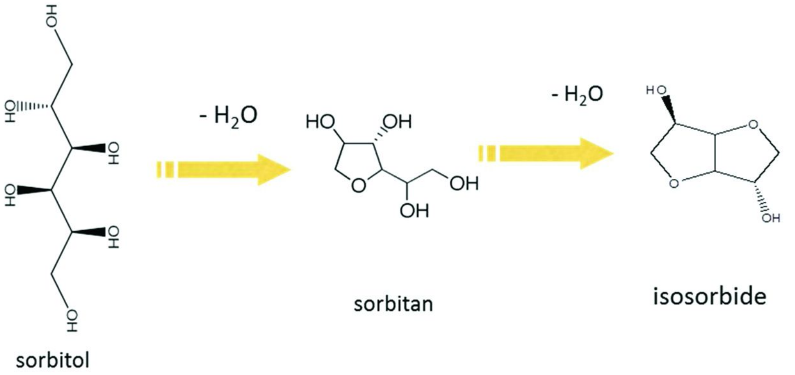
- H_2O
- H_2O
sorbitol
sorbitan
isosorbide

Figure 9. Serial kinetic pathway of the dehydration of sorbitol into isosorbide.

Isosorbide can be separated by extraction in an organic solvent at higher temperatures and further precipitated or separated in an aqueous phase at temperatures lower than 60 °C. Distillation or stripping can also be employed (*17*).

The combination of all these steps leads to a biorefinery, schematically given in Figure 10. Hemicellulose is chemically related to cellulose but it is more reactive, allowing a selective conversion at mild conditions. At more severe conditions cellulose is essentially quantitatively converted into glucose. Because the hemicellulose structure is less simple compared to cellulose more products are formed in the hydrolysis step. Several chemical conversion steps can be envisaged, giving a mix of products.

In the schematic biorefinery of Figure 10 both cellulose and hemi-cellulose are reacted in hydrolysis, hydrogenation, dehydration steps. Cellulose is converted nearly quantitatively into isosorbide, hemicellulose gives a more complex product mixture. Lignin can be separated by filtration and applied for generation of the energy needed. It can be also reformed to hydrogen or it can be subjected to a depolymerization step giving aromatic products.

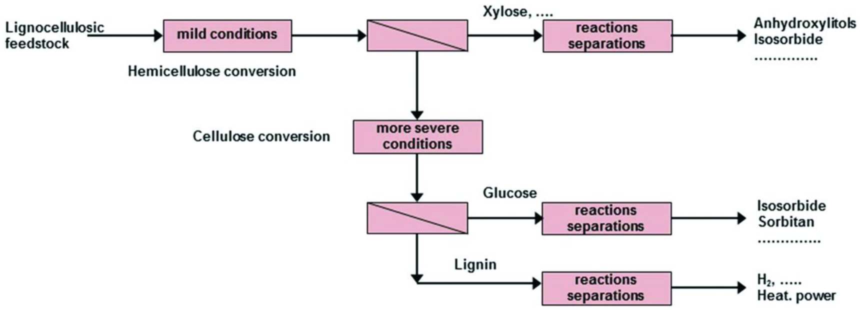
Lignocellulosic feedstock
mild conditions
Hemicellulose conversion
Xylose, ...
reactions separations
Anhydroxylitols
Isosorbide
....
Cellulose conversion
more severe conditions
Glucose
reactions separations
Isosorbide
Sorbitan
....
Lignin
reactions separations
H_2, ...
Heat. power

Figure 10. Schematic of biorefinery for lignocellulosic biomass based on hydrolysis.

Downloaded by DUKE UNIV on June 5, 2012 | http://pubs.acs.org
Publication Date (Web): December 14, 2011 | doi: 10.1021/bk-2011-1088.ch005

Given the expected large scale of biomass plants it is advisable to assess in an early stage of process development the economic value of the main products. Isosorbide is the largest bulk product. It has a molecular structure very similar to that of the monomer of cellulose. In this way isosorbide production is an efficient process as far as the chemistry and thermodynamic allow a feasible reaction pathway. Fortunately, isosorbide is an attractive platform molecule. Isosorbide is presently a commercial product (*18*) and it has applications in the fuel and the base chemical market. Options for these two markets is highly desired for large-scale products.

Biorefinery versus Oil Refinery

The biorefinery differs profoundly from the oil refinery in terms of feedstock properties, process technology, product spectrum, investments and environmental impact. Table IV gives a summary.

The oil refinery is associated with a high feedstock price and low-cost processing whereas for the biorefinery the opposite is the case: low-cost feedstock combined with high processing costs. The latter is due to several reasons such as a low energy density, a high water content, high separation costs.

Table IV. Comparison of a biorefinery and a fossil oil refinery

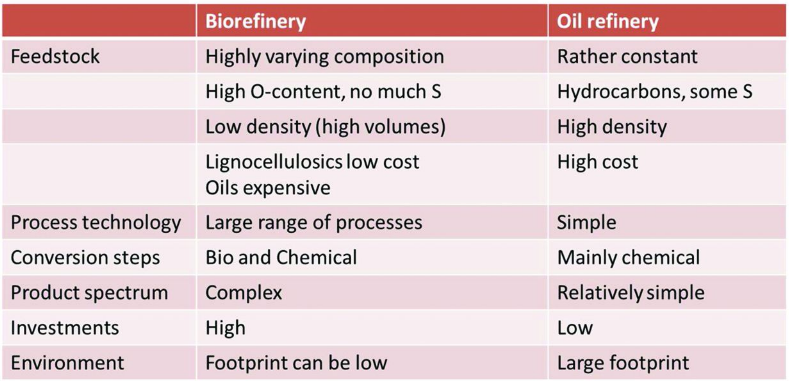

	Biorefinery	Oil refinery
Feedstock	Highly varying composition	Rather constant
	High O-content, no much S	Hydrocarbons, some S
	Low density (high volumes)	High density
	Lignocellulosics low cost Oils expensive	High cost
Process technology	Large range of processes	Simple
Conversion steps	Bio and Chemical	Mainly chemical
Product spectrum	Complex	Relatively simple
Investments	High	Low
Environment	Footprint can be low	Large footprint

A final remark on process design is the following. In biomass conversion large amounts of single molecules can be produced, a spectacular example is isosorbide in the presently described process. In this case the product mixture is simple (and not complex as stated in the Table IV) and a dedicated plant being a highly simplified version of a biorefinery might be possible, with great economics.

Conclusions, Evaluation

Biomass has a high potential both as energy carrier and as feedstock for the chemical industry. Lignocellulosics are plenty available and are the preferred biomass feedstocks. Instead of just substituting present day fossil derived fuel components and chemicals by biomass-based analogons it is better to judge the potential product spectrum of biomass conversion, taking into account the very different structure of biomass compared to fossil fuel feedstocks.

In view of the composition of biomass a biorefinery integrating several technological processes often is the best option. Because biomass is highly functionalized, dependent on the specific feedstock subtle technology in the liquid phase is most appealing. When we deal with a well-defined feedstock either a dedicated plant or a biorefinery is the best option. In all plants waste streams are present and robust, not specific technology is demanded: combustion, gasification and anaerobic fermentation usually will be most efficient.

Processing in the liquid phase calls for a suitable solvent. Metal hydrate solvents are promising and the potential for producing relevant platform molecules at high yields has been demonstrated.

Downloaded by DUKE UNIV on June 5, 2012 | http://pubs.acs.org
Publication Date (Web): December 14, 2011 | doi: 10.1021/bk-2011-1088.ch005

References

1. *World Energy Outlook 2008*, IEA Report, 2008.
2. Ladanai S.; Vinterbäck J. *Global Potential of Sustainable Biomass for Energy*, Report 013; Uppsala, Sweden, 2009, pp 1−32.
3. Hoogwijk, M.; Faaij, A.; Eickhout, B.; de Vries, B.; Turkenburg, W. *Biomass Bioenergy* **2005**, *29*, 225–257.
4. Land Available for Biomass Production for Energy. European Environment Agency. http://www.eea.europa.eu/data-and-maps/figures/land-available-for-biomass-production-for-energy.
5. *International Energy Outlook 2011*, DOE/EIA 0484; 2011.
6. Zakzeski, J.; Bruijnincx, P. C. A.; Jongerius, A. L.; Weckhuysen, B. M. *Chem. Rev.* **2010**, *110*, 3552–3599.
7. Brehmer, B.; Boom, R. M.; Sanders, J. *Chem. Eng. Res. Des.* **2009**, *87*, 1103–1119.
8. Puig-Arnavat, M.; Bruno, J. C.; Coronas, A. *Renewable Sustainable Energy Rev.* **2010**, *14*, 2841–2851.
9. Bridgwater, A. V. *Biomass Bioenergy* **2011**, in press.
10. Bulushev, D. A.; Ross, J. R. H. *Catal. Today* **2011**, in press.
11. Kamm, B.; Gruber, P. R.; Kamm, M. *Biorefineries – Industrial Processes and Products*; Wiley-VCH: Weinheim, 2006.
12. Cherubini, F. *Energy Convers. Manage.* **2010**, *51*, 1412–1421.
13. (a) Simmons, B. A.; Singh, S.; Holmes, B. M.; Blanch, H. W. *Chem. Eng. Proc.* **2010**, *106*, 50−55. (b) Zakrewska, M. E.; Bogel-Lukasik, E.; Bogel-Lukasik, L. *Energy Fuels* **2010**, *24*, 737−745.
14. Le Moigne, M. N., Ph.D. Thesis, Mines ParisTech, CEMEF, Paris, France, 2008.
15. Fischer, S.; Leipner, H.; Thümmler, K.; Brendler, E.; Peters, J. *Cellulose* **2003**, *10*, 227–236.
16. Menegassi de Almeida, R.; Li, J.; Nederlof, Ch.; O'Connor, P.; Makkee, M.; Moulijn, J. A. *Chem. Sus. Chem.* **2010**, *3*, 325–328.

17. (a) Brinegar, W. C.; Wohlers, M.; Hubbard, M. A.; Zey, E. G.; Kvakovszky, G.; Shockley, T. H.; Roesky, R.; Dingerdissen, U.; Kind, W. Patent WO 00/14081, E. I. du Pont de Nemours and Company, 2000. (b) Plucinski, J.; Durda, W.; Sinicka, S. *Stud. Mater. Monogr. - Inst. Med. Pr.* **1971**, *3*, 3–14. (c) Bhatia, K. K. U.S. Patent 6 864378, E. I. du Pont de Nemours and Company, 2005.
18. Rupp-Dahlem, C. http://www.projects.science.uu.nl/brew/BREWsymposiumWiesbaden11mei2005/WEBSITEBREWDECHEMA%20pr%E9sentationCRD.pdf.

Downloaded by DUKE UNIV on June 5, 2012 | http://pubs.acs.org
Publication Date (Web): December 14, 2011 | doi: 10.1021/bk-2011-1088.ch005

Downloaded by UNIV OF GUELPH LIBRARY on June 5, 2012 | http://pubs.acs.org
Publication Date (Web): December 14, 2011 | doi: 10.1021/bk-2011-1088.ch006

Chapter 6

Biosyngas Generation via Gasifaction of Biomass, Gas Cleaning, and Fuel Gas Upgrading

W. de Jong[*]

Delft University of Technology, Faculty 3mE,
Department of Process & Energy Technology,
Energy Technology Section, Leeghwaterstraat 44,
NL-2628 CA Delft, The Netherlands
[*]E-mail: Wiebren.deJong@tudelft.nl

Mankind uses biomass since long as food, heating and lighting source. Nowadays this renewable energy source is recognized as feedstock for combined heat and power (CHP), but increasingly for biorefineries producing chemicals, materials and fuels. Now, sustainable supply chains should be set up. Biomass conversion technology systems have been developed based on (co-)combustion, torrefaction, pyrolysis, gasification using various oxidizers, hydrolysis and anaerobic digestion. An overview is given concerning gasification for syngas generation, suitable for production of hydrogen, Fischer-Tropsch diesel, alcohols, and natural gas. Challenges result from fuel characteristics and the gasification technology determines whether pre-treatment is needed. Wet fuels are preferably processed locally using supercritical water conditions. Drier biomasses are rather converted via steam-oxygen fluidized bed and entrained flow gasification. Gas cleaning is a major issue for catalytic processes with strict limitations on particle, tar, sulphur and trace element concentrations. The paper addresses advances in research and development concerning reactor development, raw syngas cleaning and upgrading.

In Production and Purification of Ultraclean Transportation Fuels; Hu, Y., et al.;
ACS Symposium Series; American Chemical Society: Washington, DC, 2011.

Downloaded by UNIV OF GUELPH LIBRARY on June 5, 2012 | http://pubs.acs.org
Publication Date (Web): December 14, 2011 | doi: 10.1021/bk-2011-1088.ch006

1. Introduction

Biomass is being rediscovered as an attractive stored solar energy source (*1*). Major reasons for this renewed interest in biomass are that it is renewable –contrary to fossil fuels that run out-, to a large extent CO_2-neutral, widely available and it can be processed resulting in versatile energy carriers and other products. This can be achieved using technologies that exceed the widespread, traditional usage of burning for cooking. This traditional use, still applied in under developed, poor countries on a substantial scale, is associated with health issues of indoor smoke formation and substantial ineffective manual labor. Modern biomass utilization concerns highly efficient systems based on combustion for direct power and heat usage, pyrolysis leading to bio-oil production and gasification by which a gas is produced which can serve further versatile usage, like e.g. efficient combined heat and power production, chemicals and fuel production.

As the energy demand increases due to increasing (globalized) industrialization and population growth, indeed highly efficient systems for biomass conversion are required. Of course in this respect the whole chain must be considered and issues like competition with food, water usage, nutrients resupply and maintaining biodiversity on our planet should be dealt with from a sustainability point of view.

Biomass mainly consists of three major constituents: cellulose, hemi-cellulose and lignin. Besides those species, oxygen containing extractives may form a substantial part and of course moisture and mineral matter. Some biomasses contain high contents of lipids and/or proteins. The relative amounts of these determine the suitability of the fuel for a specific conversion technology and whether and which pre-treatment is needed.

Is it available in abundance? The current total energy demand in the world is around 12 GToe (*2*). Though yearly global biomass growth exceeds this number, truly sustainably produced biomass expectedly cannot cover this global primary energy next to food, fiber, materials, and chemicals demand, but a significant amount can be provided though, next to other sustainable sources. Based on different studies, Hoogwijk et al. (*3*) indicate 50 EJ as a very minimum in a scenario with bioresidues as main source. A recent report indicates that in the central and eastern European countries already 6-12 EJ could be provided by biomass plantations and that in the EU 20% of the fuels can be based on biomass (*4*). This would seriously contribute to Europe's SET plan that was issued recently, aiming at a reduction of fossil fuel usage by 20%, a CO_2 emission reduction of 20% compared to 1990, and an increase in the renewable energy share to 20% by 2020 (*5*).

One characteristic of biomass is that it is more evenly spread throughout the world than fossil energy sources, which will be advantageous for many countries and this will lead to less geo-political issues. Moreover, intensive agricultural practice will enhance rural development and its associated creation of meaningful jobs.

Among different biomass conversion technologies, this paper focuses on thermo-chemical conversion of *biomass to syngas via gasification* as it concerns a technology that can process versatile biomass sources into a spectrum of possible products while using the whole biomass. Syngas indeed is a flexible platform for generation of different chemicals and fuels. Figure 1 shows some of the main catalytic conversion routes of syngas to a spectrum of products, indicating the main catalysts used.

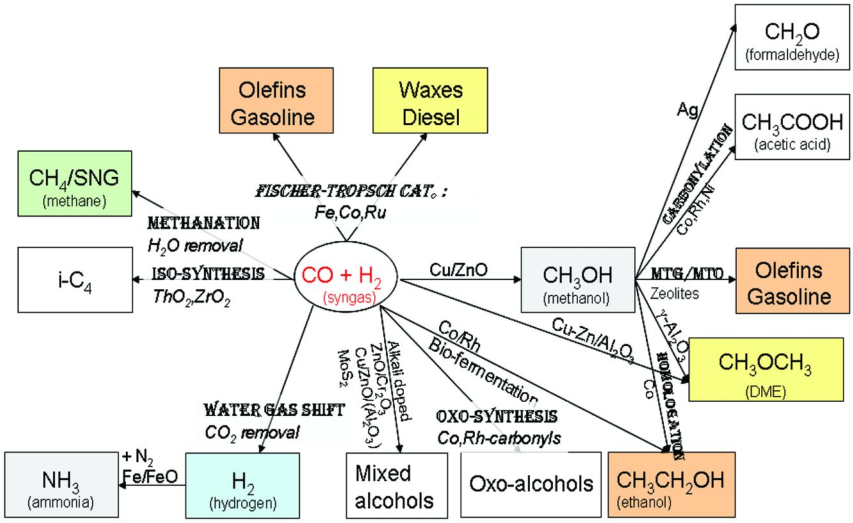

CH_2O (formaldehyde)
Olefins Gasoline
Waxes Diesel
CH_3COOH (acetic acid)
Ag
CARBONYLATION
Co,Rh,Ni
CH_4/SNG (methane)
FISCHER-TROPSCH CAT. : Fe,Co,Ru
METHANATION
H_2O removal
i-C_4
ISO-SYNTHESIS
ThO_2,ZrO_2
CO + H_2 (syngas)
Cu/ZnO
CH_3OH (methanol)
MTG/MTO
Zeolites
Olefins Gasoline
γ-Al_2O_3
Cu-Zn/Al_2O_3
CH_3OCH_3 (DME)
Co/Rh
Bio-fermentation
HOMOLOGATION
Co
Alkali doped ZnO/Cr_2O_3 Cu/ZnO/(Al_2O_3) MoS_2
WATER GAS SHIFT
CO_2 removal
OXO-SYNTHESIS
Co,Rh-carbonyls
NH_3 (ammonia)
+ N_2 Fe/FeO
H_2 (hydrogen)
Mixed alcohols
Oxo-alcohols
CH_3CH_2OH (ethanol)

Figure 1. The syngas platform for production of widely varying energy carriers.

The conversion of biomass into syngas offers the combined advantage of a flexible, renewable and potentially sustainable source for this platform, which is illustrated by Figure 2. Moreover, it is a technology that can very well be scaled up to the large industrial sizes needed for (transportation) biofuel production purposes. Furthermore, the technology has been demonstrated widely industrially for coal conversion using widely varying coal qualities on large scale and medium-scale biomass (co-)gasification technology demonstrations have shown to be successful.

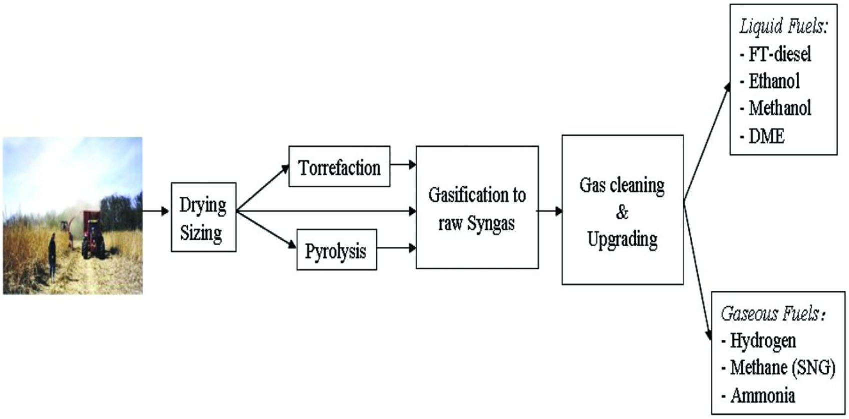

Drying
Sizing
Torrefaction
Pyrolysis
Gasification to raw Syngas
Gas cleaning & Upgrading
Liquid Fuels:
- FT-diesel
- Ethanol
- Methanol
- DME
Gaseous Fuels:
- Hydrogen
- Methane (SNG)
- Ammonia

Figure 2. Biomass to biofuels conversion schematic for relatively dry biomass.

Downloaded by UNIV OF GUELPH LIBRARY on June 5, 2012 | http://pubs.acs.org
Publication Date (Web): December 14, 2011 | doi: 10.1021/bk-2011-1088.ch006

Biomass gasification is a complex thermo-chemical process, involving many different reactions. The fuel is mainly converted into a mixture of hydrogen, carbon monoxide, carbon dioxide, methane and water. This mixture is also known as bio-syngas. The biomass gasification process can be divided into different parts, drying, pyrolysis and gasification. Pyrolysis is the thermal decomposition of the main organic constituents (carbohydrates and lignin mostly) into fragments, char, permanent gases and tars (also called bio-oil). In the gasification part the gasses, bio-liquid and char react further. During gasification hundreds of different reactions take place. The most important ones of these reactions are given in equations (1.1)-(1.13) (*6–8*). In these equations, char is assumed to consist only of carbon (C(s)), and tar to be C_nH_m.

$$C(s) + O_2 \rightarrow CO_2 \qquad \Delta_r H^0_{298} = -394 \text{ kJ/mol} \tag{1.1}$$

$$C(s) + ½ O_2 \rightarrow CO \qquad \Delta_r H^0_{298} = -111 \text{ kJ/mol} \tag{1.2}$$

$$C(s) + H_2O \leftrightarrow CO + H_2 \qquad \Delta_r H^0_{298} = +131 \text{ kJ/mol} \tag{1.3}$$

$$C(s) + CO_2 \leftrightarrow 2\,CO \qquad \Delta_r H^0_{298} = +173 \text{ kJ/mol} \tag{1.4}$$

$$C(s) + 2H_2 \leftrightarrow CH_4 \qquad \Delta_r H^0_{298} = -75 \text{ kJ/mol} \tag{1.5}$$

$$CO + ½ O_2 \rightarrow CO_2 \qquad \Delta_r H^0_{298} = -283 \text{ kJ/mol} \tag{1.6}$$

$$H_2 + ½ O_2 \rightarrow H_2O \qquad \Delta_r H^0_{298} = -242 \text{ kJ/mol} \tag{1.7}$$

$$CO + H_2O \leftrightarrow CO_2 + H_2 \qquad \Delta_r H^0_{298} = -41 \text{kJ/mol} \tag{1.8}$$

$$CH_4 + H_2O \leftrightarrow CO + 3H_2 \qquad \Delta_r H^0_{298} = +206 \text{kJ/mol} \tag{1.9}$$

$$C_nH_m\ (tars) + nH_2O \leftrightarrow n\,CO + (n+m/2)\,H_2 \tag{1.10}$$

$$C_nH_m\ (tars) + nCO_2 \leftrightarrow 2n\,CO + m/2\,H_2 \tag{1.11}$$

$$C_nH_m\ (tars) \leftrightarrow n\,C + (n+m/2)\,H_2 \tag{1.12}$$

$$C_nH_m\ (tars) + (4n-m)/2\,H_2O \leftrightarrow n\,CH_4 \tag{1.13}$$

The gasification process is usually performed with the aid of an added oxidizer. This can be steam, or air, or enriched air, or oxygen, or a combination of steam and an oxygen source, or carbon dioxide. Heat supply to drive the endothermic reactions can be provided in-situ by exothermic partial oxidation

Downloaded by UNIV OF GUELPH LIBRARY on June 5, 2012 | http://pubs.acs.org
Publication Date (Web): December 14, 2011 | doi: 10.1021/bk-2011-1088.ch006

or indirectly by integration with an external exothermic process which transfers heat to the main gasification reactor. The process is operated at relatively high temperatures, roughly ranging from 873 to 1773K depending on the reactor type and the pressure can range from atmospheric pressure up to 7 MPa. Neglected in the abovementioned main reaction overview are other elements. However, for the production of ultra-clean fuels via the gasification route, the chemistry and removal of the small amounts of impurities in the gas is of the utmost importance: particulates, tars, alkalis, nitrogen compounds, sulphur compounds, and chlorine compounds. The following chapters concentrate on gasification techniques for clean syngas production and the subsequent gas cleaning and upgrading.

Downloaded by UNIV OF GUELPH LIBRARY on June 5, 2012 | http://pubs.acs.org
Publication Date (Web): December 14, 2011 | doi: 10.1021/bk-2011-1088.ch006

2. Gasification Technologies

In the 19th century gasification was already common due to production of so called 'Town gas' based on coal; a two step process of pyrolysis and steam blowing of the remaining char. The period of the Second World War during which limited resources were available gave rise to an upcoming of biomass for gasification to generate gas for transportation purposes. Only shortly after the war, the real oil era started, which was characterized by cheap oil and biomass utilization trend was abandoned until it received the people's attention again after oil crises in the 1970ies during which time boundaries to the growth (*9*) were recognized. The past decade showed an increased momentum in development of biomass gasification related to the need for green transportation fuels with a minimum impact on net CO_2 emissions, competition with food and feed production and land usage.

Quite a variety of chemical reactors for thermo-chemical gasification of biomass are under development at different commercial companies and research institutes. Since the first (controlled) attempts regarding thermo-chemical gasification of biomass a number of reactor designs evolved considered as suitable for that process. These reactors are:

* fixed beds: updraft, downdraft, crossdraft;
* fluidized beds: bubbling, circulating, dual;
* entrained flow reactors.

Although each of these reactor types is capable of gasifying biomass, also each of them is a compromise between the product gas quality, conversion efficiency, suitability for handling of the feedstock with varying physical and chemical properties, the complexity and scalability of the design, complexity of the operation, and the investment costs.

Figure 3 illustrates the size range of application of the abovementioned classes of gasifiers; it also includes examples of current demonstrations and (semi-)commercial activities.

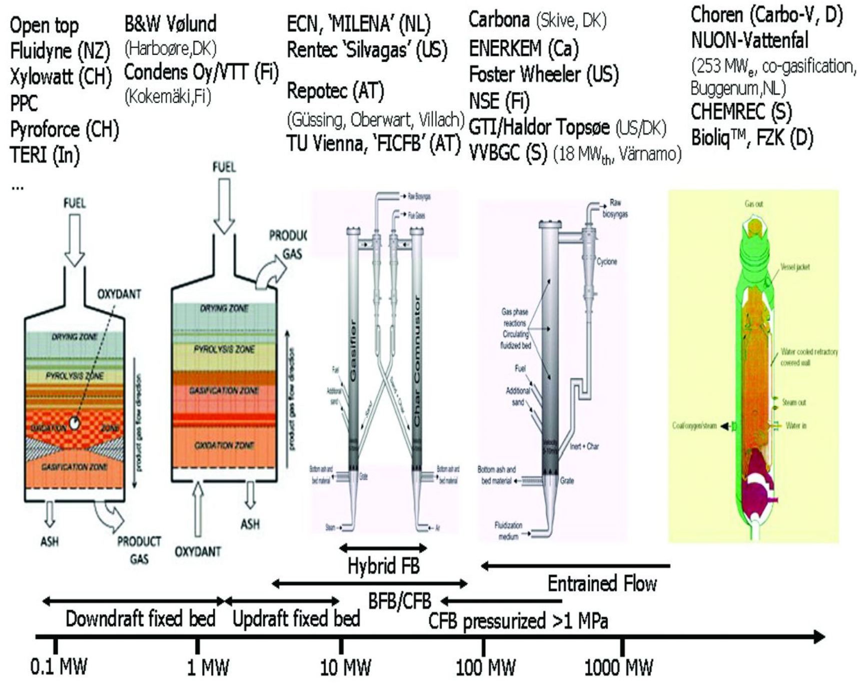
Open top
Fluidyne (NZ)
Xylowatt (CH)
PPC
Pyroforce (CH)
TERI (In)
...
B&W Vølund
(Harboøre,DK)
Condens Oy/VTT (Fi)
(Kokemäki,Fi)
ECN, 'MILENA' (NL)
Rentec 'Silvagas' (US)
Repotec (AT)
(Güssing, Oberwart, Villach)
TU Vienna, 'FICFB' (AT)
Carbona (Skive, DK)
ENERKEM (Ca)
Foster Wheeler (US)
NSE (Fi)
GTI/Haldor Topsøe (US/DK)
VVBGC (S) (18 MWth, Värnamo)
Choren (Carbo-V, D)
NUON-Vattenfal
(253 MWe, co-gasification, Buggenum,NL)
CHEMREC (S)
Bioliq™, FZK (D)
FUEL
OXYDANT
DRYING ZONE
PYROLYSIS ZONE
OXIDATION ZONE
GASIFICATION ZONE
product gas flow direction
ASH
PRODUCT GAS
FUEL
PRODUC GAS
DRYING ZONE
PYROLYSIS ZONE
GASIFICATION ZONE
OXIDATION ZONE
product gas flow direction
ASH
OXYDANT
Gasifier
Char Combustor
Raw biosyngas
Cyclone
Gas phase reactions
Circulating fluidized bed
Fuel
Additional sand
Inert + Char
Bottom ash and bed material
Grate
Fluidization medium
Gas out
Vessel jacket
Water cooled refractory covered wall
Steam out
Water in
Coal/oxygen/steam
Hybrid FB
Entrained Flow
BFB/CFB
Downdraft fixed bed
Updraft fixed bed
CFB pressurized >1 MPa
0.1 MW
1 MW
10 MW
100 MW
1000 MW

Figure 3. Overview of biomass gasifiers, their ranges and some applications.

2.1. Fixed and Moving Bed Gasifiers

The first class mentioned above, fixed bed (also called moving bed) reactors, are in particular suitable for small-scale operation of the order of a few MW_{th}. The downdraft gasifier is a co-current reactor, where the fuel and the gasification agent move in the same direction.

In Figure 4, a schematic representation is given of this reactor. The downdraft gasifier is characterized by different reaction zones: a drying zone in which moisture is evaporated from the biomass as it slowly descents towards the pyrolysis zone; a pyrolysis zone in which the biomass is converted into char, tars and gasses. Some of the pyrolysis products are combusted in the underlying combustion zone. Due to the high temperature in this combustion zone, tars are cracked. As a result, the produced gas is relatively clean, i.e. with low tar concentrations. This gasifier is simple, reliable and has been proven for certain fuels, such as relatively dry blocks or lumps with a low ash content and containing a low portion of fine and coarse particles (*10*). The physical limitations of the diameter and the particle size relation means that there is a upper limit to the capacity of this configuration of around 500 kg h^{-1} (*10*).

Another configuration of the fixed bed gasifier is the updraft gasifier, a counter-current reactor, in which the fuel and the gasification agent move in opposite directions. In Figure 4, a schematic representation of an updraft gasifier

Downloaded by UNIV OF GUELPH LIBRARY on June 5, 2012 | http://pubs.acs.org
Publication Date (Web): December 14, 2011 | doi: 10.1021/bk-2011-1088.ch006

Downloaded by UNIV OF GUELPH LIBRARY on June 5, 2012 | http://pubs.acs.org
Publication Date (Web): December 14, 2011 | doi: 10.1021/bk-2011-1088.ch006

is given (left). In the updraft gasifier, the biomass is dried by the hot producer gas, in the drying zone. Further down in the bed the biomass is pyrolyzed, the resulting char moves further down the bed. The tars and gasses follow the updraft flow in the reactor. Part of the tars will condense on the solid particles in the bed; the residual tars will remain in the gas and leave the reactor. The char slowly descents down towards the combustion zone where it is gasified. The gas produced in an updraft gasifier is characterized by a relatively high tar content and hydrocarbon content, which leads to comparatively high heating value of the gas. This producer gas needs significant cleaning before it can be processed further.

Finally, regarding fixed bed gasifier configurations, the cross-draft gasifier can be mentioned. In a cross-draft gasifier the fuel and gasification agent move perpendicular to each other, which is shown in Figure 2 at the right hand side. The cross-draft gasifer is only suitable for the gasification of charcoal. The temperatures in the combustion zone can rise to 1500°C. The construction material of the reactor has to withstand the high temperature in the reactor. Like the updraft gasifier, the cross-draft gasifier has a low tar conversion. Therefore, a high quality charcoal has to be used.

For bio-syngas generation on large-scale these gasifiers are not attractive due to their relatively small scale. Two other classes of reactors, the fluidized bed and entrained flow gasifiers can be scaled up to the large sizes needed for bio-syngas production in view of transportation fuel production.

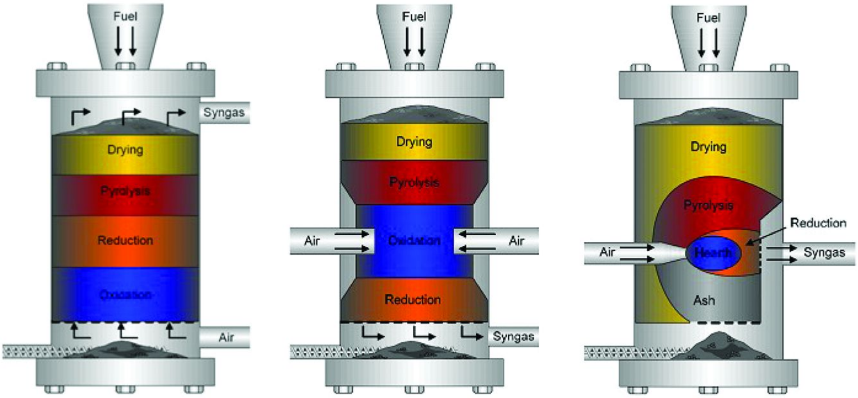

Figure 4. Diverse fixed bed reactor types: Updraft (left), downdraft (mid) and cross-draft (right), adapted with permission from Olofsson et al. (11).

2.2. Entrained Flow Gasifiers

Entrained flow (EF) gasifiers are designed for the large-scale operation (>> 100 MW_{th}) on varying fuels. The operating temperatures applied in these EF gasifiers range from approximately 1200 to 1500 °C. They are mostly operated using varying coal types. EF gasifiers generally use fuel in the form of powder or slurry. The fuel is then mixed with steam, or steam and oxygen, and gasified in a powder flame. When using biomass as fuel, it must either be ground to a powder or in some cases pyrolysed to gas, oil and coke, the latter again needs to be ground or converted to slurry. Manufacturers for "Slagging" gasifier types are Shell, Texaco, Krupp-Uhde, Future-Energy (formerly Noell / Babcock Borsig Power), Conoco-Phillips (E-gas technology, formerly Destec / Dow), MHI (Mitsubishi Heavy Industries), Hitachi and Choren (formerly UET, Germany).

Coal gasification was the initial application of the entrained flow type of gasifier, in the past century fifties by Koppers. Koppers-Totzek slagging gasifiers operating at atmospheric pressure for syngas production aimed at the production of ammonia (NH_3). The gasifier is characterized by coal and oxygen being fed via pairs of opposed burners inside niches on the side parts of a typically egg-shaped reactor. At the top part of the reactor the produced raw syngas leaves the reactor at max. about 1500 °C and this is rapidly cooled down using water to a temperature of about 900 °C, and it is cooled down further in a syngas cooler in which steam is produced. Such quenching is crucial to prevent sticky slag droplets entering and depositing on the heat exchanger. A steam jacket as reactor wall protects the steel from high temperatures. Slag which is produced mainly descends the reactor via a bottom hole.

The Prenflo and Shell Coal Gasification Process (SCGP) are processes developed later and are pressurised versions (30-40 bar) of the Koppers-Totzek process with a higher efficiency. They maintain the feature of diametrically opposed burners inside side niches of the vertically mounted cylindrical reactor. A gas quench has replaced the water quench. Also, in the processes membrane walls are applied instead of a steam jacket to protect the pressure shell from too high temperatures. These walls are used for generation of high pressure saturated steam for additional power production. Aimed at power production, the developments lead to the erection of a 2000 ton/day SCGP unit in Buggenum (The Netherlands) and a 3000 ton/day Prenflo unit in Puertollano (Spain). Both gasifiers form the heart an IGCC unit for electricity production. The power producing company NUON has demonstrated co-firing of coal with chicken manure in the Buggenum plant upto about 30wt% biomass share using the (modified) Shell process based 253 MW_e plant for electricity production, see e.g. Van Dongen and Kanaar (*12*). The concept and reactor technology can be extended to polygeneration of heat, power and syngas based chemicals. General Electric (GE) owned Texaco gasification process is also of the entrained flow type, with the main difference being that the fuel is fed as a water-slurry, whereas Koppers-Totzek and Shell based coal gasifiers use some steam. Future Energy GmbH owns a down-fired entrained flow reactor. Instead of burners in side of the reactor, this gasifier only consists of a single burner in the top part, which results in a simpler and lower cost reactor. Also, the control of this single burner is easier than the former types mentioned with a resulting lower capital and operational cost related. The German company Choren has developed a three-stage gasification process involving the following sub-processes:

1) low temperature pyrolysis/gasification;
2) high temperature gasification;
3) endothermic entrained flow gasification.

Downloaded by UNIV OF GUELPH LIBRARY on June 5, 2012 | http://pubs.acs.org
Publication Date (Web): December 14, 2011 | doi: 10.1021/bk-2011-1088.ch006

The initial process step comprises of a carbonization of relatively dry biomass (moisture contents varying up to 15-20 wt%) using partial oxidation with air/oxygen at mild temperatures of 400-500 °C. In this stage volatiles and char are formed as products. The second process step comprises the under-stoichiometric combustion of the generated volatiles with oxygen and/or air in a combustion chamber that operates above the melting point of the fuel's ash to turn it into a hot gasification medium. The third stage, finally, consists of char grinding to a pulverized fuel that is blown into the hot gasification medium created in the entrained flow reactor of the second stage (bottom part). The pulverized fuel here reacts in an endothermic process that generates a raw syngas. Further treatment of cooling and cleaning follow. The syngas can be used for different purposes, nowadays the focus is on diesel fuel production, called SunDiesel.

Downloaded by UNIV OF GUELPH LIBRARY on June 5, 2012 | http://pubs.acs.org
Publication Date (Web): December 14, 2011 | doi: 10.1021/bk-2011-1088.ch006

2.3. Fluidized Bed Gasifiers

There exist a number of basic designs of fluidized bed gasifiers. They are targeted at the mid-scale thermal capacities of 10 MW_{th} to large scale capacities of more than 100 MW_{th}. An inert or catalytic bed material is used to facilitate heat and mass transfer throughout the reactor. The bed is kept in a fluidized state by blowing a gasification agent through it, lifting the bed against gravity. Herewith, the turbulence in the bed creates an even temperature distribution in the bed. Thus no different distinct reaction zones are displayed in the bed, like in the case of fixed bed gasifiers. The prevailing temperatures in a fluidized bed are usually in the range of 700-900°C and the reactors are operated with gauge pressures between 0 and 70 bar. Even within the relatively low operating temperature, bed sintering is a common problem when a biomass with a high ash content is used. The alkali components in the ash, facilitated by Chlorine, have the tendency to form low-melting eutectics with silica being the most common bed material. These eutectics cause bed agglomeration and bed sintering, which can lead to loss of fluidization (*13*, *14*).

The most common types of fluidized beds are the bubbling fluidized bed (BFB) and the circulating fluidized bed (CFB). Also, hybrid forms, or interconnected fluidized bed reactors are encountered in modern designs. Figure 5 shows the basic reactor configurations (*11*).

In a bubbling fluidized bed, the gasification agent is blown through the bed in such a way that it forms bubbles in the bed. The gas velocity is above the minimal fluidization velocity and below the maximal settling velocity. Therefore, the bed material remains in the reactor.

In the BFB design configuration, the majority of the gasification reactions take place in the dense fluidized bed part. Some reactions, especially thermal cracking reactions and the gasification of entrained small particles continue in the freeboard. The carbon conversion in the process is well above 90%, due to the high residence time of the biomass particles and the residual conversion when entrained to the freeboard. The tar content of the gas is in between the tar content of the downdraft and updraft gasifiers. Example: steam-oxygen blown gasifier developed by IGT, now commercially manufactured by Carbona.

Downloaded by UNIV OF GUELPH LIBRARY on June 5, 2012 | http://pubs.acs.org
Publication Date (Web): December 14, 2011 | doi: 10.1021/bk-2011-1088.ch006

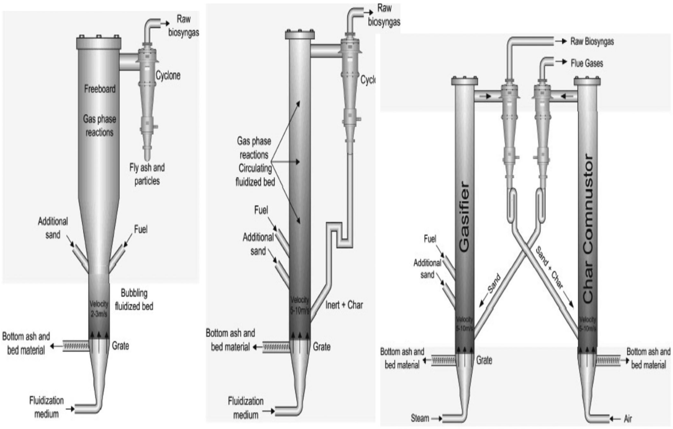
Raw biosyngas
Cyclone
Freeboard
Gas phase reactions
Fly ash and particles
Additional sand
Fuel
Bubbling fluidized bed
Velocity 2-3m/s
Bottom ash and bed material
Grate
Fluidization medium
Raw biosyngas
Cycl
Gas phase reactions
Circulating fluidized bed
Fuel
Additional sand
Velocity 5-10m/s
Inert + Char
Bottom ash and bed material
Grate
Fluidization medium
Raw Biosyngas
Flue Gases
Gasifier
Char Comnustor
Fuel
Additional sand
Sand
Sand + Char
Velocity 5-10m/s
Bottom ash and bed material
Grate
Bottom ash and bed material
Steam
Air

Figure 5. Configurations of fluidized bed reactors: bubbling fluidized bed (BFB, left), circulating fluidized bed (CFB, mid), and interconnected (indirect) fluidized beds (right). Adapted with permission from Olofsson et al. (11).

In a CFB gasifier, the oxidizing gas is introduced into the reactor with such a high velocity that large amounts of the solids are entrained with the product gas. The entrained solids are separated from the gas in a cyclone and recycled back to the gasifier. The CFB has a high carbon conversion efficiency (typically >95%), because of the recycling of the bed material. The raw product gas generated by a CFB gasifier has a relatively high dust content. Example of this technology: the 18 MW_{th} Värnamo (Sweden) pressurized gasifier.

Besides the BFB and the CFB there are also designs of gasification installations based on multiple, interconnected beds. An exellent overview is given by Corella et al. (*15*). Recent examples are the Fast Internal Circulating Fluidized Bed (FICFB) reactor concept developed at Vienna University (*16*, *17*) – now commercialized, see Table I- designed as a steam blown BFB in which biomass is gasified and char is carried over to an interconnected CFB combustor which provides heat for the endothermic reactions in the BFB reactor via internal transportation of hot bed material. Moreover, the SilvaGas process can be mentioned, which was initially developed at the Battelle Columbus labs (USA) and is characterized by two interconnected CFB’s of which one is a steam-blown gasifier of biomass and the second one a char combustor storing heat into bed material that is circulated to the gasifier reactor. Finally, the MILENA concept (*18*) developed at ECN (The Netherlands) in which the central part is a riser based on steam blown biomass gasification and an annular space is designed for combusting the char from the core part.

Table I shows an overview of large-scale fluidized bed biomass gasification demonstrations.

Table I. Some of the main fluidized bed biomass gasification demonstrations

Project / demo	*Gasifier, thermal input*	*Product gas use*	*Current status*
Güssing (Austria)	Interconnected FICFB, ~8 MW_{th}	CHP (*17*), Demo-FT (*19*) Demo-SNG	Running
Oberwart(Austria)	Interconnected FICFB, ~8 MW_{th}	CHP	Running
Villach (Austria)	Interconnected FICFB,~15 MW_{th}	CHP	Commissioned
Skive (Denmark)	BFB 28 $MW_{th,max}$	CHP	Running
NSE Biofuels, Varkaus (Finland)	CFB (Foster Wheeler) ~12 MW_{th}	Lime kiln, Demo-FT	Commissioned
HVC,Alkmaar (Netherlands)	Interconnected MILENA 10 MW	SNG (*18*)	Development
AMER (Netherlands)	CFB 84 MW_{th}	Co-firing (*20*)	Running
Värnamo (Sweden)	FosterWheeler, CFB (airblown) 18 MW	CHP (*21*)	Mothballed, after last demo in 2007; restart expected later

Downloaded by UNIV OF GUELPH LIBRARY on June 5, 2012 | http://pubs.acs.org
Publication Date (Web): December 14, 2011 | doi: 10.1021/bk-2011-1088.ch006

Factors that play a decisive roles in the selection of employing a certain reactor design for biomass gasification are:

- scale of the energy conversion process;
- feedstock flexibility (particle sizes and fuel composition);
- sensitivity to the amount of ash and its composition;
- tar generation characteristics.

The process scale of operation is most probably the primary criterion. Small, decentralized systems will benefit from a simple, easy to control and maintain, and cheap reactor. Here the feedstock is probably well-defined based on local conditions. On the other hand, a Biomass-to-Liquid (BTL) plant or maybe even a biorefinery, where the gasifier is only one of the units-of-operation will benefit from the larger scale of the reactor in terms of its thermal efficiency and the economy-of scale.

The feedstock flexibility is another issue. The structural appearance of biomass is often fibrous and tough and it will consequently be difficult to cut or pulverize. Therefore it is not desirable to reduce the biomass in size too much, because of the adverse effect on the energy efficiency of the whole process. Additionally, raw biomass is not dry, but contains a varying amount of moisture. Considering the above, the gasification reactor should be able to cope with the changes in fuel supply characteristics, which are both physical and chemical in nature.

Next to the moisture and volatile fraction, biomass also contains inorganic matter, usually referred to as ash. This ash forming matter can be variable in composition. In general wood has low ash contents with calcium and silica as main constituents, however agricultural residues can contain appreciable amounts of alkalimetals (potassium, sodium) and chlorine which can pose challenges to fluidized bed reactors (agglomeration) as well as entrained flow gasifiers (slagging and fouling).

While ash-related issues may lead to difficulties in process operation and unscheduled maintenance stops, the tar produced in the gasifier may affect the downstream equipment in a negative way, resulting in the need for downstream gas treatment and upgrading. ”Tar” is an umbrella term for various kinds of larger hydrocarbons produced during gasification. There are diverse definitions of the term, but there is a broadening global consensus in defining biomass tar as organic contaminants with a molecular weight larger than benzene (*22*, *23*), comparable to a European standard -CEN/TS 15439- for quantifying tars (*24*). Tar formation is a commonly encountered issue in gasification processes (*23*, *25–27*). Although the main issues related to tar are formed by condensation in the equipment downstream the gasifier, that operates at lower temperatures (typically below 500°C), tar also significantly contributes to the heating value of the product gas. So gas cleaning is needed with respect to this class of contaminants, which will be addressed in the next chapter.

Downloaded by UNIV OF GUELPH LIBRARY on June 5, 2012 | http://pubs.acs.org
Publication Date (Web): December 14, 2011 | doi: 10.1021/bk-2011-1088.ch006

2.4. Comparison of Gasification Technologies

An overview of the characteristics of the different gasifier technologies for the larger scale applications –so excluding the fixed and moving bed types, as these are less relevant for large-scale syngas generation- is given in Table II. The major challenges for fluidized bed gasification are in gas cleaning from particles and tars in particular, as well as agglomeration prevention. On the other hand the main challenges for entrained flow gasifiers are biomass pre-treatment to obtain finely sized fuel and slagging/fouling of heat transfer surfaces.

A development for future application is the gasification of very wet feedstock using supercritical water process conditions. Either tubular reactors can be used for this purpose or fluidized beds (*28–30*). Challenges here are construction material application due to corrosive conditions under comparatively extreme conditions and also clogging due to decreased solubilities of mineral content.

Downloaded by UNIV OF GUELPH LIBRARY on June 5, 2012 | http://pubs.acs.org
Publication Date (Web): December 14, 2011 | doi: 10.1021/bk-2011-1088.ch006

Table II. Comparison of different gasifier types

Advantages	*Disadvantages*
(Bubbling) Fluidised bed	
Flexible feed rate and composition	Operating temperature limited by ash melting temperature
High ash fuels acceptable	High tar and fine particle content in gas
High volumetric capacity	Possibility of high C content in fly ash
Temperature distribution	
Circulating fluidised bed	
Easy to scale up to medium/large scale	Corrosion and attrition problems
Medium operating temperature (about 850 °C)	Potential for agglomeration
Double (Indirect) fluidised bed	
Oxygen not required	More tar due to lower bed temperature
Temperature distribution	Difficult to operate under pressure
	Scalability more limited than common BFB/CFB
Entrained flow	
Very low tar and CO_2	Severe feedstock size reduction required
Flexible feedstock	Complex operational control
Exit gas temperature	Carbon loss with ash
	Due to high gasifier temperature, higher exergy loss
	Ash slagging

3. Gas Cleaning and Upgrading to Fuel Quality

The effects the contaminants in the product gas from biomass gasification can demonstrate are both ‘mechanical’ and ‘chemical’. To first category fouling belongs, leading to loss of surface. To the second one coking by carbonaceous species giving rise to loss of surface and plugging; moreover, poisoning by chemical adsorption is an important issue. Not directly related to contaminants in the gas - but for sure an issue that is ‘mechanical’ in nature - is catalyst particle failure leading to bed channeling and/or plugging. Finally, -also not immediately related to contaminants- catalyst deactivation in hot gas environment can take place due to component volatilization, phase changes, compound formation and sintering (*31*).

In order to meet the strict requirements of the materials used in downstream catalytic upgrading reactors, the gasification product gas must be cleaned from its contaminants. One can distinguish such gas cleaning into low temperature cleaning using scrubbers on the one hand and on the other hand hot gas cleaning. Scrubbers can be effective in removing solids and tars in particular (*32*, *33*). However, their disadvantage is that both cooling and re-heating must take place in gasification technology chains including them. Such operations are at the expense of overall process efficiency. Moreover, they create multi-component liquid streams that require either their own cleaning strategies or a recycle, complicating the process thereby (*31*). Thus in process schemes for production of syngas there are advantages of high temperature, dry gas cleaning using filters and catalysts. The challenges here are formed by (long term) filtration behaviour and catalyst performance reduction by four factors; activity, sulphur poisoning, carbon formation and sintering (*34*). In this contribution we focus on hot, dry gas cleaning.

Gas cleaning in a gasification to clean syngas process comprises primarily *particles* which contain mineral content of biomass and non-converted carbonaceous material must be removed to a very large extent. A second class of contaminants that causes issues with fouling by deposition or would at least form a loss are *tars*. Tars form an issue of serious concern for gasifiers that operate at temperatures well below ~1200 °C, so for large-scale systems fluidized bed based technology. Physical “removal” from the gas will reduce the net carbon conversion efficiency of the process, and in fact rather a “conversion” route should be preferred, where tar is broken into smaller molecules (e.g. CO and H_2). In any case, the exact extent of the “tar problem” depends on the downstream application of the product gas. For combustion applications the tolerance for tar is higher (even up to several grams per m_n^3), whereas for fuel cell applications, synthesis of chemicals, etc. it is essential to minimize the concentration of tar produced during gasification, not only to prevent the fouling of the downstream equipment, but also to make the chemical energy stored in the tar molecules available to the conversion process. A third class of minor species in the gasification product gas is formed by *sulphur* compounds. Though biomass generally does not contain high sulphur contents as opposed to coals this still may be an issue. Most catalysts applied for reforming of hydrocarbons are sensitive for such sulphur species down to low ppm or less values and thus they should be largely removed. A fourth class of compounds needing cleanup are the bound *nitrogen* species. Finally, as class of compounds that impose challenges to catalysts *alkali and trace metals* are addressed here. Final upgrading via CO_2 removal is not dealt with in this contribution.

In Figure 6 an overview of currently known contamination limitations for some representative fuels (FT-diesel, methanol) is given.

Downloaded by UNIV OF GUELPH LIBRARY on June 5, 2012 | http://pubs.acs.org
Publication Date (Web): December 14, 2011 | doi: 10.1021/bk-2011-1088.ch006

Downloaded by UNIV OF GUELPH LIBRARY on June 5, 2012 | http://pubs.acs.org
Publication Date (Web): December 14, 2011 | doi: 10.1021/bk-2011-1088.ch006

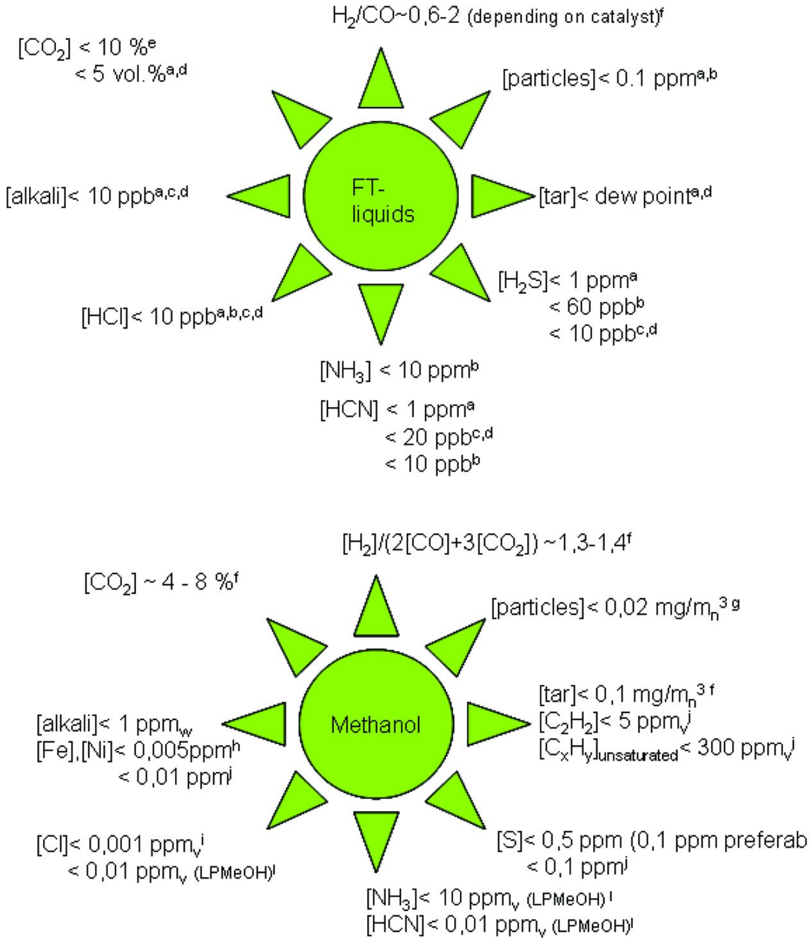
H_2/CO~0,6-2 (depending on catalyst)[f]
$[CO_2]$ < 10 %[e]
< 5 vol.%[a,d]
[particles]< 0.1 ppm[a,b]
[alkali]< 10 ppb[a,c,d]
FT-
liquids
[tar]< dew point[a,d]
[HCl]< 10 ppb[a,b,c,d]
$[H_2S]$< 1 ppm[a]
< 60 ppb[b]
< 10 ppb[c,d]
$[NH_3]$ < 10 ppm[b]
[HCN] < 1 ppm[a]
< 20 ppb[c,d]
< 10 ppb[b]
$[H_2]/(2[CO]+3[CO_2])$ ~1,3-1,4[f]
$[CO_2]$ ~ 4 - 8 %[f]
[particles]< 0,02 mg/m_n^3 [g]
[alkali]< 1 ppm_w
[Fe],[Ni]< 0,005ppm[h]
< 0,01 ppm[j]
Methanol
[tar]< 0,1 mg/m_n^3 [f]
$[C_2H_2]$< 5 ppm_v[j]
$[C_xH_y]_{unsaturated}$< 300 ppm_v[j]
[Cl]< 0,001 ppm_v[i]
< 0,01 ppm_v (LPMeOH)[l]
[S]< 0,5 ppm (0,1 ppm preferable)[h]
< 0,1 ppm[j]
$[NH_3]$< 10 ppm_v (LPMeOH)[l]
[HCN]< 0,01 ppm_v (LPMeOH)[l]

Figure 6. Some limitations to contaminant concentrations for FT-liquids and methanol production; references a) Boerrigter et al. (35),b)Newby et al. (36), c) Sasol indicated in Leibold et al. (37), d) Vogel et al. (38), e) Leibold et al. (37), f) Knoef (39), g) Spath and Dayton (40), h) Kung (41), i) Twigg and Spencer (42), j) Van Ree (43).

Different end uses of the raw synthesis gas generated demand different gas treating sections. A generic scheme of such part of the BtL technology chain is presented in Figure 7. The circle indicates that integration of particle removal and tar/hydrocarbon removal can be an option. Leibold et al. (*37*) proposed even a further simplification by adding sorbents for removal of H_2S and HCl upstream the particle removal unit so that the indicated third step is also integrated in the first cleaning step.

Downloaded by UNIV OF GUELPH LIBRARY on June 5, 2012 | http://pubs.acs.org
Publication Date (Web): December 14, 2011 | doi: 10.1021/bk-2011-1088.ch006

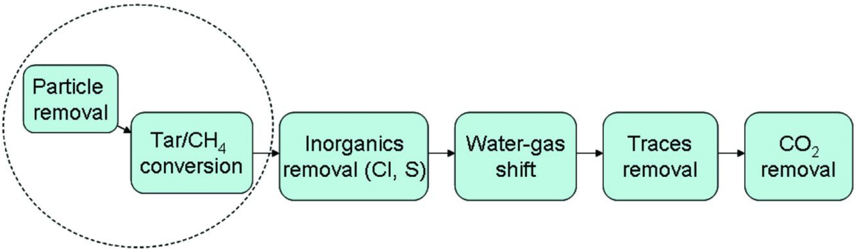

Figure 7. Simplified scheme for hot gas cleaning and gas upgrading.

3.1. Particles

Particulate matter is produced in all gasifier types together with the raw syngas and must be separated from this gas stream in order to prevent downstream gas upgrading catalytic materials to be fouled, which leads to deterioration of the gas quality improvement. Very strict requirements of particulate matter content of down to 0.02 mg/m_n^3 have been mentioned for syngas to methanol production (*39*). Gas cleaning related to particle removal is currently one of the main topics of research in the area of biomass gasification. Technologies for gas cleaning comprise mechanical methods like cyclones, hot gas filters (baffle, fabric and ceramic), and granular bed filters (*44*).

Gas cleanup from particles at near gasifier temperatures is preferred because energy loss is less due to avoidance of raw product gas cooling. The application and further development of hot gas filtrers is important in this respect. The process of filtration in general comprises separating dispersed particles from a dispersing fluid by means of a porous medium with the dispersing media being either gas or liquid. The choice of the filter medium determines the quality of the separation process and the following criteria can be applied for its selection (*45*):

1. Particle size retention objective.
2. Permeability characteristics of the clean medium.
3. The solids-holding capacity of the medium.

Current filtration systems forming the primary part of a hot gas cleaning section are fixed bed filters, ceramic filters, and metal filters (*46*) Candle filters produced using permeable ceramics are very promising filtration systems with artificially elevated porosity and adjustable pore size and shape (*47*). Ceramic materials offer the major advantage that next to exellent dust separation effieciencies (*48*) they allow temperatures up to near gasifier temperatures (*49*) and have shown to be operated at temperatures well above 400°C while synthetic fabrics and glass fibre materials are limited by maximum operating temperature of 250 and 300°C, respectively (*47*). Additional advantages include enhanced erosion and (chemical) corrosion resistance, and the possibility to remove multiple contaminants (*50*). Ceramic filters are mostly applied in the removal of dust from hot gases produced by industrial processes such as combustion and gasification. As important features, they need to comply with the following criteria (*51*) :

1. Minimized hydraulic resistance (due to a high porosity).
2. Optimal pore size distribution characteristics.
3. Resistance to reactive agents, like acids and alkaline.
4. Thermal shock resistance.
5. Physico-mechanical properties not changing too much; such as apparent density, pore diameter, compressive strength etc. on a long term exposure to hot gases.
6. Regeneration capability to its initial filtering characteristics.

Downloaded by UNIV OF GUELPH LIBRARY on June 5, 2012 | http://pubs.acs.org
Publication Date (Web): December 14, 2011 | doi: 10.1021/bk-2011-1088.ch006

Moreover, hot gas ceramic filters need to be able to withstand operating for more than 10,000 hours, maintain their high particulate removal efficiencies, high flow capacity and low pressure drop (*52*, *53*). *Advanced* ceramic filters are constructed based on two connected parts, a porous support layer ensuring mechanical strength and a denser functional top layer for the actual filtering function. The support layer must withstand the severe operating conditions, to which a candle is exposed and hence the actual life time of a candle is determined by the life of the support layer and not of the functional layer (*54*). The high filtration efficiency is ensured by the cake that is built up.

As such filters are supposed to work with gas flows at very high temperatures typically in the range of 500-900°C, they are also called hot gas filters. Hot gas filters are generally placed downstream of the main process reactor (gasifier) but recently tests have also been performed by in-situ positioning of a filter candle inside the gasifier (*55*). These hot gas filters have been applied on a large scale for particulate removal, see e.g. (*56–58*), but relatively little information is available for candle filters used with the aim to specifically reduce tar contents of syngases.

For this purpose catalytic filters have been designed and tested in lab to pilot scale (*55*, *59–65*), and are currently demonstrated on a small-scale in a demonstration unit (*66*). Companies involved in such activities are Pall Filtersystems and Madison Filter (in cooperation with Haldor Topsøe). Units including them have the advantage of combined filtration and tar removal from raw gas and also prevent energy loss because the process is carried out at high temperatures. This is a good example of process intensification.

3.2. Tar

As mentioned, tars are a challenge for low temperature (<<1200 °C) gasifiers. Acceptable limits to tar content in gasification product gas depend on the final application of such gas. Already during combustion in gas engines and gas turbines tars may cause serious operational problems. In more advanced end-use applications a virtually tar-free gas is required. In order to prevent catalyst deactivation in downstream processing of the product gas, a limit of 2g tar/m_n^3 has been suggested before further catalytic reforming (*67*). Milne et al. (*25*) reviewed many literature sources which indicate that limiting values are less than

50–500 mg/m$_n^3$, 50–100 mg/m$_n^3$ and 5 mg/m$_n^3$ recommended for compressors, internal combustion systems, and direct-fired industrial gas turbines, respectively.

The amount and composition of tar depends on several process parameters: type of feedstock, gasification conditions (temperature, pressure, oxidizer to fuel ratio), and the gasifier type. In a fluidised bed gasifier the amount of tar formed can be up to the order of magnitude of 10 g/m$_n^3$ when no primary measures (bed materials, additive feeding) are taken; an entrained flow gasifier virtually produces no tars due to its high operating temperatures.

Because of the importance of tar content reduction, several methods have been contemplated and are being used. These methods have been divided into two main categories, which are schematically depicted in Figure 8:

- Primary methods: in-situ measures taken upstream in the gasifier.
- Secondary methods: measures taken downstream the gasifier.

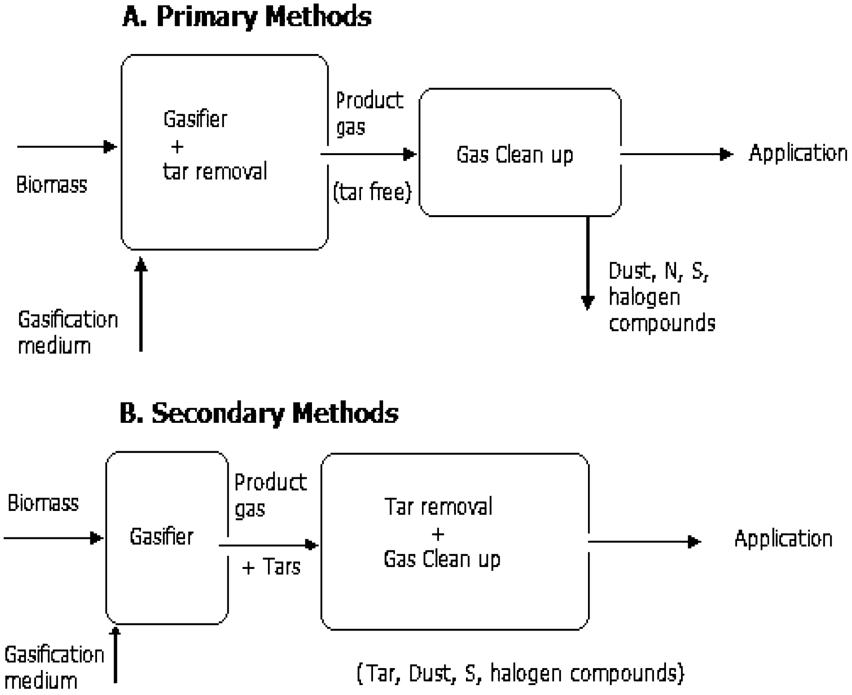
A. Primary Methods
Biomass
Gasifier
+
tar removal
Product gas
(tar free)
Gas Clean up
Application
Dust, N, S, halogen compounds
Gasification medium
B. Secondary Methods
Biomass
Gasifier
Product gas
+ Tars
Tar removal
+
Gas Clean up
Application
Gasification medium
(Tar, Dust, S, halogen compounds)

Figure 8. Tar reduction methods in biomass gasification (68).

Table III gives an overview of materials that have been investigated for tar reduction, divided into two main classes, natural rock materials and synthetic, or manufactured materials.

In Production and Purification of Ultraclean Transportation Fuels; Hu, Y., et al.;
ACS Symposium Series; American Chemical Society: Washington, DC, 2011.

Downloaded by UNIV OF GUELPH LIBRARY on June 5, 2012 | http://pubs.acs.org
Publication Date (Web): December 14, 2011 | doi: 10.1021/bk-2011-1088.ch006

Table III. Tar conversion catalysts and their characteristics, adapted with permission from Zwart (*69*)

		Positive aspects	*Negative aspects*
	Natural rock materials		
Calcined Ca/Mg	Dolomite	Availability in abundance	High attrition tendency
	Magnesite	Inexpensive	Variable qualities
	Limestone	Large tar conversions	Recarbonization with deactivation
		Disposable	
		Investigated to large extend	
Olivine		Attrition resistant Inexpensive	Lower tar reduction activity than dolomite
Clay minerals		Abundant availability and inexpensive	Loss of activity at higher T (>800°C)
		Disposal after usage less problematic	Lower activity than dolomite
Iron and iron minerals		Abundant	Without H_2 rapid deactivation
		Inexpensive	Lower activity than dolomite
	Synthetic materials		
Transition metal catalysts	e.g. Ni on carrier materials with promotors	Almost complete tar conversion ~900°C; high activity	Deactivation due to S and high tar content
		Increase CO/H_2 yields	Relatively expensive
		Commercial catalysts available	Disposal
Activated alumina		High tar conversion, comparable to dolomite	Deactivation due to coking
Alkali metals		Natural production in gasifier	Agglomeration
			Lower activity compared to dolomite
FCC catalyst		Reasonably cheap	Deactivation by coking

Continued on next page.

Downloaded by UNIV OF GUELPH LIBRARY on June 5, 2012 | http://pubs.acs.org
Publication Date (Web): December 14, 2011 | doi: 10.1021/bk-2011-1088.ch006

Table III. (Continued). Tar conversion catalysts and their characteristics, adapted with permission from Zwart (*69*)

	Positive aspects	*Negative aspects*
	Experience in industrial use	Lower activity compared to dolomite
Char	Inexpensive In-situ generation High tar conversion	Consumed Varying qualities

Downloaded by UNIV OF GUELPH LIBRARY on June 5, 2012 | http://pubs.acs.org
Publication Date (Web): December 14, 2011 | doi: 10.1021/bk-2011-1088.ch006

3.2.1. Primary Methods

An ideal primary method would eliminate the need for secondary methods (*70*). A proper selection of gasification process conditions, in particular temperature, gasifying medium, equivalence ratio (or λ), and residence time (by controlling the superficial velocity in the case of fluidised bed gasifiers) can reduce the amount of tars formed during gasification of biomass (*23*). Increased gasification temperature favours high carbon conversion and less tar formation (*71*, *72*). However, for fluidized beds gasification attention has to be paid concerning the operating temperature in order to avoid agglomeration of the bed material particles (*13*). High oxidation stoichiometric values (λ) promote tar destruction with the compromise of obtaining higher CO_2 concentrations in the product gas, due to oxidation reactions. Optimum values of 0.25-0.3 have been reported (*70*). The gasifying medium may affect the tar species distribution. It has been observed in tests with a fluidized bed gasifier (*72*) that the use of steam results in higher concentrations of phenolic compounds compared with air as gasifying medium. Pressure applied during gasification also influences tar formation and distribution. Knight (*73*) reported complete elimination of phenols during pressurized (at 21.4 atm) gasification of wood chips.

Modification of the gasifier design also impacts tar production and destruction. Secondary oxidizer injection (*74*) and two stage fast internally circulating fluidised bed gasifier (FICFB) combined with active bed material use (olivine and added Ni-species) (*75*) are some of the reported design techniques used for improving fluidized bed gasification process in terms of gas composition and tar formation.

In most of the investigations when a material is used as a in-bed catalyst for tar elimination and/or improvement of the gas composition, it is meant as an additive rather than a bed material.

Catalytic tar reduction by in-situ use of active materials in the gasifier has been studied widely and catalysts like dolomites (*72*, *76–79*), magnesites (*77*, *78*, *80*), limestones (*77*, *78*), olivines (*81–84*) and Ni-based catalysts (*75*) have been applied. As mentioned in Table III the natural rock materials among these show relatively good activity and in general are cheap, but show less favourable attrition behaviour, thus posing increased capacity requirements to particulate matter clean up. This however, has been demonstrated successfully using magnesite in the 18

MW_{th} CFB demonstration gasifier of Värnamo (*85*). The tar in-situ destruction at least reduces the treatment effort for downstream processing of the produced gas. Moreover, the use of catalytically active materials during biomass gasification can also promote char gasification, change the product gas composition and reduce the tar yield, while it can also prevent agglomeration.

3.2.2. Secondary Methods

The secondary methods involve reactor units situated downstream the gasifier unit. Mostly, fixed bed configurations have been investigated and applied, though (circulating) fluidized beds have been used as well, also commercially (TPS using dolomite CFB (*86*)). Fixed beds do not have attrition issues that soft rock materials are faced with under more severe fluidized bed conditions. To reach the very stringent requirements concerning tar, probably a combination of primary measures and downstream polishing should be used for acceptable catalyst lifetimes. Excellent reviews are available on the use of the different classes of materials mentioned in Table III, e.g. by Dayton (*87*) and updated by Abu El-Rub (*88*), Yung et al. (*31*) Regarding the use of char in downstream located beds, El-Rub has performed an extensive research (*89*), this material is active, cheap, in-situ made, but shows variable quality and is consumed so it must be suppleted.

Among the novel developments is the use of monoliths with impregnated metal (often Ni based) in relatively dusty syngas flows. Corella et al. (*90*) applied them to such a gas, but concluded that the activity was only moderate and to be improved. Also they indicate that upstream tar concentrations need to be reduced to approximately 2 g/m_n^3., another issue indicated is the presence of sticky ash due to alkali eutectics. The monolith concept is applied to reduce tar in the CHP demonstration project in Skive (Denmark). Very recently, in China a new catalyst was tested (60h run) with real gas from a fluidized bed biomass gasifier (scale: 150-300 kg/h) impregnated in a monolith that shows promising properties concerning tar conversion. It also shows prevention of coking and sintering and it consists of a $NiO\text{-}MgO/\gamma\text{-}Al_2O_3$/cordierite monolithic catalyst with a pore channel size of 7 by 7 mm. Moreover, it can operate under high dust load conditions (~330 g/m_n^3) (*91*).

When dealing with particle gas cleanup in the previous paragraph we already referred to the combination of filtration and tar conversion as a novel development which holds good promise for process integration and intensification.

3.3. Sulphur

Most virgin or fresh biomass contains little to no sulfur (0 - 2.0%). Biomass-derived feedstock such as municipal solid waste (MSW) or sewage sludge does contain sulfur, which requires e.g. limestone for the capture of it. The gasification process has an advantage over combustion in certain situations. In combustion systems, sulfur bound in the fuel is released as SO_2, which is relatively difficult to remove from the flue gas without adding an external sorbent. In a typical gasification process 93 to 96% of the sulfur appears as

Downloaded by UNIV OF GUELPH LIBRARY on June 5, 2012 | http://pubs.acs.org
Publication Date (Web): December 14, 2011 | doi: 10.1021/bk-2011-1088.ch006

Downloaded by UNIV OF GUELPH LIBRARY on June 5, 2012 | http://pubs.acs.org
Publication Date (Web): December 14, 2011 | doi: 10.1021/bk-2011-1088.ch006

H_2S^6. Among the other sulphur contaminants, comparatively small amounts of COS, CS_2 and thiophenes depending on process conditions, must be removed. In the demonstration scale woody biomass gasifier in Guessing (Austria), sulphur component levels of ~150 ppm H_2S and ~30 ppm organic sulphur (e.g. thiophene) are reported (*19*). Sulphur removal from syngas is essential to minimize poisoning of catalysts and corrosion of downstream equipment and to meet various emission requirements. Hot gas desulphurization (HGD) can improve the overall thermal efficiency due to the elimination of fuel gas cooling and associated heat exchangers. This can be established by using primary methods (in the gasifier) as well as downstream capture.

3.3.1. In Situ Sulphur Capture

Meng et al. (*92*) reviewed the various research works concerning the use of natural rock materials, limestone and dolomite, from various sources that are most commonly used sorbent for sulphur capture in fluidized bed gasification applications. Its use is explained by their widespread availability at inexpensive costs. The origin of the material though has significant effects on the final quality of the gas. Limestone already suffers from the problem of attrition and incomplete conversion below the calcining temperatures and in dolomite an increase in magnesium to calcium ratio causes an even increased attrition though these materials show an increased reaction rate and reduced sintering. Related to the abovementioned shortcomings of the natural sorbents, some studies also suggest the use of calcium acetate and calcium magnesium acetate as alternatives and such compounds have proven to show very good sulphur capture capabilities. In this context, few research work suggested the the application of a shell in core absorbent structure in which a central core of limestone or calcium sulphate hemihydrates is coated with a cement so that the absorbent simultaneously shows increased strength and absorption capacity (*93*, *94*) Therefore a good solution might be found by the use of calcium acetate salts of pelletized sorbents depending upon the quality of gas for specific application and optimal cost for the process.

3.3.2. Downstream Sulphur Capture

A diversity of metal oxides can be used for high temperature sulphur capture downstream of the gasification process but each has its own limitations and advantages. What is considered key criteria downstream sulphur sorbents are their sulphur sorption capacity and absorption reaction temperature. From these it follows that mixed oxides combining the properties of various metals and supported metal oxides are the most promising way of sulphur capture, but depending on the temperature levels other metal oxide sorbents may be used.

ZnO sorbent exhibits among these the most favorable thermodynamic properties for H_2S capture in high temperature gas cleaning chains. However, as a result of vaporization (*95*), zinc migration and agglomeration issues at high temperature, the utilization of pure ZnO as sulphur sorbent is limited to a temperature of around 600 °C. More stable zinc sorbents with inclusion of other metal elements were developed including zinc copper ferrite, which can reduce H_2S to lower levels than zinc ferrite, and manufacture of zinc ferrite doped with titanium, which shows higher stability under certain preparation conditions.

Copper oxide is able to reduce H_2S from >>1000 ppm_v to sub-ppm_v concentrations. The problem with CuO is that it is easily reduced to metallic copper by the reducing compounds H_2 and CO, major species in the fuel gases, which lowers the desulphurization efficiency.

Manganese oxides show the attractive combination of high sulphur capacity and high reactivity in the moderate temperature range, without the need for sorbent preconditioning or activation. The conditions better match biomass gasification and tar reforming process temperatures. However, manganese oxide sorbents are susceptible to the formation of sulphates and in addition need a regeneration at very high temperature.

Iron oxide desulphurization potential is slightly lower than abovementioned species, mainly because of severe reduction reaction and iron carbide formation at a temperature higher than 550 °C. Iron sulphide formed during the sulphidation or absorption step can on the other hand be well regenerated via oxidation using air or nitrogen-diluted air at considerably lower temperatures than other metal oxides. In addition, the product of sulphidation, FeS_x, is known to react with SO_2 to form Fe_3O_4 and elemental sulphur, which is the most preferred route for SO_2 fixation from the regeneration product gas.

Cerium oxide can well be regenerated with a reasonable elemental sulphur recovery. The sulphur absorption increases when the temperature and CO/CO_2 ratio increase. However, cerium oxide has lower sulphur removal efficiency than ZnO, especially at comparatively low temperatures in the range of hot gas cleaning <700 °C. In addition, in comparison with other sorbents, cerium oxide is much more expensive.

In order to overcome the abovementioned shortcomings related to the main criteria, additives, such as Ti, Al, Si, Zr, Co, Ni, and Fe, and promoters (Co, Ni, and Fe) are added to different metal oxide based sorbents to improve their sulphur capture capacity during multiple cycles as well as their regeneration properties. Also the mesoporous materials and zeolites,which mainly consist of Al_2O_3, TiO_2, Fe_2O_3 and SiO_2, are used as the supporters to create and maintain the desirable sorbent structure. Zinc oxide based sorbent ($ZnFe_2O_4$, $ZnTiO_3$, Zn_2TiO_4 and Zn_3TiO_8), mixed and dispersed copper oxide based sorbent (CuO/Al_2O_3, $CuO/Fe_2O_3/Al_2O_3$, CuO/Fe_2O_3, and CuO/MnO_2), manganese oxide based sorbent ($MnO/\gamma\text{-}Al_2O_3$, Mn–Cu, and Mn–Cu–V), iron oxide based sorbent (Fe_2O_3/SiO_2), and cerium oxide based sorbent (Ce/Mn) have been extensively studied. Therefore, some intrinsic problems using sulphur sorbents still need to be solved, even though many research works have been carried out to find suitable sorbents for different desulphurization processes.

For the development of a low cost, environmentally friendly, highly efficient, rapidly reacting and regenerable sorbent, with high sulphur capture capacity and durability still additional development work must be done applying the material under real conditions. Optimization of supported or mixed metals sorbents from zinc, copper and manganese would be one option. Binary oxides and "promoted"

Downloaded by UNIV OF GUELPH LIBRARY on June 5, 2012 | http://pubs.acs.org
Publication Date (Web): December 14, 2011 | doi: 10.1021/bk-2011-1088.ch006

binary oxides may have better attrition resistance and higher sulphidation equilibrium constants. Experimental and modeling study focus on molecular structure of different sulphur capture materials could be useful for the design and development of new sulphur sorbents. Last but not least, mechanistic information for rational design and modification of such materials can be conventionally achieved with an aid of variety of microscopic and spectroscopic characterization methods.

3.4. Chlorine

The chlorine content of the biomass can vary significantly (*37*). Chlorine is known as an alkali vaporization shuttle, by which alkali induced issues are induced in the gasifier as well as downstream equipment. Also, ash softening has to be taken into account in HT gas cleaning processes in any case due to the formation of low melting compounds mainly chlorides. Harm to relevant catalysts in the BtL chain can be done by chloride poisoning (HCl) of catalysts (Cu,Zn containing) via several parallel mechanisms (Twigg&Spencer,2001) (*42*):

i. Reaction to give adsorbed chlorine atoms that can block or modify catalytic sites.
ii. The low melting point and high surface mobility of Cu(I) chloride mean that even extremely small amounts of copper halide are sufficient to provide mobile species that accelerate the sintering of Cu catalysts.
iii. Poisoning of Cu catalysts by reduced sulphur compounds (e.g. H_2S) is exacerbated by traces of mobile Cu(I) chloride.
iv. Further, ZnO, often present in Cu catalysts, reacts to form Zn halides, which also have low melting points, and causes further poisoning and sintering problems.

Therefore, chlorine containing species need to be removed by sorbents. Natural rock materials, like dolomite and limestone, already substantially reduce HCl content. This component is absorbed and $CaCl_2$ is formed, which might contribute to stickiness of the ashes as it has a relatively low melting point.

3.5. Nitrogen

The major nitrogen compounds in biomass gasification product gases are ammonia (NH_3) and to a lesser extent hydrogen cyanide (HCN) and other species like aromatic nitrogen compounds (e.g. pyridine) and HNCO. Fuel bound nitrogen present in the producer gas originates from the feedstock. In biomass gasification relatively high NH_3 concentrations are obtained when the fuel bound nitrogen content is appreciable; HCN is much produced to a much lower extent (*96*, *97*). A 0.2 mass% of nitrogen in sawdust led to concentrations of 300-400 ppm NH_3 in the fuel gas of a pressurized fluidized bed gasifier with fuel bound nitrogen to NH_3 conversion values in the range of ~50-70% under conditions of carbon conversion > 90% (*98*).

Downloaded by UNIV OF GUELPH LIBRARY on June 5, 2012 | http://pubs.acs.org
Publication Date (Web): December 14, 2011 | doi: 10.1021/bk-2011-1088.ch006

In IGCC concepts for (combined) power and heat production, a substantial part of the fuel bound nitrogen species (NH_3,HCN etc.) is converted into NO_x in the gas turbine combustors which are difficult to remove and are highly undesirable as atmospheric pollutants.

Given experience obtained in coal to Fischer-Tropsch diesel production (SASOL company), HCN is indicated to be less tolerable than NH_3; HCN exposure leads to the deactivation of the catalyst (*11*, *37*). Thus conversion or removal of NH_3 and HCN prior to their exposure to the catalyst is required. Regarding removal of NH_3 wet scrubbing can be applied, but this creates a liquid wastes stream. Here the dry, hot gas cleaning is dealt with. Catalysts that are used for tar conversion also show activity towards ammonia. At temperatures approaching fluidized bed gasifiers (~900 °C) dolomite, steam reforming catalysts (Ni basis) (*98*, *99*) and Fe-based catalysts have all been shown to be able to largely convert NH_3 (*96*, *100*, *101*). Carbon deposition may be a problem, however high steam contents may prevent this. A high H_2 concentration limits the conversion. Novel is the application of monoliths to remove tar and NH_3 as applied by Corella et al. (*90*, *102*); these pose less strict cleaning of the gas from particles, though sticky ashes may cause deposition and related activity decrease. Catalytic filtration using ceramic filters impregnated with a Ni based catalyst can also decrease tar and NH_3 simultaneously; the configuration might also consist of an annular packed bed on the clean side of the ceramic candles.

When chlorine is in the raw syngas, this might result in the formation of a condensable (fouling) species, NH_4Cl, solidifying below 250-280°C and presents a fouling risk. Reaction of NH_3 with H_2S can result in formation of ammonium(poly)sulphide, with a melting point below 150°C.

Downloaded by UNIV OF GUELPH LIBRARY on June 5, 2012 | http://pubs.acs.org
Publication Date (Web): December 14, 2011 | doi: 10.1021/bk-2011-1088.ch006

3.6. Alkali and Trace Metals

Many biomass types among the agricultural residues show high contents of alkali salts, in particular potassium based (straw, perennial grasses). When temperature exceeds approximately 700°C these (eutectic) salts are evaporated into the gas phase (*100*). This gives rise to problems of deposition on surfaces downstream that have lower temperatures in particular to temperatures below approximately 650°C. Herewith aerosols are formed with fine particle sizes (<5 μm) or the species condense directly on any surfaces like other particulate matter or the process equipment walls. During biomass gasification, alkali vapours can be removed by cooling the hot producer gas below 600°C to allow for condensation of the material into solid particulates (*100*). These solids are subsequently removed using various dry or wet particle removal systems. These particle removal systems not only have to be designed taking into account the chemical behaviour of the condensed alkali salt, but also the effect of tar condensation (*69*). Ash stickiness often resulting from lower melting alkali species is also impacting dust filtration as sticky ash is difficult to remove.

It is preferred when alkali species can be captured upstream the gas cleaning section and thus within the gasifier. This also retards or prevents agglomeration in case of fluidized bed gasification. This is possible using ‘alkali getters’, which are clay minerals, e.g. kaolinite (*13*).

Downloaded by UNIV OF GUELPH LIBRARY on June 5, 2012 | http://pubs.acs.org
Publication Date (Web): December 14, 2011 | doi: 10.1021/bk-2011-1088.ch006

4. Conclusions and Outlook

Gasification of renewable relatively dry biomass using steam/oxygen in autothermal processing and steam in indirect gasification concepts is a promising technology to produce not only power and heat, but also biofuels and chemicals. By using biomass and aiming at systems of medium to large thermal input sizes, a substantial CO_2 reduction can be realized. When using gasification technology, also CO_2 could be captured in the process, which is called a ‘pre-combustion’ CO_2 capture scheme. In this case, one potentially would have the opportunity to create carbon sinks.

Many different gasification reactor technologies have been developed and still novel designs are worked out. For large scale biomass derived syngas generation, the major hurdle in technology progress is formed by insufficient practical experience obtained from larger scale pilots and demonstration units with integrated gas cleaning and upgrading; this holds in particular for agricultural residue processing, as wood is comparatively more common. Entrained flow gasifiers have been demonstrated for coal gasification, but only limited experience exists concerning biomass processing. These reactors pose stringent limitations to the particle size and also the mineral content of biomass being different from coals, giving rise to challenges of slagging/fouling. Pre-treatment making use of torrefaction is currently being demonstrated on semi-commericial scales. On the other hand fluidized bed based systems need to deal with relatively high particle and tar contents in the syngas generated.

Efficient, long duration and stable bio-syngas clean up from particles and tars (hydrocarbons in general in fact) is being demonstrated, though mostly for combined heat and power application and to a less intense extent for biofuels production, which poses more stringent limitations to contaminants in syngas. Process intensification by combining particle cleanup with catalytic tar/nitrogen species removal, possibly combined with upstream addition of sorbents for sulphur and chlorine species, is a promising development; also the application of monoliths in cleanup of tars and nitrogen species is promising as this technology does not require extensive upstream particle removal, which also may simplify the gas cleaning configuration. Here more active catalysts are to be investigated and solutions to improve mass transfer to the active surface.

Regarding wet biomass, supercritical water gasification offers a high potential for biofuels production. In particular streams with negative values which societies consider to be wastes, like manures and sludges, are in this respect promising. Concerning this technology, more reactor development work and scale up is needed, including gas cleaning for the process conditions which are particularly severe.

Acknowledgments

AgentschapNL in the Netherlands is acknowledged for co-financing this study via the EOS-LT-09002 project, a consortium led by ECN. We are grateful for the constructive discussions.

References

1. Sims, R. E. H. *The Brilliance of Bioenergy*; James & James Science Publishers Ltd.: London, 2002.
2. *Key World Energy Statistics*; International Energy Agency: Paris, 2009.
3. Hoogwijk, M.; Faaij, A. P. C.; Van den Broek, R.; Berndes, G.; Gielen, D.; Turkenburg, W. C. Exploration of the ranges of the global potential of biomass for energy. *Biomass Bioenergy* **2003**, *25* (2), 119–133.
4. van den Heuvel, E. *VIEWLS - Shift Gear to Biofuels, Results and Recommendations from the VIEWLS Project*; 2005.
5. *European Strategic Energy Technology Plan (SET Plan) - Towards a Low-Carbon Future*; Publications Office of the European Union: Luxemburg, 2010.
6. Higman, C.; Van der Burgt, M. *Gasification*; Elsevier - Gulf Professional Publishing: Amsterdam, 2003.
7. Moulijn, J. A.; Makkee, M.; van Diepen, A. *Chemical Process Technology*; John Wiley & Sons Ltd.: Chichester, 2001.
8. Xu, C.; Donald, J.; Byambajav, E.; Ohtsuka, Y. Recent advances in catalysts for hot-gas removal of tar and NH_3 from biomass gasification. *Fuel* **2010**, *89* (8), 1784–1795.
9. Meadows, D. H.; Meadows, D. L.; Randers, J.; Behrens, W. H. *The Limits to Growth: A Report to the Club of Rome*; Universe Publishing Co.: New York, 1972.
10. Bridgwater, A. V. The technical and economic feasibility of biomass gasification for power generation. *Fuel* **1995**, *74* (5), 631–653.
11. Olofsson, I.; Nordin, A.; Söderlind, U. *Initial Review and Evaluation of Process Technologies and Systems Suitable for Cost-Efficient Medium-Scale Gasification for Biomass to Liquid Fuels*; ETPC Report 05-02; University of Umeå/Mid Sweden University: Umeå, 2005; p 90.
12. Van Dongen, A.; Kanaar, M., Co-Gasification at the Buggenum IGCC Power Plant. In *Energetische Nutzung von Biomassen*, DGMK: Velen, Germany, 2006; pp 57−58.
13. Bartels, M. Agglomeration in Fluidized Beds: Detection and Counteraction. Ph.D. Thesis, Delft University of Technology, Delft, 2008.
14. Fryda, L.; Panopoulos, K. D.; Kakaras, E. Agglomeration in fluidised bed gasification of biomass. *Powder Technol.* **2008**, *181*, 307–320.
15. Corella, J.; Toledo, J. M.; Molina, G. A review on dual fluidized-bed biomass gasifiers. *Ind. Eng. Chem. Res.* **2007**, *46*, 6831–6839.
16. Hofbauer, H.; Rauch, R.; Loeffler, G.; Kaiser, S.; Fercher, E.; Tremmel, H. Six Years Experience with the FICFB-Gasification Process. In *12th European Conference and Technology Exhibition on Biomass for Energy, Industry and Climate Protection*, Amsterdam, 2002.
17. Pfeifer, C.; Hofbauer, H. Development of catalytic tar decomposition downstream from a dual fluidized bed biomass steam gasifier. *Powder Technol.* **2008**, *180* (1−2), 9–16.

Downloaded by UNIV OF GUELPH LIBRARY on June 5, 2012 | http://pubs.acs.org
Publication Date (Web): December 14, 2011 | doi: 10.1021/bk-2011-1088.ch006

18. van der Meijden, C. M.; Veringa, H. J.; Vreugdenhil, B. J.; van der Drift, B. Bioenergy II: Scale-up of the milena biomass gasification process. *Int. J. Chem. React. Eng.* **2009**, *7*, A53.
19. Weber, G.; Potetz, A.; Rauch, R.; Hofbauer, H. In *Development of Process Routes for Synthetic Biofuels from Biomass (BTL)*, 18th European Biomass Conference and Exhibition: From Research to Industry and Markets, Lyon, France, 2010; ETA Florence: Lyon, France, 2010; pp 1829−1833.
20. Willeboer, W. The amer demolition wood gasification project. *Biomass Bioenergy* **1998**, *15* (3), 245–249.
21. Rensfelt, E.; Gardmark, L. In *VVBGC, Växjö Värnamo Biomass Gasification Centre AB, The VVBGC Four-Year-Project*, 18th European Biomass Conference and Exhibition: From Research to Industry and Markets, Lyon, France, 2010; ETA Florence: Lyon, France, 2010; paper VP3.5.26.
22. Brown, D.; Gassner, M.; Fuchino, T.; Marechal, F. Thermo-economic analysis for the optimal conceptual design of biomass gasification energy conversion systems. *Appl. Therm. Eng.* **2009**, *29*, 2137–2152.
23. Van Paasen, S. V. B.; Kiel, J. H. A. *Tar Formation in a Fluidised-Bed Gasifier: Impact of Fuel Properties and Operating Conditions*;ECN Report Number ECN-C-04-013; ECN: Petten, The Netherlands, 2004; p 58.
24. *Biomass Gasification: Tar and Particles in Produced Gas-Sampling and Analysis*; Technical Specification CEN/TS 15439; European Committee for Standardization: Brussels, 2006.
25. Milne, T. A.; Abatzoglou, N.; Evans, R. J. *Biomass Gasifier "Tars": Their Nature, Formation, and Conversion*; National Renewable Energy Laboratory: Golden, CO, 1997.
26. Kinoshita, C. M.; Wang, Y.; Zhou, J. Tar formation under different biomass gasification conditions. *J. Anal. Appl. Pyrolysis* **1994**, *29*, 169–181.
27. Corella, J.; Toledo, J. M.; Molina, G. Calculation of the conditions to get less than 2 g tar/m_n^3 in a fluidized bed biomass gasifier. *Fuel Process. Technol.* **2006**, *87*, 841–846.
28. Basu, P.; Mettanant, V. Biomass gasification in supercritical water: A review. *Int. J. Chem. React. Eng.* **2009**, *7*, R3.
29. Matsumura, Y.; Minowa, T.; Potic, B.; Kersten, S. R. A.; Prins, W.; Van Swaaij, W. P. M.; Van de Beld, B.; Elliott, D. C.; Neuenschwander, G. G.; Kruse, A.; Antal, M. J. Biomass gasification in near- and super-critical water: Status and prospects. *Biomass Bioenergy* **2005**, *29*, 269–292.
30. Matsumura, Y.; Minowa, T. Fundamental design of a continuous biomass gasification process using a supercritical water fluidized bed. *Int. J. Hydrogen Energy* **2004**, *29* (7), 701–707.
31. Yung, M. M.; Jablonski, W. S.; Magrini-Blair, K. A. Review of catalytic conditioning of biomass-derived syngas. *Energy Fuels* **2009**, *23*, 1874–1887.
32. Zwart, R. W. R.; Van der Drift, A.; Bos, A.; Visser, H. J. M.; Cieplik, M. K.; Könemann, J. W. Oil-based gas washing: Flexible tar removal for high-efficient production of clean heat and power as well as sustainable fuels and chemicals. *Environ. Prog. Sustainable Energy* **2009**, *28* (3), 324–335.
33. Rabou, L. P. L. M.; Zwart, R. W. R.; Vreugdenhil, B. J.; Bos, L. Tar in Biomass Producer Gas. The Energy Research Centre of The Netherlands

Downloaded by UNIV OF GUELPH LIBRARY on June 5, 2012 | http://pubs.acs.org
Publication Date (Web): December 14, 2011 | doi: 10.1021/bk-2011-1088.ch006

Downloaded by UNIV OF GUELPH LIBRARY on June 5, 2012 | http://pubs.acs.org
Publication Date (Web): December 14, 2011 | doi: 10.1021/bk-2011-1088.ch006

(ECN) Experience: An Enduring Challenge. *Energy Fuels* **2009**, *23* (12), 6189–6198.

34. Sehested, J. Four challenges for nickel steam-reforming catalysts. *Catal. Today* **2006**, *111* (1−2), 103–110.
35. Boerrigter, H.; Den Uil, H.; Calis, H. P. Pyrolysis and Gasification of Biomass and Waste. In *Green Diesel from Biomass via Fischer-Tropsch Synthesis: New Insights in Gas Cleaning and Process Design*; CPL Press: Strasbourg, 2003; pp 371−383.
36. Newby, R. A.; Smeltzer, E. E.; Lippert, T. E.; Slimane, R. B.; Akpolat, O. M.; Pandya, K.; Lau, F. S.; Abbasian, J.; Williams, B. E.; Lepping, D.*Novel Gas Cleaning/Conditioning for Integrated Gasification Combined Cycle*; Project DOE, DE-AC26-99FT40674; U.S. Department of Energy: Washington, DC, 2001.
37. Leibold, H.; Hornung, A.; Seifert, H. HTHP syngas cleaning concept of two stage biomass gasification for FT synthesis. *Powder Technol.* **2008**, *180*, 265–270.
38. Vogel, A.; Kaltschmitt, M.; Bolhar-Nordenkampf, M.; Hofbauer, H., Festbettvergaser zur Stromerzeugung—Lessons Learned. In *Biomassevergasung der Königsweg für eine Effiziente Strom-und Kraftstoffbereitstellung?*; Landwirtschaftsverlag GmbH ed.: Leipzig, 2003; pp 170−187.
39. Knoef, H. *Handbook Biomass Gasification*; BTG Biomass Technology Group: Enschede, The Netherlands, 2005.
40. Spath, P. L.; Dayton, D. C. *Preliminary Screening - Technical and Economic Assessment of Synthesis Gas to Fuels and Chemicals with Emphasis on the Potential for Biomass-Derived Syngas*; NREL/TP-510-34929; NREL: Golden, CO, 2003.
41. Kung, H. H. Deactivation of methanol synthesis catalysts: A review. *Catal. Today* **1992**, *11* (4), 443–453.
42. Twigg, M. V.; Spencer, M. S. Deactivation of supported copper metal catalysts for hydrogenation reactions. *Appl. Catal., A* **2001**, *212* (1-2), 161–174.
43. Van Ree, R. *Technical and Economic Data Biomass-Based Energy Conversion Systems for the Production of Gaseous and/or Liquid Energy Carriers*; NOVEM, GAVE 9915; ; Utrecht, The Netherlands, 2000.
44. Han, J.; Kim, H. The reduction and control technology of tar during biomass gasification/pyrolysis: An overview. *Renewable Sustainable Energy Rev.* **2008**, *12*, 397–416.
45. Orr, C. *Filtration Principles and Practices (Part 1)*; Marcel Dekker: New York, 1977.
46. Chung, J.-D.; Hwang, T.-W.; Park, S.-J. Filtration and dust cake experiment by ceramic candle filter in high temperature conditions. *Korean J. Chem. Eng.* **2008**, *20* (6), 1118–1122.
47. Val'dberg, A. Y.; Kaznacheeva, T. O.; Krasnyi, B. L.; Tarasovskii, V. P. Filtering behavior of ceramic materials. *Chem. Pet. Eng.* **2005**, *41* (1−2), 28–31.

Downloaded by UNIV OF GUELPH LIBRARY on June 5, 2012 | http://pubs.acs.org
Publication Date (Web): December 14, 2011 | doi: 10.1021/bk-2011-1088.ch006

48. Heidenreich, S.; Haag, W.; Salinger, M. Next generation of ceramic hot gas filter with safety fuses integrated in venturi ejectors. *Fuel* **2011**, accepted proof, in press.
49. Heidenreich, S.; Scheiber, B. Hot gas filtration with ceramic filters: Experiences and new developments. *Filtr. Sep.* **2002**, *39* (4), 22–25.
50. Krasnyi, B. L.; Tarasovskii, V. P.; Valsecchi, B.; Kaznacheeva, T. O. Porous permeable ceramics for filter elements cleaning hot gases from dust. *Glass Ceram.* **2005**, *62* (5−6), 134–138.
51. Krasnyi, B. L.; Tarasovskii, V. P.; Val'dberg, A. Y. Ceramic filters and their use for cleaning dust-laden hot exit gases. *Refract. Ind. Ceram.* **2005**, *46* (2), 116–119.
52. Pastila, P.; Helanti, V.; Nikkilä, A.-P.; Mäntylä, T. Environmental effects on microstructure and strength of SiC-based hot gas filters. *J. Eur. Ceram. Soc.* **2001**, *21* (9), 1261–1268.
53. Pastila, P.; Lara-Curzio, E.; Nikkilä, A.-P.; Mäntylä, T. In *Microstructure and Fracture of Some SiC-based Clay Bonded Hot Gas Filter Materials after Exposure to Thermal Cycling and/or High Temperature Water Vapour*, 5th International Symposium on Gas Cleaning at High Temperature, Morgantown, WV, 2002, paper 4.8.
54. Westerheide, R.; Von der Wehd, C.; Adler, J.; Rehak, P. In *Evaluation of Mechanical Properties and Structural Changes of Ceramic Filter Materials for Hot Gas Cleaning under Simulated Process Conditions*, 5th International Symposium on Gas Cleaning at High Temperature, Morgantown, WV, 2002; paper 4.06.
55. Rapagna, S.; Gallucci, K.; Di Marcello, M.; Foscolo, P. U.; Nacken, M.; Heidenreich, S. In situ catalytic ceramic candle filtration for tar reforming and particulate abatement in a fluidized-bed biomass gasifier. *Energy Fuels* **2009**, *23* (7), 3804–3809.
56. Lehtovaara, A.; Mojtahedi, W. Ceramic-filter behavior in gasification. *Bioresour. Technol.* **1993**, *46* (1−2), 113–118.
57. Ståhl, K.; Neergaard, M. IGCC power plant for biomass utilisation, Värnamo, Sweden. *Biomass Bioenergy* **1998**, *15* (3), 205–211.
58. Heidenreich, S.; Wolters, C. Hot gas filter contributes to IGCC power plant's reliable operation. *Filtr. Sep.* **2004**, *41* (5), 22–24.
59. Zhao, H.; Draelants, D. J.; Baron, G. V. Performance of a nickel-activated candle filter for naphthalene cracking in synthetic biomass gasification gas. *Ind. Eng. Chem. Res.* **2000**, *39* (9), 3195–3201.
60. Nacken, M.; Ma, L.; Heidenreich, S.; Baron, G. V. Performance of a catalytically activated ceramic hot gas filter for catalytic tar removal from biomass gasification gas. *Appl. Catal., B* **2009**, *88* (3−4), 292–298.
61. Nacken, M.; Ma, L.; Engelen, K.; Heidenreich, S.; Baron, G. V. Development of a tar reforming catalyst for integration in a ceramic filter element and use in hot gas cleaning. *Ind. Eng. Chem. Res.* **2007**, *46*, 1945–1951.
62. Ma, L.; Baron, G. V. Mixed zirconia–alumina supports for Ni/MgO based catalytic filters for biomass fuel gas cleaning. *Powder Technol.* **2008**, *180* (1−2), 21–29.

Downloaded by UNIV OF GUELPH LIBRARY on June 5, 2012 | http://pubs.acs.org
Publication Date (Web): December 14, 2011 | doi: 10.1021/bk-2011-1088.ch006

63. Ma, L.; Verelst, H.; Baron, G. V. Integrated high temperature gas cleaning: Tar removal in biomass gasification with a catalytic filter. *Catal. Today* **2005**, *105* (3-4), 729–734.
64. Engelen, K.; et al. A novel catalytic filter for tar removal from biomass gasification gas: improvement of the catalytic activity in the presence of H_2S. *Chem. Eng. Sci.* **2003**, *58* (3−6), 665–670.
65. Zhao, H.; Draelants, D. J.; Baron, G. Preparation and characterization of nickel-activated ceramic filters. *Catal. Today* **2000**, *56* (1-3), 229–237.
66. Varga, C.; Koppatz, S.; Pfeifer, C.; Hofbauer, H. In *Hot Gas Cleaning of Biomass Derived Syngas by Catalytic Filter Candles*, 18th European Biomass Conference & Exhibition: From Research to Industry and Markets, Lyon, France, 2010; ETA Florence: Lyon, France, 2010.
67. Aznar, M. P.; Caballero, M. A.; Gil, J.; Martín, J. A.; Corella, J. Commercial steam reforming catalysts to improve biomass gasification with steam-oxygen mixtures. 2. Catalytic tar removal. *Ind. Eng. Chem. Res.* **1998**, *37* (7), 2668–2680.
68. Litinas, A. Biomass Gasification in a Steam-Oxygen Blown Circulating Fluidised Bed Gasifier: Effect of Bed Material on Tar Formation and Gas Composition. MSc. Report, Delft University of Technology, Delft, 2009.
69. Zwart, R. *Gas Cleaning Downstream Biomass Gasification*; Report Number ECN-E-08-078; ECN: Petten, The Netherlands, 2009; p 65.
70. Devi, L.; Ptasinski, K. J.; Janssen, F. J. J. G. A review of the primary measures for tar elimination in biomass gasification processes. *Biomass Bioenergy* **2003**, *24*, 125–140.
71. Narvaez, I.; Orio, A.; Aznar, M. P.; Corella, J. Biomass gasification with air in an atmospheric bubbling fluidized bed. Effect of six operational variables on the quality of produced raw gas. *Ind. Eng. Chem. Res.* **1996**, *35* (7), 2110–2120.
72. Gil, J.; Caballero, M. A.; Martín, J. A.; Aznar, M. P.; Corella, J. Biomass gasification with air in a fluidized bed: Effect of the in-bed use of dolomite under different operation conditions. *Ind. Eng. Chem. Res.* **1999**, *38* (11), 4226–4235.
73. Knight, R. A. Experience with raw gas analysis from pressurized gasification of biomass. *Biomass Bioenergy* **2000**, *18*, 67–77.
74. Pan, Y. G.; Roca, X.; Velo, E.; Puigjaner, L. Removal of tar by secondary air injection in fluidised bed gasification of residual biomass and coal. *Fuel* **1999**, *78*, 1703–1709.
75. Pfeifer, C.; Rauch, R.; Hofbauer, H. In-bed catalytic tar reduction in a dual fluidized bed biomass steam gasifier. *Ind. Eng. Chem. Res.* **2004**, *43* (7), 1634–1640.
76. Ising, M. Zur katalytischen Spaltung teerartiger Kohlenwasserstoffe bei der Wirbelschichtvergasung von Biomasse. Ph.D. Dissertation, Universität Dortmund, Dortmund, 2002.
77. Corella, J.; Aznar, M. P.; Delgado, J.; Martinez, M. P.; Aragues, J. L. Deactivation of tar cracking stones (dolomites, calcites, magnesites) and of commercial steam reforming catalysts in the upgrading of the exit gas from

steam fluidized bed gasifiers of biomass and organic wastes. *Stud. Surf. Sci. Catal.* **1991**, *68*, 249–252.

78. Delgado, J.; Aznar, M. P.; Corella, J. Calcined dolomite, magnesite, and calcite for cleaning hot gas from a fluidized bed biomass gasifier with steam: Life and usefulness. *Ind. Eng. Chem. Res.* **1996**, *35* (10), 3637–3643.
79. Olivares, A.; Aznar, M. P.; Caballero, M. A.; Gil, J.; Francés, E.; Corella, J. Biomass gasification: Produced gas upgrading by in-bed use of dolomite. *Ind. Eng. Chem. Res.* **1997**, *36*, 5220–5226.
80. Siedlecki, M.; Nieuwstraten, R.; Simeone, E.; de Jong, W.; Verkooijen, A. H. M. Effect of magnesite as bed material in a 100 kW_{th} steam-oxygen blown circulating fluidized-bed biomass gasifier on gas composition and tar formation. *Energy Fuels* **2009**, *23*, 5643–5654.
81. Devi, L.; Craje, M.; Thüne, P.; Ptasinski, K. J.; Janssen, F. J. J. G. Olivine as tar removal catalyst for biomass gasifiers: Catalyst characterization. *Appl. Catal., A* **2005**, *294*, 68–79.
82. Devi, L.; Ptasinski, K. J.; Janssen, F. J. J. G. Pretreated olivine as tar removal catalyst for biomass gasifiers: Investigation using naphthalene as model biomass tar. *Fuel Process. Technol.* **2005**, *86*, 707–730.
83. Aznar, M. P.; Toledo, J. M.; Sancho, J. A.; Francés, E., The effect the amount of olivine has on gas quality in gasification with air of different mixtures of biomass and plastic waste in fluidized bed. In *15th European Biomass Conference & Exhibition*, ETA Florence: Berlin, 2007; pp 1176−1179.
84. Corella, J.; Toledo, J. M.; Padilla, R. Olivine or dolomite as in-bed additive in biomass gasification with air in a fluidized bed: Which is better? *Energy Fuels* **2004**, *18* (3), 713–720.
85. Ståhl, K.; Waldheim, L.; Morris, M.; Johnsson, U.; Gårdmark, L. In *Biomass IGCC at Värnamo, Sweden - Past and Future*, GCEP Energy Workshop, Stanford University, Palo Alto, CA, April 27, 2004.
86. Rensfelt, E., Atmospheric CFB Gasification. In *Gasification and Pyrolysis of Biomass: The Greve Plant and Beyond*; Stuttgart, Germany, 1997; Vol. 1, pp 139−159.
87. Dayton, D. C. *A Review of the Literature on Catalytic Biomass Tar Destruction*; Report Number NREL/TP-510-32815; NREL: Golden, CO, 2002.
88. Abu El-Rub, Z.; Bramer, E. A.; Brem, G. Review of catalysts for tar elimination in biomass gasification. *Ind. Eng. Chem. Res.* **2004**, *43*, 6911–6919.
89. Abu El-Rub, Z.; Bramer, E. A.; Brem, G. Experimental comparison of biomass chars with other catalysts for tar reduction. *Fuel* **2008**, *87*, 2243–2252.
90. Corella, J.; Toledo, J. M.; Padilla, R. Catalytic hot gas cleaning with monoliths in biomass gasification in fluidized beds. 1. Their effectiveness for tar elimination. *Ind. Eng. Chem. Res.* **2004**, *43*, 2433–2445.
91. Wang, T.; Li, Y.; Wang, C.; Zhang, X.; Ma, L.; Wu, C. Synthesis gas production with NiO-MgO/γ-Al2O3/cordierite monolithic catalysts in a pilot-scale biomass-gasification-reforming system. *Energy Fuels* **2011**, *25*, 1221–1228.

Downloaded by UNIV OF GUELPH LIBRARY on June 5, 2012 | http://pubs.acs.org
Publication Date (Web): December 14, 2011 | doi: 10.1021/bk-2011-1088.ch006

92. Meng, X.; de Jong, W.; Verkooijen, A. H. M. In bed and downstream hot gas desulphurization during solid fuel gasification: A review. *Fuel Process. Technol.* **2010**, *91* (8), 964–981.
93. Akiti, T. T.; Constant, K. P.; Doraiswamy, L. K.; Wheelock, T. D. A regenerable calcium-based core-in-shell sorbent for desulfurizing hot coal gas. *Ind. Eng. Chem. Res.* **2002**, *41*, 587–597.
94. Akiti, T. T.; Constant, K. P.; Doraiswamy, L. K.; Wheelock, T. D. An improved core-in-shell sorbent for desulfurizing hot coal gas. *Adv. Environ. Res.* **2002**, *6*, 419–428.
95. Westmoreland, P. R.; Harrison, D. P. Evaluation of candidate solids for high-temperature desulfurization of low-Btu gases. *Environ. Sci. Technol.* **1976**, *10*, 659–661.
96. Leppälahti, J.; Koljonen, T. Nitrogen evolution from coal, peat and wood during gasification: Literature review. *Fuel Process. Technol.* **1995**, *43*, 1–45.
97. De Jong, W. Nitrogen Compounds in Pressurised Fluidised Bed Gasification of Biomass and Fossil Fuels. Ph.D. Dissertation, Delft University of Technology, Delft, 2005.
98. Wang, W.; Padban, N.; Ye, Z.; Anderson, J. R.; Bjerle, I. Kinetics of ammonia decomposition in hot gas cleaning. *Ind. Eng. Chem. Res.* **1999**, *38*, 4175–4182.
99. Wang, W.; Padban, N.; Ye, Z.; Olofsson, G.; Andersson, A.; Bjerle, I. Catalytic Hot gas cleaning of fuel gas from an air-blown pressurized fluidized-bed gasifier. *Ind. Eng. Chem. Res.* **2000**, *39*, 4075–4081.
100. Stevens, D. J. *Hot Gas Conditioning: Recent Progress with Larger-Scale Biomass Gasification Systems: Update and Summary of Recent Progress*; NREL/SR-510-29952; National Renewable Energy Laboratory: Golden, CO, 2001.
101. Leppälahti, J.; Simell, P.; Kurkela, E. Catalytic conversion of nitrogen compounds in gasification and combustion. *Fuel Process. Technol.* **1991**, *29*, 43–56.
102. Corella, J.; Toledo, J. M.; Padilla, R. Catalytic hot gas cleaning with monoliths in biomass gasification in fluidized beds. 3. Their effectiveness for ammonia elimination. *Ind. Eng. Chem. Res.* **2005**, *44*, 2036–2045.

Downloaded by UNIV OF GUELPH LIBRARY on June 5, 2012 | http://pubs.acs.org
Publication Date (Web): December 14, 2011 | doi: 10.1021/bk-2011-1088.ch006

Downloaded by OHIO STATE UNIV LIBRARIES on June 5, 2012 | http://pubs.acs.org
Publication Date (Web): December 14, 2011 | doi: 10.1021/bk-2011-1088.ch007

Chapter 7

Carbon Dioxide-Selective Facilitated Transport Membranes for Hydrogen Purification

He Bai[1] and W. S. Winston Ho*

William G. Lowrie Department of Chemical and Biomolecular
Engineering and Department of Materials Science and Engineering,
The Ohio State University, 2041 College Road,
Columbus, Ohio 43210-1178, U.S.A.
[1]Current address: Momentive Performance Materials, Inc.,
3500 South State Route 2, Friendly, West Virginia 26146-9750, U.S.A.
***Tel.: (614) 292-9970. Fax: (614) 292-3769.**
E-mail: ho@chbmeng.ohio-state.edu.

This review covers carbon dioxide- and hydrogen sulfide-selective facilitated transport membranes for applications of low-pressure hydrogen purification for fuel cells and high-pressure hydrogen purification for refining and petrochemical industries. We have synthesized new carbon dioxide- and hydrogen sulfide-selective facilitated transport polymeric membranes containing amino groups with high carbon dioxide and hydrogen sulfide permeabilities and selectivities vs. hydrogen or carbon monoxide. This type of membranes has the potential for hydrogen purification for environmentally friendly fuel cells, including the use of the membrane in the membrane reactor configuration to enhance water gas shift reaction. At high feed gas pressures, the membranes showed reduced separation performance compared to that at low feed gas pressures, due to the typical carrier satuation phenomenon. However, the membranes still showed a carbon dioxide selectivity vs. hydrogen greater than 50 and a carbon dioxide permeability greater than 1000 Barrers (1 Barrer = 10^{-10} cm^3 (STP) • cm / (cm^2 • s • cmHg)) at a carbon dioxide feed partial pressure of 44 psia, which is very desirable for refining and petrochemical applications.

In Production and Purification of Ultraclean Transportation Fuels; Hu, Y., et al.;
ACS Symposium Series; American Chemical Society: Washington, DC, 2011.

Introduction

Synthesis Gas Purification

Hydrogen is a foundamental chemical used for petrochemical and refining hydrogenation processes, and it has been proposed as an energy carrier for fuel cells. The production of hydrogen is expected to increase as petrochemical and refinery demands, as well as its applications (e.g., fuel cells), expand (*1*). Most feasible strategies to produce hydrogen in a commercial scale are based on the reforming of hydrocarbon fuels such as CH_4, which convert hydrocarbon fuels to H_2, CO and CO_2, and followed by the water gas shift (WGS) reaction (*2*), which converts CO to more H_2 (eq 1).

$$CO + H_2O \Leftrightarrow CO_2 + H_2 \qquad (\Delta H = -41.16\, kJ/mol) \tag{1}$$

As a result, the resulting synthesis gas consists of CO_2/H_2 mixture, and the removal of CO_2 from H_2 to produce high purity H_2 has become a very important industrial process. In addition, after WGS reaction, the resulting synthesis gas generally still consists of 0.5 – 1% of CO due to the equilibrium of the reversible WGS reaction (*3*). For proton-exchange membrane fuel cell (PEMFC) applications, even a small amount of CO, e.g., greater than 10 parts per million (ppm), deteriorates the platinum catalyst on the electrodes and decreases the fuel cell performance. Therefore, the CO level in synthesis gas needs to be reduced to 10 ppm or lower for this application (*4*).

Currently, the most commonly used processes to remove CO_2 and H_2S from synthesis gas mixtures are absorption technology (such as amine or amine-promoted hot potassium carbonate aqueous solutions), pressure swing adsorption, and membrane technology (*5*). The amine absorption process is highly energy-intensive, and it requires regeneration steps and additional chemicals. Pressure swing adsorption consists of adsorption and desorption steps each limited by thermodynamic equilibrium, resulting in a low degree of hydrogen recovery (< 90%). Compared to these conventional CO_2 and H_2S separation processes, membrane separation process has the advantages of separating and capturing CO_2 and H_2S with enhanced weight and space efficiency, operational simplicity, reduced energy consumption, lower operating costs, and absence of moving parts (*6*).

To reduce CO level to 10 ppm or lower for fuel cell applications, several CO cleanup methods are currently used or under development, which include methanation, preferential oxidation (PROX), sorption-enhanced reaction, and WGS membrane reactor. Methanation is one of the most widely used processes for CO cleanup. However, both methanation of CO and CO_2 consume H_2, which result in a reduced degree of H_2 recovery (*7*). In preferential oxidation, a small amount of O_2 is introduced into the process to convert CO to CO_2 by precious metal catalysis. Generally, to reduce the CO level below 10 ppm, an excess amount of O_2 needs to be introduced, which consumes H_2 by combustion and causes the potential of an accidental explosion (*8*). Sorption-enhanced reaction

Downloaded by OHIO STATE UNIV LIBRARIES on June 5, 2012 | http://pubs.acs.org
Publication Date (Web): December 14, 2011 | doi: 10.1021/bk-2011-1088.ch007

uses high surface area adsorbents, such as activated carbon, to remove one of the WGS reaction products (i.e., CO_2), thus shift the equilibrium of the WGS reaction (eq 1) to the forward direction and increase the CO conversion (*9–11*). However, as described previously, this process consists of adsorption and desorption steps each limited by thermodynamic equilibrium, resulting in a low degree of hydrogen recovery (< 90%).

Methanation, PROX, and sorption-enhanced reaction all consume valuable hydrogen at various degrees and add additional steps and costs. The WGS membrane reactor offers the most promising approach to overcome the thermodynamic constraint (reaction equilibrium) and achieve nearly complete conversion of CO not only without consuming valuable H_2 but also producing additional H_2 from the CO conversion. A membrane reactor is a combination of a chemical reactor and a semipermeable membrane that can extract products. In a WGS membrane reactor, one of the reaction products (either H_2 or CO_2) is continuously removed from the process, which shifts the equilibrium of the WGS reaction (eq 1) to the forward direction to achieve a CO level of less than 10 ppm.

Downloaded by OHIO STATE UNIV LIBRARIES on June 5, 2012 | http://pubs.acs.org
Publication Date (Web): December 14, 2011 | doi: 10.1021/bk-2011-1088.ch007

Solution-Diffusion Membranes for Synthesis Gas Purification

For conventional inorganic membranes (such as palladium (*12*) and silica (*13*)) and polymeric membrane materials (*14*), overall gas selectivity is mainly dependent on diffusivity selectivity. Thus, the membranes are more permeable to H_2 compared to CO_2. As a result, the H_2 product is produced at low pressure on the permeate side. However, downstream utilization generally requires H_2 at high pressure, and expensive compression of the H_2 product significantly decreases the advantages of membrane technology. To avoid this problem, membrane materials with high CO_2/H_2 selectivity and high CO_2 permeability are of great interest. In addition, the CO_2-selective membrane materials offer the following advantages: (a) a H_2 rich product is recovered at high pressure (feed gas pressure) and ready for downstream applications; (b) CO_2 is the minor component in synthesis gas, and selective removal of the minor component CO_2 across the membrane potentially reduces the overall membrane area required for the separation; (c) air or steam can be used to sweep the permeated CO_2 on the permeate side of the membrane to obtain a high driving force for the separation in the case of a low-pressure feed gas; and (d) CO_2 at high concentration (> 99%) can be obtained on the permeate side for sequestration when steam is used as the sweep gas.

Current CO_2-selective membranes are based on either solution-diffusion mechanism or facilitated transport mechanism. For solution-diffusion CO_2-selective membranes, Lin et al. synthesized and characterized a family of highly branched crosslinked amorphous poly(ethylene oxide) (PEO)-based membranes by UV crosslinking (*15–21*). The resulting membranes displayed CO_2-selective separation performance because ethylene oxide (EO) units interacted more favorably with CO_2, resulting in high solubility selectivity. However, these membranes only showed reasonably good CO_2/H_2 selectivity (about 30) at a very low temperature (i.e., - 20 °C). When the temperature increased, CO_2/H_2 selectivity of the membranes dropped significantly. In

Downloaded by OHIO STATE UNIV LIBRARIES on June 5, 2012 | http://pubs.acs.org
Publication Date (Web): December 14, 2011 | doi: 10.1021/bk-2011-1088.ch007

industrial applications, high operating temperatures (> 100 °C) are highly desirable because of the high operating temperatures of reforming and WGS reactions. Moreover, PEO is a very soft rubbery polymer, which has relatively poor mechanical properties. Thus, it was very difficult to make thin membranes, and the reported membrane thicknesses were all more than 100 μm. Even though the membrane showed a CO_2 permeability of around 500 Barrers, its permeance (< 5 GPU) or flux might not be high enough for realistic industrial applications.

Most of WGS membrane reactors reported were based on H_2-selective inorganic membranes, e.g., silica (*22–24*) and palladium (*25–29*) membranes. Giessler et al. used silica as the membrane material to remove H_2 (*22*). They packed $Cu/Zn/Al_2O_3$ catalyst on the top of a molecular sieve silica membrane and obtained a CO conversion of 99% at 280 °C. Basile et al. prepared Pd-based WGS membrane reactor by a co-condensation technique (*25*, *26*). An ultra-thin double-layer Pd film was deposited on a tubular ceramic support. By continuously removing H_2 through membrane during WGS reaction, a CO conversion as high as 99.89% was obtained. To improve the mechanical strength and H_2 permeability of the membrane, Tosti et al. used Pd-Ag complex as the membrane material (*27*). They coated a thin (50 μm thickness) Pd-Ag film on the inside wall of the ceramic porous support. With this kind of WGS membrane reactor, reaction conversions close to 100% were achieved at 325 – 330 °C, which were well above the equilibrium value of 80%. For silica-based membranes, their performance and mechanical strength are still issues. On the other hand, for palladium and palladium alloy membranes, the cost of such precious metals is a concern. According to the economic study by Criscuoli et al. (*30*), only with a thickness of less than 20 μm, such Pd-based membrane reactors could be a potential alternative to conventional reactors. However, the difficulty of preparing such thin, flawless and durable membranes is still the remaining challenge for the commercial applications of this kind of membrane reactors (*31*).

Facilitated Transport Membranes for Synthesis Gas Purification

The facilitated transport mechanism, involving a reversible reaction in addition to penetrant dissolution and diffusion, is a desirable approach to achieving high CO_2/H_2 selectivity and high CO_2 permeation. For conventional solution-diffusion membranes, the increase of selectivity for the gas of interest is normally accompanied by the decrease of permeability, and vice versa (*14*). However, facilitated transport membranes can achieve high selectivity without the sacrifice of permeabililty (*32*). This type of membrane is based on the reversible reaction of the targeted gas with the reactive carriers inside the membrane. In literature, supported liquid membranes (SLMs) (*33–38*), ion-exchange membranes (*39–45*), and membranes with bonded reactive carriers (*46–59*) are three common CO_2-selective facilitated transport membranes.

For SLMs, three major problems exist: loss of solvent, loss of carriers, and degradation of carriers. The loss of solvent is caused by its evaporation, particularly in high temperature applications, and/or its leakage through the SLM. The loss of carriers is due to the washout of the carrier solutions from the SLM

Downloaded by OHIO STATE UNIV LIBRARIES on June 5, 2012 | http://pubs.acs.org
Publication Date (Web): December 14, 2011 | doi: 10.1021/bk-2011-1088.ch007

at high trans-membrane pressure. The degradation of carriers is the result of irreversible reactions between feed components and carriers, which make carriers lose effectiveness for facilitated transport (*39*, *40*). To overcome these instability issues, a "bulk flow liquid membrane" has been proposed, in which a carrier solution was forced to permeate through the SLM and then recycled continuously (*60–62*).

In recent years, one of the most interesting strategies for improving the stability of SLMs was proposed, using room temperature ionic liquids (RTILs) as the immobilized phase within the pores of SLMs. RTILs are organic salts that are liquid at room temperature, thermally stable at high temperatures (above 300 °C), non-flammable, and nonvolatile. These properties make them ideal candidates as the separation medium for supported liquid membranes. Particularly, the fact that RTILs have a negligible vapor pressure eliminates the problem of solvent evaporation that typically occurs in SLMs and significantly improves the membrane stability (*63*). Supported ionic liquid membranes (SILMs) have been investigated for natual gas purification, i.e., CO_2/CH_4 separation (*64–66*), flue gas CO_2 capture, i.e., CO_2/N_2 separation (*65–68*), and synthesis gas purification, i.e., CO_2/H_2 separation (*68*), based on the solution-diffusion mechanism due to the high solubility of CO_2 in selected RTILs (*69*). A more desirable way of using SILMs is the incorporation of an amine-functionalized ionic liquid, which could significantly improve the membrane CO_2 separation performance since the CO_2 transport mechanism is facilitated transport in this case. The resulting facilitated transport-based SILMs exhibited very desirable CO_2/CH_4 (*70*, *71*) and CO_2/H_2 (*72*, *73*) separation performances, which are much improved compared to those for the solution diffusion-based SILMs.

In ion-exchange membranes, carriers are retained in the membrane by electrostatic forces to minimize the washout of carriers, resulting in improved stability of the facilitated transport membranes. Membranes with polymer backbones bound with reactive carriers are believed to have better stability than SLMs, and great progress has been made in recent years (*46–59*). In addition, various models of facilitated transport mechanism have been developed and established using numerical and analytical methods, which can be used to guide the experimental work (*74–84*).

Ho et al. have synthesized CO_2-selective polymeric membranes based on the facilitated transport mechanism, which have shown desirable CO_2 permeance and CO_2/H_2 selectivity at high operating temperatures (> 100 °C) due to the chemical reactions between CO_2 and amine carriers (*85–97*). In addition, it appears that no report on a WGS membrane reactor using a CO_2-selective membrane has existed prior to the recent work of Ho's group (*88*). As described earlier, there are several advantages of using CO_2-selective WGS membrane reactors instead of H_2-selective WGS membrane reactors. According to the modeling work by Ho's research group (*87*, *92*), CO concentration of less than 10 ppm and H_2 recovery of more than 97% could be achieved by using CO_2-selective WGS membrane reactors with commercial $Cu/ZnO/Al_2O_3$ catalyst from both steam reforming syngas and autothermal reforming syngas.

Downloaded by OHIO STATE UNIV LIBRARIES on June 5, 2012 | http://pubs.acs.org
Publication Date (Web): December 14, 2011 | doi: 10.1021/bk-2011-1088.ch007

Facilitated Transport Mechanism

Figure 1 shows a schematic of the CO_2 transport mechanism in the facilitated transport membranes (*93*). In the facilitated transport process, the CO_2-carrier reaction products (carbamate and bicarbonate) diffuse along their concentration gradients in addition to the diffusion of the unreacted CO_2 across the membrane. In the downstream permeate side with a lower CO_2 concentration than the upstream retentate side, CO_2 is released from the CO_2-carrier reaction products since the CO_2-carrier reactions are reversible. Thus, the membrane can be highly CO_2-selective since the other gases (e.g., H_2, N_2 and CO) cannot react with these carriers (*98*).

For facilitated transport, there are two types of amine carriers: non-sterically hindered amine and sterically hindered amine. The following eqs 2 – 4 present the reactions between CO_2 and the non-sterically hindered amine. Firstly, CO_2 reacts with the amine to form an intermediate zwitterion (eq 2):

$$CO_2 + RNH_2 \Leftrightarrow RNH_2^+COO^- \qquad (2)$$

which can be deprotonated by bases such as amine itself to form the carbamate (eq 3):

$$RNH_2^+COO^- + RNH_2 \Leftrightarrow RNHCOO^- + RNH_3^+ \qquad (3)$$

Thus, the combination of the eqs 2 and 3 gives the following eq 4:

$$CO_2 + 2\ RNH_2 \Leftrightarrow RNHCOO^- + RNH_3^+ \qquad (4)$$

This shows that 2 moles of amines react only with 1 mole of CO_2 for the non-sterically hindered amine (*99*).

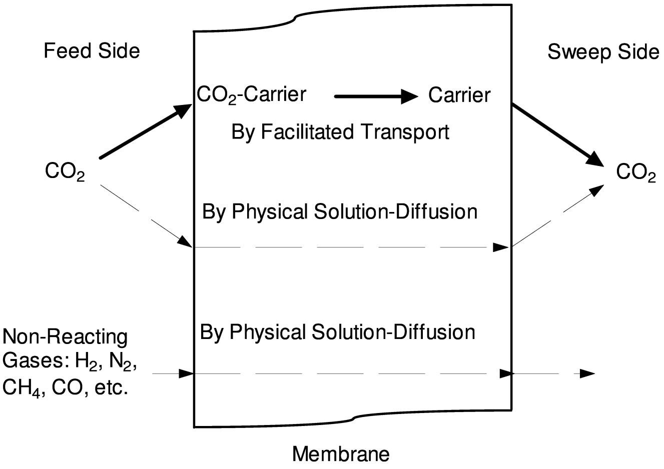
Feed Side
Sweep Side
CO2-Carrier
Carrier
By Facilitated Transport
CO2
CO2
By Physical Solution-Diffusion
Non-Reacting Gases: H2, N2, CH4, CO, etc.
By Physical Solution-Diffusion
Membrane

Figure 1. Schematic of CO_2 transport mechanism in the facilitated transport membrane. (Figure reproduced from reference (93).)

Downloaded by OHIO STATE UNIV LIBRARIES on June 5, 2012 | http://pubs.acs.org
Publication Date (Web): December 14, 2011 | doi: 10.1021/bk-2011-1088.ch007

However, a sterically hindered amine can be defined as either of the following classes: (a) a primary amine in which the amino group is attached to a tertiary carbon and (b) a secondary amine in which the amino group is attached to a secondary or tertiary carbon (*99*). The carbamate of the sterically hindered amine carrier is not stable, and it reacts with H_2O to form the bicarbonate as shown in eq 5:

$$RNHCOO^{-} + H_2O \Leftrightarrow RNH_2 + HCO_3^{-} \qquad (5)$$

Thus, the combination of the eqs 4 and 5 gives the following eq 6:

$$CO_2 + RNH_2 + H_2O \Leftrightarrow HCO_3^{-} + RNH_3^{+} \qquad (6)$$

This shows that 1 mole of amine can react with 1 mole of CO_2 for the sterically hindered amine (*99*). Therefore, the sterically hindered amine can have a higher efficiency for the facilitated transport of CO_2.

The reaction mechanism of CO_2 with K_2CO_3-$KHCO_3$ is described in eq 7 (*100*, *101*):

$$CO_3^{2-} + CO_2 + H_2O \Leftrightarrow 2HCO_3^{-} \qquad (7)$$

In addition, for facilitated transport, there are two types of reactive carriers: the fixed carrier and the mobile carrier. In the fixed carrier membranes, since the fixed carrier only has limited mobility around its equilibrium position, the target component reacts at one carrier site and then hops to the next carrier site from upstream to downstream by the “hopping” mechanism (*74*). However, in the mobile carrier membranes, the mobile carrier reacts with the target component on the high-pressure retentate side, and the reaction product moves across the membrane and releases the target component on the low-pressure permeate side. Regardless of the carrier type, the component being facilitated is removed from the upstream retentate side to the downstream permeate side. However, the other components that are not affected by facilitated transport are retained on the retentate side. Thus, the different components can be separated. Generally, the mobile carriers contribute to the CO_2 flux more than the fixed carriers (*85*). On the other hand, since the mobile carriers are small molecules, they are not bound as strongly as the fixed carriers in the membranes.

There are two parameters to characterize the separation performance of a membrane. One is the selectivity (or separation factor), which is defined as

$$\alpha_{ij} = \frac{y_i / y_j}{x_i / x_j} \qquad (8)$$

Another parameter is the permeability P_i, which is defined as

$$P_i = \frac{J_i}{\Delta p_i / \ell} \qquad (9)$$

The common unit of P_i is Barrer, which is 10^{-10} cm^3 (STP) • cm / (cm^2 • s • cmHg). (P_i / ℓ) is referred to as the permeance, and its common unit is the gas permeation unit (GPU), which is 10^{-6} cm^3 (STP) / (cm^2 • s • cmHg) (*98*).

Compositions of Facilitated Transport Membranes

Polymer Matrix Materials for Facilitated Transport

Not many polymer materials can be used as the polymer matrix in the facilitated transport membranes since most of polymers have shown either undesirable stability or incompatibility with amine carriers. Ho and co-workers have extensively studied the CO_2-selective facilitated transport membranes based on both crosslinked poly(vinyl alcohol) (PVA) matrix and sulfonated polybenzimidazole (SPBI) copolymer matrix.

PVA was chosen as the matrix for the facilitated transport membranes because of its high hydrophilicity, good compatibility with carriers, and good film forming ability. However, PVA without crosslinking could be easily dissolved in water at a temperature of 70 °C or higher (*102*). For certain applications where a temperature of more than 100 °C is required, crosslinking of PVA is very crucial to improve its thermal stability. Both formaldehyde and glutaraldehyde could be used as the crosslinking reagent. When formaldehyde was used as the crosslinking reagent, the crosslinking degree of 60 mol% and the crosslinking time of 16 h at 80 °C were required (*103*). However, when glutaraldehyde was used as the crosslinking reagent, the crosslinking degree of 15 mol% and the crosslinking time of 2 h at 80 °C were already sufficient (*103*). Moreover, the membranes crosslinked with glutaraldehyde have been found to show better separation performance (*103*). Figure 2 shows the schematic of synthesis of the crosslinked PVA with formaldehyde (*91*).

Downloaded by OHIO STATE UNIV LIBRARIES on June 5, 2012 | http://pubs.acs.org
Publication Date (Web): December 14, 2011 | doi: 10.1021/bk-2011-1088.ch007

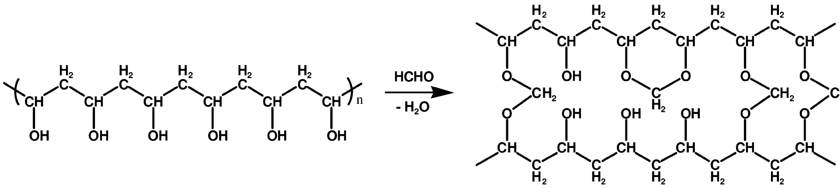

Figure 2. Schematic of synthesis of the crosslinked PVA with formaldehyde. (Figure reproduced from reference (91).)

In addition, SPBI copolymers with excellent thermal and hydrolytic stability (*104*), good compatibility with amine carriers, and a desirable membrane forming property, were also successfully synthesized. Figure 3 shows the schematic of synthesis of the SPBI copolymers (*93*).

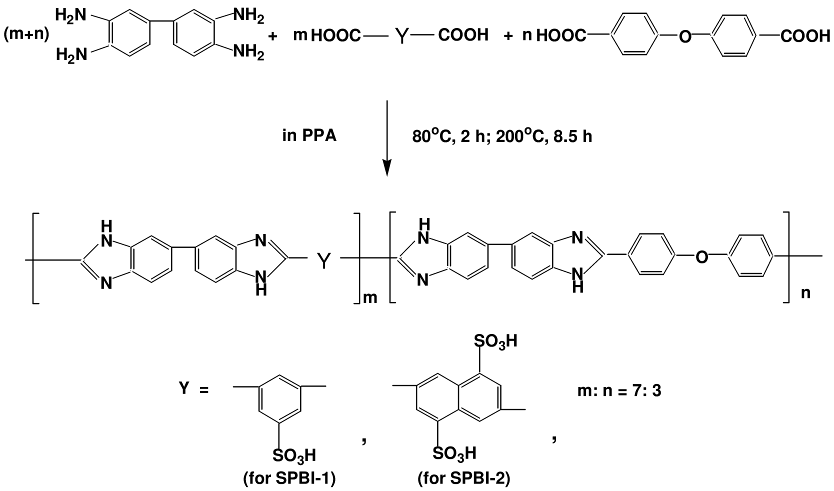

Figure 3. Schematic of the synthesis of new sulfonated polybenzimidazole copolymers. (Figure reproduced from reference (93).)

Thermal stability of the crosslinked PVA and SPBI-1 copolymer was investigated by thermogravimetric analysis (TGA) measurements. The TGA curve of the crosslinked PVA has been shown in the reference (*105*), and the TGA curve of the SPBI-1 copolymer has also been illustrated in the references (*93*, *106*). The TGA curves clearly indicate that the crosslinked PVA and SPBI-1 copolymer were thermally stable up to around 230 °C and 460 °C, respectively. Thus, they are all suitable for gas separation applications at relatively high temperatures.

The glass transition temperatures (Tg) of the crosslinked PVA and SPBI-1 copolymer-based facilitated transport membranes were investigated by differential scanning calorimetry (DSC) measurements. The DSC curve of the crosslinked PVA-based membrane has been illustrated in the reference (*103*), and the DSC curve of the SPBI-1 copolymer-based membrane has also been discussed in reference (*93*). For both the membrane with 50 wt.% crosslinked PVA/50 wt.% carriers (membrane composition: 50 wt.% crosslinked PVA with 60 mol% crosslinking by glutaraldehyde, 20.3 wt.% 2-aminoisobutyric acid-potassium salt (AIBA-K), 18.7 wt.% KOH, and 11 wt.% poly(allylamine) (PAA)) and the membrane with 50 wt.% SPBI-1/50 wt.% carriers (membrane composition: 50 wt.% SPBI-1-potassium salt, 5 wt.% AIBA-K, and 45 wt.% polyethylenimine (PEI)), only one Tg could be observed. This suggested that a

Downloaded by OHIO STATE UNIV LIBRARIES on June 5, 2012 | http://pubs.acs.org
Publication Date (Web): December 14, 2011 | doi: 10.1021/bk-2011-1088.ch007

Downloaded by OHIO STATE UNIV LIBRARIES on June 5, 2012 | http://pubs.acs.org
Publication Date (Web): December 14, 2011 | doi: 10.1021/bk-2011-1088.ch007

desirable homogeneous blending was achieved in these systems. In other words, both crosslinked PVA and SPBI-1 copolymer had good compatibility with the amine carriers. However, the SPBI-1-based membrane showed a much higher Tg (226 °C) than that of the crosslinked PVA-based membrane (84 °C). Thus, the SPBI-1-based membrane has the advantage of being used for asymmetric thin membrane preparation by the phase inversion technique based on the following two reasons: (1) the resulting asymmetric membrane could maintain its sustainable porous structure in the bottom of the membrane, even at high temperatures and pressures. Thus, a very thin dense separation layer (~ 0.1 µm) is possible to be prepared, and the flux of the membrane could be significantly improved in comparison with the membrane prepared by the solution-casting method, which generally has a membrane thickness of greater than about 2 µm. (2) The SPBI copolymer is soluble in organic solvents (such as dimethyl sulfoxide) but insoluble in water. Therefore, water can be used as the non-solvent in the phase inversion process, which is in line with the industrial operation.

Carriers for Facilitated Transport

In Ho's research group, AIBA-K and potassium carbonate-potassium bicarbonate (K_2CO_3-$KHCO_3$, converted from KOH) have been used as the mobile carriers (*85–97*), and PAA, 2-bromobutane functionalized PAA (PAA-C_4H_9) and PEI have been used as the fixed carriers (*85–97*) for CO_2 transport. The chemical structures of the carriers are displayed in Figure 4.

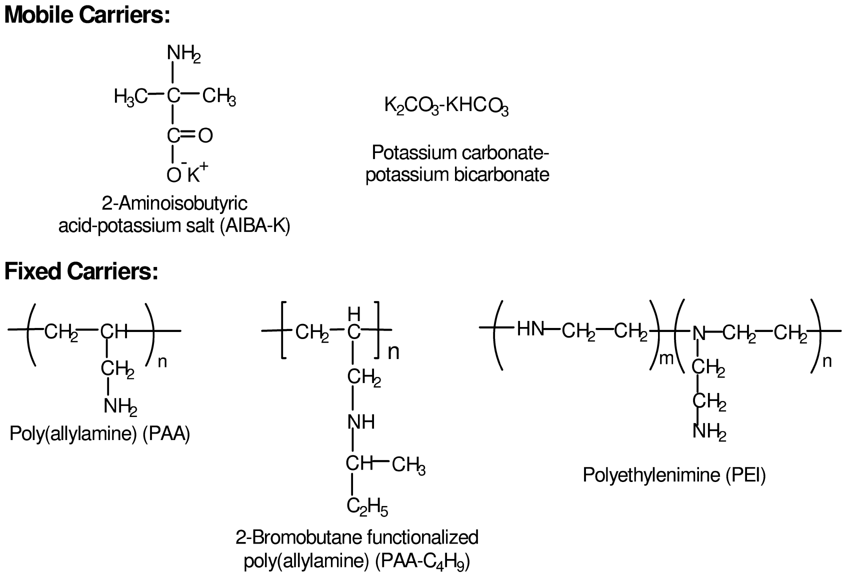
Mobile Carriers:
2-Aminoisobutyric acid-potassium salt (AIBA-K)
K2CO3-KHCO3
Potassium carbonate-potassium bicarbonate
Fixed Carriers:
Poly(allylamine) (PAA)
2-Bromobutane functionalized poly(allylamine) (PAA-C4H9)
Polyethylenimine (PEI)

Figure 4. Chemical structures of the mobile and fixed carriers for CO_2 facilitated transport.

Downloaded by OHIO STATE UNIV LIBRARIES on June 5, 2012 | http://pubs.acs.org
Publication Date (Web): December 14, 2011 | doi: 10.1021/bk-2011-1088.ch007

The reaction mechanisms of CO_2 with both fixed and mobile carriers have been described in details in the previous section. Generally, the mobile carriers contribute to the CO_2 flux more than the fixed carriers (*85*). However, since the mobile carriers are small molecules, they are not bound as strongly as the fixed carriers in the membranes. The mobile carrier AIBA-K and fixed carrier PAA-C_4H_9 belong to the sterically-hindered amine whereas the fixed carrier PAA and PEI belong to the unhindered amine. The reaction mechanisms of CO_2 with both hindered and unhindered amine carriers have been described in details in the previous section (eqs 2 – 6). The sterically hindered amine can have a higher efficiency for the facilitated transport of CO_2. The reaction mechanism of CO_2 with K_2CO_3-$KHCO_3$ is also described in the previous section (eq 7).

Synthesis Gas Purification for Fuel Cells

Majority of CO_2-selective facilitated transport membranes synthesized in Ho's research group for fuel cell applications contained crosslinked PVA as the polymer matrix, both AIBA-K and K_2CO_3-$KHCO_3$ (converted from KOH) as the mobile carriers, and PAA as the fixed carrier for CO_2 transport (*85–92*). This will be the membrane composition in case of no specifications in the context. Figure 5 shows the scanning electron microscopy (SEM) image of the cross-section of the above mentioned crosslinked PVA-based membrane on the GE A1 microporous polysulfone support (*86*). It can be seen that the membrane mainly consisted of two portions: a dense active layer at the top to provide separation and the microporous polysulfone support at the bottom to provide mechanical strength. This composite structure maximizes the mechanical strength while minimizes the mass transfer resistance of the membrane.

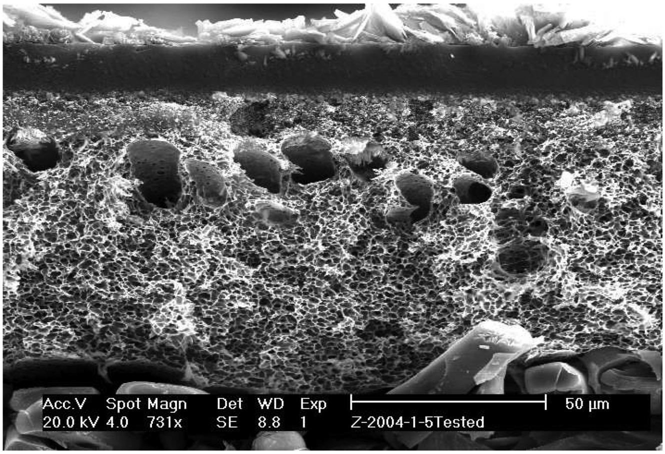

Figure 5. SEM image of the cross-section of the facilitated transport membrane synthesized on a microporous polysulfone support. (Figure reproduced from reference (86).)

Downloaded by OHIO STATE UNIV LIBRARIES on June 5, 2012 | http://pubs.acs.org
Publication Date (Web): December 14, 2011 | doi: 10.1021/bk-2011-1088.ch007

CO_2 Transport Properties of Facilitated Transport Membranes

In gas permeation experiments, both the feed and the sweep gases were fed with controlled amounts of water before entering the permeation cell. Higher water contents on both the feed side and the sweep side increased the CO_2 permeability of the membrane (*86*). Presumably, this was due to the fact that the higher water content on the feed or sweep side increased the water retention inside the membrane, which resulted in the increased mobility of both fixed and mobile carriers as well as the enhanced reaction rates of CO_2 with these carriers (eqs 2 – 7). In addition, CO_2/H_2 selectivity also increased as the water content on the feed or sweep side increased (*86*). The reason is that the CO_2 permeability increased with the increase of water content as described above, while the transport of H_2 was not significantly affected by the increase of the water content.

Both CO_2 permeability and CO_2/H_2 selectivity increased with temperature from 50 to 100 $_0$C (*85*). This is unusual in view of typical membranes based on the solution-diffusion mechanism, for which the permeability increase is always accompanied with selectivity reduction (*14*). The selectivity increase for the synthesized facilitated transport membrane was due to (1) a significant CO_2 permeability increase from the facilitated transport with a higher CO_2-amine reaction rate as temperature increased and (2) a much less H_2 permeability increase due to lower H_2 solubility in the membrane as temperature increased. In this temperature range, an activation energy of 62.9 kJ/mol for CO_2 permeation was obtained through the Arrhenius equation (*85*).

The CO_2 permeability and CO_2/H_2 selectivity as a function of temperature from 100 °C to 180 °C are shown in Figure 6 at a feed gas pressure of 2.1 atm and a sweep gas pressure of 1.0 atm (*88*). The feed gas composition was 20% CO_2, 40% H_2 and 40% N_2.

As shown in Figure 6, the CO_2 permeability was about 3500 Barrers or higher for the temperatures ranging from 100 °C to 150 °C. However, the permeability reduced to about 1900 Barrers as the temperature increased to 180 °C. This was due to the reduction of water retention in the membrane as the temperature increased. Also shown in this figure, the CO_2/H_2 selectivity was about 80 or higher for the temperatures ranging from 100 °C to 150 °C. The selectivity reduced slightly as the temperature increased to 170 °C. This was a result of CO_2 permeability decrease due to the reduction of water retention in the membrane as described above. At 180 °C, the selectivity reduced significantly to slightly greater than 10 due to the significant swelling of this membrane at this high temperature. Nonetheless, the selectivity of 10 is still good enough to give a reasonably high H_2 recovery of about 90% (*88*).

N_2 is a principal component in autothermal reforming synthesis gas. Similar to H_2, N_2 also transports through the facilitated transport membranes by the solution-diffusion mechanism only. Since N_2 is a much bigger molecule than H_2, it is expected to permeate through the membranes more slowly by the solution-diffusion mechanism. Therefore, the synthesized CO_2-selective facilitated transport membranes have more desirable CO_2/N_2 separation properties. As shown in Figure 7, the CO_2/N_2 selectivity was 260 or higher for the temperatures ranging from 110 °C to 150 °C. The selectivity was still quite high (around 100) at the temperature of 180 °C (*86*).

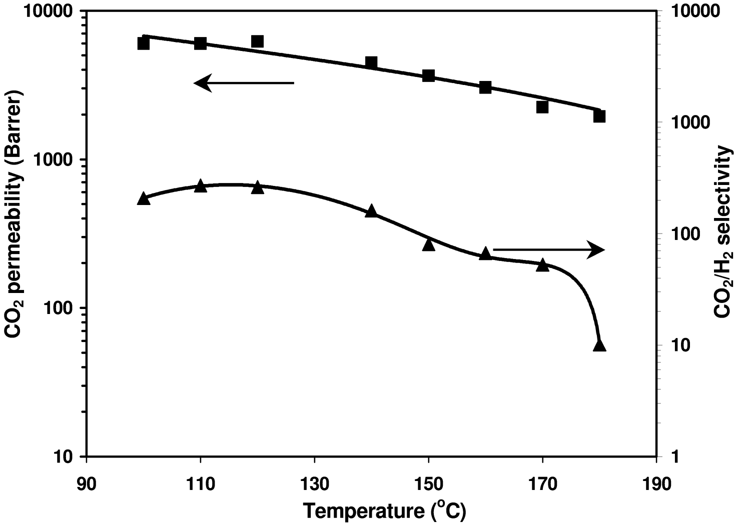

Figure 6. CO_2 permeability and CO_2/H_2 selectivity as a function of temperature (Figure reproduced from reference (88)). (▪) CO_2 permeability; (▴) CO_2/H_2 selectivity. (Small circular cell, feed gas: 20% CO_2, 40% H_2 and 40% N_2, p_f = 2.1 atm, p_s = 1.0 atm, membrane thickness = 26 μm).

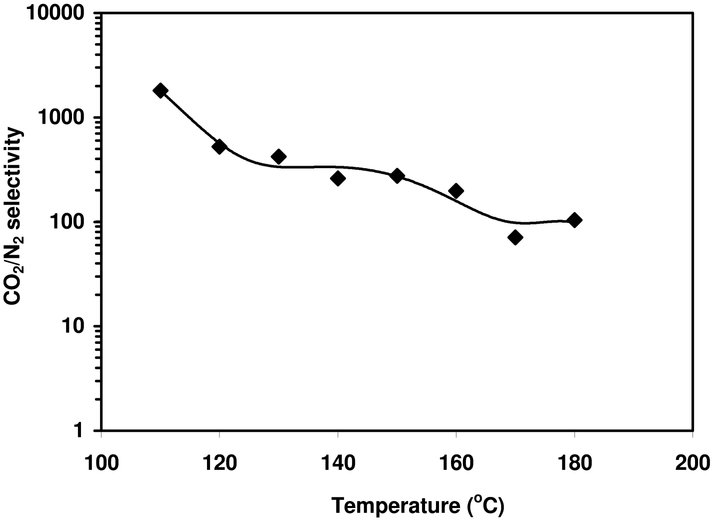

Figure 7. CO_2/N_2 selectivity as a function of temperature (Figure reproduced from reference (86)). (Small circular cell, feed gas: 20% CO_2, 40% H_2 and 40% N_2, p_f = 2.0 atm, p_s = 1.0 atm, membrane thickness = 70 μm).

Downloaded by OHIO STATE UNIV LIBRARIES on June 5, 2012 | http://pubs.acs.org
Publication Date (Web): December 14, 2011 | doi: 10.1021/bk-2011-1088.ch007

The membranes synthesized also showed very desirable CO_2/CO separation performance. Figure 8 presents the CO_2/CO selectivity as a function of temperature from 100 °C to 170 °C at the feed gas pressure of 2.0 atm and sweep gas pressure of 1.0 atm (*86*). The feed gas composition was 1% CO, 17% CO_2, 45% H_2 and 37% N_2. As shown in the figure, CO_2/CO selectivity reduced as the temperature increased. This was due to the reduction of water retention in the membrane as described earlier. However, even at 170 °C, the CO_2/CO selectivity was still greater than 150, which is high enough for syngas applications (*86*). A high CO_2/CO selectivity is desirable because a higher CO_2/CO selectivity means a less CO loss. Therefore, more CO can be converted into H_2 in the WGS reaction step, which increases the overall H_2 recovery.

Downloaded by OHIO STATE UNIV LIBRARIES on June 5, 2012 | http://pubs.acs.org
Publication Date (Web): December 14, 2011 | doi: 10.1021/bk-2011-1088.ch007

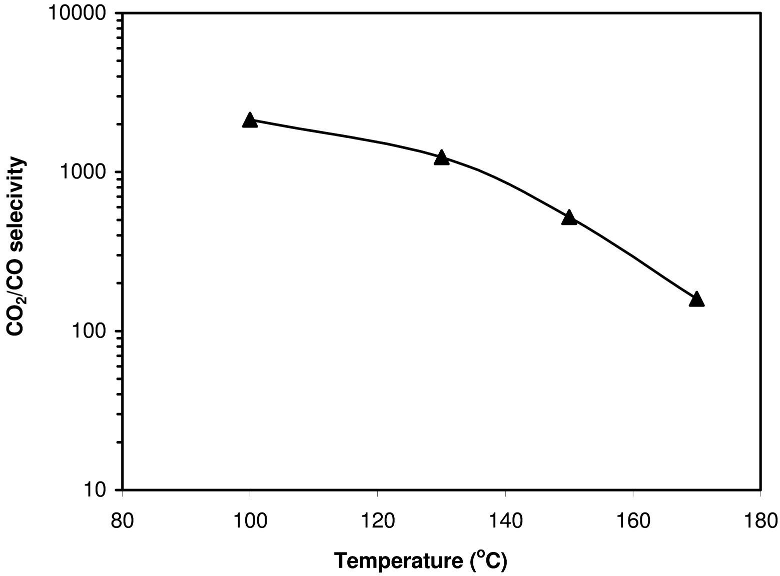

Figure 8. CO_2/CO selectivity as a function of temperature (Figure reproduced from reference (86)). (Small circular cell, feed gas: 1% CO, 17% CO_2, 45% H_2 and 37% N_2, p_f = 2.0 atm, p_s = 1.0 atm, membrane thickness = 70 μm).

As depicted in Figure 6, the membrane showed the most desirable CO_2 permeability at 100 – 120 °C. Thus, the temperature of 120 °C was chosen for CO_2 removal ability study of the membrane. Since the previously used circular permeation cell had a relatively small membrane area (45.6 cm^2) and more chance of the channeling effect, a rectangular flat-sheet membrane permeation cell (342.7 cm^2) was constructed for the CO_2 removal experiments. The new “big cell” had 7.5 times the membrane area of the previous circular permeation cell and a well-defined gas flow and velocity profile on both the feed and sweep sides. The feed gas consisted of 1% CO, 17% CO_2, 45% H_2 and 37% N_2. The feed gas pressure was about 2 atm, and the sweep gas pressure was about 1 atm. The water contents on the feed and sweep sides were approximately 32 – 37 mol% and 95 mol%, respectively.

Figure 9 shows the final exit CO_2 concentration in the retentate (dry basis) as a function of the feed gas flow rate (dry basis) in this rectangular cell (*89*). As shown in the figure, at a feed rate of 60 cm^3/min, CO_2 concentration in the feed side could be reduced from 17% to about 10 ppm, nearly complete removal of CO_2. Even with a feed rate of 120 cm^3/min, CO_2 concentration could still be reduced to as low as 1000 ppm. Thus, by using the above feed gas composition, a CO_2 removal of > 99.4% could be achieved with this big rectangular cell even with a flow rate around 100 – 120 cm^3/min (*89*). Such effectiveness in CO_2 removal could be attributed to the high CO_2 permeability demonstrated in Figure 6.

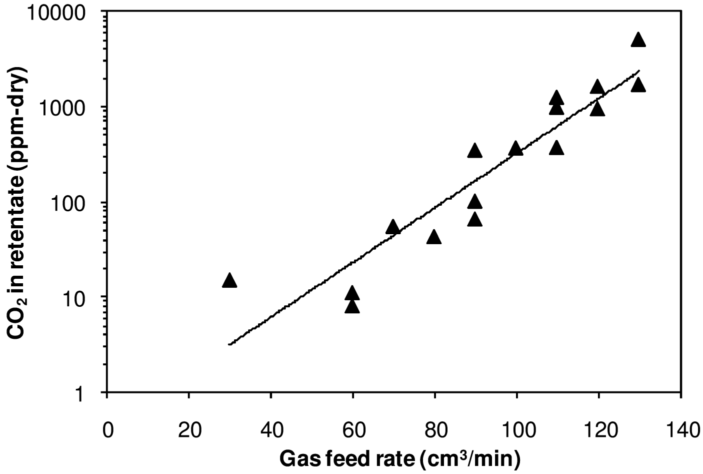

Figure 9. CO_2 concentration in retentate as a function of feed gas flow rate (Figure reproduced from reference (89)). (Big rectangular cell, feed gas: 1% CO, 17% CO_2, 45% H_2 and 37% N_2, feed water content: 32 – 37 mol%, sweep water content: 95 mol%, $p_f = 2.0$ atm, $p_s = 1.0$ atm, average membrane thickness = 40 μm, T = 120 °C, feed/sweep ratio = 1/1 (dry basis)).

As depicted in Figures 6 – 8, the membranes synthesized were much more selective to CO_2 compared to other gas components, such as H_2, N_2 and CO. Thus, mainly CO_2 could pass through the membrane and go to the permeate side. In laboratory studies, argon can be used as the sweep gas for ease of gas chromatographic analysis. In real industrial applications, it is more feasible to use steam alone as the sweep gas. As a result, the permeated CO_2 will be easily separated from steam to obtain a high concentration (> 98%) for sequestration. The high permeate CO_2 concentration (> 98%) has been achieved by using steam alone as sweep gas in the CO_2 capture experiments by Ho's research group (*91*).

In addition to crosslinked PVA polymer matrix, CO_2-selective facilitated transport membranes containing both the mobile (AIBA-K) and fixed (PEI or PAA) carriers in the SPBI copolymer matrix were also synthesized in Ho's research group (*93*). The SPBI copolymer-based facilitated transport membranes showed the best separation performance at 100 °C (*93*) instead of around 106 °C for crosslinked PVA-based membranes (*85–92*) because of the lower

Downloaded by OHIO STATE UNIV LIBRARIES on June 5, 2012 | http://pubs.acs.org
Publication Date (Web): December 14, 2011 | doi: 10.1021/bk-2011-1088.ch007

Downloaded by OHIO STATE UNIV LIBRARIES on June 5, 2012 | http://pubs.acs.org
Publication Date (Web): December 14, 2011 | doi: 10.1021/bk-2011-1088.ch007

hydrophilicity of SPBI compared to crosslinked PVA. In addition, compared to the crosslinked PVA-based membranes (*85–92*), the SPBI-based facilitated transport membranes showed lower CO_2 permeability and CO_2/H_2 selectivity (*93*). The reason is that the SPBI copolymers are less hydrophilic than the crosslinked PVA matrix. Thus, the crosslinked PVA-based membranes could maintain more water, particularly at high temperatures. As described earlier, water is very important for both the reaction between CO_2 and carriers and the diffusion of CO_2-carrier reaction products (*86*). However, the SPBI-based facilitated transport membrane with an optimized composition still showed a CO_2/H_2 selectivity as high as 64.9 and a CO_2 permeability as high as 2539 Barrers (*93*), which is very desirable in synthesis gas purification for fuel cell applications. As mentioned earlier, the SPBI copolymer-based facilitated transport membranes have the advantage of being used for asymmetric membrane preparation by the phase inversion technique.

H_2S Transport Properties of Facilitated Transport Membranes

The CO_2-selective membranes synthesized in Ho's research group as previously discussed (*85–92*), which consist of crosslinked PVA polymer matrix, AIBA-K/K_2CO_3-$KHCO_3$ mobile carriers and PAA fixed carrier, are also desirable to be used for H_2S removal. H_2S has a much higher reaction rate with the amine than CO_2 as the former reacts with the amine via proton transfer (eq 10) and the latter reacts with the amine via carbamate formation (eq 4) primarily.

$$H_2S + RNH_2 \Leftrightarrow HS^- + RN^+H_3 \qquad (10)$$

Thus, H_2S can permeate through the membrane much faster than CO_2, and H_2S can be completely removed from the synthesis gas before WGS reaction, e.g., using a separate membrane module for the H_2S removal before a WGS membrane reactor or in the front section of the WGS membrane reactor without the H_2S removal module.

Initial results achieved in Ho's group showed that the membranes exhibited much higher permeability of H_2S, which was about 3 times that of CO_2 (*107–109*). Using the feed gas composition with 50 ppm H_2S, 1% CO, 17% CO_2, 45% H_2 and 37% N_2, and at a feed gas pressure of 2.0 atm and a sweep gas pressure of 1.0 atm, a high H_2S permeability of greater than 20000 Barrers and a high H_2S/H_2 selectivity of greater than 600 were obtained at 110 – 130 °C (*107–109*). The "big rectangular cell" with an active membrane area of 342.7 cm^2 as mentioned previously was also used for the removal of H_2S from the synthesis gas containing 50 ppm H_2S, 6.5% CO, 12% CO_2, 40% H_2, 1.5% CH_4 and 40% N_2. At 120 °C with the feed gas pressure of 2.5 atm and sweep gas pressure of 1.0 atm, a low H_2S concentration of about 10 part per billion (ppb) in retentate was obtained at a feed gas flow rate of 5 cm^3/min, indicating a nearly complete removal of H_2S from the synthesis gas. Even at the high feed flow rate of 60 cm^3/min, the H_2S concentration in the exit retentate stream was still less than 1000 ppb (1 ppm) (*107–109*). Thus, the H_2S existing in synthesis gas can be almost completely removed by the facilitated

Downloaded by OHIO STATE UNIV LIBRARIES on June 5, 2012 | http://pubs.acs.org
Publication Date (Web): December 14, 2011 | doi: 10.1021/bk-2011-1088.ch007

transport membranes before feeding into the WGS membrane reactor, and the poisoning of the WGS catalyst, e.g., Cu/Zn/Al_2O_3, can be prevented.

CO Conversion/Reduction by WGS Membrane Reactor

Ho's research group has successfully used the synthesized CO_2-selective polymeric membranes with very desirable CO_2/H_2, CO_2/N_2 and CO_2/CO selectivities as well as very high CO_2 permeability at 110 – 180 °C (*85–92*) for CO_2-selective WGS membrane reactor work. Figure 10 shows the schematic of the water gas shift membrane reactor (*88*).

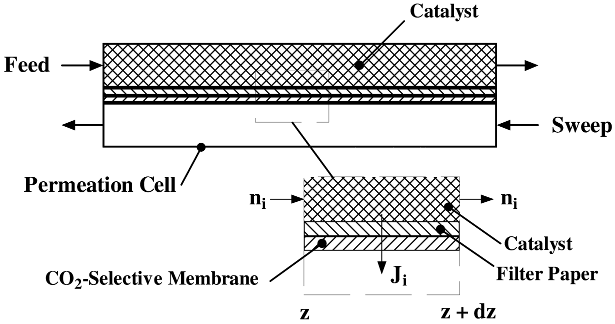

Figure 10. Schematic of the water gas shift membrane reactor. (Figure reproduced from reference (88).)

The membranes consisted of crosslinked PVA polymer matrix, PAA fixed carrier and AIBA-K/K_2CO_3-$KHCO_3$ mobile carriers. In the work, a "big cell" membrane reactor was used for studying the WGS membrane reactor and its scale-up. The "big cell" membrane reactor was a rectangular cell with well defined flow channels, a width of 17.5 cm and an active membrane area of 342.7 cm^2. The catalyst used in the study was commercial Cu/ZnO/Al_2O_3 WGS catalyst. In the membrane reactor experiments, the synthesis gas feed containing 1% CO, 17% CO_2, 45% H_2 and 37% N_2 entered into the membrane reactor after the catalyst activation. The operating temperature was 150 °C. The feed gas pressure was 2.0 atm and the sweep gas pressure was 1.0 atm. The water content of the feed stream was between 40 mol% and 50 mol%, and the water content of the sweep stream was remained at 93 mol% (*88*).

The results obtained from the "big cell" WGS membrane reactor are shown in Figure 11. As presented in the figure, the CO concentration in the exit retentate stream, i.e., the H_2 product, was less than 10 ppm (equivalent to almost 100% CO conversion) for various feed flow rates of the synthesis gas ranging from 20 to 70 cm^3/min (*88*). With the increase of the feed flow rate, the retentate CO concentration increased, which was due to the reduced CO residence time in the membrane reactor. In addition, as shown in the figure, the experimental data agreed reasonably with the prediction of the mathematical model, which was developed based on the material and energy balances, membrane permeation, and the low-temperature WGS reaction kinetics for the commercial catalyst (*87*, *88*, *92*).

Downloaded by OHIO STATE UNIV LIBRARIES on June 5, 2012 | http://pubs.acs.org
Publication Date (Web): December 14, 2011 | doi: 10.1021/bk-2011-1088.ch007

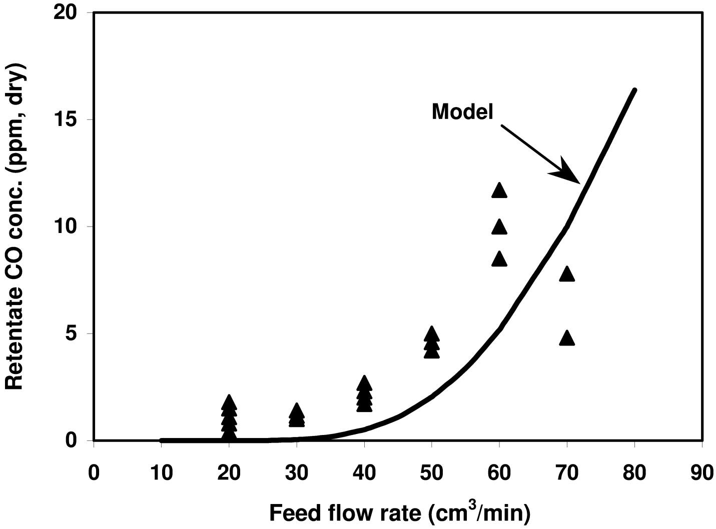

Figure 11. Retentate CO concentration as a function of feed flow rate in the rectangular WGS membrane reactor (Figure reproduced from reference (88)). (Big rectangular cell, feed gas: 1% CO, 17% CO_2, 45% H_2 and 37% N_2, feed water content: 40 – 50 mol%, sweep water content: 93 mol%, $p_f = 2.0$ atm, $p_s = 1.0$ atm, average membrane thickness = 53 μm, T = 150 °C, feed/sweep ratio = 1/1 (dry basis)).

From the modeling work, the exit CO concentration without CO_2 removal should be at an equilibrium value of about 190 ppm at 150 °C and 40 mol% water content. The much lower CO level (< 10 ppm) obtained in this work was due to the use of membrane reactor to continuously remove CO_2 during the WGS reaction and shift the equilibrium of the reaction to the forward direction (eq 1) (*87*, *88*, *92*).

In addition, the percentage of H_2 loss due to its permeation through the membrane was very small. A retentate with a H_2 concentration of greater than about 50% was achieved, which was significantly enhanced in comparison with its original concentration (45%) (*88*, *89*). The rest of the retentate consisted of N_2, CO_2 and a trace amount of CO. The N_2 concentration ranged from 50% to 42%, and the CO_2 concentration ranged from 0.1% to 10%, depending on the feed flow rate. The CO concentration in the retentate has been presented previously in Figure 11. Moreover, as described earlier, the permeate CO_2 dry concentration of greater than 98% could be obtained at various feed gas flow rates when steam only was used as the sweep gas, using this kind of CO_2-selective facilitated transport membranes (*87*, *88*, *92*).

Ho's research group also investigated a new two-step process for H_2 purification and CO reduction (*89*). The first step was the nearly complete removal of CO_2 (> 99%), and the second step was the low temperature WGS reaction. Since CO_2 has been almost completely removed in the first step, the WGS reaction equilibrium could be significantly shifted forward (eq 1) to

Downloaded by OHIO STATE UNIV LIBRARIES on June 5, 2012 | http://pubs.acs.org
Publication Date (Web): December 14, 2011 | doi: 10.1021/bk-2011-1088.ch007

reduce the exit rententate CO concentration to less than 10 ppm. As discussed earlier, the new CO_2-selective facilitated transport membranes showed the best performance at 110 – 120 °C. However, the WGS reaction performed the best at the temperature of 140 – 150 °C. The advantage of using two-step process is that the CO_2 removal by membrane can be carried out in the first step at 120 °C, and the WGS reaction can be done in the second step at 150 °C. As a result, both of these two steps can perform at their preferable temperatures, respectively. Thus, the system performance can be optimized.

Figure 9 already shows that by using a big rectangular cell and the feed gas composition of 1% CO, 17% CO_2, 45% H_2 and 37% N_2, a CO_2 removal of > 99.4% with the resulting concentration of < 1000 ppm (0.1%) could be achieved even with a flow rate around 100 – 120 cm^3/min at 120 °C (*89*). Thus, after the first CO_2 removal step, the resulting synthesis gas composition would be 1.19% CO, 0.10% CO_2, 53.87% H_2 and 44.84% N_2, and this feed composition was introduced into the second step, WGS reactor. At 140 and 150 °C with a feed pressure of 2 atm and a steam content of about 42 mol%, the CO concentration in the exit stream from the WGS reactor was reduced to less than 10 ppm (on dry basis) (*89*), which met the requirement for PEMFC applications. In addition, the percentage of H_2 loss due to its permeation through the membrane was very low. The H_2 concentrations at the exit were increased to 55.1% and 54.4% at 140 °C and 150 °C, respectively, compared to the concentration of 45% going into the first CO_2 removal step and the concentration of 53.9% going into the second WGS reaction step (*89*).

Synthesis Gas Purification for Petrochemical and Refining Applications

As described in the last section, Ho and co-workers have extensively studied the CO_2-selective facilitated transport membranes based on both crosslinked PVA matrix and SPBI copolymer matrix for low-pressure synthesis gas purification for fuel cell applications (*85–95*). However, the requirements by the refining and petrochemical industries for the applications of CO_2-selective membranes for CO_2/H_2 separation are more challenging since feed pressures of 220 psia or higher are preferred. At high pressures, the facilitated transport membranes generally suffer from the carrier saturation phenomenon, which results in lower CO_2/H_2 selectivity and CO_2 permeability (*86*). The CO_2-selective membranes synthesized in Ho's research group as previously discussed (*85–92*), which consisted of crosslinked PVA polymer matrix, AIBA-K/K_2CO_3-$KHCO_3$ mobile carriers and PAA fixed carrier, were also investigated for high-pressure petrochemical and refining applications (*97*, *103*).

A study with non-optimized membrane compositions showed that with the increase of feed gas pressure, both CO_2 permeability and CO_2/H_2 selectivity reduced as expected. For example, with feed gas composition of 20% CO_2 and 80% H_2, at 110 °C and a sweep gas pressure of 15 psia, the non-optimized membrane with a thickness of around 48 μm showed a CO_2 permeability of 1073 Barrers and a CO_2/H_2 selectivity of 52.8 at the feed gas pressure of 100 psia, a CO_2 permeability of 756 Barrers and a CO_2/H_2 selectivity of 42.3 at the feed gas pressure of 225 psia, and a CO_2 permeability of 383 Barrers and a CO_2/H_2 selectivity of 24.2 at the feed gas pressure of 440 psia (*103*). Increasing feed gas pressure caused the decrease of CO_2 permeability, which was due to the carrier saturation phenomenon (*82*, *86*). This is the characteristic of facilitated transport membranes. As described by Ho and Dalrymple (*82*), when the CO_2 partial pressure is high, carrier saturation will occur. In this situation, the CO_2 flux of the membrane reaches constant. The increase of CO_2 partial pressure does not further increase the CO_2 flux, and hence CO_2 permeability drops according to eq 9. The CO_2/H_2 selectivity also reduced as the feed gas pressure increased, which again can be explained using the carrier saturation phenomenon as described earlier. CO_2 permeability reduced as the feed gas pressure increased; unlike CO_2, H_2 has no chemical association with the carriers and its permeability does not subject to the carrier saturation phenomenon, and thus does not change with feed gas pressure significantly. As a result, the CO_2/H_2 selectivity reduced as the feed gas pressure increased.

The above study shows that increasing feed gas pressure caused both the decrease of CO_2/H_2 selectivity and the decrease of CO_2 permeability due to the carrier saturation phenomenon. However, through membrane composition and process optimization, the crosslinked PVA-based facilitated transport membranes synthesized in Ho's research group have shown CO_2/H_2 selectivity higher than 30 (30 – 70) and CO_2 permeability as high as close to 1000 Barrers for a membranes thickness of 15 – 30 μm at a feed gas pressure of 220 psia (*97*), which have great potential to be used for high-pressure synthesis gas purification for petrochemical and refining applications.

In addition to crosslinked PVA polymer matrix, CO_2-selective facilitated transport membranes containing both the mobile (AIBA-K) and fixed (PAA) carriers in the SPBI copolymer matrix were also investigated for high-pressure synthesis gas purification by Ho's research group (*97*). As described earlier, the SPBI copolymer-based facilitated transport membranes showed the best separation performance at 100 °C. Again, due to the lower copolymer hydrophilicity, the SPBI-based facilitated transport membranes showed lower CO_2 permeability and CO_2/H_2 selectivity compared to the crosslinked PVA-based membranes even for this high-pressure feed gas application. However, the SPBI-based facilitated transport membrane with a thickness of 50 μm still showed a CO_2/H_2 selectivity as high as 20 and a CO_2 permeability as high as 892 Barrers (*97*), which is still desirable in high-pressure synthesis gas purification for petrochemical and refining applications. As mentioned earlier, the SPBI copolymer-based facilitated transport membranes have the advantage of being used for asymmetric membrane preparation by the phase inversion technique.

Polymer/silica mixed matrix membranes have gained interest in recent years because the introduction of silica particles into polymers could not only improve thermal and mechanical propeties of membranes but also enhance gas transport properties of membranes (i.e., increase target gas selectivity, permeability or both) (*6*, *110–114*). Merkel et al. reported that both gas permeability and selectivity of large organic molecules were simultaneously enhanced by introducing nonporous, nanosize fumed silica (FS) particles into poly(4-methyl-2-pentyne) (*6*). This was

Downloaded by OHIO STATE UNIV LIBRARIES on June 5, 2012 | http://pubs.acs.org
Publication Date (Web): December 14, 2011 | doi: 10.1021/bk-2011-1088.ch007

Downloaded by OHIO STATE UNIV LIBRARIES on June 5, 2012 | http://pubs.acs.org
Publication Date (Web): December 14, 2011 | doi: 10.1021/bk-2011-1088.ch007

attributed to the FS-induced disruption of polymer chain packing, resulting in subtle increase in the size of free volume elements. Gomes et al. also reported similar gas transport behavior for poly(1-trimethylsilyl-1-propyne)/silica mixed matrix membranes (*115*).

In Ho's research group, mixed matrix membranes containing both amine carriers (AIBA-K/K_2CO_3-$KHCO_3$ mobile carriers and PAA fixed carrier) and hydrophilic fumed silica nanoparticles based on either crosslinked PVA matrix or crosslinked PVA-polysiloxane matrix were synthesized and investigated for high-pressure synthesis gas purification (*96*). TGA analysis shows that the thermal stability of the mixed matrix membranes was significantly improved by incorporating fumed silica nanoparticles (*96*). The CO_2 permeance and CO_2/H_2 selectivity as a function of fumed silica content from 4% to 31% are shown in Figure 12 at a temperature of 107 °C, a feed gas pressure of 220 psia, and a sweep gas pressure of 15.7 psia (*96*). The feed gas composition was 20% CO_2 and 80% H_2.

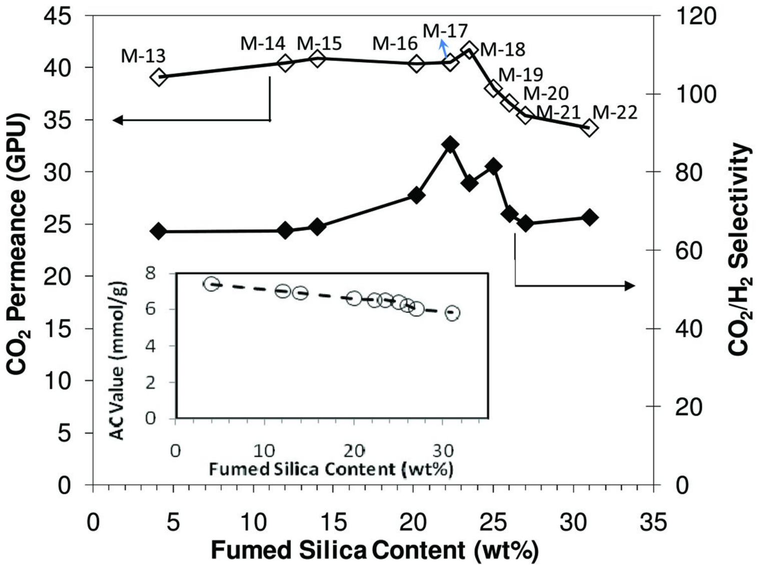

Figure 12. CO_2 permeance and CO_2/H_2 selectivity vs. FS loading content (Figure reproduced from reference (96)). (Small circular cell, feed gas: 20% CO_2 and 80% H_2, $T = 107$ °C, $p_f = 220$ psia, $p_s = 15.7$ psia, membrane thickness = 25 – 32 μm).

Figure 12 shows that with the increase of the fumed silica content, the amine concentration value (AC value) of the resulting membrane, which is defined as the molar equivalents of effective amine functional groups (carriers) per mass of dry membrane in the unit of mmol/g (*93*), reduced because of the decreased relative ratio of amine carriers in membranes (*96*). However, the CO_2/H_2 selectivity and CO_2 permeance of the resulting facilitated transport membranes increased with the FS content (even though not a very significant effect) upto a FS loading of 23%. This was due to the fact that the incorporated FS nanoparticles disrupted

Downloaded by OHIO STATE UNIV LIBRARIES on June 5, 2012 | http://pubs.acs.org
Publication Date (Web): December 14, 2011 | doi: 10.1021/bk-2011-1088.ch007

the packing of the polymer chains and increased the free volume of membranes, which was in consistence with other literature findings (*6*). Further increase of the FS content to over 23% reduced both CO_2/H_2 selectivity and CO_2 permeance of the resulting facilitated transport membranes due to the reduced total AC value. As a result, at 107 °C and 220 psia, the facilitated transport membrane synthesized in Ho's research group with 22.3 wt% FS loading showed the optimized performance with a CO_2/H_2 selectivity of 87 and a CO_2 permeability of 1296 Barrers for a membrane thickness of 32 μm (*96*).

In addition to hydrophilic fumed silica nanoparticles, multi-walled carbon nanotubes (MWNTs) were also used as inorganic fillers for making mixed matrix facilitated transport membranes (*116*). The MWNTs were functionalized with hydrophilic groups to improve the resulting membrane hydrophilicity. The resulting mixed matrix facilitated transport membranes showed both desirable synthesis gas purification performance and long-term membrane stability (*116*).

By incorporating hydrophilic FS nanoparticles or MWNTs (*96*, *116*), the resulting mixed matrix facilitated transport membranes not only showed improved high-pressure synthesis gas purification performance, but also exhibited improved membrane thermal and mechanical properties, increased resistance to membrane compression at high temperatures and pressures, reduced membrane swelling at high temperatures and high water contents, and stable membrane gas transport properties. Thus, the mixed matrix facilitated transport membranes synthesized in Ho's research group have great potential to be used for synthesis gas purification, particularly for high-pressure petrochemical and refining applications.

Conclusions

In summary, Ho's research group first proposed, synthesized, and experimentally demonstrated novel CO_2-selective membranes capable of possessing high CO_2 permeability and CO_2/H_2 selectivity (> 80) at relatively high temperatures (100 – 180 °C), and elucidated the unusual phenomenon of both permeability and selectivity increases with temperature. Less than 10 ppm of CO in the H_2 product was achieved with a WGS membrane reactor using the membrane to drive the WGS reaction to the product side via CO_2 removal. The data were in good agreement with model predictions. This was the first WGS membrane reactor using a CO_2-selective membrane. In addition, less than 10 ppb of H_2S in the H_2 product was also achieved since the membrane was also highly H_2S-selective.

The membrane performance (CO_2/H_2 selectivity and CO_2 permeability) reduced with increased feed gas pressure due to the typical carrier satuation phenomenon at high CO_2 partial pressures. However, through membrane composition improvement, a CO_2/H_2 selectivity of over 50 and a CO_2 permeability of over 1000 Barrers could still be obtained at a CO_2 feed partial pressure of 44 psia, which is very desirable for high-pressure petrochemical and refining applications. The mixed-matrix facilitated transport membranes with inorganic fillers showed both improved gas separation performance and enhanced membrane mechanical strength and stability, particularly for high-pressure applications.

Downloaded by OHIO STATE UNIV LIBRARIES on June 5, 2012 | http://pubs.acs.org
Publication Date (Web): December 14, 2011 | doi: 10.1021/bk-2011-1088.ch007

Acknowledgments

We would like to thank the National Science Foundation, the Office of Naval Research, and the Ohio Department of Development for the financial support of this work. Part of this material is based upon work supported by the National Science Foundation under Grant No. 1033131.

Nomenclature

J = steady-state permeation flux (cm^3 (STP)/(cm$^2 \cdot$ s))
ℓ = membrane thickness (cm)
P = permeability (Barrer)
p = pressure (cmHg)
p_f = feed side pressure (cmHg)
p_s = sweep (permeate) side pressure (cmHg)
Δp = pressure difference between the feed and permeate sides (cmHg)
x = retentate molar fraction
y = permeate molar fraction

Greek Letter

α = selectivity

Subscripts

i, j = species

References

1. Ghenciu, A. F. *Curr. Opin. Solid State Mater. Sci.* **2002**, *6* (5), 389–399.
2. In *Encyclopedia of Chemical Technology*, 4th ed.; Kroschwitz, J. I., Howe-Grant, M., Eds.; John Wiley & Sons: New York, 1995.
3. In *Catalyst Handbook*, 2nd ed.; Twigg, M. V., Ed.; Wolfe Publishing: London, 1989.
4. Song, C. *Catal. Today* **2002**, *77*, 17–49.
5. In *Gas Purification*, 5th ed.; Kohl, A. L.; Nielson, R., Eds.; Gulf Publishing: Houston, TX, 1997.
6. Merkel, T. C.; Freeman, B. D.; Spontak, R. J.; He, Z.; Pinnau, I.; Meakin, P.; Hill, A. J. *Science* **2002**, *296*, 519–522.
7. In *Fuel Cell Systems Explained*, 2nd ed.; Larminie, J., Dicks, A., Eds.; John Wiley & Sons: Chichester, U.K., 2003.
8. Igarashi, H.; Uchida, H.; Suzuki, M.; Sasaki, Y.; Watanabe, M. *Appl. Catal., A* **1997**, *159*, 159–169.
9. Ortiz, A. L.; Harrison, D. P. *Ind. Eng. Chem. Res.* **2001**, *40*, 5102–5109.
10. Lin, S.; Harada, M.; Suzuki, Y.; Hatano, H. *Fuel* **2002**, *81*, 2079–2085.
11. Yi, K. B.; Harrison, D. P. *Ind. Eng. Chem. Res.* **2005**, *44*, 1665–1669.

Downloaded by OHIO STATE UNIV LIBRARIES on June 5, 2012 | http://pubs.acs.org
Publication Date (Web): December 14, 2011 | doi: 10.1021/bk-2011-1088.ch007

12. Tong, J.; Matsumura, Y.; Suda, H.; Haraya, K. *Ind. Eng. Chem. Res.* **2005**, *44*, 1454–1465.
13. Tsuru, T.; Yamaguchi, K.; Yoshioka, T.; Asaeda, M. *AIChE J.* **2004**, *50*, 2794–2805.
14. Robeson, L. M. *J. Membr. Sci.* **1991**, *62*, 165–185.
15. Lin, H.; Freeman, B. D. *Macromolecules* **2005**, *38*, 8394–8407.
16. Lin, H.; Freeman, B. D.; Kalakkunnath, S.; Kalika, D. S. *J. Membr. Sci.* **2007**, *291*, 131–139.
17. Lin, H.; Kai, T.; Freeman, B. D.; Kalakkunnath, S.; Kalika, D. S. *Macromolecules* **2005**, *38*, 8381–8393.
18. Lin, H.; Wagner, E. V.; Freeman, B. D.; Toy, L. G.; Gupta, R. P. *Science* **2006**, *311*, 639–642.
19. Lin, H.; Freeman, B. D. *J. Mol. Struct.* **2005**, *739*, 57–74.
20. Lin, H.; Wagner, E. V.; Swinnea, J. S.; Freeman, B. D.; Pas, S. J.; Hill, A. J.; Kalakkunnath, S.; Kalika, D. S. *J. Membr. Sci.* **2006**, *276*, 145–161.
21. Lin, H.; Freeman, B. D. *Macromolecules* **2006**, *39*, 3568–3580.
22. Giessler, S.; Jordan, L.; Diniz da Costa, J. C.; Lu, G. Q. *Sep. Purif. Technol.* **2003**, *32*, 255–264.
23. Brunetti, A.; Barbieri, G.; Drioli, E.; Lee, K. H.; Sea, B. K.; Lee, D. W. *Desalination* **2006**, *200*, 681–683.
24. Battersby, S.; Duke, M. C.; Liu, S.; Rudolph, V.; Diniz da Costa, J. C. *J. Membr. Sci.* **2008**, *316*, 46–52.
25. Basile, A.; Drioli, E.; Santella, F.; Violante, V.; Capannelli, G.; Vitulli, G. *Gas Sep. Purif.* **1996**, *10*, 53–61.
26. Basile, A.; Criscuoli, A.; Santella, F.; Drioli, E. *Gas Sep. Purif.* **1996**, *10*, 243–254.
27. Tosti, S.; Basile, A.; Chiappetta, G.; Rizzello, C.; Violante, V. *Chem. Eng. J.* **2003**, *93*, 23–30.
28. Basile, A.; Paturzo, L.; Gallucci, F. *Catal. Today* **2003**, *82*, 275–281.
29. Iyoha, O.; Enick, R.; Killmeyer, R.; Howard, B.; Ciocco, M.; Morreale, B. *J. Membr. Sci.* **2007**, *306*, 103–115.
30. Criscuoli, A.; Basile, A.; Drioli, E.; Loiacono, O. *J. Membr. Sci.* **2001**, *181*, 21–27.
31. Armor, J. N. *J. Membr. Sci.* **1998**, *147*, 217–233.
32. Gottschlich, D. E.; Roberts, D. L.; Way, J. D. *Gas Sep. Purif.* **1988**, *2*, 65–71.
33. Ward, W. J.; Robb, W. L. *Science* **1967**, *156*, 1481–1484.
34. Meldon, J. H.; Smith, K. A.; Colton, C. K. *Chem. Eng. Sci.* **1977**, *32*, 939–950.
35. Ilconich, J.; Myers, C.; Pennline, H.; Luebke, D. *J. Membr. Sci.* **2007**, *298*, 41–47.
36. Hanioka, S.; Maruyama, T.; Sotani, T.; Teramoto, M.; Matsuyama, H.; Nakashima, K.; Hanaki, M.; Kubota, F.; Goto, M. *J. Membr. Sci.* **2008**, *314*, 1–4.
37. Bara, J. E.; Gabriel, C. J.; Carlisle, T. K.; Camper, D. E.; Finotello, A.; Gin, D. L.; Noble, R. D. *Chem. Eng. J.* **2009**, *147*, 43–50.
38. Gorji, A. H.; Kaghazchi, T.; Kargari, A. *Chem. Eng. Technol.* **2009**, *32*, 120–128.

39. LeBlanc, O. H.; Ward, W. J.; Matson, S. L.; Kimura, S. G. *J. Membr. Sci.* **1980**, *6*, 339–343.
40. Way, J. D.; Noble, R. D.; Reed, D. L.; Ginley, G. M.; Jarr, L. A. *AIChE J.* **1987**, *33*, 480–487.
41. Yamaguchi, T.; Koval, C. A.; Noble, R. D.; Bowman, C. N. *Chem. Eng. Sci.* **1996**, *51*, 4781–4789.
42. Langevin, D.; Pinoche, M.; Selegny, E.; Metayer, M.; Roux, R. *J. Membr. Sci.* **1993**, *82*, 51–63.
43. Matsuyama, H.; Teramoto, M.; Iwai, K. *J. Membr. Sci.* **1994**, *93*, 237–244.
44. Matsuyama, H.; Teramoto, M.; Sakakura, H.; Iwai, K. *J. Membr. Sci.* **1996**, *117*, 251–260.
45. Matsuyama, H.; Teramoto, M.; Matsui, K.; Kitamura, Y. *J. Appl. Polym. Sci.* **2001**, *81*, 936–942.
46. Yoshikawa, M.; Ezaki, T.; Sanui, K.; Ogata, N. *J. Appl. Polym. Sci.* **1988**, *35*, 145–154.
47. Yamaguchi, T.; Boetje, L. M.; Koval, C. A.; Noble, R. D.; Brown, C. N. *Ind. Eng. Chem. Res.* **1995**, *34*, 4071–4077.
48. Matsuyama, H.; Teramoto, M.; Sakakura, H. *J. Membr. Sci.* **1996**, *114*, 193–200.
49. Matsuyama, H.; Terada, A.; Nakagawara, T.; Kitamura, Y.; Teramoto, M. *J. Membr. Sci.* **1999**, *163*, 221–227.
50. Quinn, R.; Laciak, D. V. *J. Membr. Sci.* **1997**, *131*, 49–60.
51. Quinn, R.; Laciak, D. V.; Pez, G. P. *J. Membr. Sci.* **1997**, *131*, 61–69.
52. Ho, W. S. W. U.S. Patent 5,611,843, 1997.
53. Ho, W. S. W. U.S. Patent 6,099,621, 2000.
54. Zhang, Y.; Wang, Z.; Wang, S. C. *Desalination* **2002**, *145*, 385–388.
55. Kim, T.; Li, B.; Hagg, M. *J. Polym. Sci., Part B: Polym. Phys.* **2004**, *42*, 4326–4336.
56. Shil, G.; Ho, W. S. W. *J. Environ. Eng. Manage.* **2006**, *16*, 233–241.
57. Zhao, J.; Wang, Z.; Wang, J.; Wang, S. *J. Membr. Sci.* **2006**, *283*, 346–356.
58. El-Azzami, L. A.; Grulke, E. A. *Ind. Eng. Chem. Res.* **2009**, *48*, 894–902.
59. Du, J. R.; Liu, L.; Chakma, A.; Feng, X. *Chem. Eng. J.* **2010**, *156*, 33–39.
60. Teramoto, M.; Takeuchi, N.; Maki, T.; Matsuyama, H. *Sep. Purif. Technol.* **2001**, *24*, 101–112.
61. Teramoto, M.; Takeuchi, N.; Maki, T.; Matsuyama, H. *Sep. Purif. Technol.* **2002**, *27*, 25–31.
62. Teramoto, M.; Kitada, S.; Ohnishi, N.; Matsuyama, H.; Matsumiya, N. *J. Membr. Sci.* **2004**, *234*, 83–94.
63. Fortunato, R.; Afonso, C. A. M.; Reis, M. A. M.; Crespo, J. G. *J. Membr. Sci.* **2004**, *242*, 197–209.
64. Barghi, S. H.; Adibi, M.; Rashtchian, D. *J. Membr. Sci.* **2010**, *362*, 346–352.
65. Neves, L. A.; Crespo, J. G.; Coelhoso, I. M. *J. Membr. Sci.* **2010**, *357*, 160–170.
66. Jiang, Y.; Wu, Y.; Wang, W.; Li, L.; Zhou, Z.; Zhang, Z. *Chin. J. Chem. Eng.* **2009**, *17* (4), 594–601.
67. Jindaratsamee, P.; Shimoyama, Y.; Morizaki, H.; Ito, A. *J. Chem. Thermodyn.* **2011**, *43*, 311–314.

Downloaded by OHIO STATE UNIV LIBRARIES on June 5, 2012 | http://pubs.acs.org
Publication Date (Web): December 14, 2011 | doi: 10.1021/bk-2011-1088.ch007

68. Cserjesi, P.; Nemestothy, N.; Vass, A.; Csanadi, Z.; Belafi-Bako, K. *Desalination* **2009**, *245*, 743–747.
69. Baltus, R. E.; Counce, R. M.; Culbertson, B. H.; Luo, H.; Depaoli, D. W.; Dai, S.; Duckworth, C. *Sep. Sci. Technol.* **2005**, *40*, 525–541.
70. Iarikov, D. D.; Hacarlioglu, P.; Oyama, S. T. *Chem. Eng. J.* **2011**, *166*, 401–406.
71. Hanioka, S.; Maruyama, T.; Sotani, T.; Teramoto, M.; Matsuyama, H.; Nakashima, K.; Hanaki, M.; Kubota, F.; Goto, M. *J. Membr. Sci.* **2008**, *314*, 1–4.
72. Myers, C.; Pennline, H.; Luebke, D.; Ilconich, J.; Dixon, J. K.; Maginn, E. J.; Brennecke, J. F. *J. Membr. Sci.* **2008**, *322*, 28–31.
73. Yokozeki, A.; Shiflett, M. B. *Appl. Energy* **2007**, *84*, 351–361.
74. Cussler, E. L.; Aris, R.; Bhown, A. *J. Membr. Sci.* **1989**, *43*, 149–164.
75. Ward, W. J. *AIChE J.* **1970**, *16*, 405–410.
76. Smith, D. R.; Quinn, J. A. *AIChE J.* **1979**, *25*, 197–200.
77. Donaldson, T. L.; Lapinas, A. T. *Chem. Eng. Sci.* **1982**, *37*, 715–718.
78. Noble, R. D. *J. Membr. Sci.* **1990**, *50*, 207–214.
79. Noble, R. D. *J. Membr. Sci.* **1991**, *60*, 297–306.
80. Kalachev, A. A.; Kardivarenko, L. M.; Plate, N. A.; Bagreev, V. V. *J. Membr. Sci.* **1992**, *75*, 1–5.
81. Noble, R. D. *J. Membr. Sci.* **1992**, *75*, 121–129.
82. Ho, W. S. W.; Dalrymple, D. C. *J. Membr. Sci.* **1994**, *91*, 13–25.
83. Kang, Y. S.; Hong, J.; Jang, J.; Kim, U. Y. *J. Membr. Sci.* **1996**, *109*, 149–157.
84. Hong, J.; Kang, Y. S.; Jang, J.; Kim, U. Y. *J. Membr. Sci.* **1996**, *109*, 159–163.
85. Tee, Y. H.; Zou, J.; Ho, W. S. W. *J. Chin. Inst. Chem. Eng.* **2006**, *37*, 37–47.
86. Zou, J.; Ho, W. S. W. *J. Membr. Sci.* **2006**, *286*, 310–321.
87. Huang, J.; El-Azzami, L.; Ho, W. S. W. *J. Membr. Sci.* **2005**, *261*, 67–75.
88. Zou, J.; Huang, J.; Ho, W. S. W. *Ind. Eng. Chem. Res.* **2007**, *46*, 2272–2279.
89. Zou, J.; Ho, W. S. W. *J. Chem. Eng. Jpn.* **2007**, *40*, 1011–1020.
90. Mandal, B.; Ho, W. S. W. *Int. J. Chem. Sci.* **2007**, *5*, 1938–1946.
91. Huang, J.; Zou, J.; Ho, W. S. W. *Ind. Eng. Chem. Res.* **2008**, *47*, 1261–1267.
92. Huang, J.; Ho, W. S. W. *J. Chin. Inst. Chem. Eng.* **2008**, *39*, 129–136.
93. Bai, H.; Ho, W. S. W. *Ind. Eng. Chem. Res.* **2009**, *48*, 2344–2354.
94. Huang, J.; Zou, J.; Ho, W. S. W. In *Hydrogen and Syngas Production and Purification Technologies*; Liu, K., Song, C., Subramani, V., Eds.; John Wiley & Sons: New York, 2010; pp 385−413.
95. Bai, H.; Ho, W. S. W. *Polym. Int.* **2011**, *60*, 26–41.
96. Xing, R.; Ho, W. S. W. *J. Membr. Sci.* **2011**, *367*, 91–102.
97. Bai, H.; Ho, W. S. W. *Ind. Eng. Chem. Res.* **2011**, in peer review.
98. In *Membrane Handbook*; Ho, W. S. W., Sirkar, K. K., Eds.; Chapman & Hall: New York, 1992; Kluwer Academic Publishers: Boston, MA, 2001, reprint edition.
99. Sartori, G.; Ho, W. S. W.; Savage, D. W.; Chludzinski, G. R.; Wiechert, S. *Sep. Purif. Methods* **1987**, *16*, 171–200.
100. Shulik, L. J.; Sartori, G.; Ho, W. S. W.; Thaler, W. A.; Milliman, G. E.; Wilbur, J. C. *Sep. Sci. Technol.* **1996**, *31*, 1663–1673.
101. Sartori, G.; Savage, D. W. *Ind. Eng. Chem. Fund.* **1983**, *22*, 239–249.

Downloaded by OHIO STATE UNIV LIBRARIES on June 5, 2012 | http://pubs.acs.org
Publication Date (Web): December 14, 2011 | doi: 10.1021/bk-2011-1088.ch007

102. In *Poly(vinyl Alcohol), Basic Properties and Uses*; Pritchard, J. G., Ed.; Gordon and Breach Science Publishers: London, 1970.
103. Zou, J., Ph.D. Thesis, The Ohio State University, Columbus, OH, 2007.
104. Li, Q.; He, R.; Jensen, J. O.; Bjerrum, N. J. *Fuel Cells* **2004**, *4* (3), 147–159.
105. Huang, J., Ph.D. Thesis, The Ohio State University, Columbus, OH, 2006.
106. Bai, H.; Ho, W. S. W. *J. Taiwan Inst. Chem. Eng.* **2009**, *40*, 260–267.
107. Bai, H.; Ho, W. S. W. In *Proceedings of the Minerals, Metals & Materials Society Annual Meeting*; New Orleans, LA, March 9−13, 2008; Supplemental Volume 1: Materials Processing and Properties; Vol. 1, pp 529−535.
108. Bai, H.; Ho, W. S. W. In *Proceedings of MACRO 2008, Polymers at Frontiers of Science and Technology*; Taipei, June 29–July 4, 2008.
109. Bai, H.; Ramasubramanian, R.; Ho, W. S. W. *Prepr. Symp. ACS Div. Fuel Chem.* **2009**, *54*, 820–822.
110. Zou, H.; Wu, S. S.; Shen, J. *Chem. Rev.* **2008**, *108*, 3893–3957.
111. Hu, Q.; Marand, E.; Dhingra, S.; Fritsch, D.; Wen, J.; Wilkes, G. *J. Membr. Sci.* **1997**, *135*, 65–79.
112. Nunes, S. P.; Schultz, J.; Peinemann, K. V. *J. Mater. Sci. Lett.* **1996**, *15*, 1139–1141.
113. Joly, C.; Goizet, S.; Schrotter, J. C.; Sanchez, J.; Escoubes, M. *J. Membr. Sci.* **1997**, *130*, 63–74.
114. Merkel, T. C.; Freeman, B. D.; Spontak, R. J.; He, Z.; Pinnau, I.; Meakin, P.; Hill, A. J. *Chem. Mater.* **2003**, *15*, 109–123.
115. Gomes, D.; Nunes, S. P.; Peinemann, K. V. *J. Membr. Sci.* **2005**, *246*, 13–25.
116. Zhao, Y.; Ho, W. S. W. In *American Institute of Chemical Engineers Annual Meeting, Fuel Cell Membranes*; Minneapolis, MN, 2011.

Downloaded by OHIO STATE UNIV LIBRARIES on June 5, 2012 | http://pubs.acs.org
Publication Date (Web): December 14, 2011 | doi: 10.1021/bk-2011-1088.ch007

Downloaded by STANFORD UNIV GREEN LIBR on June 5, 2012 | http://pubs.acs.org
Publication Date (Web): December 14, 2011 | doi: 10.1021/bk-2011-1088.ch008

Chapter 8

Reduction of Carbon Dioxide to Energy-Rich Products

Jian Gao, Bing Yu, and Liang-Nian He[*]

**State Key Laboratory and Institute of Elemento-Organic Chemistry,
Nankai University, Weijin Rd. 94, Tianjin 300071, P. R. China**
[*]E-mail: heln@nankai.edu.cn

Carbon dioxide is very attractive as a typical renewable feedstock for manufacturing commodity chemicals, fuels and various materials since it is an abundant, nontoxic, nonflammable and easily available C1 resource. In this context, development of catalytic methodologies for chemical transformation of CO_2 into fuels and value-added chemicals is of paramount importance from a standpoint of green chemistry and sustainable development. The aim of this chapter is to demonstrate the versatile use of CO_2 in organic synthesis, with the main focus on the reduction of CO_2 to energy-rich products such as formic acid and its derivatives, methanol, carbon monoxide, and other higher hydrocarbons which can be used as liquified fuels; and features advances in catalytic processes for the production of clean transportation fuels. The prospects and challenges for the direct catalytic hydrogenation of CO_2 to produce value-added chemicals are also discussed.

Introduction

With the development of human society and economy, energy demand is also growing dramatically, accompanying with severe environment concerns. Undoubtedly, energy and the environment are two of the most important and challenging issues in the 21st century. It is estimated that more than 80% of our energy comes from the combustion of fossil fuels, which will still remain the dominant energy source for years to come. However, from the perspective

In Production and Purification of Ultraclean Transportation Fuels; Hu, Y., et al.;
ACS Symposium Series; American Chemical Society: Washington, DC, 2011.

of long-term, research and development novel energy would be particularly important for the sustainable development of our society.

In recent years, the role of CO_2 as a greenhouse gas and its contribution to global warming are widely recognized by both scientists and governmental agencies. Thus, controlling CO_2 emission has become one of the most strategic issues for most of the governments. Obviously, CO_2 capture and storage looks particularly effective for temporarily preserving large volumes of CO_2 (*1*). On the other hand, as an abundant, nontoxic, nonflammable, easily available, and renewable C1 resource, CO_2 is very attractive as an environmentally friendly feedstock for making commodity chemicals, fuels, and materials. In this context, there is a more far-reaching significance to convert CO_2 into value-added energy, materials, and other chemical products while reducing its emission on a large scale. Since thermodynamic stability and kinetic inertness of CO_2 molecule limit its utilization in industry, chemical transformation of CO_2 represents a continuing scientific challenge. To our delight, a great progress has been seen on chemical utilization of CO_2 as a raw material, as a sound green solvent, or as a Lewis acid catalyst or tunable reagent which could offer profound advantages for both green chemistry and economical benefits in terms of creating novel chemistry, reaction control, product separation, and operation simplification. In this chapter, we would like to illustrate potential applications of CO_2 in the synthesis of valued-added chemicals and energy-rich products such as formic acid and its derivatives, methanol, carbon monoxide, and other higher hydrocarbons which can be used as alternative energy and fuels. Both traditional chemical strategies and novel photochemical/electrochemical approaches will be discussed. CO_2 chemistry disclosed herein will stimulate further interest in research that may lead to the development of CO_2 as a new source for a wide set of value-added organic compounds like solvents, fuels, fine/bulk chemicals, pharmaceuticals and polymers.

Downloaded by STANFORD UNIV GREEN LIBR on June 5, 2012 | http://pubs.acs.org
Publication Date (Web): December 14, 2011 | doi: 10.1021/bk-2011-1088.ch008

Reduction of CO_2 to Formic Acid and Its Derivatives

Formic acid, a useful chemical and important organic intermediate, is widely used in chemical industry and organic synthesis. Recently, it is also recognized as a very promising fuel for low-temperature fuel cell and a carrier for hydrogen storage. The direct catalytic hydrogenation of CO_2 could be performed to produce formic acid, which has 100% of atom economy (equation 1), consistent with the contemporary trend of green chemistry.

$$CO_2 + H_2 \xrightleftharpoons{\text{Cat.}} HCOOH \qquad (1)$$

In 1976, Inoue *et al.* firstly reported the direct catalytic hydrogenation of CO_2 to formic acid using transition metal complexes although conversion and the yield for formic acid was very low (*2*). Up to now, in this aspect, transition-metals such as Ru, Rh, Pd, Ni and Ir catalyzed hydrogenation of CO_2 to afford formic acid and its derivatives e.g. formamide, formic ether, has so far been extensively studied (*3–12*). Those catalysts based on transition metals can be used to promote hydrogenation of CO_2 to formic acid in organic solvent, water, ionic liquid (IL) and supercritical CO_2 ($scCO_2$).

Generally speaking, the presence of free amine can further covert the formic acid formed in situ into ammonium formate which could improve the reduction of CO_2 to formic acid. That is because formation of ammonium formate can shift the equilibrium (equation 1) to right as a consequence of formation of a weaker acid (based on the Brønsted/Lowry acid/base theory). Additionally, ligands bearing amine functional groups as pendant arms are found to be able to improve the catalytic activity of metal complexes even at a inferior level compared with an external amine.

Noyori *et al.* (*13*) investigated selective hydrogenation of CO_2 using Ru complexes as catalysts bearing PMe_3 or PPh_3 as a ligand. The TOF (turnover frequency) could reach up or exceed 4000 h^{-1} in the presence of deliquescent H_2, tertiary amine, and Ru complex with PMe_3 as a ligand at 50 °C. In addition, water and alcohols have accelerating effect on this transformation. The high reaction rate could be ascribed to the fast diffusion rate, the weak dissolution effect of catalyst and the high mutual miscibility of H_2 in $scCO_2$.

Jessop *et al.* investigated the effect of different phosphine ligands and Ru precursors on the direct hydrogenation of CO_2 to formic acid (*14*, *15*). It is found that using the following six phosphine ligands (PMe_3, $PPhMe_2$, $Ph_2PCH_2PPh_2$, $Ph_2PC_2H_4PPh_2$, and cis- and trans-$Ph_2PCH{=}CHPPh_2$) could result in very high reaction rates. Based on the experimental results, the authors concludes that there is no correlation between the basicity of monophosphine (PR_3) ligand and the catalytic activity. In the case of biphosphine as ligand, weak basic ligand with small bite angels gives high activity, whereas stronger basic diphosphine ligand shows the opposite trend. In addition, $scCO_2$ is found to be an excellent reaction medium in the presence of CO_2 soluble catalyst for example, $RuCl(OAc)(PMe_3)_4$, and thus TON (Turnover number) and TOF could reach up to 28500 and 95000 h^{-1}, respectively.

Homogeneous catalysts have been widely used for this transformation, and high reaction rate can be achieved. On the other hand, heterogeneous catalysts fabricated by immobilizing ruthenium on silica and polystyrene (PS) resin have also been employed (*16*) to facilitate separation of catalyst from the reaction mixture. In particular, inorganic and organic bases, including high-boiling organic bases, such as imidazole, quinoline and other heterocyclic nitrogen containing compounds are often added to the reaction system in order to attain reasonable conversion (*17*, *18*). However, development of an ideal process to realize the recovery of formic acid and reuse of bases and precious metal catalysts still remains challenging. This could also account for limitation in industrial scale production. Recently, Han's group (*19*, *20*) used a kind of basic ionic liquid (IL) to promote selective hydrogenation of CO_2 to formic acid for the first time. Using the new basic ILs bearing a tertiary amino group on the cation as the base and silica immobilized Ruthenium as the catalyst, hydrogenation of CO_2 to produce formic acid with satisfactory activity and high selectivity in aqueous solution is performed successfully (Scheme 1).

Downloaded by STANFORD UNIV GREEN LIBR on June 5, 2012 | http://pubs.acs.org
Publication Date (Web): December 14, 2011 | doi: 10.1021/bk-2011-1088.ch008

Downloaded by STANFORD UNIV GREEN LIBR on June 5, 2012 | http://pubs.acs.org
Publication Date (Web): December 14, 2011 | doi: 10.1021/bk-2011-1088.ch008

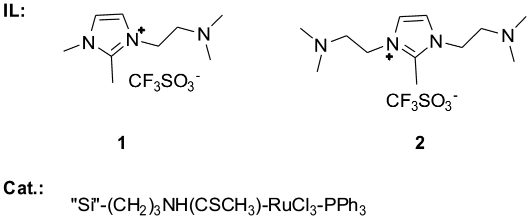
IL:
CF3SO3-
CF3SO3-
1
2
Cat.:
"Si"-(CH2)3NH(CSCH3)-RuCl3-PPh3

Scheme 1. Task-specific basic ILs used in this study.

The unique feature of this approach would be that: the task-specific ionic liquid could fix the formed formic acid which could be released easily at a certain temperature; and both the immobilized Ru catalyst and the basic IL can be reused after a simple separation process (Scheme 2). No decrease of TOF is evident after recycling the catalyst and IL for five times, which is very favorable from a practical point of view.

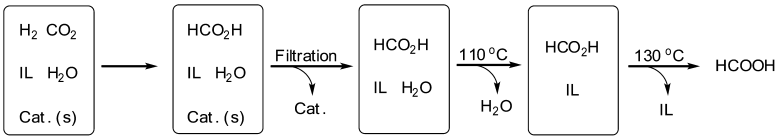
H2 CO2
IL H2O
Cat. (s)
HCO2H
IL H2O
Cat. (s)
Filtration
Cat.
HCO2H
IL H2O
110 °C
H2O
HCO2H
IL
130 °C
IL
HCOOH

Scheme 2. Recovery/separation strategy.

Himeda and co-workers developed a self-precipitation strategy to recover the catalyst for selective hydrogenation of CO_2 to formate (*21*, *22*). As shown in Scheme 3, the Ir-complex catalyst, viz. [Cp*Ir(H_2L)-Cl]Cl (**3**-Cl) is almost insoluble in acidic aqueous solutions but completely soluble in CO_2-saturated KOH solution under 3 MPa of CO_2. Furthermore, a hydride complex (**5**) from the deprotonated complex (**4**) would act as a reductant to convert bicarbonate (a species of CO_2 in alkaline solution) into formate. Simultaneously, the regenerated **4** would be protonated to the initial catalyst **3**. In other words, the catalyst precursor can be precipitated with generation of the formate product.

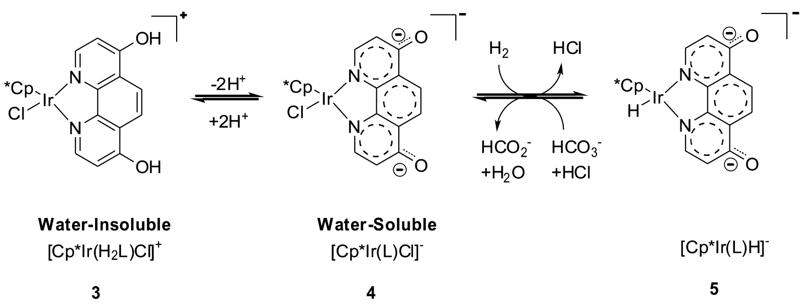
*Cp
Cl
Ir
OH
OH
-2H+
+2H+
H2
HCl
HCO2-
+H2O
HCO3-
+HCl
H
Water-Insoluble
[Cp*Ir(H2L)Cl]+
3
Water-Soluble
[Cp*Ir(L)Cl]-
4
[Cp*Ir(L)H]-
5

Scheme 3. Proposed mechanism for hydrogenation of bicarbonate catalyzed by the Iridium complex with 4,7-dihydroxy-1,10-phenanthroline.

Downloaded by STANFORD UNIV GREEN LIBR on June 5, 2012 | http://pubs.acs.org
Publication Date (Web): December 14, 2011 | doi: 10.1021/bk-2011-1088.ch008

This process has several significant features as follows: (i) catalyst recycling by self-precipitation/filtration, (ii) waste-free process, (iii) ease of product separation, (iv) high efficiency under relatively mild conditions, and (v) aqueous catalysis. Furthermore, the authors proposed triple roles of the oxyanion as a ligand: catalyst recovery by acid-base equilibrium; rendering the catalyst water-soluble; and activating the catalyst due to its electron-donating ability.

Later on, the same group reported a highly active cationic Cp*Ir(III) catalyst containing phenanthroline derivatives as ligands for the direct hydrogenation of CO_2 to formic acid (*22*). The maximum turnover number (TON) of the hydrogenation could reach up to 222000 in a basic aqueous solution which is an important milestone in this field. The presence of electron-donating ligands could presumably accelerate the reaction.

Pincer ligands are known as multidentate ligands that is strongly bound to a metal center resulting in hindering dissociation of the ligand from the metal (*23–30*). Based on this principle, Nozaki and co-workers (*31*) developed an efficient catalytic system consisting of an alkylphosphine-based pincer ligand bearing strong electron-donating group and a transition metal center (Ir) for selective hydrogenation of CO_2. This process could feature a significant advancement in catalyst efficiency. Using this defined Ir-pincer trihydride complex [Ir^{III}PNP] **(6)** containing two diisopropylphosphino substituents (Scheme 4), excellent TON value of 3500000 and TOF of 150000 h^{-1} are obtained in aqueous KOH with the formation of potassium formate HCOOK (*31*, *32*). It is worth noting that this catalyst system give the highest TON reported so far.

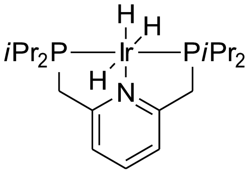

6

Scheme 4. Highly active Ir^{III}-pincer complex in hydrogenation of CO_2.

Additionally, a catalytic cycle was proposed as depicted in Scheme 5. The resulting formate complex (**7**) is believed to react with hydroxide to give the amidoiridium dihydride species (**8**), which has been independently prepared by addition of CsOH•H_2O to the corresponding chloroiridium dihydride complex. Notably, converting **8** into **6** in the presence of molecular hydrogen, thus could let the catalytic cycle completion.

Downloaded by STANFORD UNIV GREEN LIBR on June 5, 2012 | http://pubs.acs.org
Publication Date (Web): December 14, 2011 | doi: 10.1021/bk-2011-1088.ch008

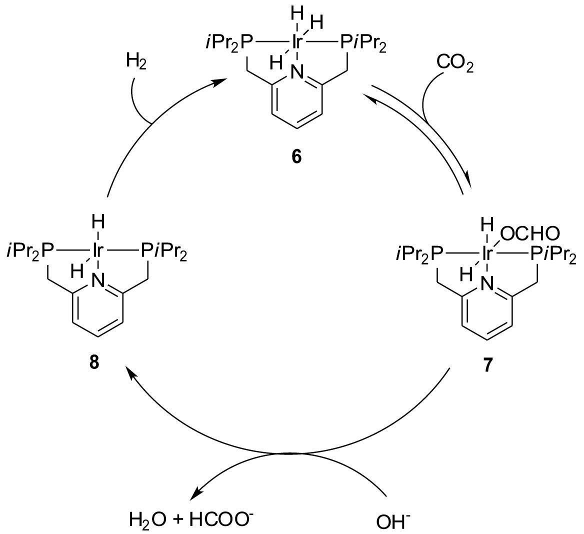
H
H
*i*Pr2P
Ir
P*i*Pr2
H
N
H2
CO2
6
H
*i*Pr2P
Ir
P*i*Pr2
H
N
8
H
OCHO
*i*Pr2P
Ir
P*i*Pr2
H
N
7
H2O + HCOO-
OH-

*Scheme 5. Plausible mechanism for hydrogenation of CO_2 using Iridium trihydride complex **(6)**.*

Recently, Peris and co-workers (*33*) reported a new approach to reduction of CO_2 to formate in which a series of Ir and Ru complexes were tested in the presence of H_2 (Scheme 6). The basic NHC (Nitrogen Heterocyclic Carbene) ligand shows better catalytic performance with high TON up to 1800. It is also worth mentioning that the reaction could go through a hydrogen transfer process by using *i*PrOH as proton donor. TON of 150 could be obtained.

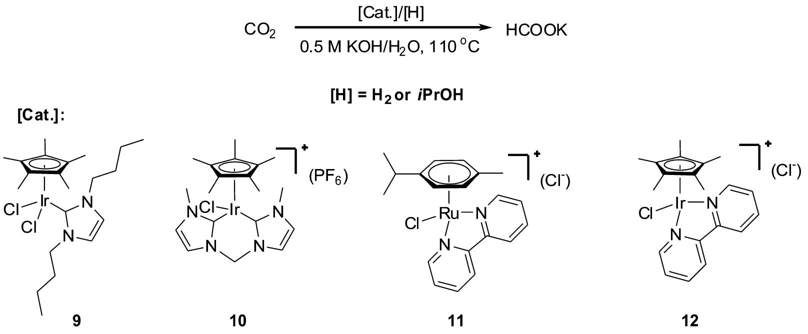
CO2
[Cat.]/[H]
0.5 M KOH/H2O, 110 °C
HCOOK
[H] = H2 or *i*PrOH
[Cat.]:
Cl
Ir
Cl
N
N
(PF6)
N
Cl
Ir
N
N
N
(Cl-)
Cl
Ru
N
N
(Cl-)
Cl
Ir
N
N
9
10
11
12

Scheme 6. Hydrogenation of CO_2 using H_2 or iPrOH as the hydrogen source.

Besides the aforementioned precious metals, much cheaper and greener iron derived compound can also be used as a catalyst for selective hydrogenation of CO_2 to formic acid. Very recently, Beller and co-workers (*34*) described for the first time that an active iron catalyst system works well for the catalytic reduction of both CO_2 and bicarbonates to afford formates, alkyl formates and formamides. The authors ascribe the success to combination of the iron source $Fe(BF_4)_2{\bullet}6H_2O$ (**13**) with the tetradentate ligand $P(CH_2CH_2PPh_2)_3$ (PP_3) which can further be transformed into the defined iron hydride complexes $[FeH(PP_3)]BF_4$ **(14)** and $[FeH(H_2)(PP_3)]BF_4$ (**18**) under the reaction conditions. In the presence of alcohol, methyl formate is formed in high yield (56%) with a TON of 585; in the presence of amine, formamides product was formed in 75% yield with a TON of 727. A possible catalytic cycle is also proposed as shown in Scheme 7.

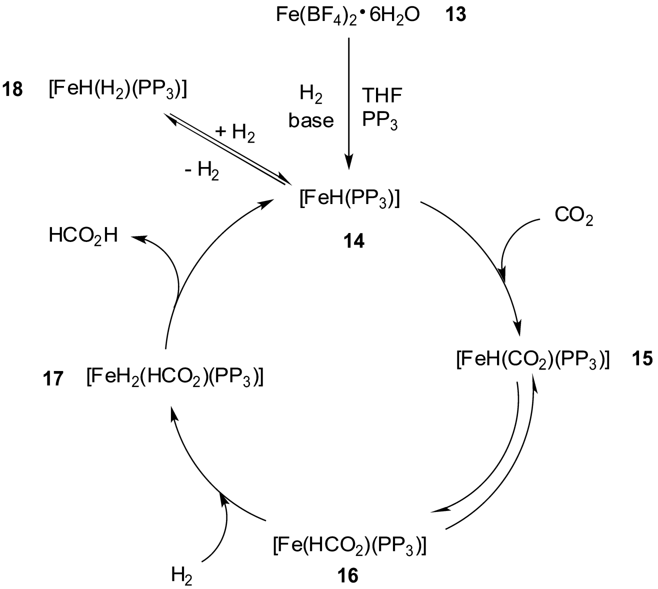

$Fe(BF_4)_2{\bullet}6H_2O$ **13**
18 $[FeH(H_2)(PP_3)]$
H_2
base
THF
PP_3
$+ H_2$
$- H_2$
$[FeH(PP_3)]$
14
CO_2
HCO_2H
$[FeH(CO_2)(PP_3)]$ **15**
17 $[FeH_2(HCO_2)(PP_3)]$
$[Fe(HCO_2)(PP_3)]$
16
H_2

Scheme 7. Proposed catalytic cycle for the hydrogenation of CO_2 using $Fe(BF_4)_2{\bullet}6H_2O/PP_3$.

Reduction of CO_2 to Methanol

Methanol, a valuable product in chemical industry being stored and transported safely, is now regarded as a novel and alternative fuel resource that can replace fossil fuels owing to its high octane number. At the same time, methanol has also been widely used as an important starting material/ intermediate for the production of other fuels and value-added chemicals. World demand for methanol is currently increasing enormously, thus the synthesis of methanol can be of great significance in view of energy utilization and sustainable development.

CO_2 can be reduced to methanol via direct catalytic hydrogenation with 100% selectivity (equation (2), Scheme 8) and this kind of reduction reaction could be thermodynamically favorable. However, it needs an excess amount of H_2 in comparison with the reduction of CO_2 to CO (equation (1), Scheme 8) most likely due to a different reaction mechanism.

Downloaded by STANFORD UNIV GREEN LIBR on June 5, 2012 | http://pubs.acs.org
Publication Date (Web): December 14, 2011 | doi: 10.1021/bk-2011-1088.ch008

$$CO_2\ (aq) + H_2\ (aq) \longrightarrow CO\ (aq) + H_2O\ (l) \qquad \textbf{(1)}$$

$$\Delta G^0 = 11\ kJmol^{-1};\ \Delta H^0 = 11\ kJmol^{-1};\ \Delta S^0 = -0.8\ Jmol^{-1}K^{-1}$$

$$CO_2\ (aq) + 3\ H_2\ (aq) \longrightarrow CH_3OH\ (l) + H_2O\ (l) \qquad \textbf{(2)}$$

$$\Delta G^0 = -79\ kJmol^{-1};\ \Delta H^0 = -106\ kJmol^{-1};\ \Delta S^0 = -88\ Jmol^{-1}K^{-1}$$

$$CO_2\ (aq) + 4\ H_2\ (aq) \longrightarrow CH_4\ (l) + 2\ H_2O\ (l) \qquad \textbf{(3)}$$

$$\Delta G^0 = -193\ kJmol^{-1};\ \Delta H^0 = -230\ kJmol^{-1};\ \Delta S^0 = -125\ Jmol^{-1}K^{-1}$$

Scheme 8. Thermodynamic parameters for hydrogenation of CO_2 to various C1 products.

Ipatieff and Monoroe reported for the first time in 1945 that methanol could be synthesized from the direct catalytic hydrogenation of CO_2 using Cu-Al based catalysts (*35*). The effect of catalyst composition, reaction temperature, H_2/CO_2 ratio and the pressure on the reaction were investigated. Although great progress has been made in the reduction of CO_2 to methanol and this technology has been commercialized on a pilot scale, developing greener process for large-scale industrial production of methanol from CO_2 still remains challenging due to limitation of catalysts and hydrogen sources. In general, effective catalysts for this reaction can be classified as follows: Cu-based catalyst, heterogeneous catalyst containing precious metal, and non-metal catalysts.

Among those catalysts, Cu-based catalysts being composed of Cu, Zn active component and a carrier like Al_2O_3 or SiO_2 or ZrO_2 have been studied well and could give the best catalytic activity probably thanks to large surface area, high dispersion and good thermal stability.

Fujiware and co-workers (*36*, *37*) reported that combination of CuO-ZnO-CrO_3 oxides and zeolites would be effective for methanol formation, although generation of long chain hydrocarbons is favorable rather than methanol. They also found that preparative procedure of the catalyst could have obvious impact on the catalytic activity. The addition of copper-zinc carbonate to an aqueous solution of CrO_3 could lead to an excellent efficacy catalyst.

In addition, the Cu/ZnO/ZrO_2 catalyst commonly used for syngas production is also active for methanol formation from CO_2 and H_2 (*38–41*). In this aspect, various metal oxides are often used as an additive to improve the catalytic activity and stability. Besides ZrO_2, other irreducible oxides such as Al_2O_3, TiO_2 and Ga_2O_3 are measured (*42*). The effects of other additives such as boron, chromium, vanadium, tungsten, manganese, VO_x, MnO_x and MgO are also evaluated (*41*, *43–45*). When it comes to heterogeneous catalysts, the active components are mainly transition metals or precious metals such as Pd, Pt, Au, and Rh and so

Downloaded by STANFORD UNIV GREEN LIBR on June 5, 2012 | http://pubs.acs.org
Publication Date (Web): December 14, 2011 | doi: 10.1021/bk-2011-1088.ch008

on. SiO_2, Nb_2O_5, ZrO_2, ThO_2, MgO, and TiO_2 are often used as carriers for the immobilization of the active metal components.

Very recently, Guan and co-workers (*46*) reported a highly efficient nickel catalyst for the catalytic hydroboration of CO_2 to methoxyboryl species, followed by hydrolysis using a simple borane to afford methanol. Using a PCP-pincer nickel hydride (**19**) as a catalyst, catecholborane (HBcat) as the reducing reagent, CO_2 is reduced to methoxide compound with the highest TOF (495 h^{-1} based on B-H) under very mild reaction conditions (Scheme 9). It is also worth noting that this could be the first example for catalytic hydroboration of CO_2.

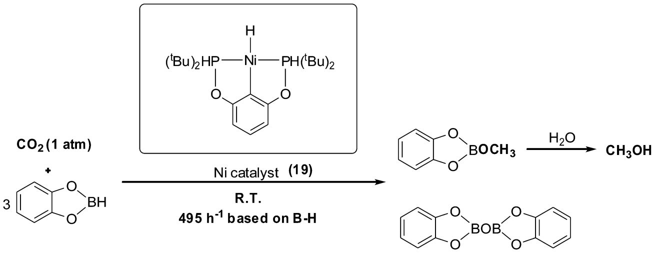

H
(ᵗBu)₂HP—Ni—PH(ᵗBu)₂
O
O
CO₂ (1 atm)
+
3
BH
Ni catalyst (19)
R.T.
495 h⁻¹ based on B-H
BOCH₃
H₂O
CH₃OH
BOB

Scheme 9. Nickel-catalyzed hydroboration of CO_2 to methonal.

In addition, a catalytic cycle is proposed as shown in Scheme 10. The catalytic reduction of CO_2 begins with a reversible insertion of CO_2 into an active Ni-H bond. The subsequent cleavage of the Ni-O bond with a reducing reagent i.e. HBcat regenerates the nickel hydride **19** and produce HCOOBcat, followed by further reduction to formaldehyde. A second cycle involves the hydroboration of formaldehyde, which is analogous to the nickel-catalyzed hydrosilylation of aldehydes through the formation of a Ni-methoxide intermediate. The final methoxide product is obtained in the presence of HBcat and the whole catalytic cycle is completion as the initial catalyst is regenerated.

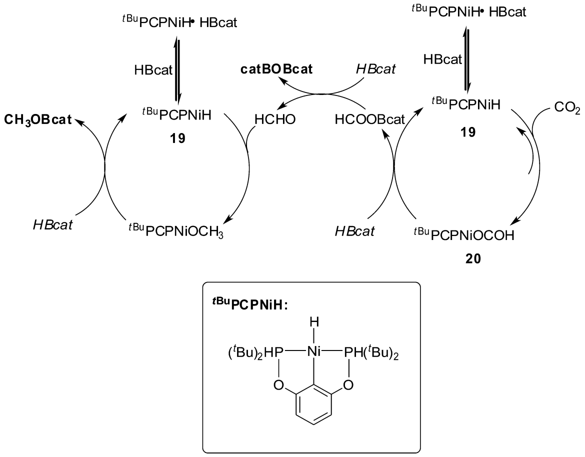

ᵗᴮᵘPCPNiH• HBcat
HBcat
ᵗᴮᵘPCPNiH
19
CH₃OBcat
HBcat
ᵗᴮᵘPCPNiOCH₃
catBOBcat
HBcat
HCHO
HCOOBcat
ᵗᴮᵘPCPNiH• HBcat
HBcat
ᵗᴮᵘPCPNiH
19
CO₂
HBcat
ᵗᴮᵘPCPNiOCOH
20
ᵗᴮᵘPCPNiH:
H
(ᵗBu)₂HP—Ni—PH(ᵗBu)₂
O
O

Scheme 10. Proposed catalytic cycle of Nickel-catalyzed hydroboration of CO_2.

In Production and Purification of Ultraclean Transportation Fuels; Hu, Y., et al.;
ACS Symposium Series; American Chemical Society: Washington, DC, 2011.

Downloaded by STANFORD UNIV GREEN LIBR on June 5, 2012 | http://pubs.acs.org
Publication Date (Web): December 14, 2011 | doi: 10.1021/bk-2011-1088.ch008

Furthermore, a metal-free process for conversion of CO_2 to methanol has also been developed. In 2008, Ying and co-workers (*47*) reported the first hydrosilylation of CO_2 to methanol using silane as the reducing reagent in the presence of NHC as the organocatalyst under very mild conditions (Scheme 11).

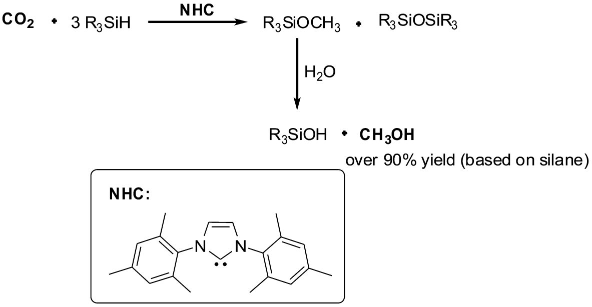

$CO_2 + 3\,R_3SiH \xrightarrow{NHC} R_3SiOCH_3 + R_3SiOSiR_3$
H_2O
$R_3SiOH + CH_3OH$
over 90% yield (based on silane)
NHC:
N
N

Scheme 11. N-heterocyclic carbenes catalyzed reduction of CO_2 to methanol.

Although detailed mechanism for the overall catalytic system is unclear yet, a possible reaction pathway (Scheme 12) is proposed on basis of spectroscopic investigation for identifying the intermediates. First, the nucleophilic carbene NHC would activate CO_2 with the formation of an imidazolium carboxylate and then interact with a silane to form formoxysilanes **22** and **3**. **23** could be an important intermediate in the catalytic cycle, and can react with other free hydrosilanes to afford intermediates **24**-**26** and the final methoxide products $Ph_2Si\text{-}(OMe)_2$ (**27**) and $(Ph_2(MeO)SiO\text{-})_n$ (**28**). This catalytic cycle would continue until hydrosilane is exhausted.

It is worth particularly noting that in this system, dry air can serve as the feedstock, and the organocatalyst NHC which present superior efficiency than transition-metal catalysts, are amenable to milder and less stringent reaction conditions. This approach offers a very promising protocol for chemical CO_2 activation and fixation.

In recent years, Stephan and co-workers have been developing a novel concept of “frustrated Lewis pairs” (FLPs) (*48*, *49*). In this system, combination of sterically encumbered Lewis acid and Lewis base do not undergo the ubiquitous neutralization reaction to form the “classical” Lewis acid/Lewis base adduct. Rather, it has been proposed that both the unquenched Lewis acidity and basicity of such sterically “frustrated Lewis pairs” are able to run unusual reactions. For instance, such Lewis acid/Lewis base pair can activate H_2 heterolytically (*50–54*) and thus promote metal-free catalytic hydrogenation of unsaturated compounds. With the development of this new concept, it has also been found that this “frustrated Lewis pairs” system can achieve activation of other small molecules, including CO_2 (*55*), NH_3 (*52*), B-H bond (*56*), whereby have been applied in ring-opening of THF (*57*), and addition to alkenes (*58–60*), alkynes (*61*).

As ongoing project in FLP chemistry for activation of small molecules, it is interesting to find that $B(C_6F_5)_3$ and *t*Bu_3P in C_6H_5Br can bind CO_2 reversibly

Downloaded by STANFORD UNIV GREEN LIBR on June 5, 2012 | http://pubs.acs.org
Publication Date (Web): December 14, 2011 | doi: 10.1021/bk-2011-1088.ch008

under mild conditions (*55*). However, irreversible capture of CO_2 using commonly available "frustrated Lewis pairs" comprising AlX_3 (X = Cl, Br) and $PMes_3$ (Mes = 2,4,6-$C_6H_2Me_3$) has also been achieved (*62*). When the acid-base ratio is 2:1, the FLP could react with CO_2 irreversibly with the formation of the FLP-CO_2 adduct **31** or **32** (Scheme 13). These species have remarkable stability to CO_2 loss even on heating to 80 °C in vacuo.

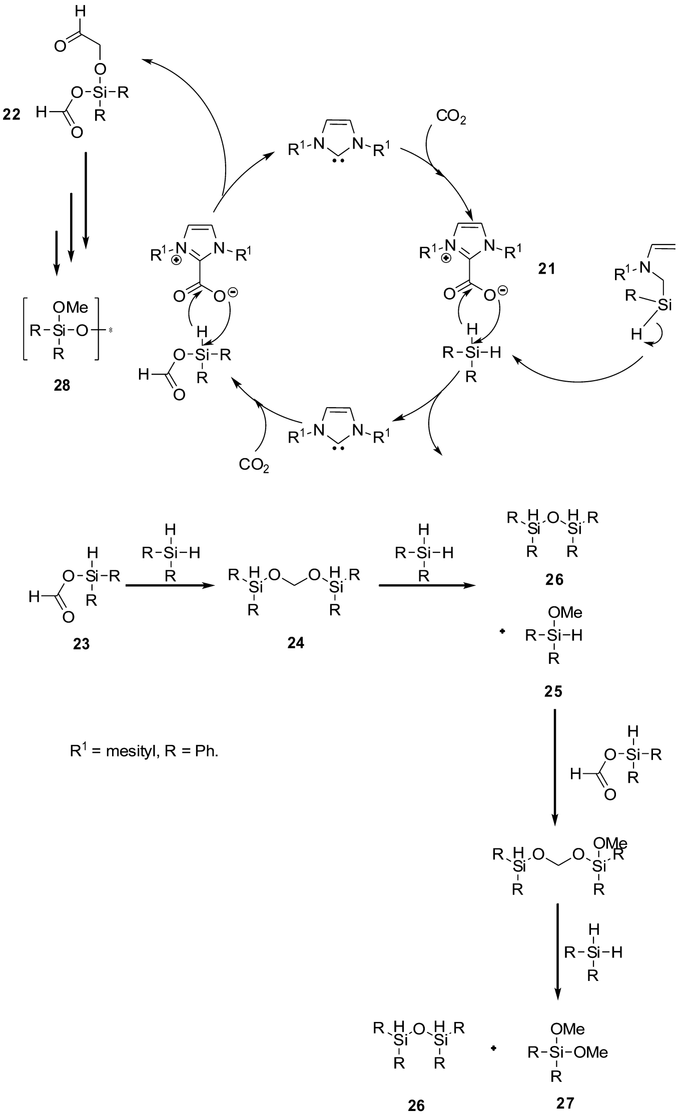

Scheme 12. Possible mechanism of NHC-catalyzed reduction of CO_2 to MeOH.

Downloaded by STANFORD UNIV GREEN LIBR on June 5, 2012 | http://pubs.acs.org
Publication Date (Web): December 14, 2011 | doi: 10.1021/bk-2011-1088.ch008

Downloaded by STANFORD UNIV GREEN LIBR on June 5, 2012 | http://pubs.acs.org
Publication Date (Web): December 14, 2011 | doi: 10.1021/bk-2011-1088.ch008

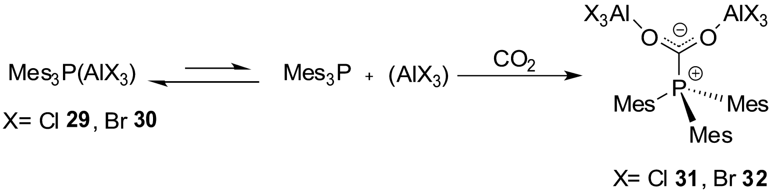

Scheme 13. Irreversible capture of CO_2 by frustrated Lewis pairs.

Remarkably, these species could react rapidly with excess ammonia borane at r. t. to give CH_3OH with 37-51% yields upon quenching with water (Scheme 14). Yet, detailed mechanism is not clear and further study is needed.

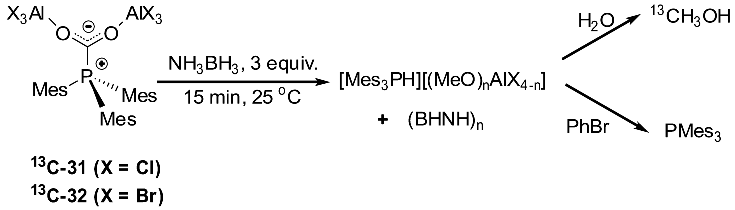

Scheme 14. Stoichiometric reduction of CO_2 to CH_3OH using FLP.

The FLPs has been widely used in heterolytic activation of hydrogen for the subsequent hydrogenation of unsaturated compounds. Ashley and O'Hare described a heterolytic activation of hydrogen and subsequent insertion of CO_2 into a B-H bond for homogeneous catalytic conversion of CO_2 into methanol for the first time (*63*). Upon addition of CO_2 (1 equiv) to a 1:1 mixture of TMP (2,2,6,6-tetramethylpiperidine)/$B(C_6F_5)_3$ (4 equiv) in C_7D_8 under an H_2 atmosphere, quantitative conversion into $CH_3OB(C_6F_5)_2$ via a formatoborate complex [TMPH]-[$HCO_2B(C_6F_5)_3$] **(34)** is achieved at 160 °C for 6 d. Finally, removal of solvent leads to the isolation of CH_3OH in 17-25% yields as the sole C1 product, alongside C_6F_5H and TMP (Scheme 15).

Additionally, a catalytic cycle is proposed as shown in Scheme 16. First, a equilibrium concentrations of CO_2 and **33** from **34** would be established followed by reversible decomposition of the borohydride salt into free H_2, TMP, and $B(C_6F_5)_3$; then attack of $B(C_6F_5)_3$ on the acyl oxygen atom of **34** gives an intermediate **A**; and hydride reduction of the activated formate **A** by an equivalent of **33** leads to the formaldehyde acetal (intermediate **B**) and $B(C_6F_5)_3$. In the presence of $[TMPH]^+$ counterions which might serve as H^+ donor, a cleavage of **B** occurs with the formation of $H_2CO\text{-}B(C_6F_5)_3$ (intermediate **C**) and **35**. Intermediate **C** is expected to be a potent electrophile and undergoes a final hydride reduction in the presence of (**33**) to afford (**36**), which can be then converted to methanol upon distillation.

Downloaded by STANFORD UNIV GREEN LIBR on June 5, 2012 | http://pubs.acs.org
Publication Date (Web): December 14, 2011 | doi: 10.1021/bk-2011-1088.ch008

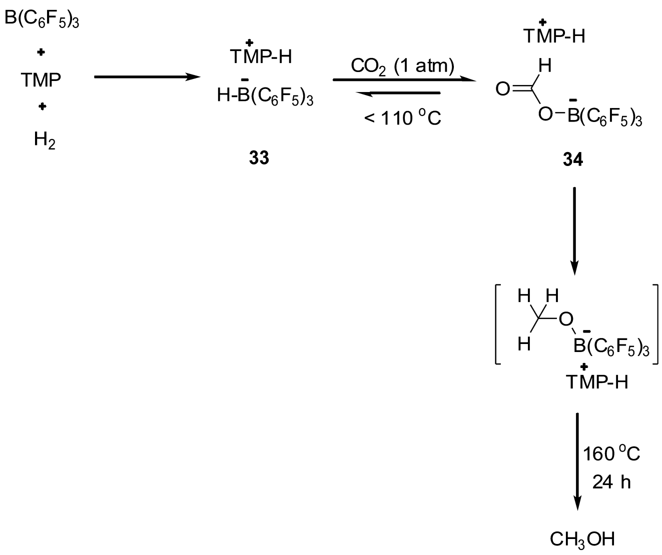
B(C6F5)3
+
TMP
+
H2
TMP-H
H-B(C6F5)3
33
CO2 (1 atm)
< 110 °C
TMP-H
H
O
O-B(C6F5)3
34
H H
O
H
B(C6F5)3
TMP-H
160 °C
24 h
CH3OH

Scheme 15. Reduction of CO_2 to methanol with H_2 activated by a frustrated Lewis acid-base pair.

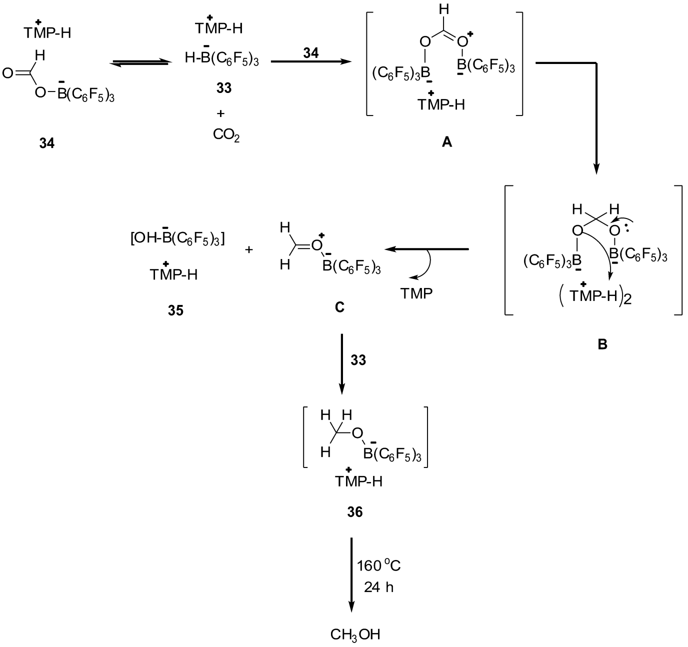
TMP-H
H
O
O-B(C6F5)3
34
TMP-H
H-B(C6F5)3
33
+
CO2
34
H
O
O
(C6F5)3B
B(C6F5)3
TMP-H
A
H H
O
O
(C6F5)3B
B(C6F5)3
(TMP-H)2
B
TMP
H
H
O
B(C6F5)3
C
[OH-B(C6F5)3]
+
TMP-H
35
33
H H
O
H
B(C6F5)3
TMP-H
36
160 °C
24 h
CH3OH

Scheme 16. Proposed mechanism.

Downloaded by STANFORD UNIV GREEN LIBR on June 5, 2012 | http://pubs.acs.org
Publication Date (Web): December 14, 2011 | doi: 10.1021/bk-2011-1088.ch008

Reduction of CO_2 to CO

The dissociation of CO_2 to CO is the simplest reaction for CO_2 reduction, and also the primary reaction for all the reactions involving CO_2 utilization (eq. 2):

$$CO_2 \rightarrow CO + 1/2\ O_2\ ,\ \Delta G_{1000K} = 190.5\ kJmol^{-1} \qquad (2)$$

It is clear that, even for this reaction, there exist certain difficulties in the thermodynamics, because Δ*G* increases when the reaction going from left to right. That is to say, a great amount of energy is necessary for this transformation. In addition, even with strong reducing agents, overcoming the enthalpy of 532 kJ/mol of C=O bond in CO_2 molecule often presents kinetic difficulties (*64–66*).

It has been reported that certain metal complexes can abstract oxygen readily from CO_2 (*67–71*), but the obtained metal-oxygen bonds are so strong that catalytic turnover is rare (*72*, *73*). Thus, the chemical pathways involved are obscure, making it difficult to improve the reduction system, and CODH (carbon monoxide dehydrogenase) remains the most effective catalyst for this reaction (*74*).

Recently, Sadighi and co-workers (*75*) reported a novel carbene-supported Cu(I) boryl complex that could abstract oxygen from CO_2 and undergoes subsequent turenover readily. Using an easily handled diboron reagent as the oxygen acceptor, a catalytic reduction of CO_2 to CO in homogeneous system is achieved with unprecedented TON and TOF (Scheme 17). In this system, higher TON could be achieved at higher reaction temperature or using less sterically demanding ligands for copper.

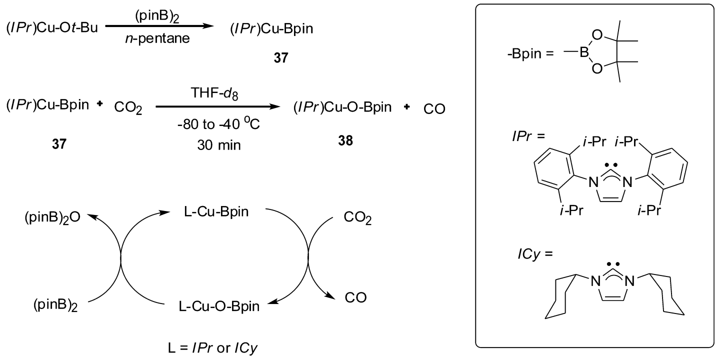

Scheme 17. Homogeneous reduction of CO_2 to CO catalyzed by Cu(I) boryl complex.

As mentioned above, transition metals-promoted reduction of CO_2 to give CO and CO_3^{2-} has been observed in many systems, and this type of transformation is known as reductive disproportionation (equation 3).

$$2\ CO_2 + 2e^- \rightarrow CO + CO_3^{2-} \qquad (3)$$

Downloaded by STANFORD UNIV GREEN LIBR on June 5, 2012 | http://pubs.acs.org
Publication Date (Web): December 14, 2011 | doi: 10.1021/bk-2011-1088.ch008

Peters *et al.* reported the reductive cleavage of CO_2 by a low-coordinate iron(I) system in which a diiron(II) complex with a Fe(μ-CO)-(μ-O)Fe core was obtained as the major product (*76*). Later, Holland and co-workers (*77*) described another iron(I) system for the reduction of CO_2 to CO in which different results was obtained while the mechanism would be similar. Treating $L^{tBu}FeNNFeL^{tBu}$ (L^{tBu} = 2,2,6,6-tetramethyl-3,5-bis-[(2,6-diisopropylphenyl)imino]hept-4-yl) with 2 equiv of dry CO_2 in pentane, benzene, or diethyl ether affords a mixture of dicarbonyliron(I) compound $L^{tBu}Fe(CO)_2$ (**39**) and the bridging carbonarodiiron(II) compound $L^{tBu}Fe(\mu\text{-}OCO_2)\text{-}FeL^{tBu}$ (**40**). The theoretical stoichiometry of this reaction is shown in equation 4. In this reaction, 8 moles of Fe are oxidized from Fe^{I} to Fe^{II}, concomitant with the reduction of 8 moles of CO_2. And 4 moles of carbonate anions bound to Fe^{II}, as well as 4 moles of CO trapped by Fe^{I} is formed in this reaction.

$$5L^{tBu}FeNNFeL^{tBu} + 8CO_2 \rightarrow 2L^{tBu}Fe(CO)_2\ (\mathbf{39}) + 4L^{tBu}Fe(CO_3)FeL^{tBu}\ (\mathbf{40}) \quad (4)$$

A reasonable mechanism for this CO_2 reduction reaction is proposed as shown in Scheme 18, in which an oxo complex is assumed to be an intermediate in the formation of **40**.

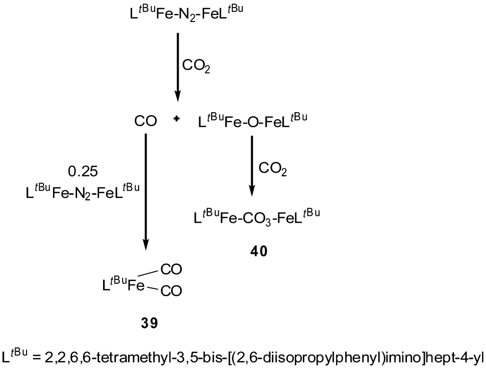

Scheme 18. Proposed mechanism for the reduction of CO_2 to CO mediated by iron complex.

Very recently, Kato and Baceiredo (*78*) reported the synthesis of the first stable disilyne bisphosphine adduct (**41**) (Scheme 19) and its application in the reduction of CO_2. Herein, this adduct would act as an efficient CO_2-reducing agent allowing the non-metal-mediated direct reduction of CO_2 to CO. It is observed that the reaction of **41** with CO_2 is complete upon mixing to afford the aminosilicate **42** with two pentacoordinated silicon arms (78% isolated yield) and CO gas which is quantified and characterized by using {Rh^{I}(cod)} (cod= cycloocta-l,5-diene) complex based on the corresponding ligand-exchange reaction. As a result, disilyne **41** reacts with 4 equivalents of CO_2, formally extracting 3 mole of oxygen and capturing one CO_2 molecule in the obtained product.

Downloaded by STANFORD UNIV GREEN LIBR on June 5, 2012 | http://pubs.acs.org
Publication Date (Web): December 14, 2011 | doi: 10.1021/bk-2011-1088.ch008

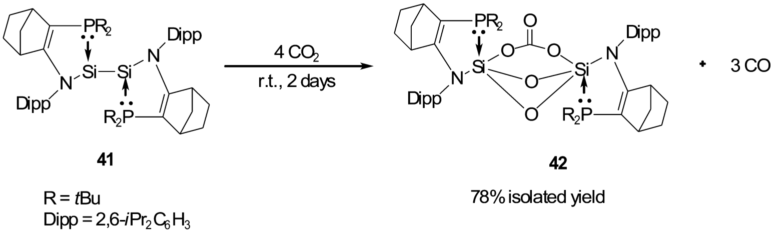

Scheme 19. Reduction of CO_2 to CO mediated by disilyne derivative.

For this reduction reaction, a Peterson olefination type reaction instead of a Wittif type reaction is proposed by the authors as illuminated in Scheme 20. The addition of the first equivalent of CO_2 probably gives the intermediate (**43**) featuring a silaketene and silaketone function. Since silaketene derivatives are known to be labile molecules, the pentacoordinated silaketene (**43**) could readily release CO to give the transient oxadisilirene derivative (**44**). After a similar process with a second equivalent of CO_2, the 2,4-dioxabicyclo-[1.1.0]tetrasilane derivative (**45**) could react with a third equivalent of CO_2, leading to formation of **46**. Since intermediate **46** can not be involved in a Peterson type reaction, the last Coreleasing reaction is probably assisted by the nucleophilic attack of one of the phosphine ligands, leading to **47** and then **48** after CO elimination. Finally, the highly reactive tricyclic silicate (**48**) would be trapped by a fourth equivalent of CO_2 to give the isolated aminosilicate **42**. Compound **42** is highly stable, and no decomposition is observed even after heating at 180 °C for 12 h.

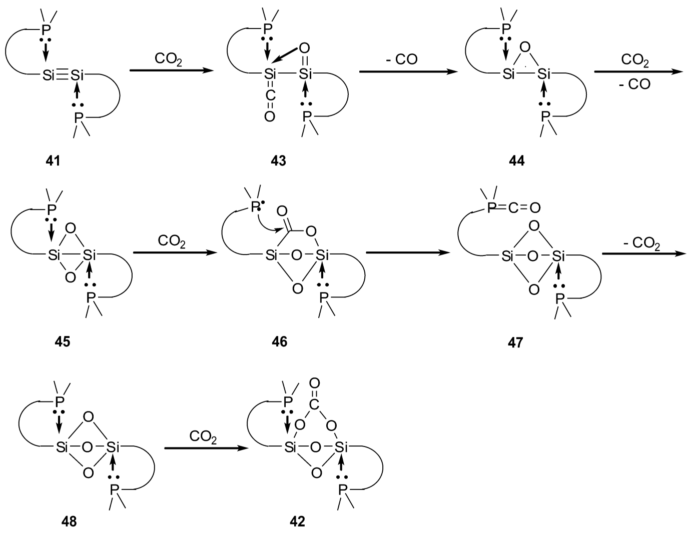

Scheme 20. Proposed reaction mechanism for the reduction of CO_2 to CO mediated by disilyne derivative.

Downloaded by STANFORD UNIV GREEN LIBR on June 5, 2012 | http://pubs.acs.org
Publication Date (Web): December 14, 2011 | doi: 10.1021/bk-2011-1088.ch008

Reduction of CO_2 to CH_4 and Higher Hydrocarbons

From the perspective of environmental protection, the appeal for conversion of CO_2 into hydrocarbons is that CO_2, the main greenhouse gas, could be recycled as hydrocarbon fuels instead of being pumped into the atmosphere. It is of great significance for both environmental protection and the development of clean energy.

Homogeneous catalytic system has been reported for the direct reduction of CO_2 to methane. Matsuo *et al.* (*79*) realized the homogeneous reduction of CO_2 into methane with hydrosilanes as the reductant catalyzed by zirconium-borane complexes via a bis(silyl)acetal intermediate. The overall reaction stoichiometry described here proceeds as illustrated in equation 5.

$$CO_2 + 4\text{Si-H} \rightarrow CH_4 + 4\text{Si-O} \qquad (5)$$

The catalytic system being composed of zirconium complex with a tridentate-phenoxide ligand (**L**^{3})Zr(CH_2Ph)$_2$ and tris(pentafluorophenyl)borane ($B(C_6F_5)_3$) exhibits the best catalytic activity for the reduction of CO_2 affording methane and the corresponding siloxanes product (Scheme 21). In addition, various hydrosilanes are shown to be effective although bulkier ones reacts slowly.

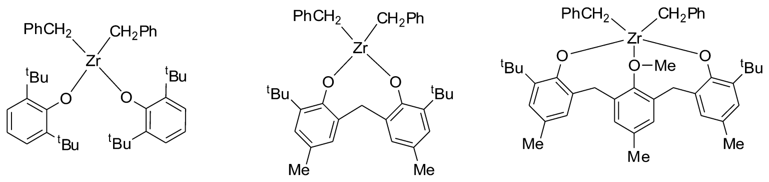

(L^1)$_2$Zr(CH_2Ph)$_2$ **(49)** (L^2)Zr(CH_2Ph)$_2$ **(50)** (L^3)Zr(CH_2Ph)$_2$ **(51)**

Scheme 21. Various zirconium complex bearing phenoxide ligands.

Although a detailed pathway for the overall catalytic process can not be deduced, an outline of a potential mechanism is provided (Scheme 22). First, the zirconium cationic complex forms a adduct with CO_2 due to highly electrophilic character of the phenoxide-supported zirconium(IV) cationic species (*80*). This coordination might render CO_2 reactive toward hydrosilation to yield the initial product $CH_2(OSiR_3)_2$. The resulting bis(silyl)acetal is subsequently reduced by R_3SiH to CH_4 and $(R_3Si)_2O$. It is worth noting that the final step is found to be facilitated by a catalytic amount of $B(C_6F_5)_3$ alone.

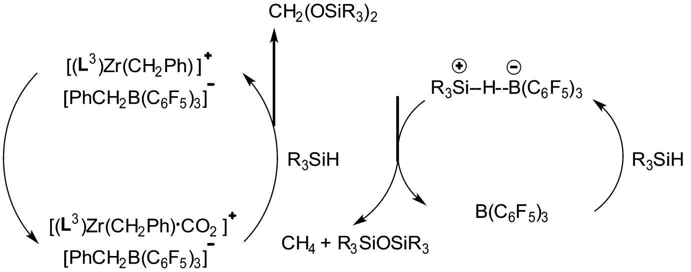

Scheme 22. Proposed mechanism for reduction of CO_2 to CH_4.

Heterogeneous catalysis has also been reported for the direct hydrogenation of CO_2 to light olefins and liquid hydrocarbons, similar to Fischer-Tropsch chemistry of CO and H_2. CO_2 can be directly reduced to light olefins and liquid hydrocarbons over various kinds of Fe-based catalysts, for example, K-, Cu-, and Mn/K-promoted iron catalysts (*81–91*).

For the MnO/K_2O-promoted Fe/silicalite (*84*) catalyzed hydrogenation of CO_2, addition of MnO into the Fe catalyst enhances the selectivity toward light olefins although no positive effect is observed on CO_2 conversion. With the addition of K_2O onto the Fe-Mn/silicalite catalyst, the selectivity to light olefins increases further and an obvious increase in CO_2 conversion is also observed. Capacity of the Fe/silicalite catalyst to absorb CO_2 is remarkably enhanced with the incorporation of MnO/K_2O promoter, being favorable for improving the activity as well as for enhancing C_2H_4 and C_3H_6 selectivities during CO_2 hydrogenation.

Choi *et al.* (*91*) developed two kinds of iron-based catalysts ($Fe-K/Al_2O_3$ and Fe-Cu-Al-K) which were prepared through a co-precipitated method for the direct hydrogenation of CO_2. The Fe-Cu-Al-K catalyst has much higher reducibility and catalytic activity at low temperature than $Fe-K/Al_2O_3$. Additionally, using Fe-Cu-Al-K catalyst, the effect of different types of reactors on the reduction of CO_2 is also studied. It is observed that the performance of fluidized bed or slurry reactors is superior to that of fixed bed reactor over Fe-Cu-Al-K catalyst in terms of CO_2 conversion and hydrocarbon productivity. Moreover, light olefins and heavy hydrocarbons are selectively synthesized in fluidized bed and slurry reactors, respectively. These improved performance using fluidized bed and slurry reactors can be ascribed to their removal of heat generated during the hydrogenation reaction which is highly exothermic.

Photochemical and Electrochemical Conversion

During the four main methodologies to transform CO_2 into useful chemicals, one of them is to supply physical energy such as light and electricity to overcome the tremendous obstacle both in thermodynamics and kinetics. There will be of great significance using such energy from nature to realize the transformation of CO_2 which is an abundant and renewable C1 source for the sustainable development of our society.

Downloaded by STANFORD UNIV GREEN LIBR on June 5, 2012 | http://pubs.acs.org
Publication Date (Web): December 14, 2011 | doi: 10.1021/bk-2011-1088.ch008

Recent research has shown that the reduction of CO_2 by photochemical or electrochemical methods can efficiently produce various organic compounds such as HCOOH, CO, CH_4, $CH_2{=}CH_2$ (*92–97*). Those products can be used as starting materials for chemical synthesis or production of hydrocarbon fuels.

The potential for the reduction of CO_2 to $CO_2^{\bullet -}$ is -1.90 V *versus* normal hydrogen electrode (NHE), making the one-electron reduction highly unfavorable. Because the first added electron must occupy the lowest energy π* orbital of the linear molecule (CO_2), then the bent radical anion ($CO_2^{\bullet -}$) is generated. In contrast, proton-coupled multielectron steps are much more favorable since thermodynamically more stable molecules are produced (*97–101*) as shown in Table 1.

Table 1. Reduction Potentials for Various CO_2 Reduction Reactions[a]

Reaction	*E^a / V*
$CO_2 + e^- \rightarrow CO_2^{\bullet -}$	-1.90
$CO_2 + 2H^+ + 2e^- \rightarrow CO + H_2O$	-0.52
$CO_2 + 2H^+ + 2e^- \rightarrow HCOOH$	-0.61
$CO_2 + 4H^+ + 4e^- \rightarrow C + 2H_2O$	-0.20
$CO_2 + 4H^+ + 4e^- \rightarrow HCHO + H_2O$	-0.48
$CO_2 + 6H^+ + 6e^- \rightarrow CH_3OH + H_2O$	-0.38
$CO_2 + 8H^+ + 8e^- \rightarrow CH_4 + 2H_2O$	-0.24

[a] Potentials were measured in aqueous solution (pH = 7) *versus* NHE, 25 °C, 1 atmosphere pressure, and 1 M for the other solutes.

Photochemcal Reductions

Generally, a photosensitizer is required in the photochemical systems which can convert light energy into stored chemical energy. The photosensitizer first absorbs photons, producing a reactive excited state that is capable of reducing CO_2 by charge transfer. After that, the oxidized photosensitizer receives an electron to regenerate the initial ground-state species and complete the catalytic cycle. Transition-metal complexes are usually employed as catalysts since they can absorb a significant part of the solar spectrum, have long-lived excited states, and can promote the activation of small molecules (*102*).

The photosensitizer $[Ru(bpy)_3]^{2+}$ was applied in photochemical reduction of CO_2 by Lehn *et al.* (*98*). Visible light irradiation of CO_2 saturated solutions of $[Ru(bpy)_3]^{2+}$, $CoCl_2$ and NEt_3 in $CH_3CN/H_2O/$ NEt_3 (3:1:1, vol/vol) generates CO and H_2. The amount of gas produced and the ratio CO/H_2 depend markedly on the composition of the system. Addition of free bipyridine strongly decreases CO generation but increases H_2 production. However, the selectivity for CO could be enhanced by replacement of NEt_3 with triethanolamine (TEOA). $CoCl_2$ is the most efficient mediator for both CO and H_2 generation and specifically promotes CO

In Production and Purification of Ultraclean Transportation Fuels; Hu, Y., et al.;
ACS Symposium Series; American Chemical Society: Washington, DC, 2011.

Downloaded by STANFORD UNIV GREEN LIBR on June 5, 2012 | http://pubs.acs.org
Publication Date (Web): December 14, 2011 | doi: 10.1021/bk-2011-1088.ch008

formation, whereas salts of other cations studied only yield H_2. The mechanism is proposed to pass through a reductive quenching. The reduction of Co(II) generated Co(I) species, which could then reduce CO_2. Further study shows that the active Co(I) species is $[Co(bpy)_n]^+$ (*103*).

By using 1-benzyl-1,4-dihydronicotinamide (BNAH) as electron donor, $[Ru(bpy)_3]^{2+}$ as a photosensitizer and $[Ru(bpy)_2(CO)_2]^{2+}$ as a cocatalyst, Tanaka *et al.* (*104*) converted CO_2 into CO (Scheme 23). When TEOA is employed as quenching agent, the solution pH is higher and the conversion of CO_2 into $HCOO^-$ (quantum yield up to 14%) is achieved.

Downloaded by STANFORD UNIV GREEN LIBR on June 5, 2012 | http://pubs.acs.org
Publication Date (Web): December 14, 2011 | doi: 10.1021/bk-2011-1088.ch008

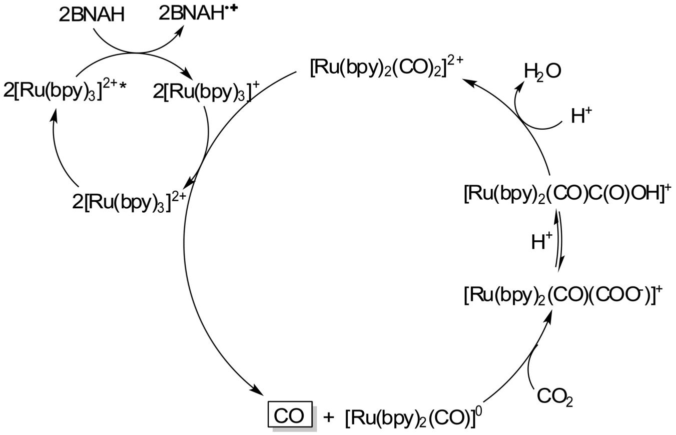

Scheme 23. Photochemical reduction of CO_2 in the BNAH solution.

Neumann *et al.* (*105*) examined the photoreduction of CO_2 to CO with tertiary amines as reducing agents catalyzed by ${}^6Q_5[Ru^{III}(H_2O)SiW_{11}O_{39}]$ in which ${}_6Q = (C_6H_{13})_4N^+$. Results of UV/vis, EPR spectrum and ^{13}C NMR reveal that the coordination of CO_2 to Ru^{III} active site yields ${}^6Q_5[Ru^{III}(CO_2)SiW_{11}O_{39}]$. Reaction mechanism is also proposed based on the experimental and computed results (Scheme 24).

Hori *et al.* (*106*) used the photocatalyst $\{Re(bpy)(CO)_3[P(OEt)_3]\}SbF_6$ to obtain reduction product (CO) in the CO_2 saturated DMF/TEOA solution, with a quantum yield of 38%. When using $Re(bpy)(CO)_3Cl$ under the same conditions, the quantum yield is only 16%. Both the quantum yield and turnover number of the photocatalytic reaction are strongly dependent on the irradiation light intensity and wavelength because of the unusual stability of the one-electron-reduced species. When $[Re(4,4'\text{-}X_2\ bpy)(CO)_3PR_3]^+$ ($X = H, CH_3$; $R = P(OC_2H_5)_3, P(O\text{-}i\text{-}C_3H_7)_3$) is employed, the quantum yield of CO is only 16-20% (*107*). The soluble rhenium-bipyridine complexes in compressed CO_2 were also prepared by Hori *et al.* (*108*) and successfully applied to photochemical reduction of CO_2 without use of an organic liquid solvent.

Downloaded by STANFORD UNIV GREEN LIBR on June 5, 2012 | http://pubs.acs.org
Publication Date (Web): December 14, 2011 | doi: 10.1021/bk-2011-1088.ch008

In the $[Re^{I}(L)(CO)_3X]$ photocatalyzed reduction of CO_2 to CO and H_2O, replacement amine sacrificial donors by H_2 has drawn much attention in recent years. In the presence of Pt(0), polyoxometalates can oxidize H_2 to two protons and two electrons.

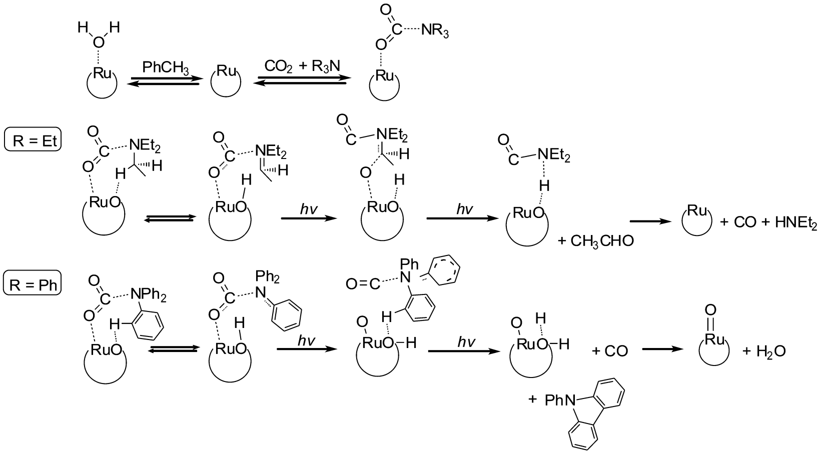
PhCH3
CO2 + R3N
NR3
R = Et
NEt2
hv
+ CH3CHO
+ CO + HNEt2
R = Ph
NPh2
Ph2
Ph
+ CO
+ H2O
+ PhN

Scheme 24. Mechanism of CO_2 photoreduction by Ru complex.

Neumann *et al.* (*109*) prepared a metalorgano polyoxometalate hybrid complex $Re^{I}(L)(CO)_3CH_3CN\text{-}MHPW_{12}O_{40}$ (L = 15-crown-5-phenanthroline, M = Na^+, H_3O^+) by modifying the 5,6-position of phenanthroline ligand with 15-crown-5 ether. Under visible light irradiation, the complex can oxidize H_2 to protons and electrons and this can catalyze the photoreduction of CO_2 to CO in the present of Pt/C. But the turnover frequency and quantum yield observed in the present reduction of CO_2 with H_2 is lower than previous report. The concept of replacing the sacrificial tertiary amine reducing agent by H_2 is depicted in Scheme 25.

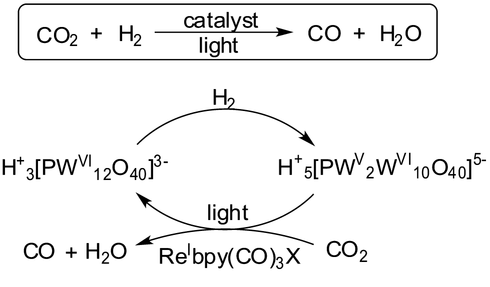
CO2 + H2 catalyst light CO + H2O
H2
H+3[PWVI12O40]3-
H+5[PWV2WVI10O40]5-
light
CO + H2O
ReIbpy(CO)3X
CO2

Scheme 25. Proposed photoreduction of CO_2 with H_2.

Downloaded by STANFORD UNIV GREEN LIBR on June 5, 2012 | http://pubs.acs.org
Publication Date (Web): December 14, 2011 | doi: 10.1021/bk-2011-1088.ch008

Frei *et al.* (*110*) studied the photoreduction of CO_2 over mesoporous ZrCu(I)-MCM-41 silicate sieve. By using a stepwise grafting procedure, binuclear redox sites consisting of a Zr oxo-bridged to a Cu(I) center have been obtained on the pore surface of MCM-41 silicate sieve. The absorption of metal-to-metal charge-transfer (MMCT), Zr(IV)-O-Cu(I) to Zr(III)-O-Cu(II), shifts from the UV region to about 500 nm. Irradiation of ZrCu(I)-MCM-41 loaded with 1 atm of CO_2 at room temperature produces CO and H_2O (Scheme 26). Isotope labelled experiments by using $^{13}CO_2$ and $C^{18}O_2$ ravel that CO and the oxygen of H_2O product would originate from CO_2. This indicates splitting of CO_2 by the excited MMCT moiety to CO and a surface OH radical, followed by trapping of the products at Cu(I) centers (OH is reduced to H_2O).

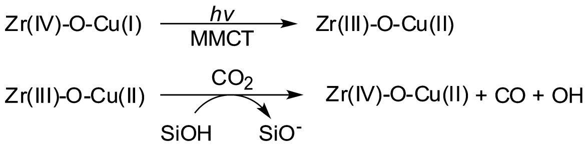

Scheme 26. Photochemical CO_2 splitting.

Homogenous photosensitizer systems with metal cocatalysts have been observed to produce only CO and $HCOO^-$ (*98*, *103*, *104*, *106–108*). Recently, Bocarsly *et al.* (*111*) reported selective conversion of CO_2 to methanol by utilizing light energy at a p-GaP semiconductor electrode. The reduction system, driving by light energy, features a homogeneous pyridinium ion catalyst and faradaic efficiencies near 100% at potentials well below the standard potential is achieved.

Chen *et al.* (*112*) studied the reduction of CO_2 in the supercritical state by Fe_3O_4 powder,. Valuable products such as ethanol, acetaldehyde, acetic acid and, especially, phenol can be obtained. The reduction is suggested to occur on the surface of the Fe_3O_4 particles and to go through a multielectron reductive coupling of a pair of or several carbonyls to produce an intermediate. The increased polarity in a high pressure system is favorable for CO_2 absorption on the surface of Fe_3O_4 particles, and may accelerate the reduction. The maximum transformation ratio for CO_2 to phenol is found to be as high as 7.6% at temperatures > 300 °C.

The selective and reversible conversion of CO into CO_2 can be catalyzed by CODH, which belongs to the family of oxidoreductases, specifically those acting on the aldehyde or oxo group of donor with other acceptors. Two different types of CODH are found in nature (*113–115*). CODH from the anaerobic microbe *Carboxydothermus hydrogenoformans* (*Ch*) is Ni-Fe containing enzymes ($CODH_{Ni}$) and the Mo-Cu containing enzyme ($CODH_{Mo}$) is found in *Oligotropha carboxidovorans* (*Oc*). The active site structure of the enzymes is shown in Scheme 27. Studies has shown that the pathway of CO_2 formation is different but in both enzymes, a direct reversible two-electron transfer is observed (*116–118*).

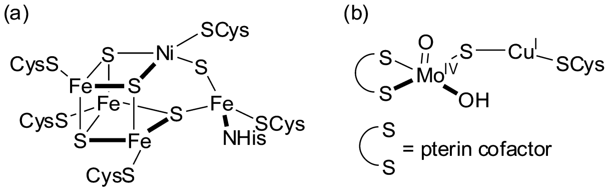

Scheme 27. Active site structures of (a) $CODH_{Ni}$ and (b) $CODH_{Mo}$.

The usual TiO_2-based systems provide only a single electron transfer forming a highly reactive $CO_2^{\bullet -}$ radical (*119*). This high energy pathway typically leads to a mixture of products, including methane and ethanol. Recently, Armstrong *et al.* (*120*) reported the photoreduction of CO_2 to CO by $CODH_{Ni}$ modified TiO_2 nanoparticles (NPs) using visible light. The enzyme bypasses the one-electron radical pathway, instead catalyzing a controlled, two-electron reduction (E = -0.46 V *versus* saturated calomel electrode (SHE) at pH = 6) giving CO (250 μmolh^{-1} CO per g of TiO^2) as a clean product (Figure 1).

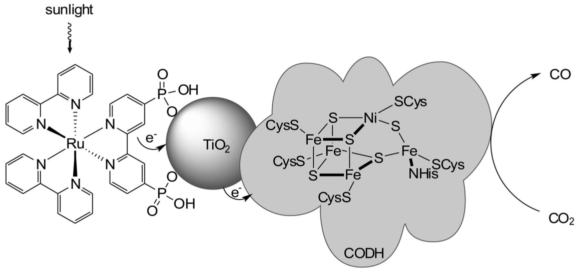

Figure 1. The photoreduction of CO_2 to CO by $CODH_{Ni}$ modified NPs.

Similarly, Cummins *et al.* (*121*) also achieved the two-electron reduction of CO_2 into CO by using a Nb_V nitrido complex. Strong metal-oxygen bonds are avoided through the nitrido ligand. And the nitrido ligand reacts with CO_2 to give a carbamate species (Scheme 28), which has been confirmed by ^{13}C-labeling experiments. Deoxygenation of the carbamate by reaction with RC(O)X (such as Ac_2O) results in an isocyanato acetato complex. Subsequently, dissociation of the acetate ligand occurs induced either by electrochemical reduction or by treatment with SmI_2. Additional one-electron reduction leads to CO release and re-forms the Nb^V nitrido complex. The final loss of the CO group is confirmed by the reaction with [Cp*RuCl(PCy_3)] which gives [Cp*RuCl-(PCy_3)(CO)] (Cp* = cyclopentadienyl ligand) and shows a dramatic color change from blue to yellow.

Downloaded by STANFORD UNIV GREEN LIBR on June 5, 2012 | http://pubs.acs.org
Publication Date (Web): December 14, 2011 | doi: 10.1021/bk-2011-1088.ch008

Downloaded by STANFORD UNIV GREEN LIBR on June 5, 2012 | http://pubs.acs.org
Publication Date (Web): December 14, 2011 | doi: 10.1021/bk-2011-1088.ch008

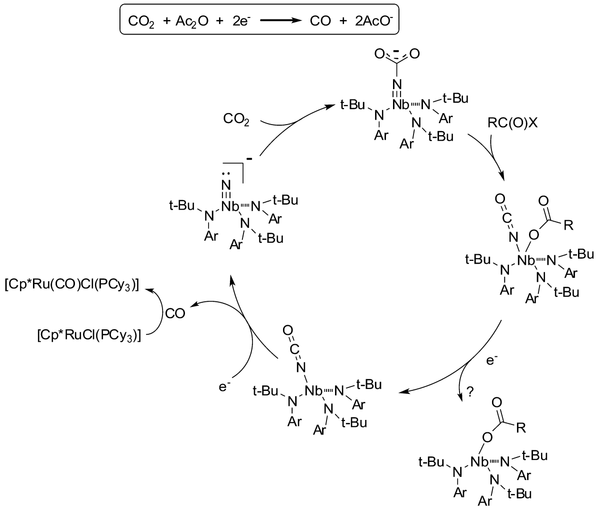

Scheme 28. CO_2 reduction by Nb^V nitrido complexes.

Zou *et al.* prepared single-crystalline hexagonal prism Zn_2GeO_4 nanorods with different aspect ratios using a solution phase route (*122*). Under UV-vis light irradiation, CO_2 can be photoreduced to CO and CH_4 in the presence of water vapor by using RuO_2 loaded Zn_2GeO_4 as the photocatalyst. The results indicate that Zn_2GeO_4 nanorods exhibit higher activity than Zn_2GeO_4 bulks due to the low crystal defects, high specific surface area and beneficial microstructure on the catalyst's surface (*123*).

The reaction can be described as follow: the photogenerated hole on the valence band top (potential: +3.8 V *versus* NHE) of Zn_2GeO_4 can lead to oxidation of water to produce hydrogen ions and the photogenerated electron on the conduction band bottom (potential: -0.7 V *versus* NHE) of Zn_2GeO_4 can drive the reduction of CO_2 into CO (*124*).

Electrochemical Reductions

Electrochemical reductions of CO_2 to liquid fuels occur on solid electrodes and are therefore heterogeneous processes which can be slower than homogeneous ones. However, an appropriate electrocatalysts can be applied for lowering the overpotential, increasing the reaction kinetics, and improving reaction selectivity. Many reports have appeared in the literature concerning transition metal complexes or macrocyclic complexes as catalyst.

In 1980, the first reported of electrochemical reduction of CO_2 using transition metal catalysts with high current efficiencies was demonstrated by Eisenberg *et al.* (*125*). The cobalt and nickel tetraazomacrocyclic complexes employed in this work are shown in Scheme 29. These catalysts are able to provide high current efficiencies (up to 98%), but displays low TOF (from 2 to 9 h^{-1}) at 23 °C.

Downloaded by STANFORD UNIV GREEN LIBR on June 5, 2012 | http://pubs.acs.org
Publication Date (Web): December 14, 2011 | doi: 10.1021/bk-2011-1088.ch008

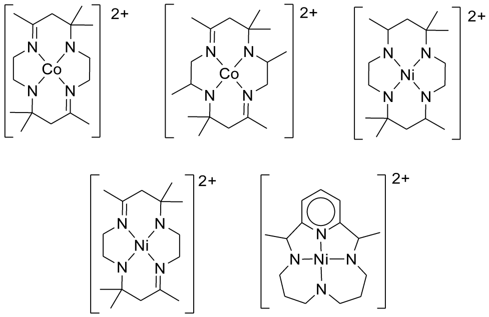

Scheme 29. Transition metal catalysts for the reduction of CO_2 to CO.

Using cyclic voltammetry (CV) and controlled-potential electrolysis (CPE) techniques, Viswanathan *et al.* (*126*) studied electroreduction of CO_2 with Ni(II) complex of 1,3,6,9,11,14-hexaazatricyclo[12.2.1.1]octadecane as electrocatalyst. The mechanism of producing CO and HCOOH is proposed (Scheme 30).

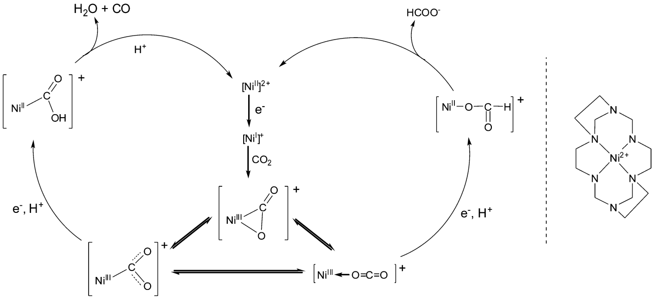

Scheme 30. Structure of electrocatalyst and the proposed mechanism.

Aguirre *et al.* studied electrochemical reduction of CO_2 on a glassy carbon electrode modified with either polymeric M-tetrakis aminophthalocyanines (M-TaPc, M = Co, Ni, Fe, Scheme 31) or with the polymeric free ligand in aqueous electrolyte (*127*). The products are dependent on the chemical nature of central ion by affecting the kinetics of polymerization and the polymer morphology.

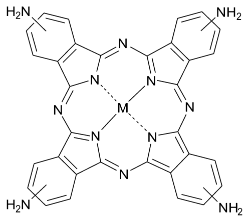

Scheme 31. Structrues of M-TaPc (M = Co, Ni, Fe).

Very recently, Chang *et al.* (*128*) proposed and synthesized Ni(II) complexes with N-heterocyclic carbene-pyridine ligands (Scheme 32), which are able to reduce CO_2 to CO with high selectivity for activating CO_2 over H_2O under electrocatalytic conditions.

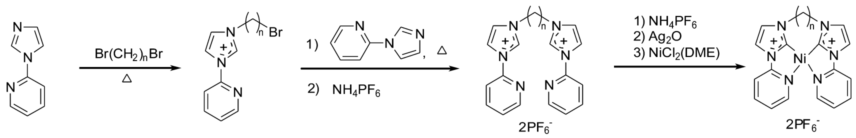

Scheme 32. Synthesis of nickel N-heterocyclic carbene-pyridine complexes.

Generally, electrochemical reduction of CO_2 in nonaqueous solution is more effective than that in aqueous solution. This is mainly because of increased CO_2 solubility in nonaqueous media. On the other hand, aqueous solutions provides a readily available proton source to generate methanol and hydrocarbons. Recently, Irvine et al. (*129*) applied an efficient electrolyser with configuration of (anode) $(La_{0.8}Sr_{0.2})_{0.95}MnO_{3-\delta}/YSZ/La_{0.2}Sr_{0.8}TiO_{3+\delta}$ (cathode) (YSZ = yttria-stabilized zirconia) to reduce CO_2 into methane in aqueous system. In the whole process, heterogeneous catalysis is the rate limitation. Electroreduction of cathode is the main process at low electrical voltages while the coelectrolysis is the main process at high voltages.

Conclusions

As an abundant, nontoxic, nonflammable, easily available, and renewable C1 resource, the transformation of CO_2 into useful and value-added chemicals is particularly important and deserves the worldwide research efforts. Especially, facing two of the most austere and challenging issues nowadays all over the world, viz. energy and environment, there is a more far-reaching significance to convert CO_2 into value-added and precious energy and fuels while reducing its emission. In this aspect, the transformation and utilization of CO_2, which can be upgraded to huge CO_2 industry, are particularly important for the sustainable development of our society and economy.

Although a great progress has been made on chemical transformation and utilization of CO_2, there remain many opportunities and challenges to be explored further in this field. In terms of catalytic hydrogenation and reduction of CO_2 into fuels and value-added chemical products, many ingenious and innovative strategies have been developed in laboratory. However, thermodynamic stability and kinetic inertness of CO_2 would prevent its utilization in industry. Thus the exploration of milder reaction conditions, more efficient catalysts, and more practical catalytic systems is highly desired for conversion of CO_2 into value-added chemical products, in particular, CO_2 reductive transformation into clean energy and sustainable transportation fuels (*130–132*).

Downloaded by STANFORD UNIV GREEN LIBR on June 5, 2012 | http://pubs.acs.org
Publication Date (Web): December 14, 2011 | doi: 10.1021/bk-2011-1088.ch008

In general, the main challenge for advancing CO_2 reduction is increasing the energy efficiency, which is primarily hindered by high over-potentials for CO_2 reduction. The challenges presented here are great, but the potential rewards are enormous. We hope this presentation will stimulate further interest in academic research and industrial utilization that may lead to development of CO_2 as a building block for the synthesis of value-added chemical products, specifically for fuel production.

Acknowledgments

We are grateful to the National Natural Science Foundation of China (Grant No. 20872073), and Research Fellowship for International Young Scientists from NSFC (21150110105), and the Committee of Science and Technology of Tianjin for financial support.

References

1. Chen, C.; Yang, S.-T.; Ahn, W.-S.; Ryoo, R. *Chem. Commun.* **2009**, *24*, 3627–3629.
2. Inoue, Y.; Izumida, H.; Sasaki, S.; Hashimoto, H. *Chem. Lett.* **1976**, *8*, 863–864.
3. Jessop, P. G.; Ikaryia, T.; Noyori, R. *Nature* **1994**, *368*, 231–233.
4. Jessop, P. G.; Ikaryia, T.; Noyori, R. *Chem. Rev.* **1995**, *95*, 259–272.
5. Jessop, P. G.; Joò, F.; Tai, C. C. *Coord. Chem. Rev.* **2004**, *248*, 2425–2442.
6. Gassun, F.; Leitner, W. *J. Chem. Soc., Chem. Commun.* **1993**, *19*, 1465–1466.
7. Munshi, P.; Main, A. D.; Linehan, J.; Jessop, P. G. *J. Am. Chem. Soc.* **2002**, *124*, 7963–7971.
8. Krocker, O.; Koppel, R. A.; Froba, M.; Baiker, A. *J. Catal.* **1998**, *178*, 284–298.
9. Jessop, P. G.; Hsiao, Y.; Ikaryia, T.; Noyori, R. *J. Am. Chem. Soc.* **1994**, *116*, 8851–8852.
10. Munshi, P.; Heldebrandt, D. J.; McKoon, E. P.; Kelly, P. A.; Tai, C.-C.; Jessop, P. G. *Tetrahedron Lett.* **2003**, *44*, 2725–2726.
11. Elek, J.; Nádasdi, L.; Papp, G.; Laurenczy, G. *Appl. Catal., A* **2003**, *255*, 59–67.
12. Kathó, Á.; Opre, Z.; Laurenczy, G.; Joó, F. *J. Mol. Catal. A: Chem.* **2003**, *204-205*, 143–148.
13. Jessop, P. G.; Hsiao, Y.; Ikariya, T.; Noyori, R. *J. Am. Chem. Soc.* **1996**, *118*, 344–355.
14. Tai, C.-C.; Pitts, J.; Linehan, J. C.; Main, A. D.; Munshi, P.; Jessop, P. G. *Inorg. Chem.* **2002**, *41*, 1606–1614.
15. Munshi, P.; Main, A. D.; Linehan, J. C.; Tai, C.-C.; Jessop, P. G. *J. Am. Chem. Soc.* **2002**, *124*, 7963–7971.
16. Zhang, Y.-P.; Fei, J.-H.; Yu, Y.-M.; Zheng, X.-M. *Catal. Commun.* **2004**, *5*, 643–646.

Downloaded by STANFORD UNIV GREEN LIBR on June 5, 2012 | http://pubs.acs.org
Publication Date (Web): December 14, 2011 | doi: 10.1021/bk-2011-1088.ch008

17. Anderson, J.-J.; Hamlin, J.-E. European Patent Application 0 126 524, 1984.
18. Anderson, J.-J.; Drury, D.-J.; Hamlin, J.-E.; Kent, A.-G. European Patent Application 0 181 078, 1986.
19. Zhang, Z.-F.; Xie, Y.; Li, W.-J.; Hu, S.-Q.; Song, J.-L.; Jiang, T.; Han, B.-X. *Angew. Chem., Int. Ed.* **2008**, *47*, 1127–1129.
20. Zhang, Z.-F.; Hu, S.-Q.; Song, J.-L.; Li, W.-J.; Yang, G.-Y.; Han, B-X. *ChemSusChem* **2009**, *2*, 234–238.
21. Himeda, Y.; Onozawa-Komatsuzaki, N.; Sugihara, H.; Kasuga, K. *J. Am. Chem. Soc.* **2005**, *127*, 13118–13119.
22. Himeda, Y.; Onozawa-Komatsuzaki, N.; Sugihara, H.; Kasuga, K. *Organometallics* **2007**, *26*, 702–712.
23. Moulton, C. J.; Shaw, B. L. *J. Chem. Soc., Dalton Trans.* **1976**, 1020–1024.
24. Gupta, M.; Hagen, C.; Flesher, R. J.; Kaska, W. C.; Jensen, C. M. *Chem. Commun.* **1996**, 2083–2084.
25. Gupta, M.; Hagen, C.; Kaska, W. C.; Cramer, R. E.; Jensen, C. M. *J. Am. Chem. Soc.* **1997**, *119*, 840–841.
26. Liu, F. C.; Pak, E. B.; Singh, B.; Jensen, C. M.; Goldman, A. S. *J. Am. Chem. Soc.* **1999**, *121*, 4086–4087.
27. Haenel, M. W.; Oevers, S.; Angermund, K.; Kaska, W. C.; Fan, H. J.; Hall, M. B. *Angew. Chem., Int. Ed.* **2001**, *40*, 3596–3600.
28. Van Der Boom, M. E.; Milstein, D. *Chem. Rev.* **2003**, *103*, 1759–1792.
29. Göttker-Schnetmann, I.; White, P. S.; Brookhart, M. *Organometallics* **2004**, *23*, 1766–1776.
30. *The Chemistry of Pincer Compounds*; Morales-Morales, D., Jensen, C. M., Eds.; Elsevier; Amsterdam, 2007.
31. Tanaka, R.; Yamashita, M.; Nozaki, K. *J. Am. Chem. Soc.* **2009**, *131*, 14168–14169.
32. Federsel, C.; Jackstell, R.; Beller, M. *Angew. Chem., Int. Ed.* **2010**, *49*, 6254–6257.
33. Sanz, S.; Benítez, M.; Peris, E. *Organometallics* **2010**, *29*, 275–277.
34. Federsel, C.; Boddien, A.; Jackstell, R.; Jennerjahn, R.; Dyson, P. J.; Scopelliti, R.; Laurenczy, G.; Beller, M. *Angew. Chem., Int. Ed.* **2010**, *49*, 9777–9780.
35. Ipatieff, V. N.; Monroe, G. S. *J. Am. Chem. Soc.* **1945**, *67*, 2168–2171.
36. Fujiwara, M.; Souma, Y. *J. Chem. Soc., Chem. Commun.* **1992**, *10*, 767–768.
37. Fujiwara, M.; Ando, H.; Tanaka, M.; Souma, Y. *Bull. Chem. Soc. Jpn.* **1994**, *67*, 546–550.
38. Amenomiya, Y. *Appl. Catal.* **1987**, *30*, 57–68.
39. Koeppel, R. A.; Baiker, A.; Wokaun, A. *Appl. Catal., A* **1992**, *84*, 77–102.
40. Sahibzada, M.; Chadwick, D.; Metcalfe, I. S. *Catal. Today* **1996**, *29*, 367–372.
41. Wambach, J.; Baiker, A.; Wokaun, A. *Phys. Chem. Chem. Phys.* **1999**, *1*, 5071–5080.
42. Słoczyński, J.; Grabowski, R.; Olszewski, P.; Kozlowska, A.; Stoch, J.; Lachowska, M.; Skrzypek, J. *Appl. Catal., A* **2006**, *310*, 127–137.
43. Chinchen, G. C.; Denny, P. J.; Jennings, J. R.; Spencer, M. S.; Waugh, K. C. *Appl. Catal.* **1988**, *36*, 1–65.

Downloaded by STANFORD UNIV GREEN LIBR on June 5, 2012 | http://pubs.acs.org
Publication Date (Web): December 14, 2011 | doi: 10.1021/bk-2011-1088.ch008

44. Kanoun, N.; Astier, M. P.; Pajonk, G. M. *Catal. Lett.* **1992**, *15*, 231–235.
45. Słoczyński, J.; Grabowski, R.; Kozłowska, A.; Olszewski, P.; Lachowska, M.; Skrzypek, J.; Stoch, J. *Appl. Catal., A* **2003**, *249*, 129–138.
46. Chakraborty, S.; Zhang, J.; Krause, J. A.; Guan, H.-R. *J. Am. Chem. Soc.* **2010**, *132*, 8872–8873.
47. Riduan, S. N.; Zhang, Y.-G.; Jackie, Y. Y. *Angew. Chem., Int. Ed.* **2009**, *48*, 3322–3325.
48. Stephan, D. W. *Dalton Trans.* **2009**, *17*, 3129–3136.
49. Stephan, D. W.; Erker, G. *Angew. Chem., Int. Ed.* **2010**, *49*, 46.
50. Welch, G. C.; Juan, R. R. S.; Masuda, J. D.; Stephan, D. W. *Science* **2006**, *314*, 1124–1126.
51. Welch, G. C.; Stephan, D. W. *J. Am. Chem. Soc.* **2007**, *129*, 1880–1881.
52. Chase, P. A.; Stephan, D. W. *Angew. Chem., Int. Ed.* **2008**, *47*, 7433–7437.
53. Sumerin, V.; Schulz, F.; Atsumi, M.; Wang, C.; Nieger, M.; Leskelä, M.; Repo, T.; Pyykkö, P.; Rieger, B. *J. Am. Chem. Soc.* **2008**, *130*, 14117–14119.
54. Ramos, A.; Lough, A. J.; Stephan, D. W. *Chem. Commun.* **2009**, *9*, 1118–1120.
55. Mömming, C. M.; Otten, E.; Kehr, G.; Fröhlich, R.; Grimme, S.; Stephan, D. W.; Erker, G. *Angew. Chem., Int. Ed.* **2009**, *48*, 6643–6646.
56. Dureen, M. A.; Lough, A.; Gilbert, T. M.; Stephan, D. W. *Chem. Commun.* **2008**, *36*, 4303–4305.
57. Welch, G. C.; Cabrera, L.; Chase, P. A.; Hollink, E.; Masuda, J. D.; Wei, P. R.; Stephan, D. W. *Dalton Trans.* **2007**, *31*, 3407–3414.
58. Mömming, C. M.; Froemel, S.; Kehr, G.; Froehlich, R.; Grimme, S.; Erker, G. *J. Am. Chem. Soc.* **2009**, *131*, 12280–12289.
59. Ullrich, M.; Kelvin, K. S. H.; Lough, A. J.; Stephan, D. W. *Chem. Commun.* **2009**, *17*, 2335–2337.
60. McCahill, J. S. J.; Welch, G. C.; Stephan, D. W. *Angew. Chem., Int. Ed.* **2007**, *46*, 4968–4971.
61. Dureen, M. A.; Stephan, D. W. *J. Am. Chem. Soc.* **2009**, *131*, 8396–8397.
62. Ménard, G.; Stephan, D. W. *J. Am. Chem. Soc.* **2010**, *132*, 1796–1797.
63. Ashley, A. E.; Thompson, A. L.; O’Hare, D. *Angew. Chem., Int. Ed.* **2009**, *48*, 9839–9843.
64. Data taken from *CRC Handbook of Chemistry and Physics*, 73rd ed.; Lide, D. R., Ed.; CRC Press, Inc.: Boca Raton, FL, 1992−1993.
65. Ueno, A.; Sato, T.; Todo, N.; Kotera, Y.; Takasaki, S. *Chem. Lett.* **1980**, 1067–1070.
66. For general reviews of metal-mediated CO_2 chemistry, see for example: (a) Yin, X. L.; Moss, J. R. *Coord. Chem. Rev.* **1999**, *181*, 27−59. (b) Leitner, W. *Coord. Chem. Rev.* **1996**, *153*, 257−284.
67. Castro-Rodriguez, I.; Meyer, K. *J. Am. Chem. Soc.* **2005**, *127*, 11242–11243.
68. Procopio, L. J.; Carroll, P. J.; Berry, D. H. *Organometallics* **1993**, *12*, 3087–3093.
69. Ziegler, W.; Nicholas, K. M. *J. Organomet. Chem.* **1992**, *423*, C35–C37.
70. Bryan, J. C.; Geib, S. J.; Rheingold, A. L.; Mayer, J. M. *J. Am. Chem. Soc.* **1987**, *109*, 2826–2828.

Downloaded by STANFORD UNIV GREEN LIBR on June 5, 2012 | http://pubs.acs.org
Publication Date (Web): December 14, 2011 | doi: 10.1021/bk-2011-1088.ch008

Downloaded by STANFORD UNIV GREEN LIBR on June 5, 2012 | http://pubs.acs.org
Publication Date (Web): December 14, 2011 | doi: 10.1021/bk-2011-1088.ch008

71. Fachinetti, G.; Floriani, C.; Chiesi-Villa, A.; Guastini, C. *J. Am. Chem. Soc.* **1979**, *101*, 1767–1775.
72. Bogdanovic, B.; Leitner, W.; Six, C.; Wilczok, U.; Wittmann, K. *Angew. Chem., Int. Ed.* **1997**, *36*, 502–504.
73. Eisenschmid, T. C.; Eisenberg, R. *Organometallics* **1989**, *8*, 1822–1824.
74. Shin, W.; Lee, S. H.; Shin, J. W.; Lee, S. P.; Kim, Y. *J. Am. Chem. Soc.* **2003**, *125*, 14688–14689.
75. Laitar, D. S.; Mueller, P.; Sadighi, J. P. *J. Am. Chem. Soc.* **2005**, *127*, 17196–17197.
76. Lu, C. C.; Saouma, C. T.; Day, M. W.; Peters, J. C. *J. Am. Chem. Soc.* **2007**, *129*, 4–5.
77. Sadique, A. R.; Brennessel, W. W.; Holland, P. L. *Inorg. Chem.* **2008**, *47*, 784–786.
78. Gau, D.; Rodriguez, R.; Kato, T.; Saffon-Merceron, N.; Cózar, A. De.; Cossío, F. P.; Baceiredo, A. *Angew. Chem., Int. Ed.* **2011**, *50*, 1092–1096.
79. Matsuo, T.; Kawaguchi, H. *J. Am. Chem. Soc.* **2005**, *127*, 17198–17199.
80. Hill, M.; Wendt, O. F. *Organometallics* **2005**, *24*, 5772–5775.
81. Barrault, J.; Forquy, C.; Menezo, J. C. *Catal. Lett.* **1981**, *17*, 373–378.
82. Lee, M. D.; Lee, J. F.; Chang, C. S. *Bull. Chem. Soc. Jpn.* **1989**, *62*, 2756–2758.
83. Ando, H.; Xu, Q.; Fujiwam, M.; Matsumura, Y.; Tanaka, M.; Souma, Y. *Catal. Today* **1998**, *45*, 229–234.
84. Xu, L.-Y.; Wang, Q.-X.; Liang, D.-B.; Wang, X.; Lin, L.-W.; Cui, W.; Xu, Y.-D. *Appl. Catal., A* **1998**, *173*, 19–25.
85. Choi, P. H.; Jun, K.-W.; Lee, S.-J.; Choi, M.-J.; Lee, K.-W. *Catal. Lett.* **1996**, *40*, 115–118.
86. Nam, S.-S.; Kim, H.; Kishan, G.; Choi, M.-J.; Lee, K.-W. *Appl. Catal., A* **1999**, *179*, 155–163.
87. Yan, S.-R.; Jun, K.-W.; Hong, J.-S.; Choi, M.-J.; Lee, K.-W. *Appl. Catal., A* **2000**, *194-195*, 63–70.
88. Hong, J.-S.; Hwang, J. S.; Jun, K.-W.; Sur, J. C.; Lee, K-W. *Appl. Catal., A* **2001**, *218*, 53–59.
89. Choi, M.-J.; Kim, J.-S.; Kim, H.-K.; Lee, S.-B.; Kang, Y. *Korean J. Chem. Eng.* **2001**, *18*, 646–651.
90. Kim, J.-S.; Lee, S.-B.; Kang, M.-C.; Lee, K-W.; Choi, M.-J. *Korean J. Chem. Eng.* **2003**, *20*, 967–972.
91. Kim, J.-S.; Lee, S.; Lee, S.-B.; Choi, M.-J.; Lee, K.-W. *Catal. Today* **2006**, *115*, 228–234.
92. Collin, J. P.; Sauvage, J. P. *Coord. Chem. Rev.* **1989**, *93*, 245–268.
93. Andres, S.; Escuder, B.; Domenech, A.; Garcia-Espana, E.; Luis, S. V.; Marcelino, V.; Llinares, J. M.; Ramirez, J. A.; Soriano, C. *J. Phys. Org. Chem.* **2001**, *14*, 495–500.
94. Grodkowski, J.; Neta, P.; Fujita, E.; Mahammed, A.; Simkhovich, L.; Gross, Z. *J. Phys. Chem. A* **2002**, *106*, 4772–4778.
95. Laitar, D. S.; Muller, P.; Sadighi, J. P. *J. Am. Chem. Soc.* **2005**, *127*, 17196–17197.

96. Raebiger, J. W.; Turner, J. W.; Noll, B. C.; Curtis, C. J.; Miedaner, A.; Cox, B.; DuBois, D. L. *Organometallics* **2006**, *25*, 3345–3351.
97. Benson, E. E.; Kubiak, C. P.; Sathrum, A. J.; Smieja, J. M. *Chem. Soc. Rev.* **2009**, *38*, 89–99.
98. Lehn, J.; Ziessel, R. *Proc. Natl. Acad. Sci. U.S.A.* **1982**, *79*, 701–704.
99. Taniguchi, I. *Mod. Aspects Electrochem.* **1989**, *20*, 327–400.
100. Sutin, N.; Creutz, C.; Fujita, E. *Comments Inorg. Chem.* **1997**, *19*, 67–92.
101. Fujita, E. *Coord. Chem. Rev.* **1999**, *185-186*, 373–384.
102. Doherty, M. D.; Grills, D. C.; Muckerman, J. T.; Polyansky, D. E.; Fujita, E. *Coord. Chem. Rev.* **2010**, *254*, 2472–2482.
103. Ziessel, R.; Hawecker, J.; Lehn, J.-M. *Helv. Chim. Acta* **1986**, *69*, 1065–1084.
104. Ishida, H.; Tanaka, K.; Tanaka, T. *Chem. Lett.* **1988**, *17*, 339–342.
105. Khenkin, A. M.; Efremenko, I.; Weiner, L.; Martin, J. M. L.; Neumann, R. *Chem. Eur. J.* **2009**, *16*, 1356–1364.
106. Hori, H.; Johnson, F. P. A.; Koike, K.; Ishitani, O.; Ibusuki, T. *J. Photochem. Photobiol., A* **1996**, *96*, 171–174.
107. Koike, K.; Hori, H.; Ishizuka, M.; Westwell, J. R.; Takeuchi, K.; Ibusuki, T.; Enjouji, K.; Konno, H.; Sakamoto, K.; Ishitani, O. *Organometallics* **1997**, *16*, 5724–5729.
108. Hori, H.; Koike, K.; Takeuchi, K.; Sasaki, Y. *Chem. Lett.* **2000**, *29*, 522–523.
109. Ettedgui, J.; Diskin-Posner, Y.; Weiner, L.; Neumann, R. *J. Am. Chem. Soc.* **2010**, *133*, 188–190.
110. Lin, W.; Frei, H. *J. Am. Chem. Soc.* **2005**, *127*, 1610–1611.
111. Barton, E. E.; Rampulla, D. M.; Bocarsly, A. B. *J. Am. Chem. Soc.* **2008**, *130*, 6342–6344.
112. Chen, Q.; Qian, Y. *Chem. Commun.* **2001**, 1402–1403.
113. Lindahl, P. A. *Biochemistry* **2002**, *41*, 2097–2105.
114. Groysman, S.; Holm, R. H. *Biochemistry* **2009**, *48*, 2310–2320.
115. Huang, D.; Holm, R. H. *J. Am. Chem. Soc.* **2010**, *132*, 4693–4701.
116. Apfel, U.-P.; Weigand, W. *Angew. Chem., Int. Ed.* **2011**, *50*, 4262–4264.
117. Jeoung, J.-H.; Dobbek, H. *Science* **2007**, *318*, 1461–1464.
118. Dobbek, H.; Gremer, L.; Kiefersauer, R.; Huber, R.; Meyer, O. *Proc. Natl. Acad. Sci. U.S.A.* **2002**, *99*, 15971–15976.
119. Rudolph, M.; Dautz, S.; Jager, E. G. *J. Am. Chem. Soc.* **2000**, *122*, 10821–10830.
120. Woolerton, T. W.; Sheard, S.; Reisner, E.; Pierce, E.; Ragsdale, S. W.; Armstrong, F. A. *J. Am. Chem. Soc.* **2010**, *132*, 2132–2133.
121. Silvia, J. S.; Cummins, C. C. *J. Am. Chem. Soc.* **2010**, *132*, 2169–2171.
122. Yan, S.; Wan, L.; Li, Z.; Zou, Z. *Chem. Commun.* **2011**, 5632–5634.
123. Liu, Q.; Zhou, Y.; Kou, J.; Chen, X.; Tian, Z.; Gao, J.; Yan, S.; Zou, Z. *J. Am. Chem. Soc.* **2010**, *132*, 14385–14387.
124. Indrakanti, V. P.; Kubicki, J. D.; Schobert, H. H. *Energy Environ. Sci.* **2009**, *2*, 745–758.
125. Fisher, B. J.; Eisenberg, R. *J. Am. Chem. Soc.* **1980**, *102*, 7361–7363.
126. Scibioh, M. A.; Ragini, P. V.; Rani, S.; Vijayaraghavan, V. R.; Viswanathan, B. *Proc. - Indian Acad. Sci., Chem. Sci.* **2001**, *113*, 343–350.

Downloaded by STANFORD UNIV GREEN LIBR on June 5, 2012 | http://pubs.acs.org
Publication Date (Web): December 14, 2011 | doi: 10.1021/bk-2011-1088.ch008

127. Isaacs, M.; Armijo, F.; Ramirez, G.; Trollund, E.; Biaggio, S. R.; Costamagna, J.; Aguirre, M. J. *J. Mol. Catal. A: Chem.* **2005**, *229*, 249–257.
128. Thoi, V. S.; Chang, C. J. *Chem. Commun.* **2011**, *47*, 6578–6580.
129. Xie, K.; Zhang, Y.; Meng, G.; Irvine, J. T. S. *Energy Environ. Sci.* **2011**, *4*, 2218–2222.
130. He, L.-N.; Wang, J.-Q.; Wang, J.-L. *Pure Appl. Chem.* **2009**, *81*, 2069–2080.
131. He, L.-N.; Yang, Z.-Z.; Liu, A.-H.; Gao, J. In *Advances in CO_2 Conversion and Utilization*; Hu, Y. H., Ed.; ACS Symposium Series 1056; American Chemical Society: Washington DC, 2010; pp 77−101.
132. Wang, J.-L.; Miao, C.-X.; Dou, X.-Y.; Gao, J.; He, L.-N. *Curr. Org. Chem.* **2011**, *15*, 621–646.

Downloaded by STANFORD UNIV GREEN LIBR on June 5, 2012 | http://pubs.acs.org
Publication Date (Web): December 14, 2011 | doi: 10.1021/bk-2011-1088.ch008

Downloaded by UNIV OF GUELPH LIBRARY on June 4, 2012 | http://pubs.acs.org
Publication Date (Web): December 14, 2011 | doi: 10.1021/bk-2011-1088.ch009

Chapter 9

Development of Mesoporous Silica Encapsulated Pd-Ni Nanocatalyst for Hydrogen Production

Balaji Tatineni,[1] Yulia Basova,[1] Atikur Rahman,[2] Saiful Islam,[2] Mizanur Rahman,[2] Azharul Islam,[2] Joslyn Perkins,[1] James King,[1] Jasmine Taylor,[1] Dhananjay Kumar,[3] Shamsuddin Ilias,[2] and Debasish Kuila*,[1]

[1]Department of Chemistry,
North Carolina A & T State University, Greensboro, North Carolina 27411
[2]Department of Chemical and Bioengineering,
North Carolina A & T State University, Greensboro, North Carolina 27411
[3]Department of Mechanical Engineering,
North Carolina A & T State University, Greensboro, North Carolina 27411
***E-mail: dkuila@ncat.edu**

A simple one-pot procedure has been developed for the synthesis of bimetallic Pd-Ni nanoparticles with various compositions within mesoporous silica. These materials have been characterized using XRD, HRTEM, STEM, FTIR, Energy Dispersive X-ray Analysis (EDX) and nitrogen adsorption-desorption isotherm techniques. Scanning transmission electron microscope (STEM) images suggest that the size of mesoporous silica in MCM-41 varies from 100 to 300 nm. High resolution transmission electron microscopy (HRTEM) studies and EDX analyses show the presence of bimetallic Pd-Ni nanoparticles in mesoporous silica. The sizes of the metal particles are observed in the range of 5-15 nm. The specific surface area decreases with an increase in loading of Pd and Ni and the lower angle XRD features of MCM-41 are not noticeable at much higher Pd and Ni concentration. Results from magnetization studies reveal that the Pd-Ni particles in mesoporous silica exhibit a classical superparamagnetic behavior and the magnetic moment increases with a decrease

In Production and Purification of Ultraclean Transportation Fuels; Hu, Y., et al.;
ACS Symposium Series; American Chemical Society: Washington, DC, 2011.

in temperature. Preliminary studies on the catalytic activity of Pd-Ni/mesoporous silica in steam reforming of methanol (SRM) to produce hydrogen show promising results. While the conversion of methanol as high as 90% is obtained the selectivity for H_2 in the range of 15-20 is observed at 523-573 K. The superparamagnetic behavior of the catalyst is retained after the SRM reaction and the catalyst remains active for further H_2 production. Systematic studies on H_2-production are currently underway to examine its potential for H_2 production by the SRM reaction that can be extended in the future to biofuels.

Keywords: bimetallic Pd-Ni; MCM-41; nanocatalyst; magnetic properties; material characterization; mesoporous silica; SRM (steam reforming of methanol); hydrogen production

Downloaded by UNIV OF GUELPH LIBRARY on June 4, 2012 | http://pubs.acs.org
Publication Date (Web): December 14, 2011 | doi: 10.1021/bk-2011-1088.ch009

Introduction

In recent years, there has been renewed interest in porous materials due to their widespread applications as a support in catalysis, sensing, electro-optical devices, fuel cells, and separation technology (*1*). The porous materials are generally classified into three distinct categories according to their pore size: microporous (pore size < 2 nm), mesoporous (2-50 nm), and macroporous (> 50 nm). Mesoporous silica such as MCM-41, developed by Mobil Corporation, has been extensively studied previously for different applications (*2*). More recently, mesoporous materials containing metallic nanocatalysts have emerged as an exciting area of research because of unique magnetic, optical, catalytic and electronic properties due to the quantum-size effect of the corresponding individual metal particles (*3*, *4*). These properties can be further adjusted by the addition of the second metal. This is due to the fact that one metal can tune and/or modify the magnetic and catalytic properties of the other metal as a result of electronic and structural effects (*5*). A unique property of some of the bimetallic systems is the superparamagnetic transition (with no hysteresis behavior) exhibited by particles of ferromagnetic materials that are smaller than the magnetic domain size of the material (*6*). For catalysis, as examples, bimetallic Pd-Co (*7*) and Fe-Co (*8*) have shown improved catalytic activity over Co-nanoparticles in the Fischer-Tropsch synthesis. Similarly, for steam reforming of methanol, Iwasa et al (*9–12*, *19*) first reported that PdZn alloy, formed from reduction of Pd supported on ZnO, has exceptionally high activity and selectivity to CO_2 and H_2. Thus, the development of effective bimetallic nanocatalysts with proper catalyst support is an important area of research (*1*, *3*).

Steam reforming is a favored route for hydrogen (H_2) production from biofuels with the aid of a catalyst (*4*, *5*, *7*). Of the many H_2 fuel source candidates, methanol and ethanol are readily available and are being investigated intensely at present (*4–7*, *13*). If significant reductions in road transport pollution emission as well as lowering dependence on foreign oil are sought, then hydrogen is the fuel of choice that can be extracted from biofuels to provide solutions to the energy and green chemistry challenges of the 21st century (*14*)(*15*).

To date, all the technological systems developed to produce or use hydrogen rely on Cu- and Pt-group based supported or unsupported catalysts (*16*)–(*18*). However, steam reforming reactions developed using unsupported catalysts so far suffer from low active surface area and easy deactivation (*17–19*). Supports such as CeO_2, ZnO, MgO, Al_2O_3, SiO_2, and other natural oxides have been used to increase the catalyst's active surface area and improve its efficiency (*14–17*, *20*). Nevertheless, these catalysts suffer from poor metal particle distribution, steric hindrance of active sites and sintering of metal particles during the reforming reactions. We have synthesized mesoporous silica containing Pd-Ni bimetallic species using one-pot procedure to address some of these issues (*21*). In this chapter, we report synthesis, characterization, and the use of bimetallic Pd-Ni nanocatalysts in our preliminary studies on steam reforming of methanol (SRM) to produce hydrogen.

Downloaded by UNIV OF GUELPH LIBRARY on June 4, 2012 | http://pubs.acs.org
Publication Date (Web): December 14, 2011 | doi: 10.1021/bk-2011-1088.ch009

Experimental Section

Materials

Analytical grade chemicals and de-ionized H_2O were used throughout the experiments, unless otherwise indicated. Tetramethoxy silane (TMOS), cetyl trimethylammonium bromide (CTAB), nickel nitrate ($Ni(NO_3)_2.6\ H_2O$), and HPLC grade methanol were purchased from Sigma-Aldrich. Ethanol, acetone and ammonium hydroxide were obtained from Fisher Scientific, while Alfa Aesar provided palladium nitrate ($Pd(NO_3)_2$).

Catalyst Preparation

Bimetallic nanocatalysts on mesoporous MCM-41 support were prepared following our optimized (*21*) one-pot synthesis procedure. Metal salts of $Ni(NO_3)_2$ and $Pd(NO_3)_2$ were used as metal precursors while TMOS was selected as the source of silica. The CTAB surfactant was used as the structure-directing agent. The molar ratio composition of the resulting reaction mixtures are, 0.13 (CTAB) : 0.059 ($Ni(NO_3)_2$) : 0.005 ($Pd(NO_3)_2$) : 1 (TMOS) : 5.55 (NH_4OH) : 130.6 (H_2O); 0.13 (CTAB) : 0.088 ($Ni(NO_3)_2$) : 0.0075 ($Pd(NO_3)_2$) : 1 (TMOS) : 5.55 (NH_4OH) : 130.6 (H_2O); 0.13 (CTAB) : 0.088 ($Ni(NO_3)_2$) : 0.038 ($Pd(NO_3)_2$) : 1 (TMOS) : 5.55 (NH_4OH) : 130.6 (H_2O); 0.13 (CTAB) : 0.088 ($Ni(NO_3)_2$) : 0.056 ($Pd(NO_3)_2$) : 1 (TMOS) : 5.55 (NH_4OH) : 130.6 (H_2O). These materials are abbreviated as MCM- PdNi(B1), MCM- PdNi(B2), MCM- PdNi(B3) and MCM-PdNi(B4), respectively. To study how an increase in metal loading affects catalyst structure, we have prepared a few samples with higher loading of the metal salts. The molar ratio composition of the resulting reaction mixture of a typical sample is 0.135 (CTAB) : 0.409 ($Ni(NO_3)_2$) : 0.047 ($Pd(NO_3)_2$) : 1 (TMOS) : 5.3 (NH_4OH) : 174(H_2O). This material is abbreviated as MCM-PdNi(B5). Reference samples containing only Ni or Pd were also synthesized. For comparative studies, MCM-41 was prepared following the reported one-pot synthesis procedure (*22*) with a minor modification in the reaction conditions.

Catalyst Characterization

Brunauer−Emmett−Teller (BET) specific surface area, pore-size, and pore volume were determined from nitrogen adsorption–desorption isotherms measured at 77K using a Quantachrome NOVA 2200e instrument. The morphology and phase purity of the samples were analyzed using Hitachi HF2200 Transmission Electron Microscope (HRTEM). The elemental analyses of the samples were carried out using a Bruker EDX (Energy Dispersive X-ray Analysis) coupled to Hitachi HF2000 High Resolution Transmission Electron Microscope (HRTEM). The particle size, morphology and phase purity of the samples were also analyzed using a Hitachi S5500 High Resolution Scanning Transmission Electron Microscope (HRSTEM). Small–and wide-angle powder X-ray diffraction (XRD) patterns were measured using a Bruker AXS D8 Discover X-ray Diffractometer System with monochromated CuKα radiation. The FT-IR spectra of the material were recorded using a Nicolet Magna 850 IR spectrometer. The pH of the solution was measured using an Oakton digital pH meter (100 series) with a glass electrode.

Downloaded by UNIV OF GUELPH LIBRARY on June 4, 2012 | http://pubs.acs.org
Publication Date (Web): December 14, 2011 | doi: 10.1021/bk-2011-1088.ch009

Magnetic Studies

Magnetization versus magnetic field applied (M-H) of mesoporous silica containing bimetallic NiPd particles were carried out at different temperatures using vibrating sample magnetometer (VSM) interfaced with a physical property measurement system (Quantum Design). Mesoporous silica containing bimetallic species was reduced using 4% hydrogen in argon environment at 853 K for 3 hrs. The VSM characterization of the samples was carried out before and after the steam reforming of methanol (SRM) reactions.

Steam Reforming of Methanol (SRM)

The catalytic activity tests were performed for Pd-Ni under atmospheric pressure in a continuous down flow stainless steel fixed bed reactor (V=20.76 cm^3). The catalyst was activated in 4% hydrogen and argon environment in the temperature range of 823-923 K for 6 hrs. The freshly reduced catalyst was mixed with sand (white quartz, 50-70 mesh, supplier: Sigma-Aldrich) at a ratio of equal volume. The mixture was then loaded into the reactor and quartz wool (supplier: Perkin Elmer) was used at both ends to pack the reactor. Prior to each SRM reaction, the catalyst was activated further *in-situ* at 623 K for 1 h under 4% H_2 /Ar gas mixture and the reactor was finally purged with He. A feed with a constant methanol/water molar ratio of 1:3 was used in all experiments. In the SRM study, the feed flow rate was 0.2 mL/min at STP and the temperature was varied from 523 to 623 K. The composition of the reaction products was analyzed using an on-line Hewlett Packard 6890 series gas chromatograph. The unreacted reactant was trapped in a condenser immersed in ice-bath. The condensate was collected at the end of each experiment and analyzed using GC (Chromatograph: Gow-Mac Series 350) to calculate the conversion of methanol. The selectivity to hydrogen was calculated by analyzing the moles of H_2, CO and CO_2 produced in the SRM reaction.

Results and Discussion

Physicochemical Characterization of Pd-Ni in Mesoporous Silica

Physicochemical Properties of the Catalyst

Downloaded by UNIV OF GUELPH LIBRARY on June 4, 2012 | http://pubs.acs.org
Publication Date (Web): December 14, 2011 | doi: 10.1021/bk-2011-1088.ch009

The powder x-ray diffractograms of synthesized MCM-41, Pd-MCM-41, Ni-MCM-41, a typical MCM-PdNi sample and one with higher loading of Pd and Ni-salts are shown in Figure 1. Samples with different Pd-Ni ratios are shown in Table 1. The difference in the scattering power between the silica walls and the empty pores leads to produce the highly intense Bragg reflections. The three peaks observed for the MCM-41 material can be indexed to d_{100}, d_{110} and d_{200} reflections of a two dimensional hexagonal unit cell (*2*). The shift to higher values of 2θ and increase in peak intensity upon calcination corresponds to strengthening of the lattice caused by completion of silicate condensation and better crystalline order of the material (*23–25*). The unit cell parameter (a_0) values are calculated from the peak using the equation $a_0 = 2d_{100}/\sqrt{3}$. A slight decrease in the d-values and unit cell parameters are observed on incorporation of Pd, Ni and Pd-Ni in MCM-41 silica.

The XRD results show broadening of the d_{100} peak of Pd-MCM-41 when compared to that observed for MCM-41 and Ni-MCM-41 samples (Figure 1). This broadening for Pd-MCM-41 from the parent MCM-41 could be due to the bigger size of palladium compared to nickel and silicon. In contrast to Pd-MCM-41 and Ni-MCM-41, the MCM-41 material containing both Ni and Pd (B1) exhibits a strong and sharp peak at d_{100} along with higher order reflections at d_{110} and d_{200}. It indicates the formation of well-ordered bimetallic MCM-41 structure. These results are further supported by the HRTEM images that show the existence of the long-range hexagonal arrangement of nano-scale mesopores (discussed later). The XRD peaks become broader with the increase of Ni and Pd content in B2 of MCM-PdNi silica materials (Table 1), indicating some loss of long-range order. The MCM-PdNi material (B3 and B4) was prepared by varying the concentration of Pd in Pd-Ni bimetallic ((B2) silica material. The loss of order for B3 and B4 could be due to the higher loading of palladium (Table 1) that also leads to increase in scattering power within the pores and causes the intensity loss due to phase cancellation between the pore walls and the guest species such as Pd and Ni (*26*). When the total concentration of Pd-Ni is much higher (B5), the intensity of the low-angle XRD peaks are not noticeable. The results suggest that the order in the materials deteriorates with increased loading of metal ions.

The BET surface areas of different mesoporous silica samples, an important parameter for catalysis, are shown in Table 1. The nitrogen adsorption-desorption isotherms for a few samples are shown in Figure 2. All synthesized mono and bimetallic materials show type IV isotherms having inflection around

$P / P_0 = 0.2\text{-}0.4$, which is a characteristic of MCM-41 type ordered mesoporous materials. These samples also exhibit textural- and framework- confined mesoporosity, as evidenced by the presence of two separate, well defined hysteresis loops. The region - P / P_0 from 0.2 -0.4 is indicative of framework-confined mesopores and the other region - $P / P_0 \geq 0.8$ corresponds to capillary condensation in the interparticle pores (*26*). The point of inflection also shifts towards the higher relative pressure with the increase of Pd-Ni content in the synthesized materials. This shift towards higher pressure indicates an increase in the pore size. The data on pore size, pore volume and BET surface area are shown in Table 1. The BET surface areas of the prepared materials decrease with an increase in Pd-Ni loading. In more specific terms, the results indicate that with the increase in the loading of nickel (B1 and B2), the BET surface area is not affected that much; however, with the increase in Pd loading (B3, B4 and B5) the BET surface area decreased significantly. This is probably because of the larger size of Pd^{2+} compared to Ni^{2+}. The average pore diameters show an increasing trend with the increase in Pd-Ni content of the samples. The increase in pore size with incorporation of Pd and Ni is due to the larger sizes of Pd^{2+} and Ni^{2+} compared to Si^{4+}.

Downloaded by UNIV OF GUELPH LIBRARY on June 4, 2012 | http://pubs.acs.org
Publication Date (Web): December 14, 2011 | doi: 10.1021/bk-2011-1088.ch009

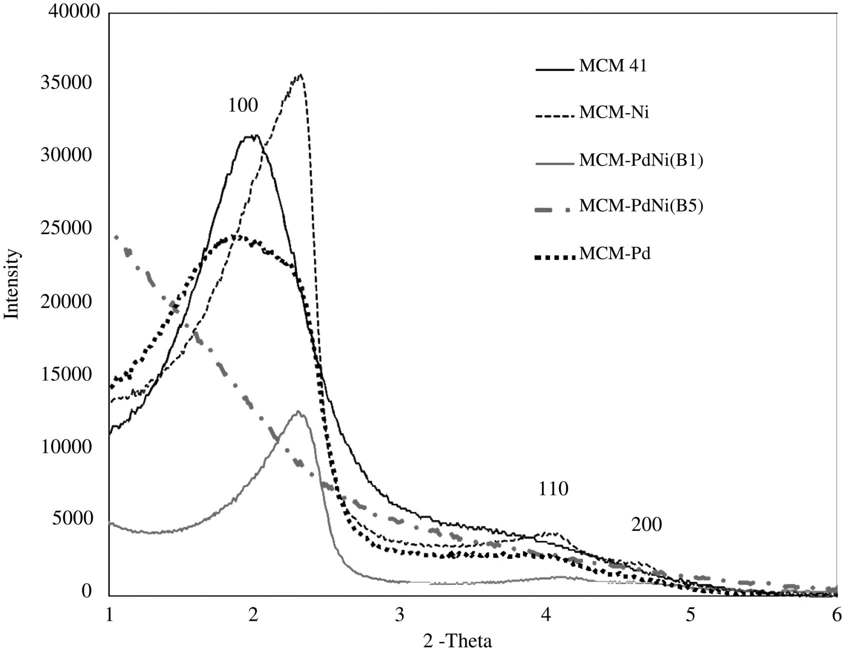

Figure 1. Small-angle XRD patterns of MCM-41, mono-metallic MCM-41, and bi-metallic MCM-PdNi samples with varying ratios of Pd and Ni.

Table 1. Physicochemical Characterization of the samples of monometallic and bimetallic mesoporous silica (Calcined materials)

Sample Name	***BET Surface area (m^2/g)***	***Average Pore diameter (BJH) (Å)***	***Pore volume (BJH) (cm^3/g)***	***Unit cell para-meter (Å)***	***Composition (%)***	
					as Ni	***as Pd***
MCM-41	1030	28	0.638	46.36		
MCM 41-Pd	857	30.6	0.709	54.57		8.26
MCM 41-Ni	876	28.22	0.732	44.13	5.36	
MCM 41-PdNi(B1)	980	30.4	0.75	46.50	3.62	0.59
MCM 41-PdNi(B2)	900	30.1	0.87	47.9	5.32	0.81
MCM 41-PdNi(B3)	861	28.22	0.837	46.73	5.15	4.01
MCM 41-PdNi(B4)	778	29.41	0.885	47.66	5.05	5.75
MCM 41-PdNi(B5)	740	31.5	0.698	NA	24.83	2.46

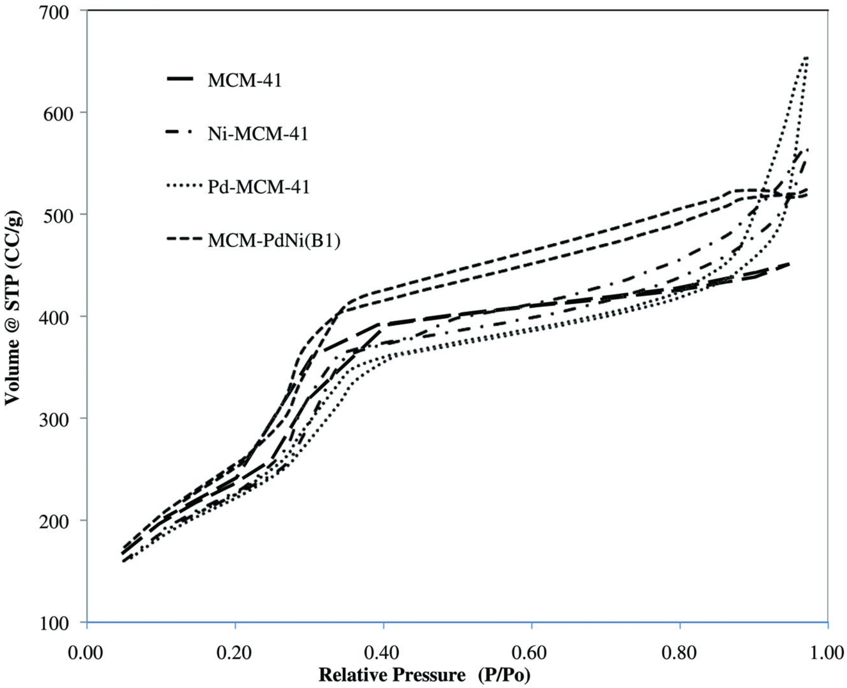

Figure 2. Nitrogen adsorption-desorption isotherms of: a) MCM-41, b) MCM-Ni, c) MCM-Pd, and d) MCM-PdNi materials.

Downloaded by UNIV OF GUELPH LIBRARY on June 4, 2012 | http://pubs.acs.org
Publication Date (Web): December 14, 2011 | doi: 10.1021/bk-2011-1088.ch009

Downloaded by UNIV OF GUELPH LIBRARY on June 4, 2012 | http://pubs.acs.org
Publication Date (Web): December 14, 2011 | doi: 10.1021/bk-2011-1088.ch009

The metal ions in mesoporous silica interact with silica. The interaction of bimetallic Pd-Ni with silica is evident in the FT-IR spectra of the samples shown in Figure 3. The bands at 1098 and 813 cm^{-1} for pure MCM-41 arise from the symmetric and asymmetric stretching vibrations of the tetrahedral SiO_4 units as reported in the literature (*23*, *25*). It has been shown previously that these peaks shift and broaden as hetero atoms such as Ti, Sn and Co are introduced (*23–25*). We observed a similar behavior and the two strong bands around 1640 and 1130 cm^{-1} may be assigned to symmetric and asymmetric stretching Si-O-Si vibrations (*28–30*). The lower absorption bands at 674 and 586 cm^{-1} might be assigned to the stretching vibrations of SiO_4 tetrahedral and NiO/PdO units present in the novel material. The presence of these bands suggests an interaction between the heteroatom and silicon in Si-O-M units (*28–30*).

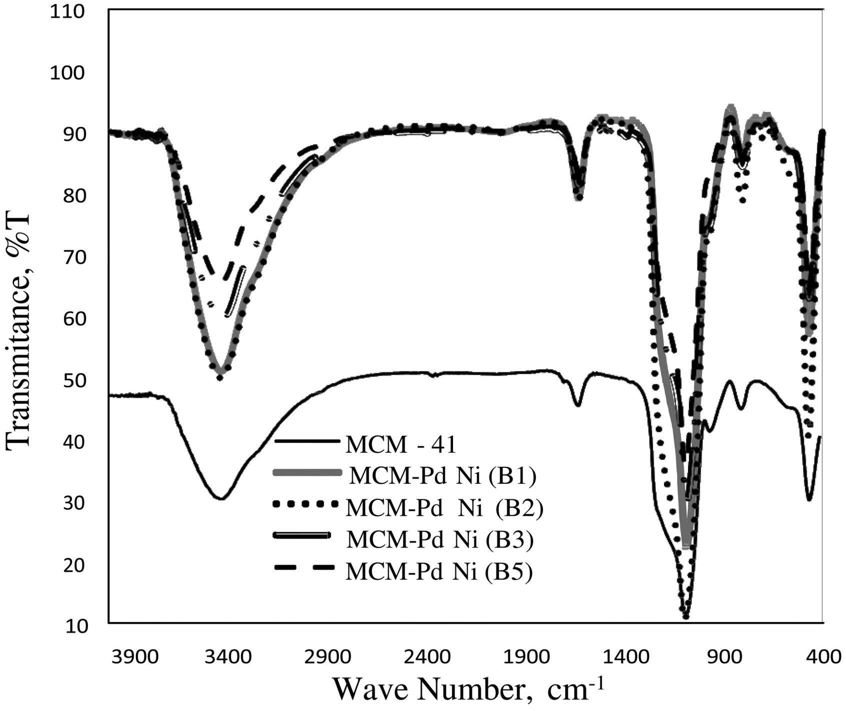

Figure 3. The FT-IR spectra of the samples of Pd-Ni with varying ratios of Pd and Ni in mesoporous silica and MCM-41.

The HRTEM measurements (Figure 4) were carried out to confirm the presence of metal particles and the existence of mesopores in the synthesized materials. The results correlate well with the N_2 adsorption-desorption measurements. The scanning transmission electron microscope (STEM) images (Figure 5) demonstrate that size of the silica particles varies from 100 to 300 nm. The presence of bimetallic Pd-Ni particles as black spots, in the range of 5-15 nm, in MCM-41 silica material is clearly evident in HRTEM images (Figure 4C and D). In addition, the elemental analysis (EDX) was carried out for Pd-Ni-MCM-41 (B1) and the results suggest the presence of bimetallic species (Ni, 4.0%; Pd, 0.06%) in mesoporous silica. The lower concentration of Pd indicates loss of Pd during preparation of the material.

Downloaded by UNIV OF GUELPH LIBRARY on June 4, 2012 | http://pubs.acs.org
Publication Date (Web): December 14, 2011 | doi: 10.1021/bk-2011-1088.ch009

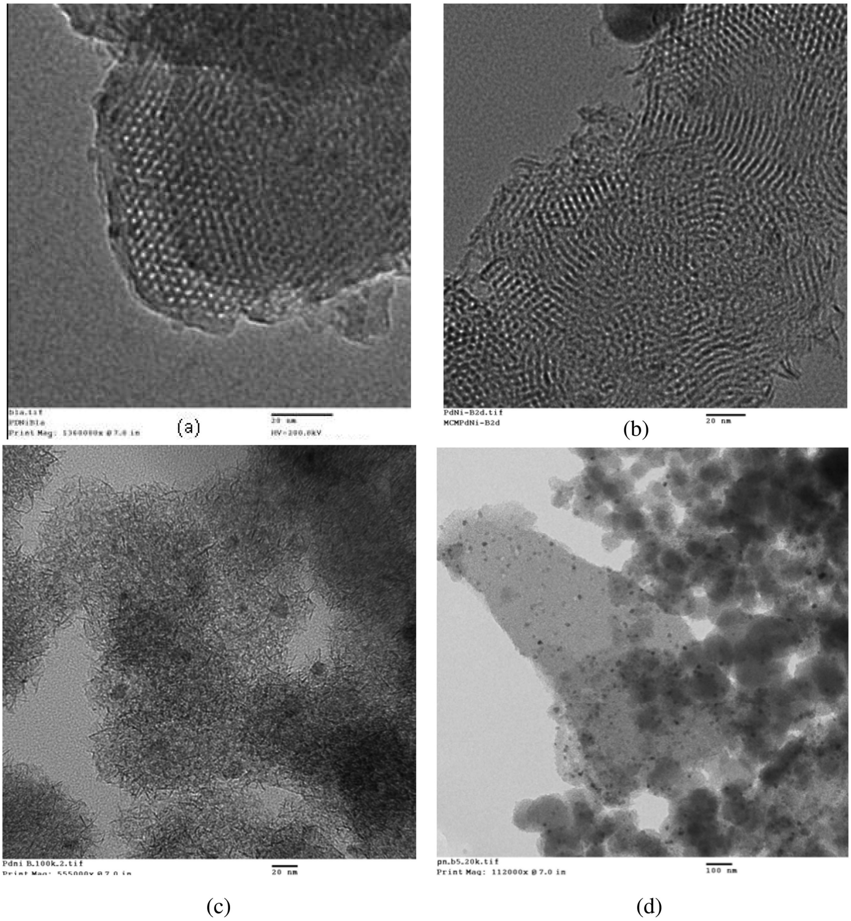
b1a.tif
PDNiB1a
Print Mag: 1360000x @ 7.0 in
(a)
20 nm
HV=200.0kV
PdNi-B2d.tif
MCMPdNi-B2d
(b)
20 nm
Pdni B.100k.2.tif
Print Mag: 555000x @ 7.0 in
20 nm
pn.b5.20k.tif
Print Mag: 112000x @ 7.0 in
100 nm
(c)
(d)

Figure 4. TEM images of calcined samples: (a) MCM-PdNi(B1), (b) MCM-PdNi(B2), (c) MCM-PdNi(B5) (Higher Magnification), and (d) MCM-PdNi(B5).

In Production and Purification of Ultraclean Transportation Fuels; Hu, Y., et al.;
ACS Symposium Series; American Chemical Society: Washington, DC, 2011.

Downloaded by UNIV OF GUELPH LIBRARY on June 4, 2012 | http://pubs.acs.org
Publication Date (Web): December 14, 2011 | doi: 10.1021/bk-2011-1088.ch009

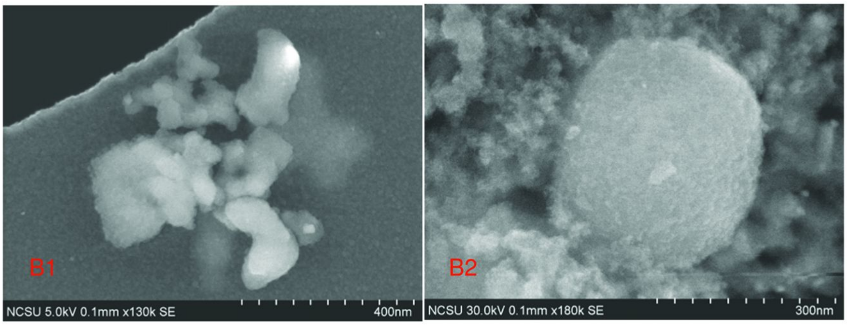

Figure 5. HRSTEM images of MCM-PdNi materials.

The mesoporous structures are partly in random arrangement and the pore sizes in MCM-PdNi sample vary from 2 to 3.4 nm. The observed disorder is consistent with d-spacing values obtained from XRD studies and can also be correlated to the high angle XRD measurements (not shown) that can provide circular evidence for the size of the PdNi nanoparticles (*22*). These particles are amorphous in nature, which is consistent with the high angle XRD data of small size bimetallic nanoparticles.

Initial Catalytic Activity Studies of Pd-Ni in the SRM Reaction

The activity of the reduced catalyst was examined for hydrogen production by steam reforming of methanol (SRM).

The SRM reaction can be expressed as:

$$CH_3OH + H_2O \leftrightarrow H_2 + CO_2; \ \Delta H_r = 49.5 \text{ kJ mol}^{-1} \tag{1}$$

However, it has been established that the reaction pathway in the SRM process is more complex as it goes through the step of methanol decomposition:

$$CH_3OH \leftrightarrow 2H_2 + CO; \Delta H_r = 90.6 \text{ kJ mol}^{-1}, \tag{2}$$

followed by a water-gas shift reaction:

$$CO + H_2O \leftrightarrow H_2 + CO_2; \Delta H_r = -41.2 \text{ kJ mol}^{-1} \tag{3}$$

producing CO and CO_2 as by-products. The H_2 selectivity in our studies is defined as:

$S_{H2} = H_{2\,(out)} / (CO_{out} + CO_{2\,out})$ and methanol conversion (%) is defined as: moles of methanol converted/ moles of methanol fed to the reactor ×100.

The initial experiments on the SRM reaction were carried out in the temperature range of 523-623 K at a reactant flow rate of 0.2 mL/min. Reference tests using catalysts containing individual metals (Pd or Ni) were also performed. Each data point corresponds to the average of at least four measurements.

From our preliminary SRM experiments, we observe that the Pd-Ni system outperforms individual metal (Pd or Ni) catalysts in terms of H_2 production and selectivity. As shown in Figure 6, methanol conversion increases with an increase in temperature, reaching conversion of ~90% or more at temperature 573 K. While for Pd (control), the conversion is observed 25 %, for Ni (control) it is 20 % at 523 K. When the conversion of methanol values is compared, the introduction of two metals enhanced the performance of the catalyst. Although the Pd-containing catalyst showed good catalytic activity and high hydrogen production, the formation of a much larger amount of byproducts, particularly CO, was observed. The selectivity to H_2 improves from 2.2 - 3.3 (Pd) and 4-6.5 (Ni) to15-20 for Pd-Ni in the temperature range of 523-573 K. These results suggest that the bimetallic system have the potential in SRM reactions and systematic studies are underway to examine them further. Further, experiments carried out at higher temperatures have shown that the bimetallic catalyst exhibits thermal stability above 750 K for a prolonged period of time. Thus, the bimetallic nanocatalysts have potential for steam reforming reactions of ethanol and other biofuels.

Downloaded by UNIV OF GUELPH LIBRARY on June 4, 2012 | http://pubs.acs.org
Publication Date (Web): December 14, 2011 | doi: 10.1021/bk-2011-1088.ch009

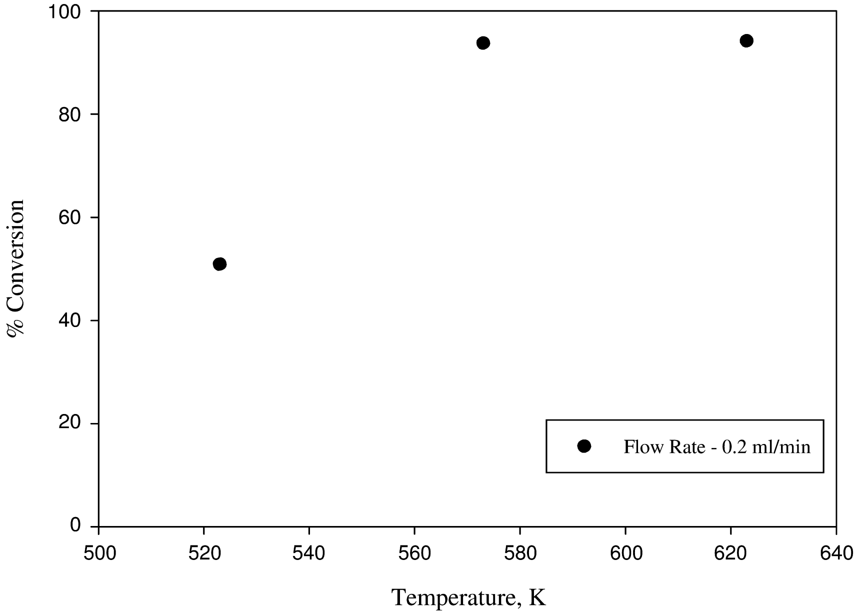

Figure 6. Effect of temperature on conversion in SRM using MCM-PdNi (B5) Catalyst (flow, 0.2 ml/min).

Downloaded by UNIV OF GUELPH LIBRARY on June 4, 2012 | http://pubs.acs.org
Publication Date (Web): December 14, 2011 | doi: 10.1021/bk-2011-1088.ch009

Magnetic Measurements of MCM-PdNi after the SRM Reaction

In order to have a better understanding of the physical properties of the very small-size bimetallic nanocatalysts and also to examine the effect of a noble metal on the ferromagnetic properties of a non-noble metal, we have carried out initial magnetization studies of MCM-PdNi(B5). Since the shape and/or crystal anisotropy play an important role in determining the magnetic properties of most fine particles (*27*), the magnetization studies on ferromagnetic nanocatalysts can provide an insight on the reducibility and activity of the catalyst during the SRM reactions. The magnetic properties of bimetallic Pd-Ni are presented in Figure 7. Magnetization increases monotonically with the decrease in temperature. The magnetic moment versus magnetic field applied curve (Figure 7) of the Pd-Ni nanocatalyst before the SRM reaction shows a typical superparamagnetic behavior of the catalyst revealing that most, if not all, of the catalyst is reduced by hydrogenation from oxides to pure metals, the active phase for the SRM reaction. The experiments were performed to estimate the catalyst's activity from the saturation magnetization value of the ferromagnetic component obtained at different stages of SRM studies.

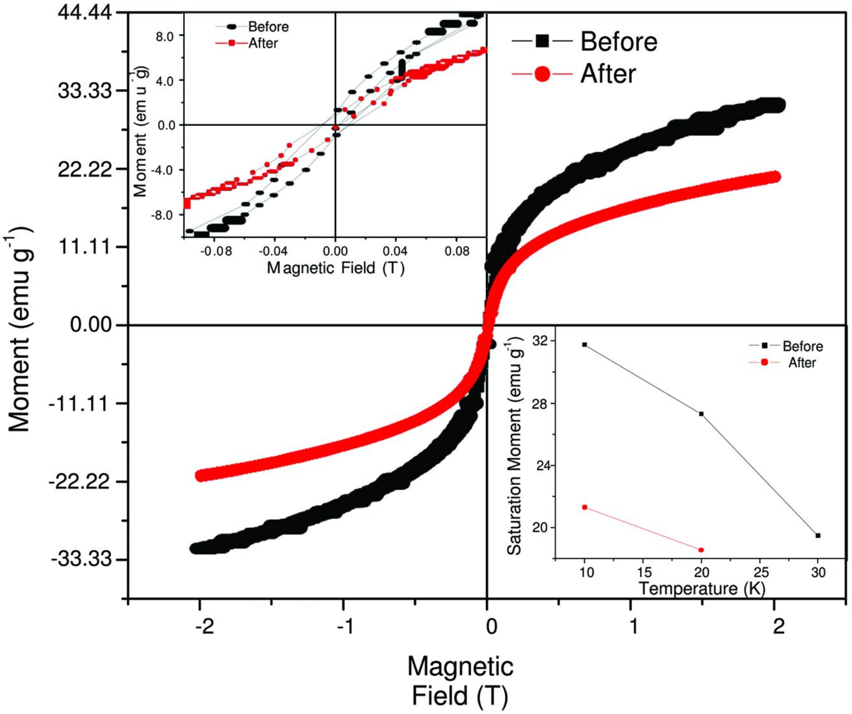

Figure 7. Magnetic data for a PdNi sample in mesoporous silica before and after SRM reaction. The lower Inset shows increase of saturation moment at lower temperature.

Downloaded by UNIV OF GUELPH LIBRARY on June 4, 2012 | http://pubs.acs.org
Publication Date (Web): December 14, 2011 | doi: 10.1021/bk-2011-1088.ch009

The magnetization experiments after the SRM reaction still shows the ferromagnetic nature of the catalyst (Figure 7), demonstrating that the metal component is not deactivated even after the longest run of the SRM reaction. This is consistent with conversion and selectivity for H_2 production, described above. The stability of the PdNi bimetallic catalyst is superior to that observed in our previous studies in sol-gel matrix with Fe-Co-Ru catalysts for Fischer-Tropsch reactions (*8*) and Co or Ni catalysts (*13*) for the SRM reactions. In both cases, the sol-gel encapsulated catalysts deactivated more easily. The current results are indeed significant and suggest the stability of the Pd-Ni catalyst in mesoporous silica. These aspects will be investigated further in our future studies with biofuels such as bioethanol.

Conclusions

We have synthesized mesoporous silica containing Pd-Ni nanoaprticles by a one-pot procedure using a surfactant as a template. Characterization of the Pd-Ni in mesoporous silica indicates that the metal nanoparticles are successfully incorporated into the structure and range in size from 5- 15 nm. The HRTEM measurements together with nitrogen adsorption-desorption studies confirm the existence of an ordered mesoporous structure with pore size from 2 to 3.4 nm. The preliminary studies on the catalysts for the SRM reaction show excellent methanol conversion and selectivity to hydrogen, compared to the catalyst containing each individual metal. The magnetic studies indicate that mesoporous silica supported Pd-Ni nanocatalysts are superparamagnetic and the reduced catalyst retains its activity after the SRM reaction. Our studies further suggest that these catalysts can be used for steam reforming reactions for a longer period of time and can be extended to biofuels for H_2 production.

Acknowledgments

Dr. Kuila would like to thank North Carolina A & T State University for the start-up grant and Department of Energy (*DE – FG26 – 09NT0008066*) for the support of this project. Dr. Kumar acknowledges the support from NSF-NIRT grant (# DMR-0403480) and the Center for Advanced Materials and Smart Structures (CAMSS). We thank Dr. Sergey Yarmolenko for catalyst activation and XRD-characterization studies, Karshak Kosaraju and Zahadul Islam for H_2-production studies, Mainul Kader Faruque for help with the magnetic measurements, and Drs. Jag Sankar and Zhigang Xu for access to the facilities at NSF-CAMSS.

References

1. Vartuli, J. C.; Shih, S. S.; Kresge, C. T.; Beck, J. S. *Mesoporous Mol. Sieves* **1998**, *117*, 13.
2. Kresge, C. T.; Leonowicz, M. E.; Roth, W. J.; Vartull, J. C.; Beck, J. S. *Nature* **1992**, *359*, 710.

Downloaded by UNIV OF GUELPH LIBRARY on June 4, 2012 | http://pubs.acs.org
Publication Date (Web): December 14, 2011 | doi: 10.1021/bk-2011-1088.ch009

3. Schmid, G. *Nanoparticles: From Theory to Application*; Wiley-VCH: Weinheim, Germany, 2004.
4. Fendler, J. H. *Nanoparticles and Nanostructured Films*; Wiley-VCH: Weinheim, Germany, 1998.
5. Sinfelt, J. H. *Bimetallic Catalysts*; Wiley: New York, 1983.
6. Vondrova, M.; Klimczuk, T.; Miller, V. L.; Kirby, B. W.; Yao, N.; Cava, R. J.; Bocarsly, A. B. *Chem. Mater.* **2005**, *17*, 6216.
7. Heemeier, M.; Carlsson, A. F.; Naschitzki, M.; Schmal, M.; Baumer, M.; Freund, H. J. *Angew. Chem., Int. Ed.* **2002**, *41*, 4073.
8. Zhao, S.; Nagineni, V. S.; Naidu, S.; Kuila, D. *Ind. Eng. Chem. Res* **2008**, *47*, 1684−1688, and references therein.
9. Iwasa, N.; Takezawa, N. *Top. Catal.* **2003**, *22*, 220.
10. Takezawa, N.; Iwasa, N. *Catal. Today* **1997**, *36*, 45.
11. Iwasa, N.; Tomoyuki, M.; Masuda, S.; Takezawa, N. *React. Kinet. Catal. Lett.* **2000**, *69*, 355.
12. Iwasa, N.; Mayanagi, T.; Wataru, N.; Arai, M.; Takewasa, T. *Appl. Catal., A* **2003**, *248*, 153.
13. Shetty, K.; Cao, W.; Zhao, S.; Seetala, N. V.; Siriwardane, U.; Kuila, D. *J. Power Sources* **2007**, *163*, 630.
14. Frusteri, F.; Freni, S.; Spadaro, L.; Chiodo, V.; Bonura, G.; Donato, S.; Cavallaro, S. *Catal. Commun.* **2004**, *5*, 611.
15. Galvita, V.; Belyaev, V. D.; Semikolenov, V. A.; Tsiakaras, P.; Frumin, A.; Sobyanin, V. A. *React. Kinet. Catal. Lett.* **2002**, *76*, 343.
16. Zhang, X.; Shi, P. *J. Mol. Catal. A: Chem.* **2003**, *194*, 99–105.
17. Breen, J. P.; Burch, R.; Coleman, H. M. *Appl. Catal., B* **2002**, *39*, 65.
18. Liu, S.; Takahashi, K.; Ayabe, M. *Catal. Today* **2003**, *87*, 247.
19. Huang, C.; Sun, Y.; Chou, C.; Su, C. *J. Power Sources* **2007**, *166*, 450.
20. Iwasa, N.; Masuda, S.; Ogawa, N.; Takezawa, N. *Appl. Catal., A* **1995**, *125*, 145.
21. Kuila, D.; Tatineni, B.; Islam, A.; Basova, Y.; Rahman, A.; Rahman, M.; Islam, S.; Ilias, S.; Taylor, J.; King, J. *Prepr. Symp. - Am. Chem. Soc., Div. Fuel Chem.* **2009**, *54* (2), 1072.
22. Grun, M.; Lauer, I.; Unger, K. *Adv. Mater.* **1997**, *9*, 254.
23. Chantrell, R. W.; Walmsey, N. S.; Gore, J.; Maylin, M. *Appl. Phys. Lett.* **1999**, *85*, 4320.
24. Cullity, B. D. In *Introduction to Magnetic Materials*; Addison Wesley Publishing Company: Boston, 1972.
25. Lee, W. R.; Kim, M. G.; Choi, J. R.; Park, J.; Ko, S. J.; Oh, S. J.; Cheon, J. *J. Am. Chem. Soc.* **2005**, *127*, 16090.
26. Noronha, F. B.; Schmal, M.; Nicot, C.; Moraweck, B.; Frety, R. *J. Catal.* **1997**, *168*, 42.
27. Jiang, S.; Kong, Y.; Wang, J.; Ren, X. *J. Porous Mater.* **2006**, *13*, 341.
28. Latham, A. H.; Williams, M. *Acc. Chem. Res.* **2008**, *41*, 411.
29. Jun, Y. W.; Seo, J. W. J. Cheon *Acc. Chem. Res.* **2008**, *41*, 179.
30. Corain, B.; Schmid, G.; Toshima, N. *Metal Nanoclusters in Catalysis and Materials Science: The Issue of Size Control*; Elsevier: The Netherlands, 2008.

Downloaded by STANFORD UNIV GREEN LIBR on June 5, 2012 | http://pubs.acs.org
Publication Date (Web): December 14, 2011 | doi: 10.1021/bk-2011-1088.ot001

Editors' Biographies

Yun Hang Hu

Yun Hang Hu received his Ph.D in physical chemistry from Xiamen University. Currently, he is an associate professor of materials science and engineering at Michigan Technological University. Before joining Michigan Tech, he was an Assistant Professor and Associate Professor at Xiamen University, Senior Staff Engineer at the ExxonMobil Research and Engineering Company, and Research Professor of Chemical and Biological Engineering at the State University of New York at Buffalo. His main research interests range from clean fuels, hydrogen storage materials, nano-structured materials, CO_2 conversion, catalysis, quantum chemistry calculations to solar energy. He has published more than 100 peer reviewed papers in reputed journals.

Xiaoliang Ma

Xiaoliang Ma, senior research scientist, is a research program manager at Kuwait Institute for Scientific Research (KISR). He has worked on the study of clean fuel production for 30 years. His research topics include hydrodesulfurization, adsorptive desulfurization/denitrogenation, oxidative desulfurization, upgrading of coal liquids, and CO_2 capture and removal of acidic gases. He has 70 publications in journals and books, and more than 110 conference papers. Dr. Ma received his Ph.D. in Chemical Engineering at Kyushu University in 1995 and his B.E. in Chemical Engineering at Zhejiang University in 1982. Before joining KISR, he worked at The Pennsylvania State University for 16 years.

In Production and Purification of Ultraclean Transportation Fuels; Hu, Y., et al.;
ACS Symposium Series; American Chemical Society: Washington, DC, 2011.

Downloaded by STANFORD UNIV GREEN LIBR on June 5, 2012 | http://pubs.acs.org
Publication Date (Web): December 14, 2011 | doi: 10.1021/bk-2011-1088.ot001

Elise Bickford Fox

Elise Bickford Fox graduated the College of Charleston (Charleston, SC) in 2001, where she received her B.S. in Chemistry. Her graduate education was completed at The Pennsylvania State University were she received a M.S. (2004) and Ph.D. (2006) in Materials with a minor in Energy and Geo-Environmental Engineering under Professor Chunshan Song. She studied hydrogen purification and production by the oxygen-assisted water-gas shift reaction and the absorptive desulfurization of fuels. She has been an employee of the Savannah River National Laboratory in Aiken, SC, since graduation from PSU. She is active in the American Chemical Society as an Associate on the Younger Chemist's Committee, the Preprint/Managing Editor for the newly formed Division of Energy and Fuels, and has served as Chair for the Savannah River Local Section. Dr. Fox's research specialty is materials chemistry with an emphasis in ionic liquids and catalytic materials for energy production. Her current research projects include the development of nanoparticle-enhanced ionic liquid heat transfer fluids for more efficient energy production, the development of ionic liquid electrolytes, and the development of catalysts for fuel cells and Li/air batteries.

Xinwen Guo

Xinwen Guo received his Ph.D in industrial catalysis from Dalian University of Technology. Currently, he is a professor of industrial catalysis and energy chemical engineering, the Dean of the School of Chemical Engineering, and Chair of the Department of Catalysis Chemistry and Engineering at Dalian University of Technology. He is also a member of the editorial board of the Chinese Journal of Catalysis and Acta Petrolei Sinica (Petroleum Processing Section). His main research interests range from clean fuels, molecular sieve catalysis, shape selective catalysis, nano-structured materials, quantum chemistry calculation to CO_2 conversion. He has published more than 120 peer reviewed papers in reputed journals, and he was awarded the second prize of the National Science and Technology Progress Award in 2003.

Subject Index

A

AC3. *See* Mesoporous carbon (AC3)
ADS. *See* Adsorptive desulfurization (ADS)
Adsorptive desulfurization (ADS), 56
  performance, 58
AED. *See* Atomic emission detector (AED)
AHP. *See* Ammonium hydrophosphate (AHP)
AIBA-K. *See* 2-Aminoisobutyric acid-potassium salt (AIBA-K)
Alkali and trace metals, 103
Amine, 121
2-Aminoisobutyric acid-potassium salt (AIBA-K), 123
Ammonium hydrophosphate (AHP), 18
ANTEK 9000, 58
Atomic emission detector (AED), 34
Autosorb-1 MP system, 36

B

Barret–Joyner–Halenda (BJH) formula, 57
Battelle Columbus labs (USA), 88
BET. *See* Brunauer–Emmett–Teller (BET)
BFB. *See* Bubbling fluidized bed (BFB)
Biomass, 65
  biofuels conversion schematic for relatively dry biomass, 81*f*
  biorefinery, 71
  characteristic, 80
  conversion technology systems, 79
  evaluation, 75
  gasification, 82
  gasifiers, their ranges and some applications, 84*f*
  industrialization and population growth, 80
  main energy sources and their potential in energy supply, 66*t*
  major constituents, 80
  modern utilisation, 80
  processes, 70
    economical reasons, 72
    oil refinery, 72
  produced via photosynthesis, 65
  resources assessed to be theoretically available, 67*f*
  routes and products, 70*f*
  stored solar energy source, 80
  sustainable basis for energy, 67
  syngas via gasification, 80
Biomass-to-Liquid (BTL) plant, 89
Biorefinery, 71
  criteria for design, 72*f*
  fossil oil refinery, 75*t*
  vs. oil refinery, 75
Bio-syngas generation, 85
BJH. *See* Barret–Joyner–Halenda (BJH) formula
BP. *See* British Petroleum (BP)
British Petroleum (BP), 57
Brunauer–Emmett–Teller (BET), 3, 19, 180
Bubbling fluidized bed (BFB), 87
Bulk flow liquid membrane, 118

C

Carbon dioxide (CO_2), 143
  catalytic cycle of nickel-catalyzed hydroboration, 151*s*
  CO catalyzed complex, 156*s*
  CO reduction, 156
  development of human society and economy, 143
  electrochemical conversion, 160
  electrochemical reductions, 166
  formic acid and its derivatives, 144
  greenhouse gas, 144
  irreversible capture of FLP, 154*s*
  methanol reduction, 149
  methanol with H_2 activated by a frustrated Lewis acid-base pair, 155*s*
  NHC-catalyzed reduction, 153*s*
  N-heterocyclic carbenes catalyzed reduction to methanol, 152*s*
  nickel-catalyzed hydroboration to methanol, 151*s*
  photochemical conversion, 160
  photochemical reduction, 161
    BNAH solution, 162*s*
    H_2, 163*s*
    Ru complex, 163*s*
  photochemical splitting, 164*s*
  photoreduction CO by $CODH_{Ni}$ modified NPs, 165*f*

Downloaded by 89.163.34.136 on June 4, 2012 | http://pubs.acs.org
Publication Date (Web): December 14, 2011 | doi: 10.1021/bk-2011-1088.ix002

Downloaded by 89.163.34.136 on June 4, 2012 | http://pubs.acs.org
Publication Date (Web): December 14, 2011 | doi: 10.1021/bk-2011-1088.ix002

- proposed catalytic cycle for hydrogenation using Fe(BF4)2•6H2O/PP3, 149*s*
- reduction by Nb^V nitrido complexes, 166*s*
- reduction CO mediated by disilyne derivative, 158*s*
- reduction CO mediated by iron complex, 157*s*
- reduction of CH_4 and higher hydrocarbons, 159
  - proposed mechanism, 160*s*
- reduction potentials for various reduction reactions, 161*t*
- stoichiometric reduction CH_3OH using FLP, 154*s*
- thermodynamic parameters for hydrogenation of C1 products, 150*s*
- transition metal catalysts for reduction to CO, 167*s*
- transport mechanism, 120*f*
  - chemical structures of the mobile and fixed carriers, 124*f*
  - CO selectivity as a function of temperature, 128*f*
  - concentration in retentate as a function of feed gas flow rate, 129*f*
  - N_2 selectivity as a function of temperature, 127*f*
  - permeability and CO_2/H_2 selectivity, 127*f*

Carbons
  - key characteristics, 43*t*
  - some parameters of the studied activated, 36*t*

Carboxydothermus hydrogenoformans, 164
Catalyst preparation method, 8
Cellulose, 67
Cetyl trimethyl ammonium bromide (CTAB), 18
CFB. *See* Circulating fluidized bed (CFB)
CGO. *See* Coker gas oil (CGO)
Chlorine, 102
CHP. *See* Combined heat and power (CHP)
Circulating fluidized bed (CFB), 87
Citric acid-modified catalyst (CMcat), 4
  - acidity, 7
  - Brunauer–Emmett–Teller characterizations, 5*t*
  - FT-IR spectrum, 7*f*
  - metal species exposed, 6
  - MSI of catalyst, 8
  - pore distribution, 5*f*
  - pore structure, 5

CLGO. *See* Coker light gas oil (CLGO)
CMcat. *See* Citric acid-modified catalyst (CMcat)
CO_2. *See* Carbon dioxide (CO_2)
Coal gasification, 86
CO conversion/reduction, water gas shift, 131
Coker gas oil (CGO), 4
Coker light gas oil (CLGO), 15, 20
  - athabasca bitumen, 20*t*

Combined heat and power (CHP), 79
Composite titania silica (CYCTS), 4
  - Brunauer−Emmett−Teller characterizations, 5*t*
  - FT-IR spectrum, 6*f*, 7*f*
  - pore distribution, 5*f*

CTAB. *See* Cetyl trimethyl ammonium bromide (CTAB)
Cu-based catalysts, 150
CV. *See* Cyclic voltammetry (CV)
Cyclic voltammetry (CV), 167
CYCTS. *See* Composite titania silica (CYCTS)

D

DAO. *See* Deasphaltene oil (DAO)
Deasphaltene oil (DAO), 4
Differential scanning calorimetry (DSC), 123
4,7-Dihydroxy-1,10-phenanthroline, hydrogenation of bicarbonate catalyzed by the Iridium complex, 146*s*
4,6-Dimethyldibenzothiophene (4,6-DMDBT), 16, 34
4,6-DMDBT. *See* 4,6-Dimethyldibenzothiophene (4,6-DMDBT)
DSC. *See* Differential scanning calorimetry (DSC)

E

EDAXr. *See* Energy-dispersive X-ray analysis (EDAX) system
Energy-dispersive X-ray analysis (EDAX) system, 19, 177
  - analysis, 26

Entrained flow gasifiers, 85
EO. *See* Ethylene oxide (EO)
EPA. *See* U.S. Environmental Protection Agency (EPA)
Ethylene oxide (EO), 117

Downloaded by 89.163.34.136 on June 4, 2012 | http://pubs.acs.org
Publication Date (Web): December 14, 2011 | doi: 10.1021/bk-2011-1088.ix002

F

Facilitated transport mechanism, 120
  carriers, 124
  CO_2 transport
    mechanism, 120*f*
    properties, 126
  compositions, 122
  H_2S transport properties, 130
  parameters, 121
  polymer matrix materials, 122
  reactive carriers, 121
  types, 120
Fast Internal Circulating Fluidized Bed (FICFB) reactor, 88
FCC. *See* Fluid catalytic cracking (FCC)
FICFB. *See* Fast Internal Circulating Fluidized Bed (FICFB) reactor
Fischer-Tropsch diesel, 79
  production, 103
Fixed and moving bed gasifiers, 84
  types, 85*f*
FLP. *See* Frustrated Lewis pairs (FLP)
Fluid catalytic cracking (FCC), 4
Fluidized bed gasifiers, 87
  biomass gasification demonstrations, 89*t*
  configurations, 88*f*
Formic acid, 144
Fourier-transform infrared (FT-IR), 3, 6
Frustrated Lewis pairs (FLP), 152
FT-IR. *See* Fourier-transform infrared (FT-IR)
FT-liquids and methanol production, limitations to contaminant concentrations, 93*f*
Fuel cells, synthesis gas purification, 125

G

Gas chromatograph equipped with sulfur-selective pulsed flame photometric detector (GC–PFPD), 58
Gas chromatography-mass spectrometry (GC-MS), 39
Gas cleaning
  alkali and trace metals, 103
  catalytic processes, 79
  chlorine, 102
  gasification to clean syngas process, 92
  nitrogen, 102
  particulate matter, 94
  sulphur, 99
  tar, 95
  upgrading to fuel quality, 91
Gasification
  biomass, 82
  technologies, 83
    comparison, 90, 91*t*
  ultra-clean fuels, 82
Gas permeation unit (GPU), 122
GC-MS. *See* Gas chromatography-mass spectrometry (GC-MS)
GC-PFPD. *See* Gas chromatograph equipped with sulfur-selective pulsed flame photometric detector (GC–PFPD)
GC-PFPD chromatograms, 51
GE. *See* General Electric (GE)
General Electric (GE), 86
GPU. *See* Gas permeation unit (GPU)

H

H_2. *See* Hydrogen (H_2)
HDN. *See* Hydrodenitrogenation (HDN)
HDO. *See* Hydrodeoxygenation (HDO)
HDS. *See* Hydrodesulfurization (HDS)
Hemicellulose, 74
Hewlett-Packard, 58
High resolution transmission electron microscopy (HRTEM), 177, 180
  MCM-PdNi materials, 186*f*
  measurements, 185, 185*f*
Hitachi-S4700 microscope, 19
Homogeneous catalysts, 145
Homogenous photosensitizer systems, 164
Hot gas cleaning, 94*f*
HPLC pump, 58
HRTEM. *See* High resolution transmission electron microscopy (HRTEM)
H_2S transport properties, 130
Hydrodenitrogenation (HDN), 4
  catalyst preparation method, 9
  citric acid coversions, 10
Hydrodeoxygenation (HDO), 71
  glucose into hexane, prices of the components involved, 71*t*
Hydrodesulfurization (HDS), 4, 33
  catalyst preparation method, 8
  citric acid coversions, 10
  effect of adsorptive pretreatment, 50
  relationship between nitrogen content in the adsorptive pretreated LCO, 51*f*
Hydrogen (H_2), 178
  catalyst characterization, 180
  catalyst preparation, 179
  experiment, 179
  material, 179
  steam reforming, 178

Downloaded by 89.163.34.136 on June 4, 2012 | http://pubs.acs.org
Publication Date (Web): December 14, 2011 | doi: 10.1021/bk-2011-1088.ix002

- technological systems, 179

Hydrolysis, 73
Hydrotreating catalysts
- catalytic activity, 20
- monophosphides, 16
- MoS_2-type phases, 16

Hydrotreatment catalyst, 3
- catalysts prepared via different methods, 10*f*
- catalytic activities, 4
- CMcat with different citric acid amounts, 10*f*
- experiment, 4
- heavy oil, 4
- results and discussion, 5

I

IL. *See* Ionic liquid (IL)
Incipient wetness impregnation (IWI) method, 56
Intertek-PARC Technical Services, 35
Ionic liquid (IL), 145
- recovery/separation strategy, 146*s*
- task-specific basic, 146*s*

Iridium trihydride complex, 148*s*
Isosorbide, serial kinetic pathway, 74*f*
IWI. *See* Incipient wetness impregnation (IWI) method

K

Koppers-Totzek slagging gasifiers, 86
Kuwait Institute for Scientific Research, 35

L

LCO. *See* Light cycle oil (LCO)
LHSV. *See* Liquid hour space velocity (LHSV); Liquid hourly speed velocity (LHSV)
Light cycle oil (LCO)
- adsorption and regeneration experiments, 37
- adsorption capacity, 41
  - nitrogen compound, 41*f*
- analysis of treated samples, 38
- breakthrough curves of nitrogen compounds, 46*f*
- breakthrough curves of sulfur compounds, 46*f*
- characterization of samples, 36
- effect of surface properties on adsorptive denitrogenation, 43
- evaluation of adsorbents, 43
- experiment material, 35
- extraction of nitrogen compounds, 37, 37*f*
- fixed-bed flow system, 45
- hydrocarbon, sulfur, and nitrogen chromatograms, 47*f*
- hydrotreating experiments, 38
- identification of nitrogen and sulfur compounds, 39
- key properties, 36*t*
- nitrogen chromatograms, 48*f*
- nitrogen-selective chromatogram, 40*f*
- predominant sulfur compounds, 40, 40*f*
- regeneration, 48
- sulfur chromatograms, 52*f*

Lignin, 67
Lignocellosic biomass biorefinery, 72
- schematic of biorefinery on hydrolysis, 74*f*

Lignocellulosic biomass, 67
- average composition, 68*f*
- components, 67
- structure, 67
- structure and chemical composition, 68*f*

Lignocellusic crops
- composition of some major, 69*f*
- productivity, 69*t*

Liquid hour space velocity (LHSV), 4
Liquid hourly speed velocity (LHSV), 58
Ludox HS-40, 18

M

MCM-41 material, 18
- HDN and HDS activities, 27*f*
- nickel phosphides, 18
- NixPy with different Ni/P ratio, 23*t*
- SEM images, 26*f*
- TEM images, 25*f*

1-MCz. *See* 1-Methylcarbazole (1-MCz)
4-MDBT. *See* 4-Methyldibenzothiophene (4-MDBT)
Mesoporous carbon (AC3), 41
- effect of adsorption temperature on adsorption capacity of nitrogen compounds, 42*f*
- nitrogen and sulfur concentrations, 50*f*

Metal component, dispersion, 8
Metal-support interaction (MSI), 3, 4
Methanation, 117

Downloaded by 89.163.34.136 on June 4, 2012 | http://pubs.acs.org
Publication Date (Web): December 14, 2011 | doi: 10.1021/bk-2011-1088.ix002

Methanol, 149
1-Methylcarbazole (1-MCz), 47
4-Methyldibenzothiophene (4-MDBT), 16, 34
Micromeritics ASAP2020 instrument, 57
Monometallic and bimetallic mesoporous silica, 183*t*
MSI. *See* Metal-support interaction (MSI)
MSW. *See* Municipal solid waste (MSW)
M-Tetrakis aminophthalocyanines, structure, 167*s*
Multi-walled carbon nanotubes (MWNT), 136
Municipal solid waste (MSW), 99
MWNT. *See* Multi-walled carbon nanotubes (MWNT)

N

N_2 adsorption-desorption isotherms
  MCM-41 supported catalysts, 24*f*
  measurement, 19
  pore size distribution, 22
NH_3-temperature-programmed desorption (NH_3-TPD), 3, 7
  profiles of NiW/CYCTS and CMcat, 7*f*
NH_3-TPD. *See* NH_3-temperature-programmed desorption (NH_3-TPD)
Nickel-based sorbents
  H_2 on ADS performance, 59
  physical properties, 58*t*
  preparation method, 57*f*
  sorption mechanism of the sulfur compounds, 61*f*
  ultra-low sulfur diesel, 56
Nickel N-heterocyclic carbene-pyridine complexes, 168*s*
Nickel nitrate hexa hydrate (NNA), 18
Nickel thiophosphate ($NiPS_3$), 17
Nicolet Magna 850 IR spectrometer, 180
$NiPS_3$. *See* Nickel thiophosphate ($NiPS_3$)
Nitrogen compounds, 102
  extractions, 37, 37*f*
NiW/CYCTS pores, 5, 5*f*
  FT-IR spectrum, 7*f*
NixPy/MCM-41 catalysts, 17
NNA. *See* Nickel nitrate hexa hydrate (NNA)

O

Oakton digital pH meter (100 series), 180
Oil refinery vs. biorefinery, 75
Oligotropha carboxidovorans, 164

P

Pd-Ni nanoparticles, 177
  FT-IR spectra, 184*f*
  magnetic data, 188*f*
  magnetization vs. magnetic field, 180
  nitrogen adsorption-desorption isotherms, 183*f*
  physicochemical characterization, 181
  small-angle XRD patterns, 182*f*
  SRM reactions, 186
    magnetic measurements of MCM-PdNi, 188
    MCM-PdNi (B5) catalyst, 187*f*
PEI. *See* Polyethylenimine (PEI)
PEMFC. *See* Proton-exchange membrane fuel cell (PEMFC)
PFPD. *See* Pulsed-flame photometric detector (PFPD)
Phosphine ligands, 145
Photochemcal reductions, 161
Pincer ligands, 147
  hydrogenation of CO_2, 147*s*
Polyethylenimine (PEI), 123
Polymer/silica mixed matrix membranes, 134
Polystyrene (PS) resin, 145
Polysulfone, SEM images, 125*f*
Poly(vinyl alcohol) (PVA) matrix, 122
  formaldehyde synthesis, 122*f*
Pore size distribution (PSD), 57
Preferential oxidation (PROX), 116
Proton-exchange membrane fuel cell (PEMFC), 116
PROX. *See* Preferential oxidation (PROX)
PS. *See* Polystyrene (PS) resin
PSD. *See* Pore size distribution (PSD)
Pulsed-flame photometric detector (PFPD), 39
PVA. *See* Poly(vinyl alcohol) (PVA) matrix
Pyrolysis, 82

Q

Quantachrome NOVA 2200e instrument, 180

R

Raney nickel, 56
  breakthrough capacities, 60*t*
Room temperature ionic liquids (RTIL), 119
RTIL. *See* Room temperature ionic liquids (RTIL)
Ru precursors, 145

S

Saturated calomel electrode (SHE), 165
SBA-15, physical properties, 58*t*
Scanning electron microscopy (SEM), 19, 125
  analysis, 24
Scanning transmission electron microscope (STEM), 177
SCGP. *See* Shell Coal Gasification Process (SCGP)
SEM. *See* Scanning electron microscopy (SEM)
SHE. *See* Saturated calomel electrode (SHE)
Shell Coal Gasification Process (SCGP), 86
Shimadzu GC-17A gas chromatograph, 39
Shimadzu QP-5000 mass spectrometer, 39
Slagging gasifier, 86
SLM. *See* Supported liquid membranes (SLM)
Sorbitol, serial kinetic pathway, 74*f*
SPBI. *See* Sulfonated polybenzimidazole (SPBI) copolymer matrix
SRGO. *See* Straight run gas oil (SRGO)
SRM. *See* Steam reforming of methanol (SRM)
Steam reforming of methanol (SRM), 178, 180
STEM. *See* Scanning transmission electron microscope (STEM)
Straight run gas oil (SRGO), 34
Sulfonated polybenzimidazole (SPBI) copolymer matrix, 122
  synthesis, 123*f*
Sulphur, 99
  downstream capture, 100
  in situ capture, 100
Supported liquid membranes (SLM), 118
Syngas platform, production of widely varying energy carriers, 81*f*
Synthesis gas purification, 116
  facilitated transport membranes, 118
  fuel cells, 125
  petrochemical and refining applications, 133
  solution-diffusion membranes, 117

T

Tar, 90
  catalytic reduction, 98
  conversion catalysts and their characteristics, 97*t*
  primary methods, 98
  reduction methods in biomass gasification, 96*f*
  secondary methods, 99
TEM. *See* Transmission electron microscopy (TEM)
Temperature-programmed desorption (TPD), 36
Temperature-programmed reduction (TPR), 17
TEOS. *See* Tetraethyl orthosilicate (TEOS)
Tetraethyl orthosilicate (TEOS), 56
Tetrahydrofuran (THF), 56
TGA. *See* Thermogravimetric analysis (TGA) measurements
TG-DSC. *See* Thermogravimetry-differential scanning calorimetry (TG-DSC)
Thermogravimetric analysis (TGA) measurements, 123
Thermogravimetry-differential scanning calorimetry (TG-DSC), 3
  CMcat, 8*f*
  NiW/CYCTS, 8*f*
THF. *See* Tetrahydrofuran (THF)
TON. *See* Turnover number (TON)
TPD. *See* Temperature-programmed desorption (TPD)
TPR. *See* Temperature-programmed reduction (TPR)
Transmission electron microscopy (TEM), 19
  analysis, 24
Turnover number (TON), 145

U

ULSD. *See* Ultra-low sulfur diesel (ULSD)
Ultra-low sulfur diesel (ULSD), 56
  breakthrough curves for ADS, 60*f*
  commercial, 56
  fuel cell applications, 56
  GC-PFPD chromatogram, 59*f*

Downloaded by 89.163.34.136 on June 4, 2012 | http://pubs.acs.org
Publication Date (Web): December 14, 2011 | doi: 10.1021/bk-2011-1088.ix002

  nickel-based sorbents, 56
  sulfur compounds, 58
  ultra-deep desulfurization, 56
U.S. Environmental Protection Agency (EPA), 16

V

VWR-Model 75T ultrasonic bath, 56

W

Water gas shift (WGS), 116
  CO conversion/reduction, 131
  membrane reactor, 117, 131
    retentate CO concentration as a function of feed flow rate, 132*f*
  product, 117
WGS. *See* Water gas shift (WGS)

X

X-ray diffraction (XRD), 3, 8
  analysis, 19
  broad angle, 21, 23*f*
  low angle, 21, 22*f*
  patterns of catalysts prepared via different methods, 9*f*
  patterns of catalysts with different citric acid amounts, 10*f*
XRD. *See* X-ray diffraction (XRD)
Xylose, 67

Z

Zirconium complex bearing phenoxide ligands, 159*s*
$ZnCl_2$ hydrate
  dissolution of cellulose, 73*f*
  dissolution of cellulose followed by depolymerization, 73*f*

Downloaded by 89.163.34.136 on June 4, 2012 | http://pubs.acs.org
Publication Date (Web): December 14, 2011 | doi: 10.1021/bk-2011-1088.ix002